IPP Max-Planck-Institut für Plasmaphysik

# Annual Report 1999

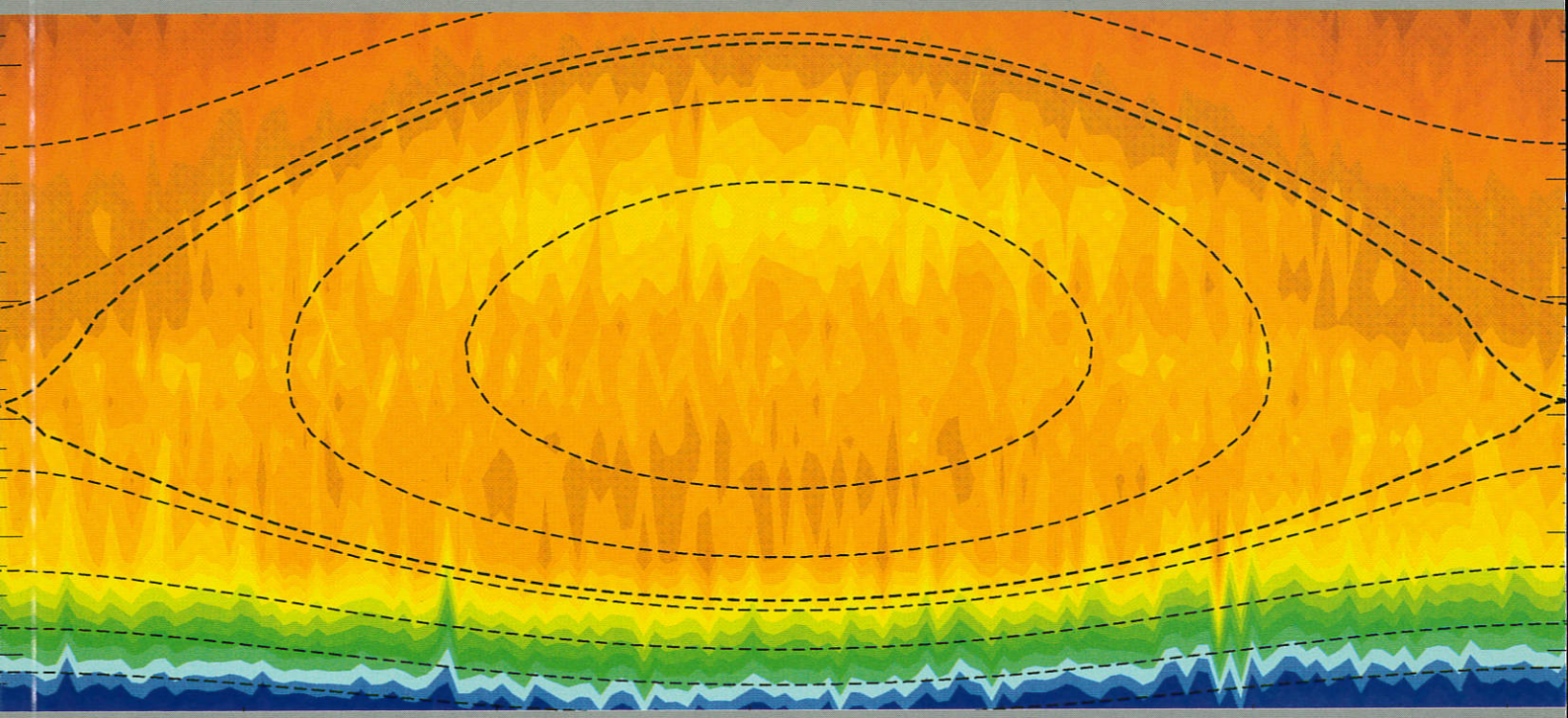

COVER ILLUSTRATION

Reconstruction of a magnetic island due to a neoclassical tearing mode in ASDEX Upgrade by means of ECE electron temperature measurements. Figure generated by J.P. Meskat (IPF Stuttgart) and H. Zohm (IPP Division "Experimental Plasma Physics 2" founded in 1999).

IPP
Max-Planck-Institut
für Plasmaphysik

EURATOM Association

# Annual Report 1999

## CONTENTS

# INTRODUCTION

The Max-Planck-Institut für Plasmaphysik (IPP) investigates the two main types of fusion devices, namely the tokamak and the stellarator. The aim of the ASDEX Upgrade divertor tokamak is to realise a reactor-compatible divertor and to study reactor-relevant plasma edge physics as well as particle and energy transport in the bulk plasma. Experiments are strongly focused on preparations for ITER: Originally mainly concerned with studies of divertor behaviour and control issues relating to ITER, ASDEX Upgrade is now also contributing to the basic understanding of instabilities as well as of particle and energy transport in the plasma core. Now that the properties of the plasma edge and core have been found to be strongly correlated, this extended research programme has become even more important. In addition, ASDEX Upgrade has recently entered the field of so-called advanced tokamak scenarios – one of the highlights of the last few years of tokamak research.

In 1999, ASDEX Upgrade was mainly concerned with investigating the advanced tokamak regime - which is characterised by formation of a hollow or very flat plasma current profile - and the effect of increased plasma triangularity on confinement: The advanced tokamak investigations with internal transport barriers cover discharges with both L-mode and H-mode signatures. Remarkable success has been achieved by prolonging the phases of inverted current profiles and hence improved energy confinement. In advanced scenarios equal ion and electron temperatures up to the reactor-relevant value of 10 keV have been achieved, thus showing the compatibility of these regimes with both electron and ion heating. Operation with moderately increased triangularity afforded a distinct improvement in the energy confinement and density operating space. Neoclassical tearing modes have been successfully stabilised by electron cyclotron current drive. The driving mechanisms of the MHD instabilities observed in advanced tokamak scenarios as well as the current and pressure profiles optimised with respect to these instabilities have been identified. Besides limiting the operating regime, MHD phenomena have been shown to contribute to quasi-stationary discharge conditions by limiting the central peaking of impurity and current density profiles. Last but not least, during 1999 ASDEX Upgrade operated routinely with neutral beam heating power capabilities of more than 20 MW, thus achieving the highest characteristic scaling power P/R in Europe.

In all areas the experimental work on ASDEX Upgrade is accompanied by a strong theoretical effort. In particular, divertor theory activities constitute the main modelling input to the ITER design. The increasing importance of high-$\beta$ scenarios for ASDEX Upgrade and steady-state tokamak reactor operation has made first-principle-based fluid turbulence studies for clarifying transport in the outer regions of the bulk plasma and the investigation of MHD stability phenomena further focal points of the theoretical programme at IPP.

In preparation for the divertor experiments on the WENDELSTEIN 7-AS stellarator ten control coils were installed in 1998 in the plasma vessel to control resonant field structures at the plasma edge. These modifications and subsequent tests were successfully concluded in 1999. The effectiveness of the control coils could be demonstrated: They are able to enlarge, decrease or compensate natural magnetic islands, can increase the plasma radius, and behaved during current ramp-up as predicted by vacuum field calculations. The high recycling conditions achieved even with this very open divertor structure afford good prospects for successful studies of a closed island divertor. Such investigations are scheduled for the second experimental campaign after installation of divertor modules, titanium getter pumps and divertor diagnostics. These further modifications to WENDELSTEIN 7-AS are due to be completed in mid-2000.

The new experiment for demonstrating the reactor relevance of the advanced stellarator principle, WENDELSTEIN 7-X, will be a 5-period Helias configuration with helical divertor and superconducting coil assembly. It is to be operated at the Greifswald Branch Institute of IPP. In 1999, the DEMO coil, an original-sized superconducting magnet, was successfully tested in the TOSKA facility at the Forschungszentrum Karlsruhe. The go-ahead for manufacture of the complete coil system for WENDELSTEIN 7-X was subsequently given. The DEMO cryostat, a one-eighth sector of the device, was completed by the contractor and prepared for the cryogenic tests to be conducted at IPP in Garching. Furthermore, in 1999 the detailed design of WENDELSTEIN 7-X was continued, and further major components were ordered, such as the planar coils, the magnet support structure, the power supply for

the magnets, and the high-voltage supply for the heating systems. The new building for the Greifswald Branch Institute of IPP was almost completed, both within schedule and budget.

Theoretical investigations in the Stellarator Theory Division formed at Greifswald are concerned with further development of the stellarator concept, equilibrium and stability investigations with advanced computational tools, development of a stellarator-specific basis of anomalous transport theory, and a three-dimensional plasma edge theory.

Since progress in plasma physics has now paved the way towards the use of fusion as an energy source, the development of materials for fusion applications has become even more necessary. To contribute to this field the Materials Research Division of IPP was newly founded in 1999, its work being complementary and closely linked to the activities of the Surface Physics Division of IPP. The aim of the new division is to develop materials for plasma-facing components; its research programme will concentrate on materials characterisation, elemental and structural analyses as well as on measurements of the thermal diffusivity of materials, thin-film synthesis, on the development of low-Z coatings, and numerical analyses of the thermomechanical behaviour of plasma-facing components.

On the national level, IPP coordinates its research effort with the Forschungszentrum Karlsruhe and the Forschungszentrum Jülich within the "Entwicklungsgemeinschaft Kernfusion". The Forschungszentrum Karlsruhe will contribute the complete ECR heating system for WENDELSTEIN 7-X. IPP also closely cooperates with a number of German universities, the collaboration with the University of Stuttgart being particularly intensive. Cooperation with the University of Greifswald is developing.

The research conducted at IPP is part of the European fusion programme: The ASDEX Upgrade tokamak and the stellarator concept of the WENDELSTEIN experiments provide essential information for preparing the next steps in the overall European programme. Furthermore, IPP hosts the European Fusion Development Agreement (EFDA) Close Support Unit, the successor of the NET group, the European reactor study group, which has been working at Garching since 1983. IPP is also involved in JET, the joint European experiment, cooperation in 1999 being organised within four Task Agreements on Pellet Injection, Plasma-Wall Interaction, H-mode Transport Studies, and Advanced Tokamak Scenarios. The experimental activities are accompanied by MHD stability analysis and modelling studies of plasma-edge-related issues. The close of 1999 saw the end of the JET activities as a Joint Undertaking: As of January 2000 the JET facility will be run under the EFDA Agreement and operated by the UKAEA. Physics exploitation will be handled by Task Forces from the various European Associations (Fusion Research Centres), coordinated by an EFDA JET Close Support Unit.

Coordination of research is also world-wide in extent. IPP is party to two Implementing Agreements: the one - with the USA - covering cooperation on the ASDEX Upgrade divertor tokamak; the other - with the USA, Japan, Australia, and Russia - regulating cooperation in the joint stellarator programme, to which the WENDELSTEIN experiments make a major contribution. From 1988 IPP provided the technical site for the American-European-Japanese-Soviet group responsible for designing ITER, the International Thermonuclear Experimental Reactor. After completion of the conceptual design, IPP was also chosen in 1992 - together with the fusion laboratories in Naka and San Diego - as an ITER site during the Engineering Design Phase. When the ITER partners decided to investigate a reduced-objective, reduced-cost version, IPP continued to be one of the hosts for the detailed technical design activities scheduled for the three-year period from 1998 to 2001.

The outline design for the redesigned ITER device was presented to the ITER Council at the beginning of 2000. The device will have an intermediate aspect ratio, a reduced plasma current of 15 MA, and a major torus radius reduced to 6.2 m. ITER-FEAT (the new designation) is thus geared to a power amplification factor of about 10 at an expected cost reduction of approximately 50 per cent. The device is also designed to study and exploit the regimes of improved tokamak confinement by internal transport barriers, which promise to give even this reduced-size device a significant chance of full ignition. ITER-FEAT will, however, achieve its base-line operating goal of $Q = 10$ without resort to advanced tokamak scenarios.

On behalf of the Directorate and Scientific Board I would like to take this opportunity of thanking all members of the institute for their substantial contribution to the success of fusion research at IPP in the last year.

Alexander M. Bradshaw

# Projects

# TOKAMAKS

A large part of the capacity at IPP is devoted to investigating plasma confinement in the tokamak configuration. IPP pioneered the divertor principle with the ASDEX tokamak (1980 - 1990), which demonstrated the favourable impurity control capabilities of this configuration and discovered the so-called H-regime characterized by markedly improved confinement. The divertor configuration has also been adopted for ITER, and ASDEX Upgrade, IPP's successor experiment to ASDEX, closely resembles a scaled-down version of ITER.

As a consequence, experiments on ASDEX Upgrade are strongly focused on the critical R&D tasks for ITER. Originally, this implied mainly studies of divertor behaviour and control issues relating to its ITER-like configuration. With the enhancement and diversification of its heating and particle control systems and the extension of its diagnostic capabilities, ASDEX Upgrade is now in addition also strongly contributing to the basic understanding of magnetohydrodynamic instabilities and particle and energy transport in the plasma core. After detection of the strong correlation of the properties of the plasma edge and core this extension of the research to core physics has become even more important. In addition, ASDEX Upgrade recently entered the field of so-called "advanced tokamak" experiments, which are characterized by formation of a hollow or at least very flat plasma current profile.

In all areas the experimental work is accompanied by strong theoretical effort. In particular, IPP's divertor theory effort also constitutes the main modelling input to the ITER design. First-principle-based fluid turbulence studies for clarifying transport in the outer regions of the bulk plasma are a further area of excellence of IPP. MHD stability phenomena have become a further focal point of our theoretical efforts due to the increasing importance of high-$\beta$ scenarios for ASDEX Upgrade and steady-state tokamak reactor operation.

During 1999, ASDEX Upgrade operated routinely with the NBI heating power capability of $P_{NBI} \leq 20$ MW, achieving the highest characteristic scaling power P/R in Europe. One part of the system delivering 10 MW was upgraded to provide 100 kV beams. ECR heating power was extended to about 1.2 MW. ICRH was operated up to 5.7 MW and extensive tests were conducted on a set of new ferrite tuners (on loan from DIII-D) which have the potential to facilitate automatic matching for nearly all plasma changes. Operation with the high-field-side pellet injector system at low injection velocities achieved further outstanding results. The ASDEX Upgrade activities in 1999 were dominated by two focal points: (i) the extension of the advanced tokamak regime and (ii) the effect of increased plasma triangularity $\delta$ on confinement. Outstanding physics results of ASDEX Upgrade in 1999 were:

- Remarkable success has been achieved by prolonging the phases of inverted q-profiles and related improved energy confinement. The advanced tokamak investigations with internal transport barriers (ITB) cover discharges with L-mode as well as discharges with H-mode signatures.
- In advanced scenarios equal ion and electron temperatures up to a reactor-relevant 10 keV have been achieved with ctr-ECCD.
- Operation with moderately enlarged triangularity showed clear impovements in the energy confinement and the density operating space in both conventional ELM'y H-modes and ITB plasmas.
- Neoclassical tearing modes have been successfully stabilized by DC ECCD in strongly NBI-heated discharges ($P_{ECCD} \ll P_{NBI}$).
- The driving mechanisms of the MHD instabilities observed in advanced tokamak scenarios as well as optimized current and pressure profiles with respect to these instabilities have been identified. Besides limiting the operating regime, MHD phenomena have been shown to contribute to quasi-stationary discharge conditions by limiting the central peaking of impurity and current density profiles.
- The existence of localized high-$\beta$ plasmoids during high-field-side pellet ablation and the correlated outward drifts have been proved. Typical densities and temperatures of the plasmoids have been determined.

In the near future, ASDEX Upgrade will adapt the divertor structure to maintain good divertor pumping properties during operation with higher triangularities. Current drive experiments will be started with the ICRH system. In addition, the NBI system will

be partly turned in the tangential direction to support current drive. The pellet-guiding system will be rebuilt to allow injection velocities of up to 1.2 km/s for deep fuelling.

ASDEX Upgrade maintains fruitful collaborations with the following institutions:
Inst. für Plasmaforschung, University of Stuttgart; University of Kiel; University of Magdeburg; University of Düsseldorf; University of Augsburg; University of Bayreuth; Culham Lab., Abingdon, UK; Centro de Fusão Nuclear, Lisbon, Portugal; University College, Cork, Ireland; Inst. Allgemeine Physik, TU Vienna, Austria; NCSR Demokritos, Athens, Greece; IESL-FoRTH, Heraklion, Greece; CRPP, École Polytechnique, Lausanne, Switzerland; CEA Cadarache, France; Istituto di Fisica del Plasma, CNR Milano, Italy; CREATE Group, Naples, Italy; University of Strathclyde, Scotland; FOM-Inst. voor Plasmafysica, Rijnhuizen, Netherlands; VTT Energy, Helsinki, Finland; Research Inst. for Particle and Nuclear Physics, Budapest, Hungary; Inst. of Applied Physics, Nizhni Novgorod, Russia; I.V.Kurchatov Institute of Atomic Energy, Moscow, Russia; Ioffe Institute, St. Petersburg, Russia; Technical University of Applied Physics, St. Petersburg, Russia; St.P.T.U., St. Petersburg, Russia; PPPL, Princeton, USA; GA, San Diego, USA; MIT, Cambridge, USA; Oak Ridge National Lab., Oak Ridge, USA; Sandia Labs, Livermore and Albuquerque, USA; Courant Institute, N.Y. University, USA; University of Toronto, Canada; Institute for Plasma Research, BHAT, Gandhinagar, India; Institute of Plasma Physics, Hefei, China; Korea Basic Science Institute, Yusung, Korea; National Institute for Fusion Science, Nagoya, Japan; University of Yokohama, Japan.

In 1998, the three remaining ITER partners (Japan, EURATOM, Russia) decided to design an experimental tokamak reactor with reduced technical objectives and cost. The target envisaged was a device capable of reaching - according to the standard ITER design rules - a value of the power amplification factor Q of 10, at an expected cost reduction of approximately 50 %. Various design options, differing essentially in the plasma aspect ratio $R/a$, were initially considered. In 1999, the design focused on a device with an intermediate aspect ratio and the following nominal parameters: (plasma current) $I_p = 15$ MA, (toroidal field) $B_t = 5.3$ T, (major torus radius) $R = 6.2$ m, (half mid-plane plasma diameter) $a = 2$ m, (elongation of the 95 % flux surface) $\kappa_{95} = 1.7$. The device was labelled ITER-FEAT, and an outline design was presented to the ITER Council at the end of 1999. A first estimate arrived at a construction cost of 55 % of that of the large ITER device, with the expectation of further cost reductions by enlisting more effective manufacturing techniques identified as part of the preceding, extensive R&D work. Tokamak research during the last few years has fortified the existing experimental data base. This was taken into account in the ITER FEAT design by remaining at a more conservative ratio of plasma density to the so-called Greenwald density.

Highlight of the last few years of tokamak research was the discovery of internal transport barriers as a means of further improving tokamak confinement. ASDEX Upgrade, in particular, has made crucial contributions to this field by demonstrating the potential steady state of one kind of such scenarios, and by showing the compatibility of this regime with both electron and ion heating. Nevertheless, the data base for this regime is at present very limited and will possibly need experimental data from ITER itself to become a reliable design instrument. ITER FEAT is therefore designed to study and exploit this regime, which also promises to give this reduced-size device a significant chance of full ignition, but it does not rely on its favourable properties to achieve its base-line operating goal of $Q = 10$.

In parallel to the design work for ITER FEAT, a special working group has been set up to study the possible legal framework for ITER construction and operation.

Besides operating ASDEX Upgrade, IPP has also been involved in JET, the Joint European Torus at Culham (UK), from the outset. In 1999, JET operation was in two campaigns, divided by a summer shutdown during which the inboard track for high-field-side (HFS) pellet launch was installed. This installation involved a combination of remote handling and manned intervention in the vacuum vessel and demonstrated once again the possibility of successfully undertaking complicated operations in a tritiated vessel. The experimental programme in both campaigns was divided into two task forces, one dealing with ELMy H-mode and Divertor Physics for ITER and one concentrating on Performance Optimization and Confinement with ITBs.

Initial assessment of the new gas box divertor was completed. H-mode performance was shown to be largely independent of divertor geometry as had been the case with previous divertor geometries. The septum dividing the two divertor legs, however, provided interesting results: Balanced detachment was obtained in L-mode discharges, and easier H-mode access was demonstrated. HFS pellet fuelling was demonstrated to be an effective fuelling method even in a large machine such as JET. Improved edge and SOL diagnosis allowed exploration of further physics issues. A novel technique using divertor tile thermocouples was used to measure the SOL energy deposition width, which in L-mode plasmas is found to be 6 mm, while in ELMy H-mode plasmas it is only 2-3 mm, integrated over the high-power heating phase of the pulse. This narrow SOL has important implications for the design of a next-step machine.

The main priority for the second task force was to obtain quasi-steady-state internal barrier (ITB) discharges: In discharges with an L-mode edge MHD events terminate the ITB due to excessive pressure peaking; in type I ELMy H-mode discharges, a high edge density and the radial extent of the ELMs erode the ITB. However, argon dosing at the edge can reduce the ELMs to type III. With argon dosing and optimum heating timing, $\beta_N = 2.6$ and $H_{89} = 2.2$ at 2.5 MA/2.5 T were obtained for several seconds. At 3.5 MA/3.45 T $\beta_N$ was limited to 2.0 at 18 MW NBI + 10 MW ICRH, the maximum combined heating power available at JET. IPP participates in scientific exploitation of the JET device and gives advice and support for the design and operation of many plasma diagnostic systems on JET. The cooperation with JET is organized within four Task Agreements on Pellet Injection (TA 1), Plasma-Wall Interaction (TF 2), H-Mode Transport Studies (TA 5), and Advanced Tokamak Scenarios (TA 8). These experimental activities are accompanied by MHD stability analysis and modelling studies of plasma-edge-related issues.

# ASDEX UPGRADE PROJECT

(Head of Project: Dr. Otto Gruber)

**Experimental Plasma Physics Division E1:** C. Aubanel, H. Bauer, K. Behler, M. Bessenrodt-Weberpals, H. Blank, H.-S. Bosch, R. Brückner, B. Brüsehaber, A. Buhler, A. Carlson, A. Cierpka, G. Conway, C. Dorn, R. Drube, J. Ernesti, H.-U. Fahrbach, J.C. Fuchs, K. Förster, O. Gehre, J. Gernhardt, D. Gonda, O. Gruber, E. Gubanka, G. Haas, M. Harnau, G. Herppich, A. Herrmann, J. Hobirk, H. Hohenöcker, L. Horton, G. Hussong, T. Härtl, D. Jacobi, S. Kamm, E. Kaplan, M. Kaufmann, B. Kleinschwärzer, H. Klement, S. Klenge, H. Kollotzek, G. Kölbl, P.T. Lang, R.S. Lang, P. Leitenstern, A. Lorenz, K.F. Mast, K. Mattes, D. Meisel, P. Meissner, R. Merkel, V. Mertens, J.P. Meskat, H.W. Müller, G. Neu, J. Neuhauser, E. Oberlander, M. Pflug, G. Prausner, G. Raupp, G. Reichert, V. Rohde, H. Röhr, M. Sator, G. Schall, H.-B. Schilling, G. Schramm, G. Schrembs, S. Schweizer, J. Schweinzer, H.-P. Schweiß, U. Seidel, S. Sesnic, Ch. Sihler, A. Sips, A. Stimmelmayr, J. Stober, B. Streibl, W. Suttrop, A. Tanga, W. Treutterer, M. Troppmann, R. Wolf, D. Zasche, T. Zehetbauer.

Guests in Division E1: S.M. Egorov, Technical University, Plasma Physics Department, St. Petersburg, CIS;
P. Fu, L. Hu, Academia Sinica, Hefei, China;
A. Khudoleev, IOFFE, St. Petersburg, CIS;
H. Weitzner, N.Y. University, USA.

**Tokamak Physics Division:** R. Arslanbekov, G. Becker, A. Bergmann, R. Bilato, D. Biskamp, K. Borrass, M. Brambilla, K. Büchl, D. Correa-Restrepo, D. Coster, W. Feneberg, S. Günter, K. Hallatschek, B. Janauschek, F. Jenko, O. Kardaun, R. Kochergov, K. Lackner, D. Lortz, P. Martin, R. Meyer-Spasche, G. Pautasso, A.G. Peeters, S. Pinches, W. Sandmann, S. Schade, R. Schneider, W. Schneider, E. Schwarz, B. Scott, E. Strumberger, G. Tardini, H. Tasso, Ch. Tichmann, R. Wunderlich, H.P. Zehrfeld, A. Zeiler.

Guests in Tokamak Physics Division: B. Braams, New York University, N.Y., USA;
C. Atanasiu, Institute of Atomic Physics, Bucharest, Romania;
J. Bowman, University of Alberta, Alberta, Canada;
V. Rozhansky, A. Ushakov, S. Voskoboynikov, I. Veselova, LPI, St. Petersburg, CIS;
O.D. Komarov, Kharkov Institute, Kharkov, Ukraine;
R. Brandenburg, H. Bürbaumer, IAP, Vienna, Austria;
J. Drake, Institute of Plasma Research, Maryland, USA;
Q. Yu, Academia Sinica, Hefei, China.

**Experimental Plasma Physics Division E2:** A. Gude, B. Kurzan, M. Maraschek, R. Monk, H. Murmann, K.-H. Steuer, H. Zohm.

**Experimental Plasma Physics Division E4:** A. Bard, K. Behringer, D. Bolshukhin, R. Dux, W. Engelhardt, J. Fink, J. Gafert, A. Geier, A. Kallenbach, H. Meister, R. Neu, R. Pugno, H. Salzmann, D. Schlögl, K. Schmidtmann, W. Ullrich, M. Zarrabian.

**Technology Division:** W. Becker, M. Beckmann, F. Braun, H. Brinkschulte, M. Ciric, H. Faugel, R. Fritsch, D. Hartmann, B. Heinemann, F. Hofmeister, K. Kirov, W. Kraus, F. Leuterer, F. Meo, F. Monaco, M. Münich, J.-M. Noterdaeme, S. Obermayer, F. Probst, S. Puri, R. Riedl, F. Ryter, W. Schärich, E. Speth, A. Stäbler, O. Vollmer, F. Wesner, R. Wilhelm, K. Wittenbecher.

**Berlin Division:** M. Laux, U. Wenzel.

**Garching Computer Centre:** P. Heimann, S. Heinzel, J. Maier, H. Reuter, A. Schott, M. Zilker.

**Materials Research:** H. Maier.

**Surface Physics Division:** K. Krieger, J. Roth, A. Tabasso.

**Central Technical Services:** R. Ammer, H. Eixenberger, F. Gresser, E. Grois, M. Huart, C.-P. Käsemann-Wilke, M. Kluger, H. Kosniowski, J. Kutsch, R. Kutzner, S. Mukherjee, J. Perchermeier, J. Stadelbauer, R. Zickert.

**University of Cork, Ireland:** M. Foley, P. McCarthy.

**IPF University of Stuttgart:** I. Altmann, G. Dodel, L. Empacher, W. Förster, G. Gantenbein, K. Hirsch, E. Holzhauer, M. Letsch, B. Roth, U. Schumacher, K. Schwörer.

**Centro de Fusão Nuclear, Lisbon, Portugal:** L. Cupido, V. Grossmann, M.-E. Manso, L. Meneses, I. Nunes, T. Ribeiro, J. Santos, F. Serra, A. Silva, P. Varela, S. Vergamoto.

**NCSR Demokritos, Athens, Greece:** G. Kyriakakis, N. Tsois, P. Xantopoulos.

**TEKES (HUT and VTT), Finland:** J.A. Heikkinen, T. Kiviniemi, T. Kurki-Suonio, S. Saarelma.

**University of Augsburg:** B. Heger, H. Paulin, U. Fantz.

# 1. OVERVIEW

## 1.1 Scientific Aims and Operation

The ASDEX Upgrade non-circular tokamak programme was largely focused on (i) investigation of scenarios and physics of advanced tokamak plasma concepts with internal transport barriers leading to stationary operation and enhanced performance, (ii) confinement and performance-related core physics in the ITER base-line scenario, the ELMy H-mode, where close interaction between the edge and core plasma was realized, (iii) MHD stability and active stabilzation of beta-limiting instabilities as well as avoidance and mitigation of disruptions., and (iv) edge and divertor physics in these high-power, high-confinement regimes, with the aim of identifying and optimizing ways of reliable power exhaust and particle control (ash removal).

The similarity of ASDEX Upgrade to ITER in the poloidal field coil system and divertor configuration makes it particularly suited to testing control strategies for shape, plasma performance, and mode stabilization. Additionally, the similarity in cross-section to other divertor tokamaks is important in determining size scalings for core and edge physics. This collaborative work, including extrapolation to ITER parameters, has continued and will even be enhanced in JET operation during the next few years.

The 1999 physics programme was based on the conclusions and findings of the last few years, ITER requirements, and tokamak concept improvement. The present version of the closed Div II, LYRE (with vertical target plates including a roof baffle in between), which is rather similar to the present ITER FEAT reference design, allows a strong reduction of the maximum heat flux to the target plates and is capable of handling heating powers of up to 20 MW or P/R of 12 MW/m. Equilibria with higher triangularities ($\delta$<0.35) have been run with the outer strike point being located on the top of the roof baffle or on the outer vertical target to get higher pumping speeds. They showed strongly improved confinement, enhanced MHD stability, and, therefore, higher plasma energies and values, and extended density operational range in both conventional and advanced scenarios.

The upgraded heating systems were extensively used for physics studies. Neutral beam injection was available with injection energies of 100 and 60 keV (both with 10 MW for deuterium), which allowed further studies of the influence of heat deposition on transport and fast-particle effects on MHD instabilities. The ICRH system allowed coupling of the full power of 5.7 MW for both on- and off-axis deposition in, respectively, minority and mode conversion heating of ions or electrons. The ECRH system consisted of three gyrotrons with a coupled power of 1.2 MW for 2 s allowing feedback stabilization of neoclassical tearing modes limiting the achievable $\beta$ in peaked plasma current density discharges with $q_{min} \approx 1$, transport studies, and on-axis heating and current drive in advanced scenarios.

In advanced scenarios, characterized by a high fraction of bootstrap current and external current drive, emphasis was placed on performance enhancement and extension by using different heating and current drive methods (NBI, ECRF), which resulted in reactor-relevant temperatures of $T_e, T_i > 10$ keV. Alignment of the internal transport barrier with the optimal magnetic shear profile and simultaneous use of a cold divertor will be one of the key elements of the ASDEX Upgrade programme. Finally, the ASDEX Upgrade programme is embedded in a framework of national (IPF Stuttgart, University of Augsburg, see also the section on University contributions to the IPP programme) and international collaborations (see section International Cooperation).

## 1.2 Summary of Main Results

The most important observation in the Div II geometry is a strongly reduced, distributed power flux to the surrounding structures during both ELMy and ELM-free phases, as already reported last year. This result is in agreement with B2-Eirene simulations, which were also used to establish the influence of the divertor geometry and different plasma shapes. The studies of reactor-compatible materials was continued by covering 1 $m^2$ of inner heat shield in the main chamber with tungsten coating to reduce carbon influx and test for possible large-area coating of the vessel walls with this material. No tungsten impurities were observed in the plasma.

The experiments with more triangular plasma shapes ($\delta \approx 0.15$ to 0.35) showed strongly improved confinement behaviour of H-mode discharges up to high densities of 80 % of the Greenwald density compared with more elliptical plasma cross-sections. Even when the Greenwald density itself is approached, the confinement times are still around 80-90 % of the ITER H97-P scaling despite deterioration due to the strong gas-puffing needed. H-mode discharges could be sustained up to very high densities, being 10 % above the Greenwald density without HFS pellet injection. These beneficial effects even exceed the values reported from the triangularity scans at JET and allow the anticipated operational regime of the RC-ITER close to the Greenwald density. The pressure at the H-mode edge barrier increases with triangularity due to the higher pressure gradients limited by edge MHD stability, and is directly coupled with the plasma stored energy via the profile stiffness. The energy losses by ELMs do not increase despite the rising ELM amplitudes, since the ELM frequency correspondingly decreases. At highest triangularities a regime with small high frequency ELMs was found, which should facilitate divertor operation in future devices.

Applications of the 100 keV neutral beam injection now available concerned the influence of particle energies between 30 and 100 keV on MHD modes, such as fishbones and TAE modes driven by fast particles, the energy transport for changed fishbone behaviour and toroidal rotation velocities, and the temperature profile resilience for quite different radial power deposition profiles.

The advanced tokamak scenarios with an internal transport barrier in combination with an H-mode edge barrier and low shear with $q_{min} \approx 1$ were extended towards higher plasma densities

close to half of the Greenwald density (to allow energy exhaust in these scenarios) either by edge gas fuelling or by improved core particle confinement with more triangular plasma shapes. Gas fuelling causes an increase of the threshold power to sustain an ITB, but on the other hand a decrease of $Z_{eff}$ below two was found. Higher plasma triangularities additionally allowed a performance increase up to $H_{ITERL-89P} \times \beta_N \approx 7$, but $\beta$ is still limited by neoclassical tearing modes (see sections 6 and 7).

The physics programme placed further emphasis on utilization of ECCD for control of $\beta$-limiting neoclassical tearing modes (achieving mode suppression also with unmodulated current drive in the islands' O-point) and on central heating and current drive to established reversed-shear, internal transport barrier discharges with $q_{min} \approx 2$. Here a substantial effect on MHD stability was found, affecting the passage of the q-profile through $q_{min} \approx 2$. A highlight was the achievement of simultaneous $T_e$ and $T_i$ values in excess of 10 keV, with ECRF counter current drive, where the performance of the ion channel was not reduced as in similar experiments at DIII-D and JET (section 5). MHD instabilities limit the operational regime in the advanced scenarios and the driving mechanisms have been identified. But MHD phenomena have also been shown to contribute to achieving quasi-stationary discharge conditions by limiting central peaking of the current density profile.

## 1.3 ASDEX Upgrade Programme in 2000

Next year, core physics studies will continue with emphasis on the improvement of plasma performance (energy and particle transport, MHD stability and limits, mode stabilization using ECRH and ECCD), on the influence of the plasma shape triangularity on both "conventional" H-mode and "advanced" tokamak scenarios, and especially on the ELMy H-mode near operational limits. As regards energy transport, it is intended to conduct studies on the relation between the core and edge and their reciprocal influence via transport, transport barrier physics, dimensionless scalings (mainly in connection with JET), and heat waves. In the advanced scenarios main items will be heating and momentum thresholds for internal barrier formation using NBI and ICRH, current profile control with ECRF and ICRF, and the influence of L- and H-mode edge controlled by limiter and divertor configurations. Particle transport and density limits remain a substantial part of our effort, including promising refuelling by pellet injection from the high-field side, where the existence of localized high-$\beta$ plasmoids and their toroidal drift have been proved. A major step is expected from a high-field side pellet launch capability with injection speeds of up to 1000 m/s.

The provisions for current drive are being continued to sustain and control flat or reversed-shear profiles in advanced mode operation in addition to the internal driven bootstrap current. This can be done in 2000 in a flexible way by means of 1.6 MW of already available coupled ECRF power with steerable mirrors (>150 kA) and on-axis fast wave (150 kA) or off-axis mode conversion current drive with the ICRF system. Major enhancement will be effort by reorientation of one beam line for more tangential injection starting in summer next year after a 9-month shut down, which will provide 250 kA of off-axis current drive. In parallel, adaptation of the divertor to the more highly triangular plasma shapes is intended in 2000, as high-$\delta$ plasma shapes now suffer from the more perpendicular inclination of the SOL to the roof baffle and reduced pumping capability. To get steady-state conditions not only on the transport and MHD time scales but also on skin time, a $I_p$ flat-top time of 10 s should be sufficient and will be provided by upgrading the power supply system. All three enhancements will be available in spring 2001.

In sections 2-4 the progress in plasma configurations and machine equipment is described. Sections 5 and 6 deal with "advanced tokamak operation" and related MHD phenomena, section 7 with the successful stabilization of neoclassical tearing modes, and section 8 with operation at increased plasma triangularity. Section 9 presents additional results concerning core physics, section 10 ICRH results, while sections 11 and 12 are particularly devoted to divertor and SOL physics.

## 2. ADVANCED PLASMA CONFIGURATIONS

In the search for scenarios with improved energy confinement, a number of discharge configurations with dedicated plasma shapes were developed and tuned. Lower single-null shapes for medium triangularity $\delta$ were designed with the outer strike point on top of the roof baffle (Fig. 2.1c)) or with both strike points in the lower divertor throats b). They are characterized by a top triangularity of 0.2 and a bottom $\delta$ of $\approx$0.4 at a plasma current of 1 MA. These shapes led to significantly improved confinement characteristics. Furthermore, high-triangularity shapes were tuned to achieve the maximum possible top triangularity, while the inner strike point was feedback-controlled to stay in the divertor area. A maximum averaged $\delta$ of about 0.36 could be achieved d). However, a number of constraints such as power supply limits, mechanical forces on the coil suspensions and geometrical distances between plasma boundary and limiters and baffles narrow severely the optimization window. A special advanced-tokamak (ITB) plasma shape with an **up-**

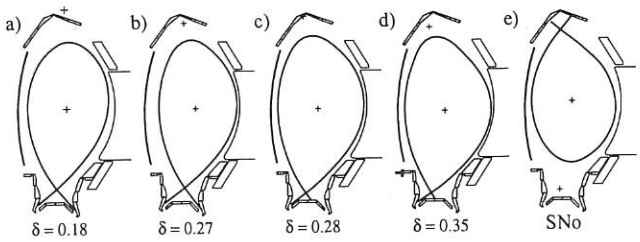


*FIG. 2.1: Conventional ASDEX Upgrade configuration a) and recently developed ones b) - e).*

**per** single-null configuration e) was designed to benefit from the enlarged L→H-mode transition threshold with ion $\nabla$B drift direction away from the active X-point. The configuration is established at the earliest possible time instant in the discharge while the plasma current is still low (0.2 MA) and is preserved

as $I_p$ is ramped up to the final value of 1 MA. Owing to the $I_p$ ramp, the early use of auxiliary NBI heating, and strong changes of $\beta_\perp$, $l_i$, and vessel currents this scenario is dominated by highly dynamic phases demanding high-quality position control.

## 3. ECRH DEVELOPMENT

The ECRH system of ASDEX Upgrade was designed particularly to achieve very localized electron heating and current drive for studies relating to electron heat transport via heat waves, to stabilization of neoclassical tearing modes, to transition of confinement regimes, etc. The basic system parameters are

| | |
|---|---|
| **frequency** | 140 ± 0.5 GHz, 2nd harmonic X-mode |
| **power** | 2 MW (2.8 MW) in Gaussian beam |
| **pulse length** | 2 sec (1 sec) |

The power is generated by 4 diode-type gyrotrons (GYCOM, Zodiak type) with a total efficiency of 30 %. They operate at 73.5 kV with beam currents of 25 to 30 A. The cavity magnetic field of 6 T is provided by cryomagnets (Oxford Instruments). The output power of the gyrotrons depends on the beam voltage. An example is shown in Fig. 3.1. One of the gyrotrons is now under repair and is expected to be returned in February 2000.

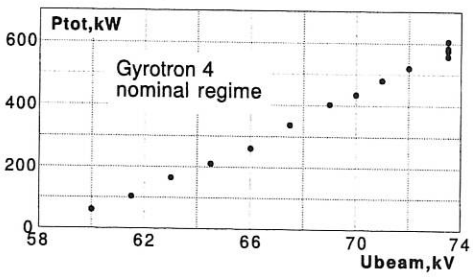


*FIG. 3.1: Total output power of gyrotron 4 for 2 sec pulses.*

Two gyrotrons at a time are driven from one thyristor-controlled power supply via one tetrode modulator (Thomson CQK 200-4A). This is used not only to switch the power on and off, but also to regulate the beam voltage to <0.5 %, and modulate the RF power. By simply switching the high voltage on and off we can achieve a modulation frequency of up to 1 kHz, but if the high voltage is only reduced to such a level that the oscillation just does not stop, we can achieve modulation frequencies of up to 30 kHz. This mode of modulation leads, however, to high loading of the tetrode and cannot be applied for the full pulse duration.

In our installation the gyrotrons suffer from magnetic perturbations. One source is the time-varying poloidal magnetic field of ASDEX Upgrade. It distorts the electron beam deposition in the collector and requires a reduced sweep amplitude across the collector surface in order not to reach uncooled areas. It may also influence the startup of the oscillation when the high voltage is switched on. This can be overcome by a slight correction of the gun magnetic field. Another source of magnetic perturbation is the magnetic field of the cryomagnet of the adjacent gyrotron. Although the distance between the tubes is 2.8 m and the perturbing magnetic field is as low as 3.5 gauss, it leads to an additional distortion of the electron beam deposition in the collector. This was compensated by a pair of Helmholtz coils.

For each gyrotron there is one transmission line to the tokamak. The lines operate under normal air pressure. A schematic of such a line is shown in Fig. 3.2.

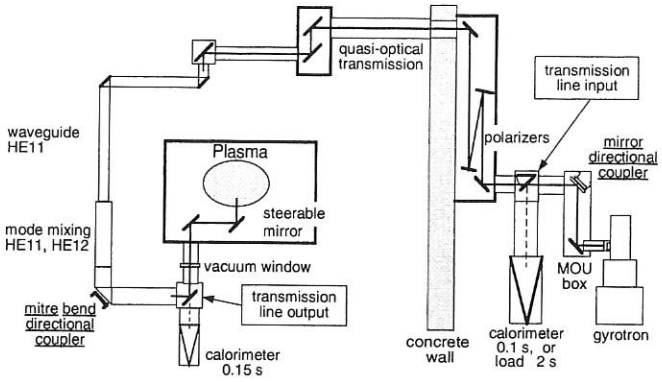


*FIG. 3.2: Schematics of ECRH transmission line.*

The output of the gyrotron is not a pure Gaussian mode and requires beam correction mirrors in the matching optics unit close to the gyroton window. The beams are then transmitted via mirror lines (lengths from 6 m to 20 m) including 2 polarizer mirrors and are finally, near the tokamak, fed into HE-11 corrugated wave guides 89 mm in diameter (lengths from 5 m to 15 m). At the end of these lines there is a mode-mixing section generating a mixture of HE-11 and HE-12 modes, such that we have a rectangular-like beam profile at the torus window (boron nitride, edge cooled). In this way the window losses occur closer to the cooled surface which is necessary to handle a 2 sec pulse. Inside the torus there are a fixed focusing mirror and a steerable plane mirror (metallized graphite) allowing the beam to be scanned by ±30° in both the poloidal and toroidal directions. Near to the plasma centre the interference of the two waveguide modes leads to a very narrow beam profile of a full half-power width of 30 mm. This allows localized deposition also with a poloidally deflected beam. The narrow deposition profiles were confirmed by measurements of the electron temperature rise on switch-on of the RF pulse.

The proper power transmission is monitored with two directional couplers at the input and output of the line, and with several arc detectors surveying the whole transmission line from the gyrotron window to the torus window.

The transmission losses were determined calorimetrically with the directional coupler signal of mirror 2 being used as reference. Right after the MOU box we have a switchable mirror to direct the RF beam into a calorimeter load. This point is taken as the input of the transmission line for the Gaussian beam, and the measured power is $P_{TLin}$. At the end of the waveguide section there is another switchable mirror to direct the beam either into the plasma or into another calorimeter load. This point is taken as the output of the transmission line, and

the power is $P_{TLout}$.

In addition, we determine the losses in the gyrotron output window which, with a factory-determined calibration factor, give the total output power $P_{tot}$ of the gyrotron. These powers are measured at different beam voltages and plotted in Fig. 3.3 as a function of the power measured at the directional coupler.

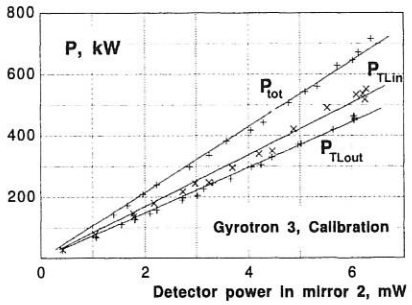


*FIG. 3.3: Calorimetric measurements of total gyrotron output power, transmission line input power and transmission line output power.*

The result of the three gyrotrons new operating is summarized in Table 1. The average loss in a transmission line is 10 % in agreement with theoretical estimates. A further loss of 6 % on the way to the plasma is estimated for the torus window and the internal mirrors.

| | Gyr. 2 | Gyr. 3 | Gyr.4 | average |
|---|---|---|---|---|
| $P_{TLin}/P_{tot}$ | 0.83 | 0.79 | 0.85 | 0.82 |
| $P_{TLout}/P_{TLin}$ | 0.93 | 0.88 | 0.88 | 0.90 |
| $P_{Plasma}/P_{TLin}$ | 0.88 | 0.84 | 0.84 | 0.85 |
| $P_{Plasma}/P_{tot}$ | 0.74 | 0.66 | 0.71 | 0.70 |

*Table 1 Power ratios determined along several transmission lines.*

There is a fairly high loss of 18 % between the gyrotron output $P_{tot}$ and the transmission line input $P_{TLin}$. Of this loss 60 % is due to beam content which could not be recoverted into a Gaussian beam, and 40 % to diffuse radiation leaving the gyrotron at a steep angle and being absorbed in the beam tunnel between the gyrotron and MOU box.

The system is working fairly satisfactory. However, there are already prospects of improvement to be realized in a new system. The most important of these are an increase of power and pulse duration, increased efficiency with depressed collector, better beam quality and reduced losses with diamond windows, frequency tunability, and fast steerability of the launching mirrors.

## 4. TECHNICAL SYSTEMS

In 1999 the experiment was operating for 98 days and the counter advanced by 1775 shots. Of this time 79 days were dedicated to physics and the remaining 18 to technical commissioning and servicing actions. The vacuum vessel was opened from mid-August to late September for the regular servicing operations and installation of two toroidal arrays of tungsten-coated carbon tiles on the inner heat shield. The additional heating systems of ICR and the second NB injector were prepared for current drive.

**Cryopump:** The high-pressure He storage capacity and the He recovery system were extended to an equivalent of 4200 litre LHe and an average throughput of up to (100 $Nm^3/h$), respectively. The recovery capacity (5 g/s LHe) is now fully adequate for the usual plasma discharge sequences with He glowing at intervals (4 g/s average). However, for stable steady-state conditions a capacity of 6 g/s would be required. Below 6 g/s the cryo line is mildly unstable. The throughput drops in about 30 minutes to the critical throughput of below 2 g/s, where serious flow instabilities then set in. By controlling the speed of the circulating pump, which can adequately changed be within several seconds, it was therefore possible to reduce the He throughput to a level between 3 and 4 g/s.

**New modular thyristor converter (Group No. 6):** In late 1999 the manufacturing contract was signed with Vonk Systems (NL) for this group. Its design is characterized by a high degree of modularity to enlarge the flexibility in plasma shape control and be able to replace or reinforce existing converters. Group No. 6 has been specified with a nominal power of 135 MVA in pulsed duty. To reduce the reactive power load in the flywheel generator grid, Group No. 6 is to be equipped with a special arrangement of freewheeling thyristors. All four modules of group No. 6 can be controlled independently of each other or jointly and operated with a fast response time in parallel, serial, and anti-parallel (four-quadrant) configuration. There is fast overcurrent protection by neutral thyristor freewheeling. The modules are short-circuit proofed by current limitation (serial chokes) and possess crowbar protection against overvoltage. The commissioning of thyristor Group No. 6 is scheduled for early 2001.

**Extension of reactive power compensation (RPC);** Having gained operational experience in about 2000 switching operations with the first two RPC units, with 15 MVAr each, a contract for another six similar RPC units was concluded with SIEMENS. The commissioning of these units is scheduled for April 2001. The new modules will again be based on phase-synchronized vacuum switches. For compensating the reactive power of the high-current converters during operation of AUG, this technical solution proved to be very reliable and economic. With all four modules (eight units) installed, a reactive power of 120 MVAr can be compensated. This extension is one of the technical requirements for long-pulse operation of AUG.

**Paralleling of the flywheel generators EZ3 and EZ4:** Another technical requirement for the long-pulse operation envisaged is parallel connection of the flywheel generators EZ3 and EZ4, which supply the PF coils and the additional heating systems. Stability analyses and parametrical studies have

shown that the parallel-connected machines can under no circumstances lose synchronism. A robust multivariable controller providing defined load sharing under all operating conditions (fast load changes, active power oscillations, harmonics, faults ...) has now been developed. A safety concept able to cope with the increased short-circuit power of the two-machine system has been elaborated. Details are to be resolved as part of a study contract to be placed with industry.

## 4.1 Optimization of Operation Procedures and Machine Protection

The highly flexible experiment operation scheme of a mid-size device and operation close to the machine's design limits makes it necessary to optimize operation procedures continuously and enhance machine protection capabilities. A number of features have been added to the real-time controllers to facilitate experimentation and guarantee the machine's integrity:
The design of new scenarios (see section 2) is subject to a large number of technical and geometrical constraints. Several tools have been developed to facilitate the design process. An equilibrium optimizer helps to attain target plasma shapes inside the ranges of power supply constraints, mechanical stress limits and plasma geometry requirements. A dynamic simulation model for magnetic plasma control is being developed to address transient issues of a discharge scenario. Finally, a scenario shot program editor was implemented to allow dedicated programming of the large numbers of signals and values and checking them against supervisory limits.

The real-time performance controller R4 is important for fine tuning of bulk and divertor properties with fuelling and heating actuators. The built-in detection of physical instabilities and activation of protection reflexes was improved for better adaption to the discharge evolution. Locked-mode recognition auto-starts when the plasma current and elapsed discharge time exceed a minimum value. If automatic counteraction is enabled, then an alarm will activate gas puff for a pre set time interval. Occurrence of the event is now broadcast to all other systems via the timing system and may be used in parallel by the killer pellet. The detachment state safety monitoring is detected from $D_\alpha$ and $l_i$ exceeding certain thresholds for a minimum time. The resulting counteraction lasts for 300 ms with increased NI power and gas puff suppressed. Repeated occurrence of the detachment state during a discharge results in an automatic stability loss request to the real-time discharge supervision controller to initiate soft landing. A video-based system to monitor the torus wall is being implemented. It will get permission to limit the discharge duration in case of excessive temperature of mechanical structures. The position and shape controller R2 was equipped with an additional oscillation detector to protect the machine from exaggerated mechanical vibrations due to marginal feedback-driven oscillations in the control coils. The detector is robust to transients but sensitive to permanent oscillations in a frequency band and alarms the machine protection system if the oscillation amplitude exceeds a threshold to terminate the discharge. The poloidal field coil monitoring system R32 now also checks the thermal load in the TF-coil power supplies. In case of an alarm, the pulse is ramped down at maximum speed. An additional procedure monitors all field coil currents after a pulse termination alarm and activates power breakers in case of improper current decay. All monitoring procedures were redesigned to adapt automatically to the coil polarities set to have full protection for any case of experiments.

## 4.2 Data Processing

The ASDEX Upgrade network is now in a transient state going from FDDI to Gigabit- and Fast-Ethernet technology. Figure 4.1 gives a schematic view of the switches and server computers involved, arranged around a central FDDI and Gigabit "wire speed" router and switch configuration. The network structures

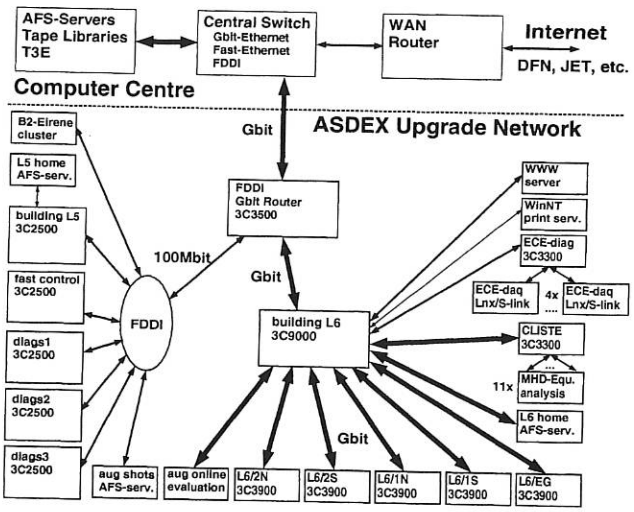


*FIG. 4.1: ASDEX Upgrade Network has moved half way from an FDDI-Backbone to Gigabit-Ethernet.*

renewed so far already have a significant performance impact on the AFS file servers storing the ASDEX Upgrade shotfiles, software, home directories, and the communication with the computer centre servers and tape libraries. It was also possible to speed up data collection and the time when first evaluation results become visible after a shot.

As next step, FDDI and Ethernet in building L5 and in the ASDEX Upgrade control room will be replaced by a Gigabit-Fast-Ethernet installation. Other projects are the replacement of CAMAC diagnostics with PCI-based DAQ systems acquiring data direct into computer memories and introducing weak real-time capabilities for selected diagnostics.

## 4.3 Neutral Beam Injection

The second injector was upgraded to an extraction voltage of 100 kV in 1998 and went into operation with 2.5 MW of injected power per source in February 1999. The maximum beam voltage is actually limited to 93 kV due to the power supplies and the maximum possible power into the calorimeter. Further regapping of the sources leading to lower extraction currents for a given extraction voltage will increase the maximum beam

voltage to 100 kV, as required for the NBI current drive experiments.

The possibility of using Helium beams for plasma diagnostics (in collaboration with the Technical University of Vienna), was checked by performing simultaneous injection of Deuterium and Helium beams. Whereas three of the four arc sources of the first injector were still run with Deuterium beams at 60 kV, the fourth source was operated with Helium at 30 keV, 22 A for 300 ms. The pulse length is limited by the gas pressure in the magnet because the Titanium getter pumps do not pump Helium. The pulse length of Helium injection will be increased in the near future by operating one arc source with a mixture of 90 % Deuterium and 10 % Helium gas.

In contrast to arc sources, the RF sources of the second injector react very fast to changes of the source input power. Hence, active beam current control of the RF sources is possible. With this possibility, the sources can be operated at the perveance optimum and the sensitivity of the RF sources to the mangetic stray field of the tokamak can be compensated, thereby increasing the beam quality and reducing the beam losses in the injector box.

Regarding the status of **tangential** NB injection for off-axis current drive one can say that detailed design of the components for the reoriented injector (see Annual Report 1997) has proceeded according to the foreseen time schedule. Major parts, e. g. the ion source flange, have been ordered. The calculations of the external magnetic screening and the field compensation by iron yokes are finished. Dismantling and rebuilding of the second injector will start on time at the end of the present series of experiments in summer 2000.

## 4.4 Ion Cyclotron Resonance Heating

The RF technical system of ICRH was modified to allow current drive in addition to pure plasma heating. This requires toroidally asymmetric spectra of the launched waves, calling for a phase difference of 90° between the two straps of an antenna. At ASDEX Upgrade this is achieved by using the outputs of the 3 dB power splitters showing this phasing. The cross-coupling between the antenna straps must be compensated for this asymmetric operation to avoid unequal power radiation.

Adequate antenna feeding lines and "compensation networks" were installed, together with coaxial switches allowing a choice between heating and current drive operation (see also Fig. 6.1 in Annual Report 1998). Since the additional line connections result in large loops enclosing poloidal flux, DC breaks had to be installed to prevent too large currents and forces from being induced upon plasma disruption.

Test were conducted on a fast stub tuner matching system, which uses premagnetized ferrites to adjust the electrical length of the tuners. This special system, developed for DIII-D and loaned to the IPP for testing is not applicable to ASDEX Upgrade in this form, but the ferrite technology used proved to be suitable for fast ICRH matching. Together with calculations it was shown that trombone-stub combinations with ferrites allow fast matching of the complex antenna impedance as well as application of a relatively simple feedback principle. Application of such automatic matching systems, which would avoid power reductions due to plasma variations, is envisaged for ASDEX Upgrade.

## 4.5 Siliconization

During the experimental campaign we used siliconization twice to coat the vacuum vessel. The more robust layers provided more constant conditions. In particular, it was possible to start up plasma operation after 8 weeks of venting without applying a new wall coating. This enables us to investigate tungsten-coated tiles at the inner heat shield without modification by an additional layer.

## 4.6 Carbon Flakes

The main disadvantage of carbon in a future fusion device is the formation of carbon hydride layers which will contain a significant amount of the Tritium inventory. As in JET, carbon layers were found on the divertor structure in ASDEX Upgrade at positions not in direct contact with the plasma. With long-term probes two different types of layers were found in ASDEX Upgrade. One type shows a ratio D/C= 0.4 which results in hard, brownish layers, the other type (D/C = 1) being soft, transparent layers. The hard layers flake off after venting. Although the positions where the layers are found are influenced by the complicated structure beyond the divertor, an asymmetry of 1:3 of the amount of carbon at the outer and inner divertor was determined. The positions where the layers are found can be correleted with the mapping of hot ions generated near the divertor slits. In laboratory experiments hot ions are required to form brownish layers with the same properties as found.

# 5. ADVANCED TOKAMAK OPERATION

## 5.1 Improved Core Confinement with H-mode Edge

In recent years fusion performance has been considerably improved in advanced tokamak operating regimes, which through optimization of the plasma shape and pressure and current profiles achieve enhanced energy and particle confinement in relation to standard ELMy H-mode plasmas. Common to these scenarios is a broad or even hollow current profile in the central region of the plasma. On ASDEX Upgrade a stationary regime of operation has been achieved which shows improved core confinement in combination with a type-I ELMy H-mode edge. Steady-state conditions are obtained by applying moderate neutral beam heating in the $I_p$ ramp up in order to reduce current diffusion and delay formation of a (m=1,n=1) resonant surface. Thus, when q=1 is reached strong (m=1, n=1) fishbones driven by neutral beam injection occur, apparently preventing sawtooth activity by clamping the q-profile at one, which is a

prerequisite for good confinement properties. On the basis of last year's results, the confinement and stability properties of such discharges with increased density and triangularity were investigated.

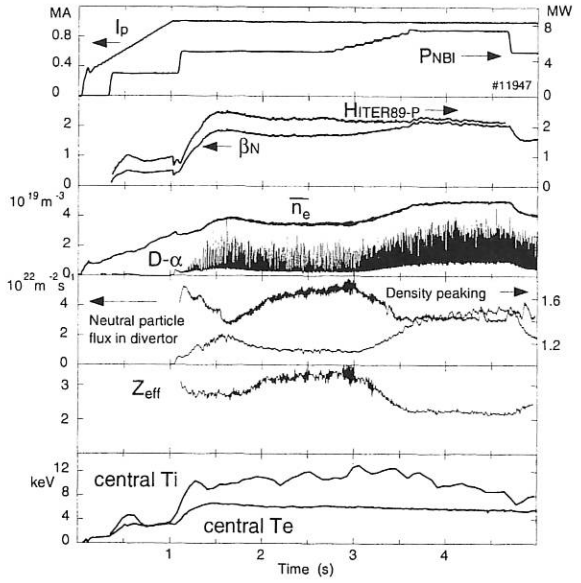


*FIG. 5.1: Typical time evolution of a discharge where the density was increased by simultaneous gas fuelling and power increase.*

To obtain high electron temperatures and hence a large reduction of the current diffusion during the initial phase of the discharge, the density is kept very low. However, for maximum fusion reactivity a higher density is desirable. If the density is raised by gas fuelling at the plasma edge at constant heating power, the confinement deteriorates, this being accompanied by a collapse of the density peaking, the almost complete loss of fishbone activity, and the appearance of sawtooth oscillations when $T_i$ approaches $T_e$, finally leading to a sawtoothing ELMy H-mode plasma. In contrast, by raising the density in conjunction with a simultaneous power increase it is possible to maintain the confinement properties. In Fig. 5.1 such a discharge is shown where $\overline{n}_e$ was increased from $3.5\times10^{19}$ m$^{-3}$ to $5.5\times10^{19}$ m$^{-3}$, corresponding to an increase of the central density from $5.5\times10^{19}$ m$^{-3}$ to $7.0\times10^{19}$ m$^{-3}$, while the neutral beam power has been raised by 50 %. Although density peaking and central $T_i$ decrease somewhat, the peaking of the profiles in general is sustained and $\beta_N$ even increases to 2.1. $H_{ITER89-P}$ stays constant, which means that the observed decrease of confinement time follows the power scaling ($\propto \sqrt{P}$). Associated with the increase of the edge density is an increase of the ELM frequency and, more important, a substantial decrease of $Z_{eff}$. Generally, this can be explained by the dependence of $Z_{eff}$ on the edge density. At low edge density the impurity screening is less effective, which leads to a higher impurity concentration in the plasma core.

To investigate the effect of the triangularity a modified regime of operation was developed. The initial phase of the discharge is similar to those presented above. After reaching the stationary phase, the top triangularity ($\delta_{top}$) is slowly increased from zero to 0.2, while the bottom one remains constant at 0.4. The main plasma parameters of such a discharge are shown in Fig. 5.2. Disregarding the initial overshooting of the plasma energy when the beam power is switched from 2.5 to 5 MW, the plasma energy increases by almost 30 % when $\delta_{top}$ reaches

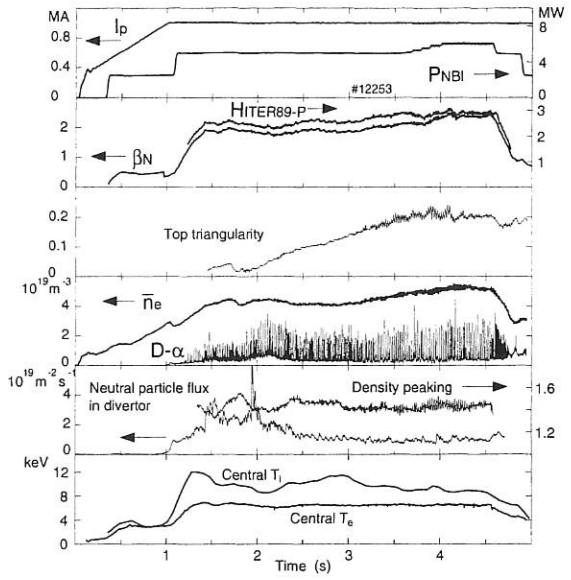


*FIG. 5.2: Typical time evolution of a discharge where the top triangularity was increased. When $\delta_{top}$ reached 0.2 the power was increased to demonstrate the higher $\beta$-limit.*

0.2, which can be mainly attributed to a density rise, reaching a central value of $7.5\times10^{19}$ m$^{-3}$. The density increase at higher triangularity occurs without gas fuelling, which can be seen on the low divertor neutral particle flux. The density peaking is unaffected by the change of $\delta$, while the central $T_i$ slightly decreases. After the maximum $\delta$ was reached, the neutral beam power was increased by 1.25 MW to demonstrate the improved MHD stability. Compared with discharges with $\delta_{top} = 0$, the maximum $\beta_N$, limited by neoclassical tearing modes (NTM), could be increased from about 2.4 to 2.6. In the discharge of Fig. 5.2 the high-performance phase was, however, terminated at a slightly lower $\beta_N$, this probably being induced by an unintentional drop of the toroidal magnetic field. In conjunction with the triangularity and the corresponding energy increase, a reduction of the ELM frequency can be observed, suggesting the edge stability is also improved. In summary, this results in the highest fusion product, $n_{D,0}T_{i,0}\tau_E = 0.9\times10^{20} keV s m^{-3}$, and the highest simultaneously achieved values of $H_{ITER89-P} = 3.0$ and $\beta_N = 2.4$ so far observed in ASDEX Upgrade.

## 5.2 Response of Internal Transport Barriers to Central Electron Heating and Current Drive

Internal transport barriers (ITBs) have hitherto been successfully attained in two extreme regimes, either with strong ion heating mostly by neutral beam injection (NBI), resulting in $T_i > T_e$, or with pure electron heating and relatively cold ions. In the first case the growth rate of ion temperature gradient (ITG) driven modes, which are considered to be responsible

for the anomalous transport in discharges with strong additional heating, are expected to be smaller than for $T_e \approx T_i$ and therefore these modes should be stabilized by rotational shear, supplied for instance by NBI. In the DIII-D tokamak, degradation of both ion and electron energy confinement has been observed, following the onset of central electron cyclotron heating (ECRH) in ITB plasmas established by ion heating through NBI. Concerning the predicted destabilization of ITG modes by increasing the ratio $T_e/T_i$, this issue has to be viewed as very critical for the prospects of a reactor based on ITB regimes. On ASDEX Upgrade central electron cyclotron heating or current drive (ECCD) was applied during neutral beam heated discharges with controlled current ramp to achieve ITBs in combination with negative central shear. In contrast to the results from DIII-D, the ion and electron confinement appears to be unaffected by the increase of $T_e/T_i$. Due to the high power density of ECRH, a central $T_e \approx T_i \geq 10$ keV could be reached with an ECRH to NBI power ratio of only 0.25.

Internal transport barriers with negative central shear are established by 5 MW of NBI in the current ramp-up phase, in order to reduce current diffusion. To avoid a transition from an L- to H-mode edge the discharges are in contact with the inner wall at the high-field side of the plasma. The ECRH gyrotrons operate at 140 GHz, requiring a toroidal magnetic field of 2.5 T for central power deposition. In the discharges presented, three gyrotrons were used to launch an ECRH power of 1.2 MW in the second-harmonic X-mode. In the ASDEX Upgrade ECRH system movable mirrors allow the poloidal and toroidal launch angles of the focused ECRH waves to be changed on a shot-to-shot basis. By varying the toroidal injection angle, in addition to electron heating, it is possible to achieve co- and counter current drive.

Starting from the reproducible regime of operation using NBI only to establish strong $T_i$ gradients combined with an L-mode edge, we added ECRH power using different launch configurations at a later phase of the discharge.

In Fig. 5.3 the time evolution of the central and minimum q-values and of the central $T_i$ and $T_e$ of three types of discharges are compared. NBI starts at $\approx 0.3$ s. The reference case with NBI alone shows strong negative central shear in the initial phase of the discharge, finally reaching values of $q_{min} \approx 1.5$ and $q_0$ above 2. A central temperature of approximately 10 keV is only observed in the ions. Since the neutral beams predominantly heat the ions and, in addition, the heating of the electrons through the ions at low densities is rather low, improved electron core confinement would not result in high electron temperatures. The sharp drop of $T_i$ observed at 0.67 s when $q_{min}$ reaches 2 is caused by a (2,1) double tearing mode (DTM) mode. However, following the drop of $q_{min}$ below 2 the core temperatures again recover, exceeding their previous levels. When counter-ECCD is added at 0.7 s, not only $T_i$, but also $T_e$ reaches central values of 10 keV. The temperature profiles show gradients of $T_e$ exceeding those of $T_i$, which is confirmed by Thomson scattering measurements (Fig. 5.5). As central ECRH does not permit ECE measurements inside $\rho_{tor} = 0.2$ and the Thomson scattering system cannot in principle reach the plasma centre in the configurations discussed here, the innermost $T_e$ measurement is located at $\rho_{tor} = 0.2$. However, the flattening of the $T_e$ profile indicates that the true central value does not lie much above that. The fast, sawtooth-like events observed on the core $T_e$ measurements are attributed to a (2,1) ideal mode, which may also be responsible for the disruptive termination of the discharge. The abrupt increase of the last $T_i$ point before the disruption coincides with the trip of two of the three gyrotrons and a $T_e$ gradient reaching an unstable value. Due to the limited time resolution of the $T_i$ measurement, the causality of this event remains unclear. The q-profiles of the NBI only and counter-ECCD cases are not very different, both showing freezing of the negative central shear after 0.8 s. For co-ECCD the behaviour is different. The central co-current drive leads to accelerated decay of the negative shear resulting in a monotonic q-profile at about 1.05 s. As the toroidal magnetic field had to be matched to the requirement of central ECRH power deposition, the early appearance of a (2,1) DTM could not be avoided. However, for NBI only and counter-ECCD the mode again disappeared due to the stabilizing effects of the decoupling of the resonant surfaces and, for counter-ECCD, of the increased pressure in the negative shear region. The latter mechanism is caused by the combined effects of bootstrap current reduction in the island and negative magnetic shear, which is the inverse process to the destabilization of NTMs in positive shear regimes. Figure 5.5 shows that the maximum of the temperature gradients are in fact located at the inner q = 2 surface in the negative shear region, while at the outer one the pressure gradient is comparatively small. In contrast, co-ECCD results in a transition of the DTM in a (2,1) and (3,1) tearing-like MHD activity which prevents recovery of the confinement, resulting in relatively low central temperatures of $T_e \approx T_i \leq 6$ keV.

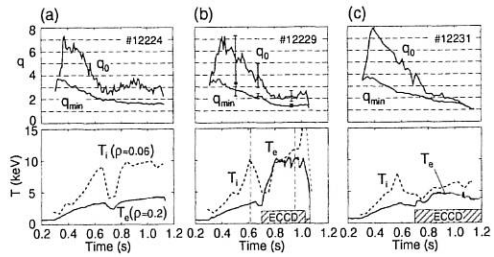


*FIG. 5.3: Comparison of three types of discharges: (a) Reference case with NBI only, (b) combination of NBI and counter-ECCD, and (c) NBI and co-ECCD. q-values are inferred from equilibrium reconstructions with the CLISTE code and measurements with the 10-channel MSE polarimeter, and the central electron and ion temperatures ($T_e$, $T_i$) from electron cyclotron emission (ECE) and CXRS, respectively. The time points for the profiles in Figs. 5.4 and 5.5 are indicated by vertical lines in (b).*

The energy transport is analyzed with the 1–1/2–dimensional ASTRA code. The electron and ion thermal conductivities are derived from the experimentally determined profiles of $T_e$ and $T_i$, $n_e$, and $Z_{eff}$ and models for the power deposition of NBI and ECRH. Ray-tracing calculations with the TORAY code show an ECRH deposition within $\rho_{tor} = 0.2$. Measured $T_e$ and $n_e$ at 0.9 s of co- and counter-current drive discharges are used (12231 and 12229 in Fig. 5.3, respectively) to determine

the power and current density distributions. For the time dependence of the current density driven by ECCD

$$j_{ECCD}\left[MA/m^{-2}\right] =$$

$$\pm 0.52 \times P_{ECRH}\left[MW/m^{-3}\right]\frac{T_e[keV]}{n_e[10^{19}m^{-3}]}$$

is assumed, with the scaling factor of 0.52 inferred from the TORAY results. Since $T_e \approx 5$ keV is much lower in the co- than in the counter-ECCD discharge ($T_e \approx 10$ keV), the resulting current driven in the co-direction (+88 kA) is also only about half of that in the counter-direction (–174 kA). These currents represent stationary values, which are only reached in a resistive equilibrium.

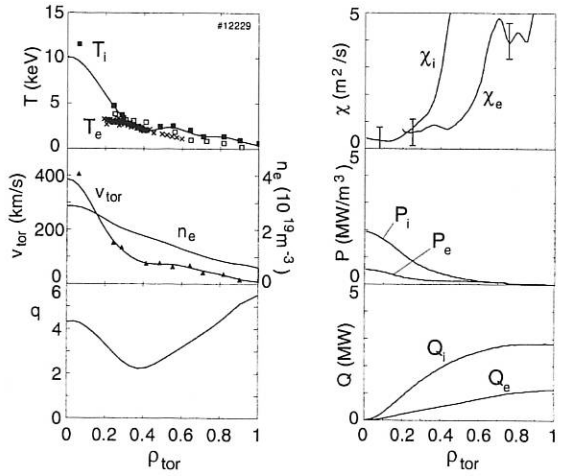


*FIG. 5.4: Discharge 12229 at 0.62 s* **before** *ECRH has been switched on. q derived from 10–channel MSE polarimeter using CLISTE, thermal heat conductivities $\chi_{i,e}$, power deposition $P_{i,e}$, and total heat flux $Q_{i,e}$ as calculated by ASTRA.*

To study the effect of electron heating in discharge 12229, the energy transport is evaluated before the onset of the (2,1) mode at 0.62 s and after the ECRH power has been switched on at 0.95 s, when $q_{min}$ has already dropped below 2. The results are shown in Figs. 5.4 and 5.5. Comparison of the two time points shows, the ion temperature profiles to be similar, with an ITB just inside the region of $q = q_{min}$. In contrast, after is switched on the ECRH the central $T_e$ more than doubles in the centre, developing a high-gradient region at $\rho_{tor} \approx 0.2$. In the plasma centre, neither the ion nor the electron thermal conductivity changes significantly. The heat conductivities show $\chi_i \leq \chi_e$, where $\chi_i$ is close to neoclassical values and $\chi_e \leq 1$ m$^2$/s. In the outer plasma regions a drop of both can be observed. This means that the confinement properties do not deteriorate, despite the strong increase of the power going into the electrons. Initially, the plasma is dominated by ion heating due to NBI, with only a small fraction of the power going into the electrons, while with ECRH electron heating even exceeds ion heating at $\rho_{tor} \leq 0.2$. In terms of heat fluxes at $\rho_{tor} = 0.2$, $Q_e$ rises by a factor of five from 0.21 to 1.20 MW, and $Q_i$ from 0.88 to 1.03 MW, the latter being mainly due to the change of the heat flux from NBI into the ions ($Q_{i,NBI}$) which increases with rising electron temperature. This reduced collisional energy transfer from the beam ions to the electrons may also be responsible for the slight $T_i$ increase observed at 0.95 s. The line-integrated density rises from 2 to $3\times10^{19}$ m$^{-3}$, which is attributed to the gas coming from the plasma limiting wall and also corresponds to an increase of the density peaking. The central toroidal rotational velocity is somewhat lower at 0.95 s than at 0.62 s. However, comparison with reference discharge 12224 shows that it finally reaches the level observed in 12224, which is close to the peak value before the appearance of the (2,1) DTM.

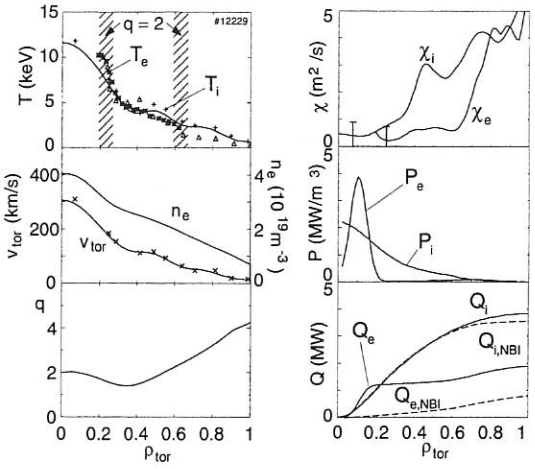


*FIG. 5.5: Discharge 12229 at 0.95 s* **after** *ECRH has been switched on: In addition to the total heat fluxes shown in Fig. 5.4, the contributions from the NBI heating separated into electrons and ions is indicated ($Q_{iNBI,eNBI}$). For discussion of the MHD stability the locations of the q=2 surfaces in the negative and positive shear regions are indicated in the temperature plot.*

## 6. MHD PHENOMENA IN REVERSED SHEAR SCENARIOS

Flat and reversed $q$-profiles allow formation of internal transport barriers and thus large pressure gradients since they permit access to second stability with respect to ideal $n \rightarrow \infty$ ballooning modes. Reversed magnetic shear gives rise to additional MHD instabilities, unknown in conventional scenarios. Whereas in tokamaks, single tearing modes are expected to be stable, resistive double tearing modes appear if a pair of rational surfaces with the same $q$-value are close to each other. Large pressure gradients in the weak magnetic shear region drive low-$n$ ballooning modes, so-called infernal modes. Resistive interchange modes can also be driven by a pressure gradient in the negative magnetic shear region. The large pressure gradient at the plasma edge, together with the resulting bootstrap current, drives external kink modes unstable, especially in H-mode discharges. Most of these instabilities have been observed in ASDEX Upgrade reversed-shear discharges. Besides limiting the normalized plasma pressure achievable in conventional scenarios, MHD instabilities might be helpful for achieving quasi-stationary discharge conditions. As already observed in improved confinement discharges with flat shear, fishbones are able to clamp the current profile locally without any con-

finement degradation, even in discharges with the minimum $q$-value ($q_{min}$) above one.

## 6.1 Double Tearing Modes (DTM)

Figure 6.1 shows the time development of the $q$-value on axis and of the minimum q-value for an ASDEX Upgrade reversed-shear discharge. When the minimal $q$-value approaches two, the onset of $(m, n) = (2, 1)$ MHD activity is observed. It starts as fishbone activity, but at about 0.68 s a continuous mode appears. Whereas the fishbone activity does not cause any confinement degradation, as soon as the continuous mode activity sets in, the ion transport barrier breaks down, and the electron temperature decreases as well (Fig. 6.2). During the mode activity, the current profile is clamped, at least in the vicinity of $q_{min}$. The end of the (2,1) activity coincides with a sudden drop of $q_{min}$ well below two. According to stability analyses using the resistive MHD code CASTOR, the most unstable mode during this time is a double tearing mode. As shown in Fig. 6.3, the calculated eigenfunction of this mode agrees well with that measured by electron cyclotron emission (ECE). The eigenfunction has two phase jumps, as expected for a DTM, and a phase shift of $180^o$ between the coupled islands. To explain the time development of the $q$-

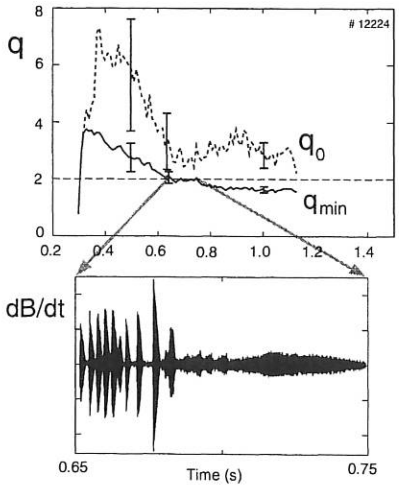


*FIG. 6.1: The time development of the q-value on axis ($q_0$) and the minimum q-value ($q_{min}$) are given for ASDEX Upgrade discharge #12224. During the time in which $q_{min}$ is about 2, the (2,1) activity measured by Mirnov coils is shown. Between 0.65 and 0.68 s, (2,1) fishbones are observed, whereas afterwards a (2,1) continuous mode appears.*

profile, non linear simulations were performed in cylindrical geometry using the TM code. It was shown that the coupled islands are able to flatten the current profile in between the two rational surfaces. This may explain the local clamping of the current profile during the time of the (2,1) DTM activity. About 70 ms after the onset of the (2,1) mode, the mode suddenly disappears, followed by a jump of $q_{min}$ from 2 to about 1.7. This is probably caused by the decoupling of the two tearing modes. Although the minimum $q$-value does not change during the time of (2,1) mode activity, global current diffusion lowers the $q$-values everywhere else, resulting in an increasing distance between the two $q = 2$ surfaces. The growth rate of the DTM,

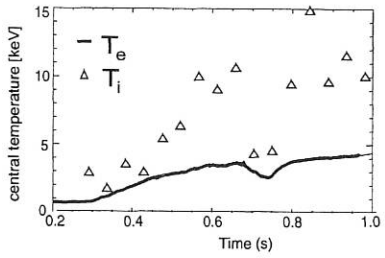


*FIG. 6.2: Central electron ($T_e$) and ion temperature ($T_i$) for the same discharge as in Fig. 6.1, measured by ECE and charge exchange spectroscopy, respectively. The breakdown of the ion transport barrier and decreased $T_e$ during the (2,1) continuous mode are clearly seen.*

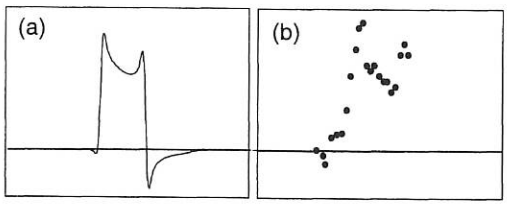


*FIG. 6.3: Eigenfunction of the (2,1) double tearing mode, resulting from the stability analysis (a) compared with that measured by ECE (b).*

however, strongly depends on the distance between the two rational surfaces. This dependence becomes even stronger if the differential rotation of the two rational surfaces is taken into account. Additional electron heating significantly changes the MHD stability of the discharges considered. With central electron heating applied, the DTM either does not appear if the electron heating is provided before the expected onset of the DTM, or disappears as soon as the ECRH is switched on. In Fig. 6.4, the time evolution of the central electron temperature is given for the discharge discussed above in comparison with a discharge with ECRH applied after the onset of the DTM. A few milliseconds after the ECRH has been switched on the electron temperature strongly rises, this being accompanied by the disappearance of the DTM. A tentative explanation for this

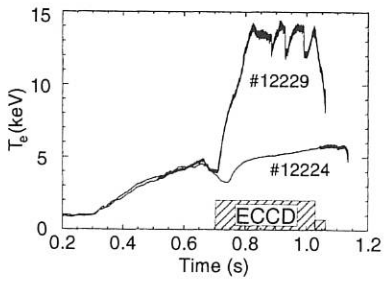


*FIG. 6.4: Time development of the central electron temperature measured by ECE for a discharge with pure NBI heating (#12224) and one with combined NBI and ECRH (#12229).*

effect could be the increased pressure gradient at the inner $q = 2$ surface, giving rise – in contrast to the dynamics leading to the neoclassical tearing modes in positive-shear regions – to stabilization of the mode due to the combined effect of bootstrap current reduction in the island and of the negative magnetic shear.

## 6.2 Ideal Modes

Sudden drops of the electron temperature during a discharge with combined NBI and EC heating (Fig. 6.4) indicate the presence of an additional MHD instability. This mode is again a (2,1) mode but grows on a much faster time scale and obviously does not always destroy the internal transport barrier. The evolution of the central electron temperature seems to be similar to that of a sawtoothing discharge with (2,1) instead of (1,1) mode activity limiting the peaking of the temperature profile. According to the stability analysis, this mode is a (2,1) infernal mode driven by the pressure gradient in the weak magnetic shear region. Even without additional electron heating, ideal modes often appear in reversed-shear discharges, primarily causing disruptions. Characteristic of the $q$-profiles just before the disruption is a low-order rational $q$-value at the plasma edge, e.g. for the discharge shown in Fig. 6.1 $q_a \approx 4$. It is obvious that this rational $q$-value at the plasma edge allows coupling of the (2,1) infernal mode to an external (4,1) kink mode. As shown in Fig. 6.5, the eigenfunction resulting from the stability analysis agrees well with the eigenfunction derived from the ECE measurements. The resulting mode is very global, which explains its disruptive character.

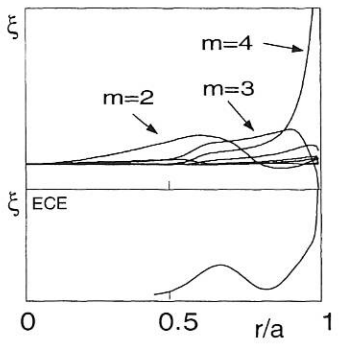


*FIG. 6.5: Calculated and measured (ECE) eigenfunctions for the mode activity right before the disruption in #12224. The mode has a large amplitude at the plasma edge, indicating coupling of the (2,1) infernal mode to the (4,1) external kink.*

## 6.3 Neoclassical Tearing Modes

In discharges with $q_{min} < 1.5$ the maximum achievable $\beta_N$ value is limited by the onset of neoclassical tearing modes (NTMs). In the improved confinement discharges with flat shear (in H-mode) we again find the scaling law for collisionless plasmas $\beta_N = c_1 \rho^*$, but the constant $c_1$ is smaller than that in conventional-scenario discharges. The stabilizing effect of triangularity increases the achievable $\beta_N$ values by about 10 %.

## 6.4 Optimized q-profiles

The MHD instabilities described above appear to be due to the occurrence of two low-order rational surfaces of the same helicity (DTMs) or to a large pressure gradient within a weak-shear region (infernal modes). An optimized $q$-profile with respect to stability of core-localized modes therefore has to avoid double rational surfaces. The shear at the low-order rational surfaces should be as large as possible, especially in regions with large pressure gradients. Furthermore, in order to avoid the occurrence of neoclassical tearing modes, $q_{min}$ should be larger than 1.5 and the pressure gradient at the $q = 2$ surface should be small.

# 7. STABILIZATION OF NEOCLASSICAL TEARING MODES

The studies of stabilization of Neoclassical Tearing Modes (NTM) by Electron Cyclotron Current Drive (ECCD) were continued. Here, the aim is to reduce or completely remove the magnetic islands associated with an NTM and thus increase the maximum $\beta$ achievable in steady state.

## 7.1 Experimental Results

Experiments were performed in lower single-null ELMy H-mode discharges with a typical density of $\bar{n}_e \approx 5 - 6 \times 10^{19}$ m$^{-3}$, a range in which a (3,2) NTM is usually triggered at $\beta_N \approx 2.2 - 2.5$ with 7.5-10 MW of NBI heating. A typical plasma current was 800 kA and $B_t = 2.1$ T, so that $q_a \approx 4$. We injected 2$^{nd}$ harmonic X-mode at 140 GHz, so that the EC resonance was on the high-field side. As a result of last year's

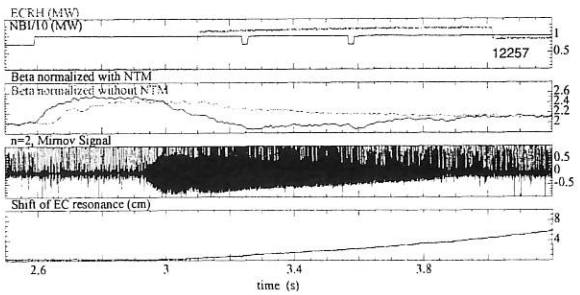


*FIG. 7.1: Complete stabilization of an NTM with ECCD.*

finding that modulated injection was not more effective than DC injection, we only focused on the DC scheme. In addition, the stabilization scheme had been found to be very sensitive to the radial positioning of the ECCD power, making reproducible experiments rather difficult. This was overcome by using slow scans of $B_t$ and hence of the deposition position. Typically $B_t$ was scanned by about 5 % in 1.5 s, so that the deposition radius changed by 8 cm during this time. This corresponds to the saturated island width and to double the estimated deposition profile width. The typical time scale for mode growth

is of the order of 100 ms, so that the scan is performed on a much slower time scale. The initial deposition was at $r > r_{res}$, where $r_{res}$ denotes the radius of the resonant surface, and then the EC resonance position was moved across $r_{res}$. The ECCD power deposited inside the island was thus effectively increased more or less linearly. Figure 7.1 shows such an experiment. It can be seen that full stabilization is achieved on the slow time scale of the deposition scan. Note that the scale for the ECCD power is 10 times that of the NBI power, so that the injected ECCD power of 1.2 MW amounted to only $\approx$10 % of the total heating power. ECCD is thus a very efficient tool to stabilize NTMs. The driven current was estimated to be between 12 and 17 kA, and so it is to roughly 2 % of the total plasma current. In Fig. 7.1, it can be seen that $\beta$ recovers during stabilization of the mode. However, it does not reach the value before mode onset. This is mainly due to a hitherto unresolved decrease of $\tau_E$ during ECRH in these discharges, which might be connected with the observation that with ECRH in these discharges the density profile changes, leading to a lower $\bar{n}_e$ and a consequent increase of the gas puff. However, $\beta$ regains the value obtained in discharges with ECRH, but without NTM: the $\beta$-trace of such a discharge is shown for comparison in Fig. 7.1, too. An interesting question is if the stabilization is due to the ECCD current driven directly by the wave or to a current driven by the local change of resistivity due to ECRH. By reversing the ECCD toroidal injection angle, so that now a ctr-current is driven with respect to $I_p$, only small variations in mode amplitude could be detected. It could thus be concluded that the effect of ECCD is at least of the same order as that of ECRH, which will always lead to stabilization, irrespective of the injection angle. Further details are given in the section of IPF, Stuttgart University. Figure 7.2 shows further details

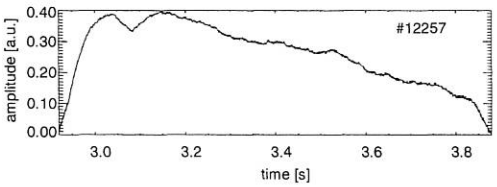


*FIG. 7.2: Temporal evolution of the mode amplitude.*

of the mode stabilization process. Plotted is the temporal evolution of the square root of the envelope of a combination of magnetic pick-up coils sensitive to even toroidal mode numbers. This should be proportional to the island width $W$ of the NTM. The signal was smoothed to remove the $n = 0$ component due to ELMs and integrated to exclude variations due to variation of the mode frequency. It can be seen that, after onset of ECCD at 3.1 s, there is an almost linear decrease of the island width until at $W/W_{max} \approx 0.25$ the time scale changes and the island suddenly decays on a much faster time scale. Our interpretation is that in the first phase we see the linear increase of the ECCD current within the island due to the scan of $B_t$ until the mode has reached such a small amplitude that $W$ drops below the seed island width. The plasma then no longer supports the magnetic perturbation, and the stabilizing terms that led to the existence of such a threshold island size rapidly drive $W$ to zero. From ECE measurements it can be estimated that $W_{max} \approx 8$ cm, so that $W_{seed} \approx 2$ cm is inferred. Furthermore, these experiments can address the question of how precise the positioning of the ECCD deposition has to be. This is studied in discharges with lower ECCD power where only partial stabilization occurs. Figure 7.3 shows such a discharge

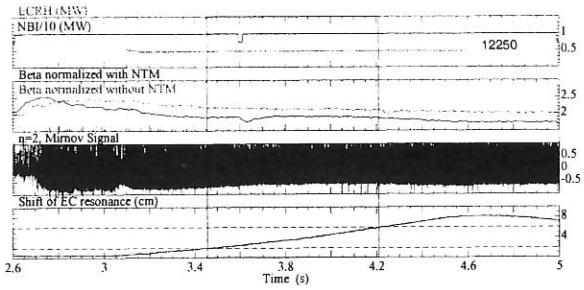


*FIG. 7.3: Positioning requirements deduced from an experiment with low ECCD power and partial stabilization.*

with an ECCD power of only 400 kW. The shaded region indicates the time during which there is a noticeable effect of ECCD on the mode amplitude as manifested by constant $\beta$ and decreasing or constant mode amplitude. In contrast, the drop of the mode amplitude in the time interval preceding the shaded region coincides with the drop in $\beta$ due to the mode. The time interval can be related to a spatial region of 4 cm in which ECCD is effective. This roughly corresponds to the deposition width, so that the required precision in positioning for stabilization can be estimated to be of the order of the deposition width. This cannot generally be achieved in ASDEX Upgrade without a $B_t$ scan. However, this method is much too slow to be used in a feedback control algorithm (and even impossible in a future reactor-size machine with superconducting coils). It follows that means of feedback control by either frequency tuning of the gyrotron or fast variation of the poloidal launch angle have to be explored if this method is to be regarded as a serious candidate for mode stabilization in future machines. The ASDEX Upgrade ECRH system will therefore be changed during the next few years to match these requirements. (At present, the gyrotrons operate at fixed frequency and the injection mirror that determines the launch angle is moveable only on a slow (several seconds) time scale.)

## 7.2 Modelling of Experimental Results

In order to extrapolate the experimental results presented above, they are compared with those of a model describing stabilization by ECCD. Here $j_{ECCD}(r,t)$ is calculated by a quasilinear Fokker-Planck code. This is taken as input to a cylindrical, nonlinear tearing mode code that takes into account the equilibration of the current density and the heat flux on flux surfaces. It is thus possible to model the effect of finite parallel heat conductivity. In addition, the bootstrap drive of the neoclassical island is incorporated into Ohm's law via realistic pressure profiles. The temporal evolution can thus be modelled, as in the example shown in Fig. 7.4. It can be seen that stabilization indeed occurs on the time scale of the deposition scan. It should be pointed out that the only free parameter used in the code is the initial current profile chosen to obtain the correct island

width. The model can thus be used to extrapolate to future machines such as ITER. This is done in collaboration with CEA Cadarache. In addition, Fig. 7.4 also shows that the two time

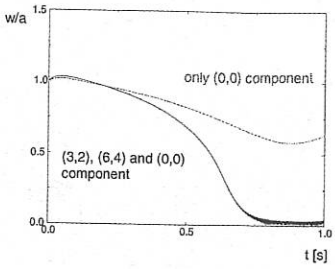


*FIG. 7.4: Modelled temporal evolution of (3, 2) amplitude.*

scales in the stabilization process that were observed in the experiment (see Fig. 7.2) are also seen in the modelling. As mentioned above, to date the seed island width is given by the ratio of the parallel-to-perpendicular heat conductivities. In the future, this will be extended to include also the polarization current. The interpretation of stabilization experiments may then in fact offer a new possibility of understanding the seed island physics.

## 8. INCREASE OF TRIANGULARITY: GOOD CONFINEMENT AT HIGH DENSITY

Variations of the triangularity was one of the key issues of the 1999 campaign. Figure 2.1 shows the equilibria which were run. The maximal value of $\delta$ is 0.36, which is about twice the old standard value. The figure shows that high bottom triangularities (c,d) had to be run with the outer strike point on the roof baffle, which resulted in a reduced compression rate for the neutral flux and reduced pumping so that the densities of steady-state phases were above 0.7 times the Greenwald density. A taller configuration with $\delta = 0.28$ and both strike points in the divertor (b) was developed later to obtain lower densities. For all equilibria the major radius $R$ and $\kappa$ were kept constant within a few per cent, but the minor radius $a$ is about 10 % larger for configurations (c) and (d) compared to (a) and (b).

### 8.1 Confinement and Density Limit

As reported earlier, increasing density in general reduces confinement in ASDEX Upgrade. An ordering parameter to describe the reduction with respect to the ITER scalings is the ratio $\bar{n}_e/\bar{n}_e^{GW}$, where $\bar{n}_e^{GW}$ is the Greenwald density. Figure 8.1a) shows the confinement data for configurations a) to d) versus the ratio $\bar{n}_e/\bar{n}_e^{GW}$. Data were taken only from stationary phases or weak density ramps with NBI heating up to 15 MW. For a given density, the confinement is better if $\delta$ is higher. It should be noted that we achieved good H-factors (viz. $\geq 1$) above the Greenwald density, which is very important for a next-step device. Nevertheless, the confinement degrades for all triangularities as the density increases. The upper limit to the

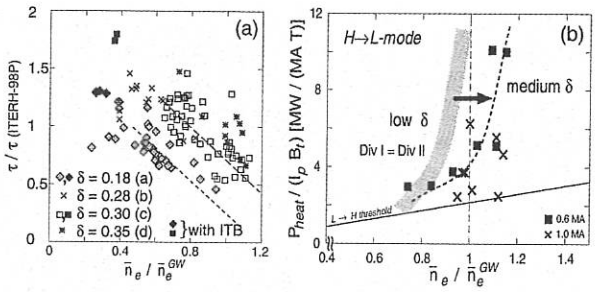


*FIG. 8.1: a): H-factor relative to the ITERH-98P scaling vs. normalized $\bar{n}_e$. Letters in brackets behind the $\delta$ values correspond to the equilibria of Fig. 2.1. Dashed lines are explained in the text. b): H→L transition at high density for two values of $\delta$: The grey-shaded area corresponds to the standard low-$\delta$ configuration Fig.2.1a) ($\delta \approx 0.18$). All data points refer to the configuration of Fig. 2.1c) ($\delta \approx 0.3$).*

density range shown in Fig. 8.1a) is the H→L back-transition, which occurs close to the Greenwald density. Figure 8.1b) shows that the increase of $\delta$ from 0.2 to about 0.3 leads to a gain in density operational space of up to 20 %. The inclined solid line corresponds to the conventional H-mode threshold power scaling $P_{thresh} \propto \bar{n}_e B_t$. The figure also shows that the experimental density limit is nearly independent of the heating power supporting the Greenwald scaling dependence. The data

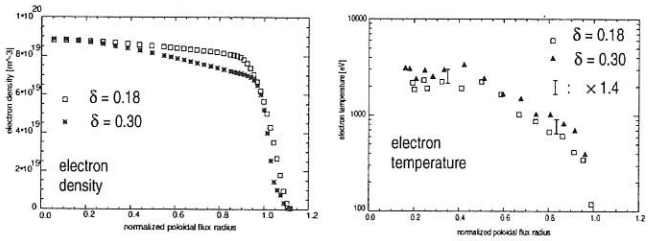


*FIG. 8.2: Comparison of $n_e$ profiles (linear) and $T_e$ profiles (logarithmic) of discharges with $\delta = 0.18$ (#11746, 3.75 s) and $\delta = 0.30$ (#11783, 4.22 s). The bar in the $T_e$ plot corresponds to a constant ratio of 1.4 as determined from the $W_{mhd}$ ratio. In both cases: $I_p = 1\ MA$, $q_{95} = 4$, $P_{NBI} = 5\ MW$.*

base used for Fig. 8.1a) contains only Deuterium discharges. $q_{95}$ is centred around 4, varying mainly between 3 and 6, so that there is also an overlap in $B_t$. The most frequent plasma current is 1 MA (additionally 0.8 MA and 1.2 MA for $\delta = 0.18$ and 0.6 MA for $\delta = 0.30$). The dashed lines in Fig. 8.1a) indicate the confinement reduction with density. The slopes of the confinement degradation are very similar to recent JET results and quantitative agreement is good for $\delta = 0.18$, but the improvement of confinement with increasing $\delta$ is larger for ASDEX Upgrade.

Figure 8.2 shows the $T_e$ and $n_e$ profiles for two discharges with different $\delta$ but similar $\bar{n}_e$. (The $T_i$ profiles match the $T_e$ profiles for this density within the experimental error.) The temperature

profiles are self-similar, as can be seen by the roughly constant shift on the logarithmic plot. The factor corresponding to this shift is in good agreement with the ratio of the stored energies, which is 1.4, corresponding to the vertical bars in Fig. 8.2. Earlier, it had already been observed that such T-profile similarity is a common feature of the low-$\delta$ H-modes, which led to the conclusion that the plasma energy content is determined by the pedestal pressure and shape of the density profile. In fact, the confinement degradation with increasing $\bar{n}_e$ was explained by an increasing ratio $n_e^{ped}/n_e(0)$ and a constant or even decreasing pedestal pressure. This behaviour is also found for higher values of $\delta$. As T-profile similarity seems to be independent of $\delta$, the beneficial effect of $\delta$ in Fig. 8.2 mainly originates from a higher pedestal pressure and, to a lesser extent, slightly higher density peaking .

## 8.2 H-mode Pedestal Shape

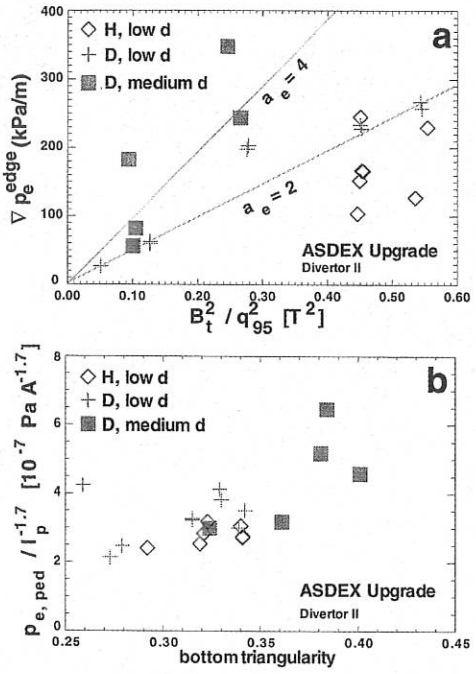


*FIG. 8.3: Stability limits: a) Edge pressure gradient vs. $B_t^2/q_{95}^2$, and b) normalized pedestal pressure vs. $\delta_{bot}$.*

As discussed above, the triangularity modifies the pressure on top of the pedestal. To understand this, it is necessary to measure the profiles in the steep gradient region very precisely. With edge Thomson scattering and radial plasma movements the spatial resolution of the $T_e$ profiles reaches the millimetre range. Further inside, they are continued with the ECE data. Density profiles are obtained from a deconvolution of local Lithium-beam data and several DCN interferometry channels. These profiles are fitted with a 5 parameter function based on a hyperbolic tangent. Figure 8.3 shows the results for the maximum gradient and the pedestal value of the electron pressure. Increasing $\delta$ increases the pressure gradient, which for constant $\delta$ seems to follow a line of constant $\alpha = -2\mu_0 R(B_t^2/q^2)dp/dr$, the critical normalized pressure gradient from ideal ballooning theory. In accordance with Fig. 8.2 the pressure on top of the pedestal increases with bottom triangularity. Note that the pressure is normalized to the $I_p$ dependence observed at low $\delta$ and that the top triangularity assumes only two discrete values due to feedback control. Another interesting question in this context is the scaling of the pedestal width. For the low-$\delta$ case, the width is almost unchanged for all type-I H-modes. For increased $\delta$ the width seems to increase with density, but the scatter in the high-resolution edge data is still too large to deduce a scaling and this remains as an important issue for the next campaign.

## 8.3 Influence of the Neutral Flux

It was checked that the scatter observed within the $\delta = 0.3$ data of Fig. 8.1a) is not due to variations in $I_p$, $B_t$, or $q_{95}$. One reason for this scatter are oscillations of the neutral gas flux outside the plasma $\Gamma_0$, which is closely related to the average density in the scrape-off layer ($\bar{n}_e^{(SOL)}$). These oscillations occur since the discharges were run in $\bar{n}_e$ feedback mode so that phases with increasing and decreasing $\bar{n}_e$ and corresponding changes in the density peaking follow each other during a nominally constant density phase. These oscillations are especially strong for the increased-$\delta$ cases since the density feedback loop was not adapted to the longer time constants due to the reduced pumping. To account for the effects of $\bar{n}_e^{(SOL)}$ and of $\delta$, a new scaling of the confinement time was proposed which uses the engineering parameter $n_{e,sol}^{D_\alpha}$ in contrast to the $\bar{n}_e$ usually used:

$$\tau_E^{scale} = 0.095 (n_{e,sol}^{D_\alpha}/\bar{n}_e^{GW})^{-0.25} I_p^{0.82} P_{tot}^{-0.5} \delta^{0.13} R_{geo}^{1.5}$$

where $n_{e,sol}^{D_\alpha}$ is a SOL density deduced from a $D_\alpha$ signal, and units in MA, MW, m. The strong dependence on $\delta$ is hidden in the relation between $\bar{n}_e$ and $n_{e,sol}^{D_\alpha}$ or $\Gamma_0$. It can be expressed by a scaling for the particle confinement time which also includes the strong influence of impurities:

$$\tau_P^{scale} = 0.14 \cdot \bar{n}_e^{GW} / n_{e,sol}^{D_\alpha} a^2 (P_{tot}/R_{geo})^{-0.7} \delta^{0.6} Z_{eff}^{0.7}$$

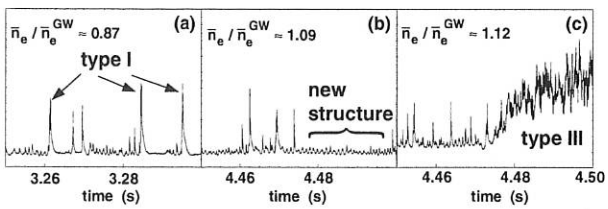


*FIG. 8.4: ELM behaviour in $D_\alpha$ at high $\delta = 0.36$.*

## 8.4 ELMs

A reduction of the type-I ELM frequency with increasing $\delta$ had been reported from other tokamaks. For lower densities, especially in comparing equilibria of Fig. 2.1a) and b), we observe in general a similar effect. Detailed interpretation

turns out to be difficult since the neutral particle flux variations described above influence the ELM frequency as well. In this density range, the energy carried by a single ELM is inversely proportional to $f_{ELM}$, i.e. the average power carried by the ELMs is roughly constant for a given input power. For higher $\delta$ and higher densities, $f_{ELM}$ is a not a well defined quantity, since bursts of smaller ELMs occur in between the common type-I ELMs and tend to prolong the period between the latter. An extreme example of this behaviour is the discharges at highest $\delta = 0.36$, which show H-factors $\geq 1$ at $1.1 \times \bar{n}_e^{GW}$. Figure 8.4 shows $D_\alpha^{div}$ traces at different densities. When the density increases (a) — b)), the type-I ELMs disappear as smaller ones come up. For the high density b) even the remaining big spikes in the $D_\alpha^{div}$ signal no longer show up in the divertor infrared thermography. This means that these H-modes not only have sufficiently good confinement above the Greenwald density, but also show a quasi-steady heat flux to the divertor, thereby combining three important goals of a reactor-relevant plasma. It should be noted that the density profile evolution with rising density appreciably differs from the lower-$\delta$ case: The profile peaks as the density increases. This does not coincide with a rise in $Z_{eff}$ (which stays at $\approx$1.7) often observed together with density peaking. The nature of the small ELMs is not yet clear. Figure 8.4c) shows a transition to a type-III ELM regime, proving that the new type is different from type III. Its connection with other H-modes with small ELMs (type II at DIII-D and JT-60U or enhanced $D_\alpha$ at Alcator C-mod) remains a topic of the next campaign.

# 9. CORE PHYSICS

## 9.1 "Non-local" Transport Studies

### 9.1.1 *Cold pulses*

A particular observation of electron transport is the so-called "non-local" transport phenomenon. It is characterized by a fast increase of the electron temperature in the plasma centre in response to edge cooling pulses. In ASDEX Upgrade, the cold pulses were produced by injection of C, Si or Fe via a repetitive laser blow-off system (LBO) or by D-gas puffs, mostly in ohmic plasmas. A rather strong enhancement of the central $T_e$ is observed as a reaction to the edge cooling which, however, appears after at least 5 ms. The results are independent of the injected species C, Si, Fe or D, indicating that the contribution of radiation does not play a role. Stronger edge cooling yields a larger enhancement in the centre. Repetitive pulses allow the use of the Fourier transform of the $T_e$ data (Fig. 9.1) to be used to extract the radial propagation of the perturbation. The inversion radius is clearly indicated at $\rho_{pol} = 0.5$, where the amplitudes of all harmonics decrease, correlated with a phase jump. The negative phase jump reflects the inversion of the pulse and is not in contradiction with causality. Except for the inversion region, the amplitude of the perturbation increases towards the centre, which is in disagreement with diffusion. As in other devices, the amplitude reversal is observed when $n_e(0)/\sqrt{T_e(0)}$ is low enough, shown by density ramps or with central ECRH. Varying $B_t$ and $I_P$ indicates that the inversion

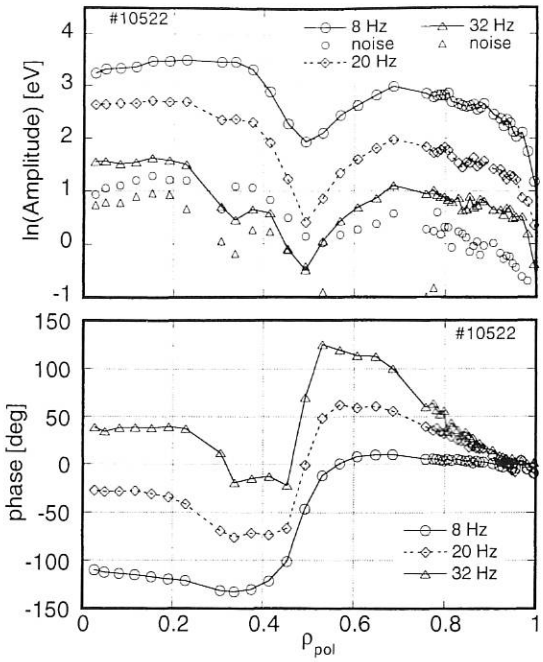


*FIG. 9.1: Fourier data for harmonics 2, 5, and 8 of Fe-LBO cold pulses showing amplitude reversal. The fundamental frequency was 4 Hz. The inversion radius of the cold pulse is clearly seen at $\rho_{pol} \approx 0.5$ on both amplitude and phase.*

radius of the cold pulse is always outside that of the sawteeth. Its position is independent of the perturbation strength, injected element, and density. Attempts to relate this behaviour to the local electron temperature or its gradient did not yield good correlation. These experiments were simulated with the IFS-PPPL model in collaboration with J. Kinsey (GA, San Diego). The calculated and experimental equilibrium temperature profiles agree. Only qualitative agreement is achieved for the pulses: the amplitude of the perturbation at the edge has to be assumed to be much stronger in the model and the response in the centre is faster. The basic effect of the model is a fast increase of the ion temperature in reaction to the edge perturbation. This would lead to a substantial increase of the neutron production rate, not observed in ASDEX Upgrade. Although the IFS-PPPL model is the only one able to reproduce amplitude reversal, several experimental observations are in disagreement with the prediction.

### 9.1.2 *Heat pulses with ECRH*

To study possible symmetry of the physics mechanism involved in the "non-local" effect of cold pulses, we applied short heat pulse (5 ms, 400 kW) at the plasma edge with ECRH in similar discharges. The ECRH absorption is close to 100 %, has a narrow width (about 5 cm) and can be varied radially with the mirror system. The comparison makes sense: the edge $T_e$ perturbation by ECRH and LBO are nearly symmetrical. However, the propagation of the ECRH pulses towards the plasma centre differs from the above description. The amplitude of the tem-

perature perturbation decreases with radius, in agreement with diffusive propagation and no amplitude reversal is observed. Instead, a delayed temperature increase is clearly visible, quite similar to that observed following the cold pulses. By varying the radial position of the ECRH deposition it could be shown that this central positive temperature reaction is not related to the original pulse but to its arrival close to the radius where inversion of the cold pulses takes place in similar discharges. Together with the absence of amplitude reversal with ECRH, this supports the assumption that the IFS-PPPL model in its present form is not able to reproduce our experiments.

## 9.2 Transport with ECRH Modulation

We have previously shown that off-axis ($\rho \approx 0.5$) ECRH causes a transport step seen in both power balance analyses ($\chi^{PB}$) and heat pulse propagation ($\chi^{HP}$). The step is located at the deposition of the ECRH, which is narrow (≈5 cm) and such that transport is low in the region between ECRH deposition and the plasma centre, but high outside this region. With two (C) of the recently available new gyrotrons we applied a constant pulse (up to 850 kW) at mid-radius to create the transport step. Launching heat waves with a modulated third gyrotron (M) depositing close to the plasma edge, we probed the radial transport. The results of the heat wave analysis are shown in Fig. 9.2. It exhibits the expected behaviour: when gyrotrons (C) are

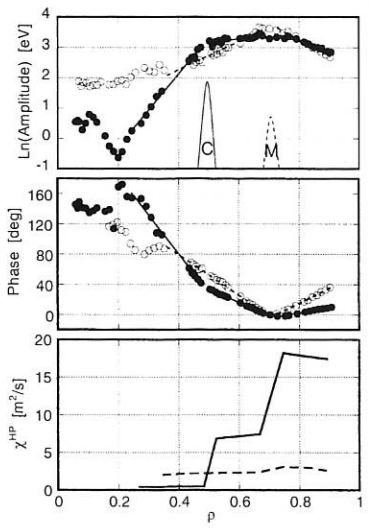


*FIG. 9.2: Amplitude and phase of the $T_e$ modulation and corresponding $\chi^{HP}$. The blank/dashed symbols/lines without gyrotrons (C), the solid ones in the presence of gyrotrons (C).*

turned on, a high transport for heat waves ($\chi^{HP} = 7-18$ m$^2/s$) is observed in the region between the edge and deposition of (C), whereas $\chi^{HP}$ is low in the region between deposition of (C) and the plasma centre. In the absence of gyrotrons (C), the propagation does not exhibit this abrupt change. Note the step at the deposition of (M), which is quite large when (C) are on. In the absence of (C), one gets $\chi^{HP}/\chi^{PB} = 1-2$. When (C) are on, $\chi^{HP}/\chi^{PB}$ reaches 5 to 10 in the region between (C) and the plasma edge, but $\chi^{HP}/\chi^{PB}$ is below 1 on the other side of the deposition of (C). The changes in transport caused by gyrotrons (C) increase with power and follow the position of the deposition. We interpret this result as a convincing indication of electron transport being determined by critical gradient physics. In fact, in the central region the heating by gyrotrons (C) flattens the temperature profile and thus drives it away from the critical gradient: transport is reduced. In the region between (C) and the edge, the temperature profile is pushed harder against the critical gradient, which is reflected in higher transport, a stiffer profile, and thus higher values of $\chi^{HP}$, $\chi^{PB}$, and $\chi^{HP}/\chi^{PB}$.

## 9.3 Beam Heating Deposition and Plasma Transport

On ASDEX Upgrade, a remarkable self-similarity of the $T_e$ and $T_i$ profiles in type-I ELMy H-mode discharges heated by neutral beams with 60 kV ($D^0$) was found over a large range of plasma parameters up to rather high densities. This so-called "profile stiffness" could be studied in more detail after upgrading the second neutral beam injector to a higher beam voltage of 93 kV. At high plasma densities ($\bar{n}_e \approx 10^{20}$ m$^{-3}$) 60 kV and 93 kV beams result in rather different beam deposition profiles. The reaction of the plasma transport to these different heating power profiles was investigated. Subsequent discharges were heated with either 60 kV or 93 kV beams at otherwise unchanged parameters with up to 7.5 MW of heating power. This was done at low and medium triangularity ($\delta = 0.15$ and 0.3) in type-I ELMy H-mode plasmas with densities of $1\times10^{20}$ m$^{-3}$ and $1.2\times10^{20}$ m$^{-3}$ respectively. Independently of triangularity, the measured temperature profiles are unaffected by the change in beam energy. An example for $T_e$ is shown in Fig. 9.3, as well as the results from power balance analysis.

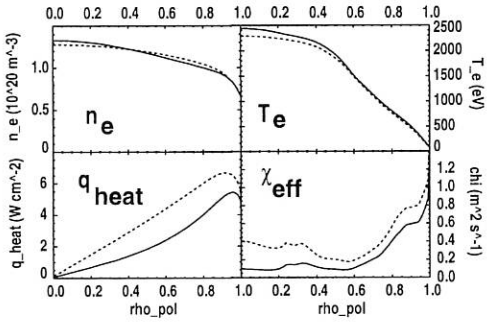


*FIG. 9.3: Profiles of $n_e$, $T_e$, heat flux, and effective heat conductivity for 5 MW NBI at 60 kV (solid lines, #11805) and 93 kV (dashed lines, #11804); 1 MA, 2 T, $\delta = 0.3$ .*

Due to the deeper beam penetration the heat flux in the core of the plasma is significantly higher for 93 kV than for 60 kV beams. At $\rho = 0.4$ the difference amounts to factor of almost 2. This leads to effective heat conductivities which are rather different: Across the whole plasma $\chi_{eff}$ for 60 kV is below the value for 93 kV beams by a factor of up to 2 despite the very similar temperature profiles in the two cases. Obviously, the heat conductivity adjusts itself to maintain the observed stiff temperature profiles. These results are independent of $\delta$. In

order to describe the above experimental results with a physics-based transport model, it is obvious that only models having a strong tendency to maintain $\nabla T/T$ will be adequate. First simulations using the IFS-PPPL model, which is based on ion temperature gradient physics, indicate rather stiff temperature profiles but are not quite able to reproduce the experimental results.

## 9.4 Transport Modeling

In recent years several theory-based transport models have become available. These models potentially lead to far more reliable extrapolation to larger devices than the empirical scalings since they are based on the underlying physics. But even if the agreement with experiment is too poor for such extrapolations, the models give a description of tokamak transport which allows discussion in terms of the parameters relevant in the theory. Potentially, comparison with experimental data will give feedback to the theory. For these reasons a comparison of ASDEX Upgrade data with the prediction of these models was started in 1999.

The transport models are mostly based on the combination of Ion Temperature Gradient (ITG) and Trapped Electron Modes (TEM). Of these models the Weiland-Nordman and the IFS-PPPL model have been used. An alternative model based on the Current Diffusive Ballooning Mode (CDBM) has also been investigated. Finally, one of the empirical models, the so-called mixed-shear model, is used for reference. A few discharges containing L- and H-mode as well as discharges with Internal Transport Barriers (ITB) have been studied. The electron and ion heat transport are modelled whereas the density profile is taken from the experiment. Neoclassical ion heat transport is added. The general trend of all models in L- and H-mode is that they give good agreement in the outer region ($\rho > 0.5$) but overpredict the transport in the central region of the discharge. The Weiland model yields the most appropriate fit to the data, whereas the CDBM model is in poor agreement with the H-mode data. In the Weiland model the E×B shear has a significant stabilizing effect on the instabilities in the H-mode, whereas it is insignificant in the L-mode.

Of particular interest is the modelling of ITB discharges. The Weiland model also gives reasonable agreement for these discharges. The high E×B shearing rate leads to the disappearance of the anomalous transport in a relatively large internal region. The ion neoclassical heat transport reasonably describes the ion temperature profile in this region, whereas the electron neoclassical heat transport is too small. This indicates that an additional instability not included in the model persists, most likely the Electron Temperature Gradient (ETG) mode. The disappearance of anomalous transport in the core region has also been studied by comparing the E×B shearing rates with the growth rates obtained from a fully kinetic dispersion relation. The shearing rate exceeded the growth rate of the most unstable mode in the central region of the discharge, and the width of this region is in reasonable agreement with the experiment. When electron heating is applied to a discharge with negative central shear and an ITB, the electron temperature was observed to increase by a factor 2 without any changes in the ion temperature. Although the electron-to-ion ratio makes the modes more unstable, it turns out that the increase of the Shafranov shift due to the increase in electron pressure can compensate for this effect. The growth rates of the most unstable mode, therefore, did not significantly change when the electron temperature was increased, and the ITG/TEM growth rate remained close to the E×B shearing rate. This explains the stationary ion temperature.

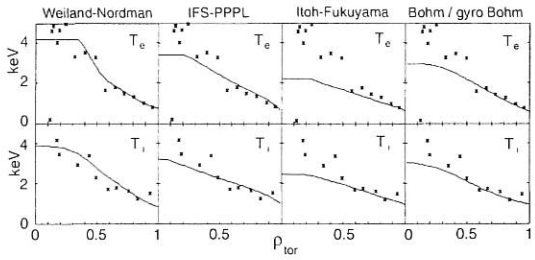


*FIG. 9.4: Simulated and measured electron and ion temperature profiles of ASDEX Upgrade shot #11127.*

## 9.5 Simulation of Gas Oscillation Experiments with New Inward Drift Scaling

Discharges with modulated neutral gas inflow were modelled by an old and a new scaling expression for the anomalous inward drift velocity $v_{in}$ by means of a special version of the 1 1/2-D BALDUR transport code. The computed phase angles between the oscillating electron density and the influx rate of Deuterium atoms were compared with DCN interferometer measurements. It was found that the new scaling $v_{in} \propto n_0$ with $n_0$ being the neutral Deuterium density, yields the observed small phase angles, whereas the old scaling independent of $n_0$ does not.

## 9.6 Scaling of the Separatrix to the Pedestal Density Ratio in H-modes

Recently, there has been increased interest in the ratio $n_{sep}/n_{ped}$, where $n_{sep}$ and $n_{ped}$ are the separatrix and pedestal densities, respectively. A semi-empirical model for this ratio was developed which puts particular emphasis on the role of edge physics. The empirical elements of the model and the detailed comparison with data rely on the extensive edge density database established at ASDEX Upgrade. The derived scaling can be cast into a form where $n_{sep}/n_{ped}$ is essentially determined by the proximity to the Greenwald limit.

## 9.7 Neoclassical Tearing Modes

The range of validity of the scaling law describing the onset conditions of neoclassical tearing modes (NTM) ($\beta_{N,crit} \propto \rho^{\star}$, for the collisionless case) was extended to smaller gyroradii by discharges with pellet injection. Fishbones were shown not only to affect the fast particle population, but also to directly influence the background plasma limiting the central peaking of the electron temperature, impurity density, and current pro-

files. Different types of fishbones have been observed when using only either the more radial or the more tangential NBI. In discharges with fast-particles provided by the more radial beams, fishbones limit the achievable $\beta$ values as soon as a critical value of the fast particle pressure is reached. If only the more tangential beam lines are used, no confinement degradation due to fishbones is observed, although the amplitude of the observed fishbones is even larger than in the radial-injection case. The ability of these strong fishbones to affect the background plasma in a similar way to sawteeth, together with their negligible effect on confinement, can help to achieve quasi-stationary discharge conditions in advanced scenarios.

Fast particles also affect NTMs. The NTM frequency often shows fast jumps to higher values followed by a frequency decrease accompanied by a (2,2) mode burst. These frequency jumps very much resemble (1,1) fishbones in the time development of the frequency and mode amplitude and therefore indicate direct interaction of fast particles and the toroidally coupled (2,2) component of the (3,2) NTM.

The effect of MHD instabilities on confinement in conventional scenarios, was summarized to develop an operational diagram in normalized space of density and heating power. The $\beta_N$ values attainable in the absence of MHD phenomena were derived by means of an empirical energy confinement scaling law for ASDEX Upgrade type-I ELMy H-mode discharges.

For high heating powers/low densities the scaling law can only be obtained with the more tangential beams (so far 10 MW available), otherwise the $\beta$ values are limited by fishbone activity. Access to the second stable regime for NTMs due to the stabilizing effect of collisionality at high densities was verified by further experiments.

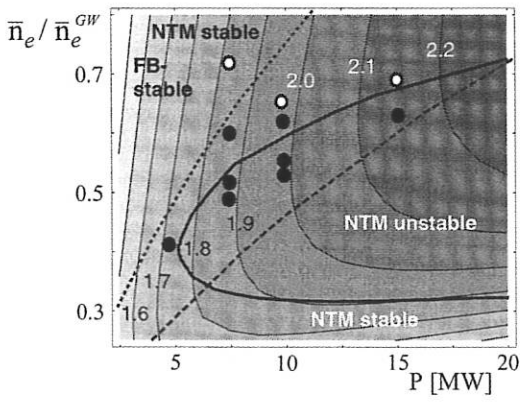


*FIG. 9.5: Operational diagram for conventional discharges with $q_{95} = 3.4$, $\delta = 0.14$, $I_P = 1$ MA. Achievable $\beta$ values according to the confinement scaling are indicated by grey scales. The NTM instability region is surrounded by a solid line. In addition, experimental data for the NTM onset (solid circles) as well as discharge conditions without NTM (blank circles) are shown. The limits for fishbone instability and the $\beta$ limit caused by fishbones in the case of radial injection are indicated by dotted and dashed lines, respectively.*

## 9.8 Observation of the High-$\beta$ Plasmoid Drift

It was shown that pellet injection from the magnetic high-field side (HFS), which is the torus inside, is preferable to low-field side (LFS) pellet injection. It was postulated that this is caused by a fast high-$\beta$ plasmoid drift which is always directed to the magnetic LFS independently of the direction of the pellet motion. This drift leads to fast particle loss for LFS pellet injection and material transport towards the plasma centre for HFS. When a pellet is injected into a hot plasma it ablates and a neutral gas cloud forms around the pellet. This ablation cloud is heated by the incoming electron heat flux parallel to the magnetic field lines. The heat flux causes ionization of the ablated material (time scale <1 $\mu$s) and a cold, dense plasmoid forms ($T_{e,pl} = 1...6$ eV, $n_{e,pl} = 1...7 \times 10^{23}$ m$^{-3}$, $r_{pl,\perp B} \sim 5$ mm). The plasmoid spreads out along the magnetic field with the ion acoustic speed of the cold plasmoid, while the electrons of the hot background plasma carry energy with their thermal velocity into the plasmoid. Strong $\beta_{pl}$ enhancement inside the plasmoid therefore takes place (typically $\beta_{pl}/\beta_0 \sim 10$). This causes a strong disturbance of the equilibrium and the diamagnetic plasmoid is accelerated out of the magnetic field to the LFS ($a_{pl} \propto T_{e,pl}/(m_i R_{pl})$ with ion mass $m_i$ and major radius position of the plasmoid $R_{pl}$). In ASDEX Upgrade an optical diagnostic with high space and time resolution was installed to observe this drift directly. At each side, LFS and HFS, the diagnostic has 10 lines of sight viewing toroidally onto the pellet path and covering a radial distance of about 15 cm. Simultaneous measurement at two wavelengths of the emitted light gives information about the plasmoid temperature and density. Additionally a spectrometer was used to determine $n_{e,pl}$ from Stark broadening. Acceleration of a sequence of discrete plasmoids to the torus outside independently of the direction of pellet injection was observed. The measured acceleration $a_{pl} \sim 10^8...10^9$ ms$^{-2}$ and velocities of up to $v_{pl} \sim 10^3...10^4$ ms$^{-1}$ agree well with theoretical expectations. From density profile measurements a material shift of about 0.1 m was determined. During the drift the plasmoid is heated (about 10 eV in 5 $\mu$s). The formation of a sequence of discrete plasmoids is correlated with the well-known **striations**. $D_\alpha$ radiation measurements in time and space show nearly periodic modulation of the radiation intensity. This is caused by modulation of the cloud density which surrounds the pellet. Detailed analysis shows that the density modulation of the ablation cloud is caused by the material removed from the high-$\beta$ plasmoid by the drift and affects the shielding of the pellet against the incoming heat flux. The ablation cloud temperature stays nearly constant during this process.

## 9.9 Improved Performance with HFS Pellet Injection

The application of HFS pellet injection allows efficient particle fuelling especially in hot target plasmas. In previous experiments density ramp-up far beyond the Greenwald limit could easily be achieved without losing typical H-mode features. However, some confinement degradation with increasing density is still faced. There are several potential limitations to performance. For example, avoiding in ASDEX Upgrade the onset of neoclassical tearing modes triggered by pellets needs operation at sufficiently high density. Since excessive confinement degradation is observed in discharges with high edge density,

sufficient pumping is essential to exhaust recycling particles. In these optimized conditions the confinement limitation is due to the occurrence of pellet-triggered ELM bursts. These ELM bursts consist of several ELMs, each stronger and longer than spontaneous ELM's. The sequence of pellet-triggered ELMs lasts typically $\approx$10 ms. In coincidence with the sequence, the plasma energy $W_{MHD}$ is observed to be reduced to an extent consistent with the assumption of thermalized pellet particles lost during the ELMs. Thus, it seems the pellet-induced ELM burst creates a particle and energy loss channel, somewhat reducing both the fuelling efficiency and the energy confinement. Whereas the particle loss is not serious, since it can easily be compensated by adapting the pellet particle flux, the additional energy losses cause a drop in confinement. With termination of the pellet train, this loss channel closes and the plasma can recover its initial energy content. Since usually the bulk particle confinement time exceeds the energy confinement time, enhanced performance can be achieved transiently while high densities are maintained and the energy has almost fully recovered. Thus, density control by injection of pellet trains causes a fuelling cycle achieving improved performance transiently but repetitively. A typical pellet fuelling sequence is shown in Fig. 9.6, where the evolution of $\bar{n}_e$ vs. $W_{MHD}$ is given and compared with a purely gas-puff-fuelled phase. Starting from conditions achieved by moderate gas puffing (1), a string of 6 pellets (P1 - P6) results in significant density enhancements (2). However, $W_{MHD}$ already drops after the 1st pellet. After termination of the pellet train (dashed arrows), $W_{MHD}$ recovers to its initial level while the pellet-induced density enhancement decays. However, $W_{MHD}$ recovers faster than the density decays, and transiently enhanced density at full inital H-mode confinement is realized (3). Optimization of the pellet fuelling cycle can be achieved by reducing the pellet flux and thus the energy loss rate to a minimum.

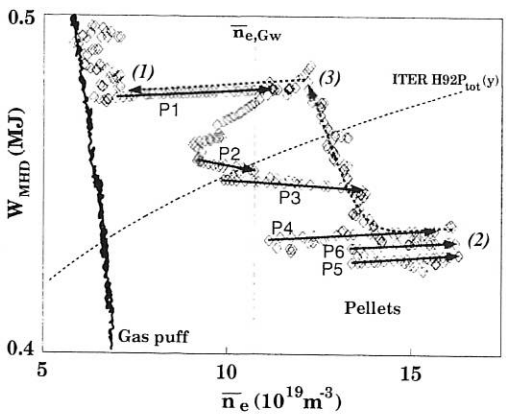


*FIG. 9.6: Evolution of a pellet fuelling sequence consisting of a string of 6 pellets.*

## 9.10 Use of a Neural Network for Prediction of Disruptions on ASDEX Upgrade

Most of the plasma disruptions in ASDEX Upgrade happen in a plasma parameter regime far from the desired operational space (H-mode, high $\beta$) and are usually announced by well-identified precursors. In this work we make use of the experience gathered in several years of operation and disruption studies to train a neural network to recognize a forthcoming disruption. An Artificial Neural Network implements a non-linear function, mapping one multidimensional space $\vec{x}$ onto another, $\vec{z}$. This function contains several parameters, which are to be determined during training. Training consists in evaluating the parameters which minimize the difference between the target output $\vec{t}$ and network output $\vec{z}$. We use a so-called feed-forward multilayer (two layers, in this work) perceptron. The $h^{th}$-component of the vector output ($h = 1, nz$) can be written as $z_h = \mathcal{F}(\sum_{i=1}^{ny} WY_{hi} y_i)$, with $y_i = \mathcal{F}(\sum_{j=1}^{nx} WX_{ij} x_j)$ and $\mathcal{F}(a) = (1 + exp(-a))^{-1}$. For training the network needs a large database of input vectors and associated outputs. The input consists of the time histories of several plasma parameters; the output of the network was chosen as the time interval up to the disruption. The database used to train and validate the network consists of shots in the range 10000 - 10800 (16398 data points from 106 shots), which ended with the disruption of a lower-single-null plasma in flat-top. Only the pre-disruption phase of these shots was selected as part of the input for the network. Several networks with different numbers of hidden neurons and different numbers of input data were trained and tested. The performance of the best network was tested off-line in the flat-top phase of 500 shots without disruption (in the shot range 10000-10850) and 36 disruptive shots (in the range 10000-11300), which were not included in training. It must be stated at this point that the performance of the neural network outside its training space is not yet reliable. Since our network was trained with only pre-disruption plasmas, the input data for the feed-forward prediction of the time-to-disruption has to be pre-processed to determine whether it belongs to the training space (novelty detection). This is now being done by modelling the unconditional distribution of the input with a histogram. The disruption alarm was defined as $\Delta t_{NN} < -50$ ms for 7.5 ms. The prediction of the disruption was defined to be correct if the disruption alarm was activated in the time interval [$t_{disr}$ − 400 ms, $t_{disr}$ − 5 ms]; a disruption alarm in shots without disruption or more than 400 ms before a disruption was considered a false alarm; a disruption was not recognized when the disruption alarm was activated too late or not at all. The results of the analysis were as follows:
(i) 97 % of the disruptions were recognized by the network, but only 78 % by our novelty detection method;
(ii) the network produced at least one false alarm in 32 of the 500 shots (6.4 %).

The present work shows that a disruption recognition system based on a neural network is feasible and relatively reliable (80 % predicted events and a few % false predictions) and encourages further development of such systems and their application. The feed-forward calculation of the output of a trained network is in fact simple and fast, making it suitable for real-time applications.

## 9.11 CLISTE Interpretive Equilibrium Code

The "Fast Mode" linear least-squares algorithm for CLISTE equilibrium interpretation, first developed towards the end of

1998, was enhanced to (i) produce confidence bands for flux surface profiles and (ii) accept MSE input data. The code was parallelized to run concurently on an arbitrary number of workstations using the Message Passing Interface for inter-processor communications. It is now running automatically after each plasma shot, delivering about 50 timepoints within 3 minutes of the FP results for the current shot being made available. Flexible current profile parametrization is desirable to fully utilize the information contained in the 10 MSE channels. To reconcile this with the need for stability and a high success rate in finding a well-converged solution to this ill-conditioned inverse problem, a lot of attention has been paid to the question of regularization. The code was recently enhanced by a dynamic regularization feature, involving both Tikhonov-like regularization (where the modulus of the solution vector is penalized) and curvature damping of the current density source profiles. The regularization parameters are progressively relaxed with progress towards convergence, but this relaxation is conditional on the solution remaining well-behaved and may be reversed. This feature has a computational price, however, since the number of iterations roughly doubles. The ultimate goal of this work is non-parametric representation of the current profile, which in the present context means spline representation with a large number of knots.

## 10. ICRH RESULTS

The experiments concentrated on two aspects:
1. Checking how the changes to the antenna affected the coupling. During the 1998 summer shutdown opening, the antennae were reconfigured to allow plasmas with higher triangularity. The consequence is that, in the equatorial plane, the antenna is 2.5 cm further from the plasma. The depth of the antenna was increased to compensate for the increase in antenna-plasma distance and avoid too large asymmetries between the two loops of the antenna. For the low-triangularity single-null plasmas (Fig. 2.1a)) the antenna coupling could be maintained, despite the increased plasma-antenna distance at the same plasma position. In the case of high triangularity, the antenna coupling is typically maintained because, for stability reasons, these plasmas are operated nearer to the antenna.
2. Influence of the location of the power depostion. At high power, the influence of the location of the power deposition was investigated by varying the position of the H-minority resonance layer in a D plasma. The application of the ICRF power strongly increases the sawtooth frequency if the H resonance layer is located on the high-field side of the plasma centre, whereas it increases this frequency only slowly if it lies on the low field side of the plasma center. Electron temperature profiles are only marginally affected. Figure 10.1 shows this variation of the sawtooth frequency as a function of the central magnetic field for an ICRF frequency of 30 MHz.

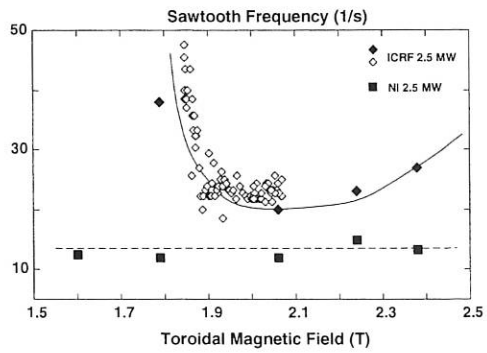


*FIG. 10.1: Variation of the sawtooth frequency with the central magnetic field. The ICRF frequency is 30 MHz. The ion cyclotron resonance position is central for B = 2 T.*

Furthermore, it was shown that ICRF could be successfully and beneficially applied quite early in the discharge: ICRF heating assisted the plasma current start-up during a period when high impurity concentration made this start-up difficult while the plasma density was still too low to use NBI.

## 11. THE ROLE OF MOLECULES IN DIVERTORS

Detached divertor plasmas are characterized by a spatial pattern of recombining and ionizing layers. $H_2$ molecules (and their isotopes) have recently been identified as important species which may influence the energy balance and ionization degree. Indeed, Molecularly Assisted Recombination (MAR) had been suggested in this context, relying on significant vibrational excitation of the electronic ground state molecules. It was speculated that, e.g. for an ITER-size machine, detachment of the divertor plasma might be achievable under upstream conditions somewhat relaxed as compared with what was predicted by the usual divertor models. The chain of reactions which played the key role in these arguments was vibrational excitation of molecules by electron impact (through resonant $H_2^-$ levels), then ion conversion, $p + H_2 \rightarrow H + H_2^+$, followed by immediate dissociative recombination, $e + H_2^+ \rightarrow H + H^*$. The excited atom decays by spontaneous emission. At the end of this chain, one electron-ion pair has recombined into an H atom, and the $H_2$ molecule has dissociated into $H + H$. The ion conversion part is resonant (comparable to resonant charge exchange between H atoms and protons) if the molecules are vibrationally excited in the $\nu = 4$ level. Under typical high-recycling divertor conditions, when molecules travel in a bath of 7-8 eV (or hotter) electrons, the molecules are destroyed before they reach such vibrational levels. Hence this chain of reactions is irrelevant there. For detached divertor plasma conditions this is not necessarily so. Inspection of the atomic database of the EIRENE code, in particular its collisional radiative models for molecules, showed that matters can be more complicated. The relaxation time for establishing a vibrational distribution of the ground-state molecule is comparable to the transport time of the molecule, hence the applicability of local collisional radiative approximations is questionable. Furthermore, one of the two atoms created in dissociative recombination is electronically excited and, hence, can be ionized very effectively even at low divertor plasma temperatures (instead of radiative decay). In this case, the whole chain of reactions would be just

enhanced ("molecularly activated") dissociation (MAD), rather than recombination (MAR). Figure 11.1 illustrates this context, taking into account the distinct dependences of MAR and MAD on $n_e$. In order to eliminate this uncertainty from current edge

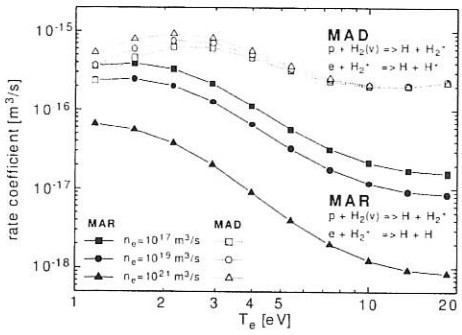


*FIG. 11.1: Rate coefficients for molecularly activated recombination and dissociation.*

plasma models, an experimental campaign was carried out at ASDEX Upgrade by using the divertor spectrometer. It was adjusted to measure lines of the molecular Fulcher band (an n=3 to n=2 transition in the molecular triplet system, in the visible range, hence corresponding closely to the $H_\alpha$ line for atomic Hydrogen). By this means, and in combination with an appro-

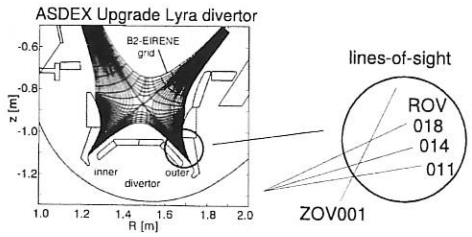


*FIG. 11.2: Divertor geometry with the grid of B2-EIRENE and lines-of-sight used in measurements.*

priate model for electronic excitation of Hydrogen molecules (e.g. as available in EIRENE), it has become possible to measure molecules directly, as distinct from various rather indirect inferences from the Balmer spectrum carried out elsewhere. The experimental setup is indicated in Fig. 11.2, also showing various lines-of-sight. Fulcher photon fluxes were measured in three identical Hydrogen plasma shots which included a transition from attachment to detachment. A series of shots is necessary in order to obtain the vibrational population of the molecules. The time-resolved and line-integrated measurements were compared with space-resolved calculations. The calculated results were obtained from a series of B2-EIRENE runs. These calculations are based on conventional 2D plasma edge models supplemented by a particular collisional radiative (multistep) approximation for the molecules and with transport parameters chosen from extensive code validation runs for ASDEX Upgrade conditions. Both attached and detached conditions were simulated and a series of different approximations of the treatment of vibrationally excited molecules has been tested. The experimentally derived vibrational polulations and photon fluxes together with the various B2-EIRENE predictions are shown in Figs. 11.3 and 11.4. The main results from comparison of predicted and measured molecular Fulcher photon fluxes, with the other major diagnostical results more or less reproduced by B2-EIRENE, are:

1. In the detached case as well in the attached plasma the molecules are significantly excited vibrationally. The relative population of the $\nu = 4$ level, being important for the ion conversion chain, reaches several per cent.
2. The Fulcher intensities can be correctly matched, but only if due consideration is given to the effect that not only is the upper level is largely populated and depopulated from the ground state (and to the lower n=2 triplet state, respectively), but also other states of the molecules are heavily involved and the light emission is truly a multistep process (the corona assumption has led to discrepancies between modelling and measurement by a factor of more than 20).
3. The modelling results can be grouped into two cases: one with explicit treatment of the vibrationally excited molecules (and the consequences thereof) and one without. Agreement can only be achieved in the first case.
4. Within the first group, the various treatments of surface effects on the establishment of the vibrational distribution did not allow experimental verification of one of them against the others. The results are robust to this detail of the model.

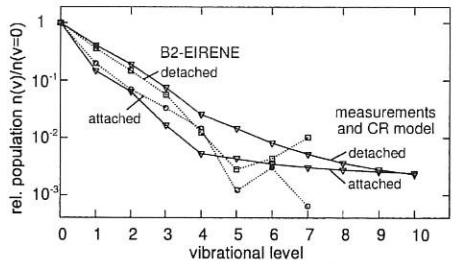


*FIG. 11.3: Vibrational population in the ground state of Hydrogen in detached and attached plasmas.*

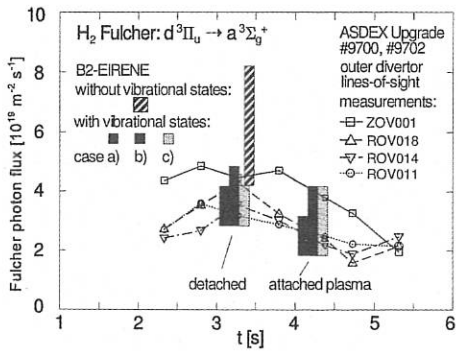


*FIG. 11.4: Comparison of measured Fulcher photon fluxes with B2-EIRENE calculations for various cases of molecular effects.*

5. Spatially resolved results demonstrate that molecular densities are only comparable to atomic densities within a small layer near the divertor walls, and much less so further inside the divertor plasma.

6. For ASDEX Upgrade, detachment is harder to achieve with the presence of vibrationally excited molecules taken into account than without. This result is exactly the opposite of what would have been expected without such detailed bookkeeping of the various competing processes and forces as provided by the B2-EIRENE code. For pure plasma conditions (no impurities were explicitly treated in these simulations, but their effects were implicitly taken into account, in the choice of boundary conditions), the upstream density for the onset of detachment had to be increased by a factor of 1.5 to 1.7 in order to recover those divertor conditions with full treatment of the molecular effect which would result with the simpler models hitherto employed. The strength of the new molecular effects may be somewhat weaker in simulations where full account is taken of the impurities in the SOL as well. However, the trends are very robust and the qualitative and even quantitative agreement with the detailed spectroscopical results are a further strong indication.

While these investigations afforded better qualitative understanding of the role of molecules in a divertor, it has to be kept in mind that quantitative predictions may be different for Hydrogen and Deuterium. Concerning Deuterium, the vibrational levels and some selected rate coefficients have to be replaced in the codes and, in addition, the application of isotopic relations has to be critically reviewed.
*(In collaboration with Universities Augsburg and Düsseldorf.)*

# 12. SOL AND DIVERTOR PHYSICS

## 12.1 Spectroscopic Investigations of Volume Recombination

In order to obtain time-resolved recombination measurement during the ELMy H-mode, highly time-resolved and spatially resolved measurements of the ratio $D_\gamma / D_\alpha$ were made (Fig. 12.1). In the outer divertor, two identical arrays with lines of sight looking radially across the strike point are available in two different toroidal positions. The lines of sight are coupled to two photomultiplier systems with interference filters, permitting measurement of the ratio with a time resolution of 100 $\mu$s. During a NI-heated H-mode density ramp with gas puffing the confinement degradation begins at about 0.6 of the Greenwald limit concurrently with the onset of volume recombination and detachment at the outer divertor (at t=3.1 s). Above this density there is full detachment and strong volume recombination alternating with phases, triggered by the heat fluxes due to ELMs, of attached plasma and low volume recombination. The recombination radiation was also used for determination of the temperature under high-density, low-temperature divertor conditions. There exist various spectroscopic methods for measurement of the temperature. They rely on the observation of bound-bound transitions and free-bound transitions in atomic Hydrogen. The Boltzmann plot is based on the measurement of the population of the Hydrogen levels above the collision limit. Temperatures can also be derived from the ratio of Hydrogen continua; the application of the Balmer and Paschen continuum is called the Balmer sprung method. It was found that the two methods, Boltzmann plot and Balmer sprung, do not yield the same result. Temperatures derived from the Boltzmann plot are significantly lower than those obtained from the Balmer sprung method (Fig. 12.2). These discrepancies are explained by taking into account the inhomogeneity of the divertor plasma. The measured intensities are line-of-sight integrated along the density and temperature gradients. Due to the different dependences of the Balmer and Paschen continua and of the Balmer lines on $T_e$, there is a weighting effect of emission which leads to deviations between the applied methods and the average temperature. The different spectroscopic methods have been applied to synthetic measurements through density and temperature profiles calculated with B2-EIRENE. In accordance with the experimental observation, it could be shown that temperatures determined by the spectroscopic methods of the Boltzmann plot and Balmer sprung tend to be lower and upper bounds of the line-averaged $T_e$ when applied to an inhomogeneous divertor plasma.

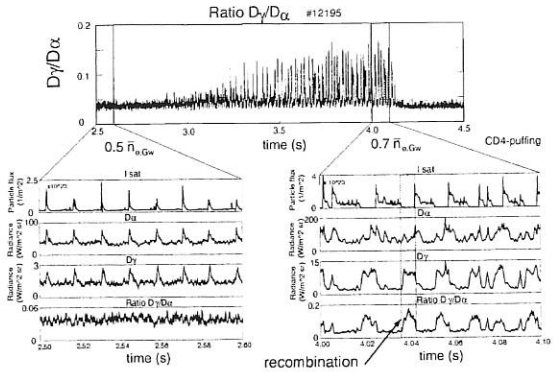


*FIG. 12.1: Time evolution of the $D_\gamma / D_\alpha$ ratio during attached and detached conditions.*

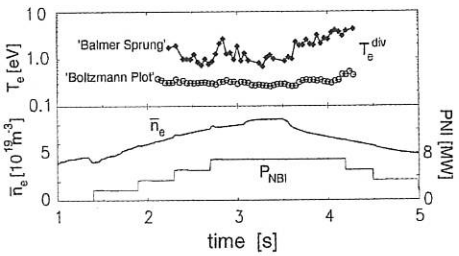


*FIG. 12.2: Temporal evolution of the temperature in the outer divertor (from channel ROV10) during simultaneous ramp-up of density and neutral beam power.*

## 12.2 In-out Divertor Asymmetry

The experiment shows a fundamental in-out asymmetry of the temperature in the divertor. In the standard configuration (single X-point at bottom, ion $\nabla$B drift to the X-point) the temperature is almost constant in the inner divertor. A variation of the power input influences mainly the temperature in the outer

divertor. The asymmetry of the divertor temperature is mostly pronounced at low line-averaged density. These experimental features were reproduced by a B2-Eirene simulation of the edge plasma without inclusion of the drift terms. It shows a transition from an almost symmetric to an asymmetric solution already known from 1D-modeling (bifurcation). In the model the symmetry is broken by geometric effects. In contrast, in the tokamak plasma the symmetry breaking is due to ExB effects. The asymmetry is then amplified by the bifurcation, which is the result of the nonlinear interplay of heat conduction and impurity radiation.

## 12.3 Heat Flux and Divertor Radiation Losses for Different Divertor Geometries.

The lyre-shaped divertor (Div II) was used to run discharges in a closed divertor geometry with the strike point at the vertical target plates as well as in an open geometry comparable to the Div I situation with the strike point at the top of the roof baffle. It was shown that the open geometry in Div II is comparable

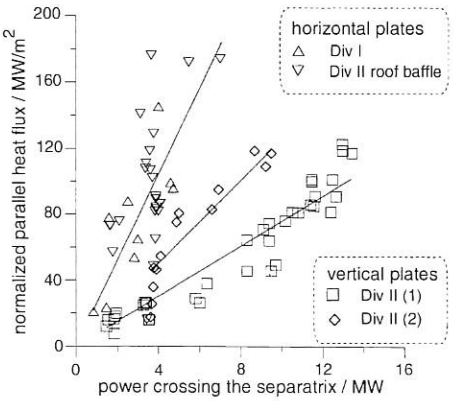


*FIG. 12.3: Maximum parallel heat flux at the outer target plate for different divertor geometries. The heat flux was normalized to a density of $10^{20}m^{-3}$ and a safety factor of 4.*

with the Div I situation. The maximum heat flux at the outer target is by a factor of about two increased in relation to the closed-divertor situation (Fig. 12.3), whereas the radiation in the divertor region decreases from about 40 % of the input power to 20 %, as was also found in Div I (Fig. 12.4).

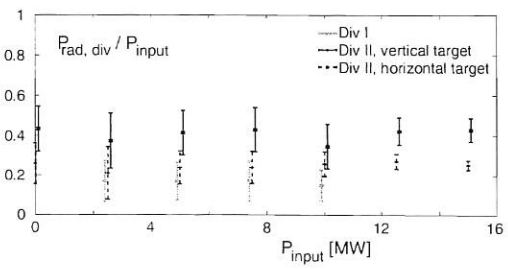


*FIG. 12.4: Fraction of the radiated power in the divertor as a function of the input power for different divertor geometries.*

## 12.4 Divertor Compression Modelling

A wide range of parameters have been simulated for AUG, with the emphasis on simulations with D+C+He and H+C+He. A range of chemical sputtering coefficients were used to determine self-consistently the C concentration in the plasma, and trace amounts of He have been included in the simulation so that He compression can be studied (see Fig.12.5). The transport

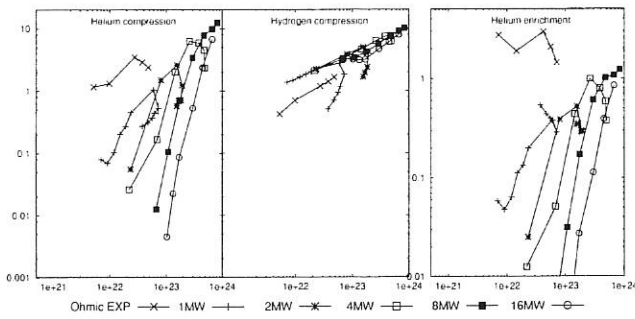


*FIG. 12.5: H compression and H enrichment as a function of the H neutral flux density at the pumping duct for simulations of ohmic shots. Some experimental results are also shown for comparison.*

coefficients and divertor geometry were varied, and the impact of these changes on the peak power to the targets, impurity radiation, and He compression were examined.

An interpretive version of the new B2 code is being developed so that the underlying transport coefficients can be extracted from the experimentally measured temperature and density profiles. So far it has been tested for a range of ASDEX Upgrade shots.

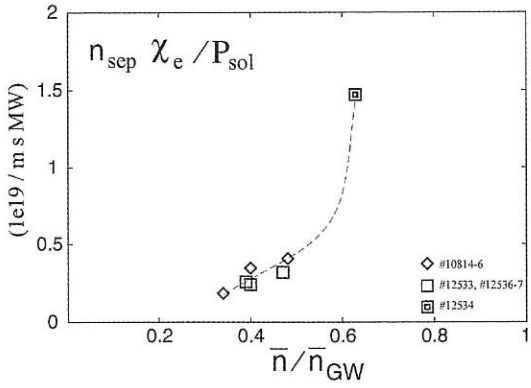


*FIG. 12.6: Normalized thermal diffusivity versus Greenwald densities.*

# INTERNATIONAL COOPERATION

The collaboration with other international institutes and universities was considerably extended. Besides the below-mentioned collaborations there was cooperation with the following institutions: Istituto de Fisica del Plasma, CNR (Italy); Ecole Polytechnique Fédérale, Lausanne (Switzerland); University of Strathclyde (Scotland); FOM-Institute voor Plasmafysica, Rijnhuizen (Netherlands); University of Toronto (Canada); Institute of Applied Physics, Nishni Novgorod (Russia); I.V. Kurchatov Institute of Atomic Energy, Moscow (Russia); IOFFE Institute, St. Petersburg (Russia); Institute for Plasma Research, Bhat, Gandhinagar (India); Southwestern Institute of Physics, Chengdu (China); Institute of Plasma Physics, Academia Sinica, Hefei (China); Korea Basic Science Institute, Yusung (Korea); NIFS, Nagoya (Japan); Kuo University, Yokohama (Japan).

## 1. DOE – ASDEX Upgrade Activities

The 14th meeting of the Executive Committee (EC) was held on September 29, 1999, at Oxford during the IAEA TCM on H-mode and internal barriers. The current contract will end in July 2000. By virtue of the fruitful collaboration during the last 10 years, which was beneficial to both sides, the EC proposes extension of the IEA ASDEX Upgrade Implementing Agreement (IA) for another 5-year period. Closer cooperation with the EC of the IA on the Three Large Tokamaks should be envisaged.

### 1.1 SOL and Divertor

B. Braams from NYU spent some weeks at IPP continuing development of the B2.5 code.
The B2-EIRENE code package has been used at ORNL for a number of years. The new B2.5 code, developed jointly by NYU and IPP, was adapted there. On the other hand, IPP benefited from ORNL's experience in modelling JET with the B2 package. A neutral model developed at PPPL includes treatment for molecular hydrogen. It will be incorporated into the IPP version of B2.5. Furthermore, the possibility of using B2.5 in modelling NSTX was discussed.

### 1.2 Plasma Turbulence

There is already close collaboration between the University of Maryland and IPP Garching focusing on the theory and numerical simulation of plasma turbulence. To further refine the description of collissionless and kinetic effects a longer stay of an IPP scientist at Maryland is envisaged.
The work on electromagnetic drift wave turbulence was extended by incooperating trapped electron dynamics within a gyrofluid model, and the model was extended to the regime of arbitrarily strong disturbances of an inhomogeneous equilibrium.

### 1.3 Impurity Transport

IPP's STRAHL code together with the appropriate atomic data basis was implemented at DIII-D, and collaboration on impurity transport and radiation in tokamak plasmas was started. Exchange of modelling and analysis techniques in this area is envisaged.

### 1.4 MHD

In collaboration with PPPL fast-particle-driven MHD instabilities were studied, and their NOVA-K code was installed at IPP. Of main interest is the theory of the MHD at the plasma boundary. The GATO code for studying the mode structure of ELM precursors was therefore adapted. Collaboration with DIII-D was started to derive scaling conditions for the occurence of tearing modes in ITER from data gained by JET, DIII-D, and ASDEX Upgrade.

### 1.5 Ion Cyclotron Resonance Frequency Heating

A Memorandum of Understanding was written under the umbrella of the IA with the goal of developing new ICRF antennas for ASDEX Upgrade. The boundary conditions for these new antennas were fixed. Tests of the ferrite tuners, borrowed from DIII-D, during plasma operation in ASDEX Upgrade were performed.

A new version of the TORIC code with an accurate evaluation of ion Bernstein waves by the electrons had been installed at MIT, and a few Alcator C-MOD shots with He3-D plasmas in the mode conversion regime were simulated. The improved code predicts the experimantal results more accurately. The MIT routine for evaluating the steady-state current driven by IC waves and an interface, also written by MIT, were adapted to the code. This interface will increase the portability of the code and, facilitate the task of keeping the versions used at different labs the same, as new physics is added to the code.

### 1.6 Plasma-wall Interaction

The use of alkaline metals such as Li in fusion devices is of interest since the low atomic number makes the impurity problem of the central plasma unimportant. Furthermore, liquid metals do not show damage, can survive disruptions, and allow higher heat transfer. At Sandia Livermore measurements and calculations regarding composition changes of Sn/Li alloys due

to ion bombardment were made.
At Oak Ridge the implantation of W ions (1 - 100 keV) and their interaction with carbon surfaces due to erosion, diffusion, and the carbidisation at temperatures up to 600 C were studied.

## 2. CEA, Cadarache

The six working groups established for collaboration between ASDEX Upgrade, W7X, and CEA had a common meeting in November 1999 to discuss special issues. A new working group concerning heating and current drive with ICRF was established.

## 3. University of Cork, Ireland

The collaboration with the University of Cork concerning MHD equilibrium identification using magnetic measurements was continued. The "CLISTE" interpretative equilibrium package includes information from magnetic probes, MSE diagnostics and rational q-values from SXR measurements. It was further developed as described in Sec. 9.5, ASDEX Upgrade Project.

## 4. DEMOKRITOS, Greece

The reciprocating divertor Langmuir Probe System (LPS) constructed and operated by Demokritos was successfully applied to a series of L- and H-mode plasmas up to medium heating power levels. Depending on the mode of operation, the LPS delivers spatial profiles of density, temperature, potential, current, and Mach number for both divertor legs along a horizontal line about 5 cm below the X-point. Beyond this routine operation there were two important discoveries in this period: (1) the observation of high current and voltage spikes during Elms at a position far from the separatrix, interpreted as unipolar arcs, and (2) a surprisingly strong change in the H-mode Elm behaviour when the active, small probe tips crossed the separatrix (probe current about 1 ampere), while the massive probe body obviously had no effect at the same posistion.

## 5. Centro de Fusão Nuclear, EURATOM IST Association, Lisbon, Portugal

This cooperation aims to investigate and exploit microwave reflectometry for profile and fluctuation measurements. In the framework of this collaboration, a multi-band fast-sweeping frequency modulation (FM) reflectometer is being operated on ASDEX Upgrade.
Techniques for automatic evaluation of density profiles have been further developed and are now being regularly used to complement the data base with reflectometry data.
Fluctuation measurements were made during formation of the H-mode (edge) transport barrier and internal transport barriers (ITB). For example, the relative timing of H-mode barrier and ITB formation was studied by making simultaneous measurements at different microwave frequencies. It is planned to extend this type of study and further develop the experimental techniques to investigate transport-relevant fluctuation properties.

## 6. UKAEA, Culham, United Kingdom

The collaboration with UKAEA Culham was continued in 1999. The main focus was discussion of neoclassical tearing mode stabilization experiments performed with LHCD in COMPASS-D as compared with those done with ECCD in ASDEX Upgrade.

## 7. Institut für Allgemeine Physik of TU Vienna and Friedrich Schiedel Foundation

In addition to the ongoing cooperation on tokamak edge diagnostics with lithium beams, first experiments were made on ASDEX Upgrade (and in parallel at JET) on the possible use of helium beams for plasma diagnostcs in fusion plasmas. In a first step, one beam source of the ASDEX Upgrade neutral injection heating system was operated with helium (30 keV) and the visible line radiation was observed with an existing, though not optimized, spectroscopic system (CXRS equipment). The results were compared with numerical modelling based on the ADAS spectroscopy data collection. The results are very encouraging and the experiments are to be continued. These activities are supported by the Austrian Friedrich Schiedel Stiftung für Energietechnik.

## 8. TEKES (HUT and VTT), Finland

The collaboration between TEKES and IPP aims to use kinetic modelling to investigate several effects in a fusion plasma: particle trajectories and ion distribution at the plasma edge, neoclassical radial electric field and ion losses. Calculations were made for real ASDEX Upgrade geometry to establish the effect of the radial electric field on measured charge exchange neutral particle spectra. In a further study, the neoclassical radial electric field is determined self-consistently in full geometry from the balance of particle losses and neoclassical viscosity. It is planned to continue and extend the studies on the L- mode to H-mode transition, effects of non-thermal distribution functions, and support of interpretation of neutral particle diagnostics. In addition to this work, a Ph.D. thesis is devoted to investigation of MHD instabilities leading to edge localized modes. A model based on coupled kink-ballooning modes has been applied to ASDEX Upgrade geometry. Regions of positive growth rates were found in keeping with experimental conditions at the onset of type I edge localized modes with realistic bootstrap current profiles.

## 9. Cooperation with Russian Institutes

The impurity pellet injector was mounted in a new sector (n.5) closer to the plasma. The development of a Simatic program now allows use of the injector in triggered or feed-forward mode. A differential pumping system for the impurity pellet injector was built by S. Egorov from SPU and is to be installed in the near future.

## 10. CREATE Group, Naples, Italy

Collaboration continued on the prediction of disruptivity using neural networks.

## JET Cooperation Project

(Head of Project: Prof. Dr. Michael Kaufmann)

In 1999, JET operation was in two campaigns, divided by a summer shutdown during which the inboard track for high-field-side (HFS) pellet launch was installed. This installation involved a combination of remote handling and manned intervention into the vacuum vessel and demonstrated once again the possibility of successfully undertaking complicated operations in a tritiated vessel. The experimental programme in both campaigns was divided into two task forces: in the January-to-May experimental campaign - Task Force A: ELMy H-mode Physics for ITER and Task Force B: Performance Optimization Physics for ITER and DTE2; in the September-to-December campaign - Task Force P: Pellet Fuelling, ELMy H-mode and Divertor Physics and Task Force C: Confinement with ITBs and Plasma Shaping in ELMy H-modes.

TFA/P Results: Initial assessment of the new gas box divertor was completed. H-mode performance was shown to be largely independent of divertor geometry, as had been the case with previous divertor geometries. Exhaust of deuterium, impurities, and, in particular, helium was shown to improve with divertor closure. The septum dividing the two divertor legs provided some interesting new physics: balanced detachment was obtained in L-mode discharges, and easier H-mode access was demonstrated. HFS pellet fuelling was demonstrated to be an effective fuelling method even in a large machine such as JET. Some confinement degradation was observed with density increase in ELMy H-modes and experiments to minimize this degradation by careful programming of the pellet size and timing were begun. Improved edge and SOL diagnosis allowed exploration of further physics issues. Unexpectedly large SOL flows were measured at the top of the machine and their influence on impurity transport is being investigated. Fluctuation measurements have begun which permitt exploration of the fundamental causes of edge and scrape-off layer transport.

TFB/C results: The main priority for this task force was to obtain quasi-steady-state internal barrier (ITB) discharges. In discharges with an L-mode edge MHD events terminate the ITB due to excessive pressure peaking. In type I ELMy H-mode discharges, a high edge density and the radial extent of the ELMs erode the ITB. However, argon dosing at the edge can reduce the ELMs to type III. With argon dosing and optimum heating timing, $\beta_N$ = 2.6 and H89 = 2.2 at 2.5MA/2.5T were obtained for several seconds. At 3.5 MA/3.45 T $\beta_N$ was limited to 2.0 at 18 MW NBI + 10 MW ICRH, the maximum combined heating power available at JET. Conditions for ITB formation concentrated on variations of the total heating power, q-profile, type of heating power (NBI or ICRH), and shear in the centre. After the summer, priority was shifted to ITER shaping studies, in which plasmas with various elongations (up to 1.9) and triangularities (up to 0.4) were checked against the existing scaling law in standard H-mode discharges. The density scaling for the scaling laws does not agree with the observations in JET. In ITB discharges pellet fuelling during the steady-state conditions show that the ITB goes away when pellets are injected due to loss density peaking.

The end of 1999 also saw the end of the JET Joint Undertaking. In 2000 a new structure in the framework of the European Fusion Development Agreement (EFDA) will oversee the operation and exploitation of JET: The JET facility will be run by the UKAEA under contract with the European Commission and the physics exploitation of JET will be done by task forces from the Associations, coordinated by a small Central Support Unit under the direction of a new JET Associate Leader.

The IPP contributions to JET mostly concentrated on the four Task Agreements:

### 1 Task Agreement No. 1

In 1999, IPP gave further advice for the design, commissioning, and operation of the injection system and supported the physics program with respect to pellet injection. For the first time, cooperation was performed by guiding experimental investigations online from the ASDEX Upgrade control room.

A number of mechanical design changes and improvements to the control system were subsequently made in the pellet centrifuge injector to improve pellet parameters and reliability. To realize sufficient pellet delivery efficiency with the continuously working JET extruders, the stop cylinder approach developed for the ASDEX Upgrade centrifuge had to be adapted accordingly. An additional in-vessel track was incorporated to facilitate pellet launch from the inboard (high-field) side of the magnetic axis. The launch point is approximately on the midplane and the trajectory is tangential to the flux surface at a normalized minor radius of about 0.5. A fast-acting selector mechanism permits individual pellets or sequences to be diverted to either the inboard or outboard track. The system is now capable of launching 4 mm cubic pellets with a maximum design repetition rate of 10 Hz from either the torus inboard or outboard.

Comparison of inboard and outboard launch readily confirmed the superior fuelling efficiency of inboard pellets with heated plasma targets at JET. The re-distribution of the pellet mass due to the ablatant drift was identified from the response of the density profile, measured promptly after injection of the pellet, and comparison with the ablation profile computed with the Neutral Gas Shielding (NGS) code and inferred from the experimental $D_\alpha$ ablation light. A range of L-mode target conditions was used to vary the parameters expected to influence the drift process, such as the magnetic field, safety factor, and target electron temperature. In the H-mode, the difference between inboard and outboard launch was more pronounced; outboard launch was found to be very ineffective for fueling, whilst average densities at or beyond the Greenwald limit were readily obtained by using inboard launch.

However, a significant reduction in energy confinement was observed with increasing density. This reduction was attributed to the occurrence of pellet-triggered ELM bursts of about 100 ms duration. ELM bursts, as observed before in ASDEX Upgrade, consist of several ELMs stronger and longer than a spontaneous ELM. Optimization of the pellet fuelling cycle was performed by adapting the pellet size and frequency as well as interrupting the pellet sequence for an appropriate time to allow energy recovery. In this way, a distinct improvement of confinement at densities close to the Greenwald limit was obtained in relation to data obtained when using gas fuelling alone.

Pellet fuelling of a pre-existing Internal Transport Barrier (ITB) discharge usually resulted in destruction of the barrier however recovery of the barrier occurred faster than the pellet-induced density enhancement decayed. Furthermore, with outboard pellets of reduced size (50-70$\%$) it was possible to raise the density within the ITB.

## 2 Task Agreement No. 2

Erosion, re-deposition, and hydrogen isotope accumulation at the vessel walls of JET were also studied for the T-discharge period by special Long Term Samples (LTS) with an area of about 0.8 $cm^2$. They had been mounted into the inner wall tiles and could be removed remotely at the first vessel opening after the T-discharge period. From the decrease in the thickness of the metal markers which had been deposited on the samples before installation at JET, it was confirmed that the inner wall is erosion-dominated. The total of T accumulated in the carbon LTS was found to be about 5 to 7 $10^{14}$ $T/cm^2$, resulting in low enough activity so that the LTS could be analyzed in some detail. An AMS (accelerator mass spectrometry) analyses performed at the Accelerator Laboratory, Technical University of Munich, showed a depth profile for the T ranging up to about 3 $\mu$m at concentrations in the $10^{-5}$ atom % range, with a minimum at the surface and a peak at a depth of about 2.5 mm. A measurement of the H and D accumulated in the LTS gave much higher concentrations in the few % range which peak closer to the surface at a depth <1 $\mu$m. The T may originate partly from DD reactions before the DT-discharge period and partly from the DT-discharge period. The much lower T and higher H and D concentrations in the near-surface region indicate very effective T removal during the glow discharge conditioning, as well during the D-discharge period after the DT-discharge period.

## 3 Task Agreement No. 8

Stationary Advanced Tokamak operation was postulated as ultimate goal to achieve a steady-state fusion reactor with highest performance. To combine the experience gained in experimental scenario development, MHD analysis, transport code modelling, and turbulence studies both on JET and ASDEX Upgrade, scientists from IPP participated in the JET experiments and their analyses. The final aim, which will be further pursued in Task Force S2 after 2000, is the development of Advanced Tokamak scenarios with experimental tests on both devices and derivation of scaling laws for power thresholds and confinement by means of similarity experiments in these new fields. Special attention was paid in 1999 to identification of limiting MHD modes, core fuelling by pellet injection from the high-field side, transport barrier control with edge radiation, current density measurements by MSE, and developments of the ASTRA transport code (implementation of an X-point equilibrium solver, comparisons with JETTO transport analyses).

## 4 Plasma-Edge Theory Contributions

In addition to the official Task Agreements, several collaborations in the field of modelling of plasma-edge-related issues were undertaken.

### *4.1 Isotope effect on the L-mode density limit*

A systematic study of the mass dependence of the L-mode density limit was conducted in JET hydrogen, deuterium, and tritium divertor plasmas [187]. A previously proposed edge-based model for the density limit was revisited to include mass dependence. The model predicts, in particular, coupling between the power and mass dependences which is in quantitative agreement with the JET data.

### *4.2 Modelling of the low-pressure boundary of ELM cycles in JET*

The trajectories of ELMy H-mode discharges in the pedestal density - pedestal temperature plane form cycles characterized by high-pressure and low-pressure boundaries. While at least for type-I ELMs the high-pressure boundary seems to be associated with the ballooning limit in the pedestal, the low-pressure boundary is poorly understood. The scaling of the low-pressure boundary was assessed for JET Type-I H-modes. Discussion is guided by a semi-empirical model emphasizing the role of scrape-off layer physics. The results suggest that the high-pressure and low-pressure boundaries are governed by distinctly different physics mechanisms.

# ITER COOPERATION PROJECT

(Head of Project: Prof. Dr. Karl Lackner)

## 1. PERFORMANCE ANALYSIS

### 1.1 H-mode Energy Confinement and Power Threshold Analysis

O. Kardaun (IPP Garching), in cooperation with the ITER Global Database Working Group.

Practical and theoretical interval estimation of the prospective energy confinement time in ITER has been described in some detail in a PPCF contribution which was elected as featured article. Salient aspects of this article, which concentrated on the ITERH.DB2 database and the ITER FDR design parameters, are the following: five different 'definitions' of a 95% interval estimate, each describing a distinct feature of the overall definition; a discussion of ITERH-92P(y) in 'dimensionless' physics variables; robustness of log-linear scalings against various types of (modelling) imperfections (database condition, sensitivity to systematically shifting the data of each tokamak, analysis of jackknife procedures, which omit data from one tokamak at a time, random coefficient models); systematic curvatures as previously found by Dorland and Kotschenreuther in relation to systematic differences in measuring the stored energy ($W_{dia}, W_{mhd}$); the influence of hitherto 'hidden' variables (such as $q_{95}/q_{cyl}$ and the definition of the elongation, as mentioned in the Annual Report 1998); robustified version of the traditional statistical interval estimate, which is too narrow in practice; variation of the interval width with the actual operating point; discussion of a number of embedding physical aspects and effects not incorporated in the scalings. The methods from this study provided the basis for the technical 95% interval estimate of the more recently designed ITER options, such as ITER IAM and ITER FEAT ($\tau_E = 3.66 \times 2^{0\%\pm 1/2} s$). The point estimate of the latter is based on the ITERH-98P(y,2) scaling, which can be considered as the successor of ITERH-92P(y) in describing ELMy confinement. At the time of writing the ITER physics basis document it was felt that the data did not warrant a preferential recommendation between ITERH-98P(y) and ITERH-98P(y,2). In the course of 1999, the database was enlarged again (ITERH.DB3v8) with additional data especially from JET and from ASDEX Upgrade, COMPASS-D, TCV, and the Canadian Tokamak TdeV. Following the Expert Group Meeting in autumn, a careful check of the ITER Physics Basis scalings against the evidence from the enlarged dataset led to recommendation of the ITERH-98P(y,2) scaling for ITER design purposes. During the year, the Threshold Database (organized by F. Ryter) was significantly improved, especially with respect to the edge data. A considerable amount of low-threshold W-divertor data from JT60-U was added, and closed divertor geometry was identified as one source of scatter. The status of the work has been well summarized in a joint PPCF article by J. Snipes et al. The interval estimate for ITER FEAT (18-55 MW) is lower than those based on the ITER Physics Basis (IAEA-1996) threshold scalings.

### 1.2 Study of Radiation Limits in Fusion Reactor Scenarios

G. Becker

Radiative mantle scenarios of the ignited ITER FDR (Final Design Report) with argon and neon seeding were explored by self-consistent simulations with a special version of the 1 1/2-D BALDUR predictive transport code. The calculations apply empirical transport coefficients and are carried out in both the bulk and scrape-off layer. Operation-relevant upper limits to the radiative power losses from the main chamber, from closed flux surfaces, and from the scrape-off layer were found. Both simulations and an analytic study of power balances show that these limits are set by the radiation profile and by the cross-field heat conduction in the scrape-off layer. For given heating power, the conductive heat flux across the separatrix and the energy flow to the divertor are also restricted. With high edge density, the required thermal energy confinement times at the radiation limits were found to be 4.4 s in the argon and 4.0 s in the neon scenario. The assumption of flat density profiles and no inward pinch in the whole plasma is supported by simulations using a new scaling relation for the anomalous inward drift. The dependence of the radiation limits on the separatrix density was investigated.

# 2. COMPONENT DEVELOPMENT

## 2.1 Development of an RF Source for Negative Ions

P. Franzen, B. Heinemann, W. Kraus, P. McNeely, W. Schaerich, E. Speth, O. Vollmer

The ITER R&D contract (within the frame of a collaboration between CEA and IPP) for development of an RF source of negative ions was continued. The incentive is the anticipated superiority of RF sources – compared with arc discharge sources – in respect of cost and maintenance. In the last year considerable progress was made by implementing magnetic confinement (cusp magnets) in order to achieve lower pressure operation and by using a suitably placed magnetic filter to achieve a lower electron temperature. An H- yield of $15 mA/cm^2$ was reached at $0.5 Pa$ (target: $20 mA/cm^2$ D, corresponding to $30 mA/cm^2$ H at 0.4 Pa). The fact that the measures taken resulted in a signigicant increase of the H yield indicates that some of the physics phenomena involved in the formation of negative ions were correctly assessed at least qualitatively. Further improvements can be expected by lowering the caesiated surface work function (heating the plasma grid up to $250^0 C$).

Further experiments are planned to demonstrate the uniformity over the full area and show the inherent long-pulse capability.

## 2.2 Design Study for an Alternative Ion Dump

P. Franzen, B. Heinemann, W. Kraus, P. McNeely, W. Schaerich, E. Speth, O. Vollmer

A scoping study for an alternative concept of the residual ion dump (RID) of the ITER NBI system has been started. The incentive is to avoid the inherent risk of the in-line electrostatic ion removal concept, presently envisaged in the NBI design. It is proposed to use conventional remote magnetic ion removal, which avoids enhanced reionization losses and potential amplification of electron currents by electrostatic acceleration. This type of RID has proved itself in almost all injection systems world-wide over the last two decades.

In a first step the study has shown the basic feasibility of the remote magnetic RID and its integration into the ITER NBI system. 2 x 8 MW of residual 1 MeV (positive and negative) deuterium ions are deflected by a horizontal magnetic field of appr. 0.2T vertically upwards and downwards onto a water-cooled ion dump. First results using a quasi-uniform model field but 3D ion orbit tracking show that the power density nowhere exceeds $15 MW/m^2$ perpendicular to the dump surface even for the lowest divergence ($0.3^0$). 3D magnetic field calculations show that the stray field of the iron magnet at the exit of the neutralizer is below the tolerable level (1 gauss).

It is planned to continue the study in the near future in order to examine engineering details of the system (subdivision of the ion dump into individual plates, 3D deflection field).

## 2.3 ICRH for ITER

F. Braun, J.-M. Noterdame

The ICRH group contributed to two ITER efforts: (i) A study contract "ICRH Radio-Frequency Generator Design Study" placed with industry in 1998. (ii) J. – M. Noterdaeme contributed to the ICRH planning for ITER as a member of the Coordinating Committee for ICRF Heating and Current Drive.

# STELLARATORS

In 1999, with Prof. Günter Grieger, a pioneer of the stellarator development retired. The relevance of helical systems for future fusion systems, as seen today, is demonstrated by the approval of the Wendelstein 7-X experiment realised in Greifswald. For decades, Prof. Grieger was the motor behind the successful development of the Wendelstein stellarator line of IPP.

New technical elements in the programme were ten control coils to manipulate the edge island structure and a double-loop antenna for ICRH heating.

The possibility of increasing the plasma radius was verified. The compensation of the natural islands in the case of $\iota = 1/2$ through the control coils allowed to increase the plasma radius. For the first time, a direct comparison of the energy content at equal plasma radius between $\iota = 1/2$ and $\iota = 1/3$ was possible.

Measurements with the poloidal Langmuir probe array showed that while ramping the control coil current the footprints of the islands behaved as expected from vacuum field calculations.

The ratio of perpendicular to parallel transport within an island could be changed by a factor of 2 by means of the control coils.

A new H-mode window was found at $\iota = 5/9$, which is marked by for distinctive transitions and better confinement times.

Experiments on EC-heating and current drive were performed with 1.5 MW ECRH power, which corresponds to extremal power densities of up to 50 $MW/m^{-3}$. The EC-driven loss of trapped particles generates radial electric fields, which lead to strongly improved confinement. Experimental investigations of the wave-particle interaction in phase-space under high power conditions were compared to nonlinear kinetic theory.

With the double-loop antenna better fitting to the plasma surface, significantly higher power could be coupled to the plasma. With ICRH minority heating, the energy of an ECRH plasma could be increased from 10 to 15 kJ. With ICRH alone, a plasma with 10 kJ was achieved.

In the middle of August 1999, the experiments on W7-AS was terminated to carry out the second step of the project "Divertor Experiment at W7-AS involving the installation of divertor modules, titanium getter pumps and divertor diagnostics. It will be completed end of June 2000.

The four counter injectors of the neutral injection heating system will be converted into co-injectors, so that after re-starting eight injectors are at disposal for high-$\beta$ studies. Considering the decisive role of the radial electrical field for the neoclassical transport, a radial injector is added to the machine. The divertor development of W7-AS prohibited the use of a large ICRH antenna. The successful high power ICRH porgramme on W7-AS had to be finished.

Theoretical investigations in the Stellarator Theory Division being built up in Greifswald concern four major areas of research: (i) further development of the stellarator concept, notably with respect to quasi-isodynamic and quasi-axisymmetric configurations; (ii) equilibrium and stability investigations with advanced computational tools, in particular in the areas of the structure of magnetic surfaces and islands at finite $\beta$ as well as of Alfvén eigenmodes; (iii) development of a stellarator-specific basis of anomalous transport theory with nonlocal investigations of linear and nonlinear ion-temperature-gradient driven modes as well as resistive drift modes; (iv) development of 3D plasma edge theory, specifically the 3D edge plasma transport code in magnetic coordinates.

# WENDELSTEIN 7-X Construction

(Head of Project: Dr. Manfred Wanner)

Members of the W7-X Construction Division and contributors to the project: see section "Division and Groups, WENDELSTEIN 7-X Construction"

## 1. INTRODUCTION

The W7-X Construction project is responsible for the design, manufacture, and assembly of the W7-X stellarator, the heating systems, the power supplies, the cooling system, and the control system. Since March 1999 the division has been operating in Greifswald.

The main components of the stellarator are the superconducting magnet system to confine the plasma, the cryostat to enclose and insulate the cryogenic parts, the ports to observe and heat the plasma, and the plasma-facing components to control the energy and particle exhaust. Steady-state plasma heating is based on powerful ECR sources. In addition, the plasma temperature and density can be increased by ICR and NBI heating. The superconducting coils are energised with high current by dedicated supplies and kept at a temperature close to absolute zero by a helium refrigeration plant. The heating systems are supplied with high voltage. A total input power of about 48 MW is required to operate the magnet system and supply the heating systems and the cryogenic refrigeration. Waste heat is removed by circulating water which is re-cooled by cooling towers.

Major R & D activities have meanwhile been completed. The DEMO coil, an original-sized superconducting magnet, which was manufactured by industry, was successfully tested under nominal and overload conditions in the TOSKA facility at Forschungszentrum Karlsruhe (FZK). With this positive result, manufacture of the coil system for W7-X was released.

The DEMO cryostat, a $^1/_8$ sector of the W7-X stellarator, was completed by the contractor. The feasibility of manufacturing the unconventionally shaped plasma vessel and other critical components of the cryostat was demonstrated. The know-how acquired will be considered in the specification of the W7-X cryostat. The DEMO cryostat was prepared for the cryogenic tests to be conducted at IPP in Garching.

The lining of the inner wall of the plasma vessel calls for cooled panels covered with low-Z material. Prototypes of water-cooled steel panels coated with boron carbide were ordered.

In 1999, design of the machine was detailed and a number of major components were ordered, such as the planar coils, the magnet support structure, the power supply for the magnets, and the high-voltage supply for the heating systems.

FZK contributes the complete ECRH system for W7-X. Joint development of a continuously working 140 GHz gyrotron by FZK, Thomson Tubes Electroniques (TTE), and CRPP Lausanne led to a first prototype, which will be tested at the facilities of FZK. Design of the microwave transmission line is handled by IPF Stuttgart.

The Low Temperature Laboratory of Commissariat á L`Énergie Atomique (CEA) at Saclay is preparing the test facilities for the cryogenic acceptance tests of all superconducting coils.

The critical path for the project is determined by delivery and testing of the superconducting coils. The project schedule aims to commission W7-X and map the magnetic field by spring 2006.

## 2. R&D ACTIVITIES

### 2.1 DEMO Coil

The cryogenic tests of the DEMO coil were performed in the TOSKA test facility at FZK. To simulate the electromagnetic conditions in W7-X, the DEMO coil was installed in the test cryostat and mounted on the European LCT (Large Coil Task) coil, which provided the necessary background field.

Mounting of the DEMO coil in TOSKA was completed in spring 1999. A series of pre-tests at ambient temperature was performed to check the hydraulic performance of the helium cooling loops as well as the integrity of the electrical circuits. After closure and evacuation of the TOSKA cryostat an integral leak test and further electrical tests were performed. Cool-down of the DEMO coil started in May at a rate of approx. 1K/h. The superconducting state was reached during the first week of June.

The functional testing of the DEMO coil entailed no major problems and was divided into three different phases.

During the first test period the coil was operated in its self-field up to the maximum possible current. The critical currents observed have to be related to the operation temperature of the conductor, agreeing well with the expected values. Quenches could be detected within fractions of a second by the quench protection system. Ramp-down of the current during rapid shutdown happened safely within 5 s. The effective forces on the coil during these first tests were well below the design limits.

During the next phase the coil was operated in the background field of the LCT coil up to the nominal current of 14.7 kA. The superposition of the magnetic fields of the two coils resulted in a maximum magnetic induction of 6.8 tesla at the DEMO coil and a corresponding force between the two coils of about 10 MN. This force causes stress and strain conditions in the winding package of the DEMO coil which are similar to those acting in the W7-X magnet system.

Finally, the DEMO coil was subjected to overload conditions to explore the margins of operation. Due to some unexpected limitations of the facility only 114 % of the nominal load could be reached. Detailed analysis revealed that additional heat was transported to the coil casing through heat conduction of residual gas in the TOSKA facility. Since the cooling on the casing of the DEMO coil was not designed for this heat load, the casing warmed up to 11 K locally instead of staying at a temperature of 4.2 K. Due to the tight mechanical embedding of the winding pack within the casing the temperature of the superconductor increased accordingly, which explains the lower critical current observed. The values for the deflections and stresses in the casing increased linearly with the magnetic force and indicated elastic behaviour. This confirmed the design of the winding pack embedding using a glass-resin compound pre-stressed during manufacture. The different thermal contraction of the conductor and the steel casing causes the pre-stress to be released at cryogenic temperature. During warm-up the stress re-appeared reversibly.

Successful testing of the DEMO coil was an essential milestone for the project. It confirmed the design of the W7-X coils and allowed to release the manufacture of the coil system in industry.

After successful testing the DEMO coil was dismantled and dispatched to the Low Temperature Laboratory of CEA at Saclay, where it will be used to gain experience with the test facilities for the series tests.

## 2.2. DEMO Cryostat

The DEMO cryostat comprises prototypes of original-sized components, except for the coils, which are replaced by dummies. Construction of the DEMO cryostat was completed in August with considerable delay. The assembly consisting of dummy coils and support structure was inserted into the lower half of the vacuum vessel. In a next step the dummy coils were electrically connected with lengths of the original-type conductor. All electrical connections were insulated with epoxy-impregnated glass fibre tapes against high voltage, which can be induced during rapid shutdown.

Heat conduction and heat radiation to the cold parts are minimised by high-vacuum radiation shields at 80 K, and multilayer insulation. The multilayer insulation was applied by means of pre-fabricated packages. In order to minimise heat leaks, the transition between the packages as well as the insulation of the transition areas to the domes and supports had to be very carefully executed. This work was performed manually and turned out to be very time consuming. Sections of the helium pipes were successively leak-tested after being mounted. During assembly, precise orientation of all components was continuously controlled by optical measurements.

After the upper half of the vacuum vessel was mounted, the ports were welded to it and to the plasma vessel. Horizontal and vertical supports were mounted to maintain the plasma vessel in a well-defined position. Glass fibre composites were used for the coil supports to reduce the heat conduction to the cryogenic parts. Temperature, pressure and strain sensors were installed to control the components during cool-down and operation. After the bulkheads of the vacuum vessel were closed, the cryostat was connected to the refrigeration system (see Fig. 1).

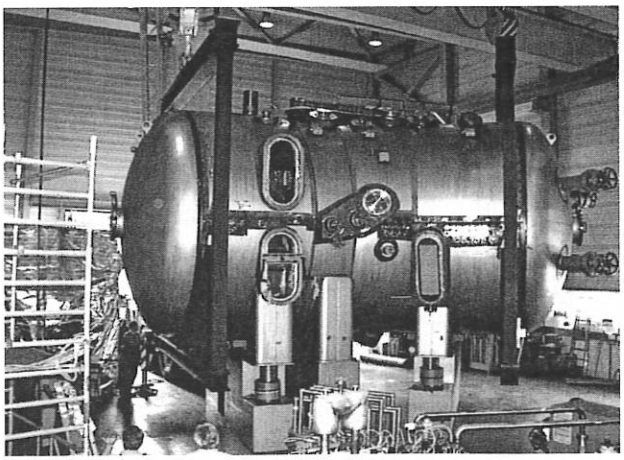

*FIG 1: W7-X DEMO cryostat during final assembly.*

Testing of the DEMO cryostat started in September with movement and adjustment of the plasma vessel supports and coil support structure. The horizontal and vertical sliding plasma vessel supports allow to compensate for movements during bake-out. The coil support structure can be independently displaced to compensate for thermal contraction during cool-down. Minor design problems have been encountered with the bearings, which, however, are of no significance for the W7-X cryostat. Deformations of the plasma vessel and the outer vessel under vacuum conditions were measured and turned out to be as predicted by calculations.

Outgassing of impurities, mainly water, was performed by bake-out of the plasma vessel and ports at 150° C by electrical heaters. After a thorough integral leak test the DEMO cryostat will be ready for the cryogenic tests at the beginning of 2000.

# 3. BASIC MACHINE

## 3.1 Magnet System

The detail design of the magnet system was continued according to schedule. The design was supported by the engineering groups of the central technical services (ZTE) of IPP at Garching. To co-ordinate and supervise the increasing number of contracts with industry additional team members were employed. Exchange of data and CAD-drawings between Garching, Greifswald and the partners in industry is performed electronically.

### *3.1.1 Coil system*

The NOELL/Ansaldo consortium has made significant progress on the fifty non-planar coils, ordered in December 1998. Since assembly of the non-planar coils represents the critical path of the project, their timely delivery is of great importance for the project. In 1999, design of the coil casings was worked out in detail and preparatory work for manufacture of the casings and winding tools was carried out. As indicated by refined structural calculation of the coil support structure, the coil casings had to be modified and stiffened locally. After some trials conducted by the contractor each coil casing will now be combined from two cast half-shells. This technique eliminates complicated welding of several segments for each half-shell and still allows adherence to the specified tolerances.

The superconducting cable is composed of 243 strands enclosed by an aluminium jacket. Pre-tests of the jacketing were performed and development of electrical joints with a resistance of less than 1 nΩ showed promising results. Joints with such a low resistance are necessary to keep the ohmic heat losses at cryogenic temperatures low.

The order for the twenty planar coils was placed with the British company, TESLA Engineering, in March 1999. Major milestones for the detailed design, conductor development, and preparation of the tools have been met. The first coils will be delivered in September 2000 to be tested in the facilities of CEA at Saclay.

### *3.1.2 Coil support structure*

Another major activity was the design of the central support structure, which has to keep the coils at their precise position. A CAD view of the coil system and support structure is given in Fig. 2. The support structure is composed of 10 identical sectors spanning a central ring with a total weight of 72 t. The design had to cater for local forces of up to 3.6 MN on the individual coils which are a result of the electromagnetic action of all other coils in a central field of 3 tesla. A detailed structural calculation of the magnet system and central support structure using finite-element techniques was made at IPP. The model took into account nonlinear transmission of the forces from the winding to the casing through elastic embedding.

Each coil is bolted to this ring at two reference planes. Additional mechanical connections are arranged between the coil casings to take up the residual compressive forces between the coils.

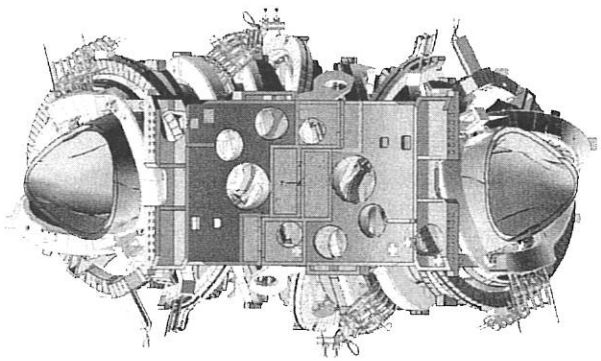

*FIG 2: CAD view of the coil system.*

The massive central support structure needs to be kept at the temperature of liquid helium to avoid heat conduction to the superconducting coils. To ensure a uniform temperature of the structure its surface will be covered by copper sheets and cooling pipes for liquid helium. On the basis of a call for European tenders, the contract for the support structure was placed with the Spanish company, Equipos Nucleares, S.A., in December 1999.

### *3.1.3 Magnet current supply*

The superconducting magnets have to be energised by direct currents of up to 20 kA at a voltage of less than 30 V. Each of

the five groups of non-planar coils and the two groups of planar coils will be independently powered. The current has to be stabilised to an accuracy of $10^{-4}$ to achieve the predicted good confinement of the plasma.

Another essential requirement for the power supplies is fast and reliable discharge of the magnets in case of a quench in the superconductor. Vacuum switches and a pyro-breaker are used to interrupt the electric circuit safely. The energy stored in the magnets amounts to approx. 620 MJ and will be dumped to resistors with a high heat capacity. At the end of 1999 the Swiss company, ABB, was awarded a contract for the power supply and protection system. System assembly will be performed by the local subsidiary of ABB at Rostock, close to the site of W7-X.

### *3.1.4 Control coil power supply*

Ten copper coils will be installed in the plasma vessel behind the baffle plates. These coils will increase experimental flexibility in several respects: They can be used to correct any minor field errors, influence the extent and location of the magnetic islands, and allow the power deposition area to be swept across the target plates. The ten power supplies for these coils will each consist of a transformer, a rectifier, and a four-quadrant controller to provide a direct current of 3 kA at a voltage of 30 V. The output can be modulated at frequencies of up to 20 Hz. The order was placed at the end of 1999 with the Spanish company, JEMA.

## 3.2 Cryostat

In 1999, design concentrated on the plasma vessel, ports, supports, and outer vessel.

The design of the plasma vessel had to maximise its volume within the space limitations given by the casings of the magnet coils and the necessary clearance for the thermal insulation. This made it necessary to reduce the manufacturing tolerances of the vessel in critical areas and decrease the thickness of the insulation at the expense of slightly higher cryogenic losses.

The structural design and buckling analysis of the plasma vessel were contracted to industry and performed by finite-element modelling with the ANSYS® numerical code. Static pressure loads and transient electromagnetic forces occurring during rapid shutdown of the magnet system were considered. The calculations where meanwhile verified at IPP by means of another ADINA® code. The wall thickness obtained from the calculations is 15-20 mm, being similar to the thickness of the sheet material used at the DEMO cryostat.
The design of the adjustable horizontal and vertical supports for the plasma vessel was also verified by a structural analysis at IPP.
The 309 ports were specified and the interfaces to the diagnostic installations and heating units were clarified. Tenders have been received and the order will be placed at the beginning of 2000.

Numerical methods were also applied to investigate the forces on the radiation shields caused by eddy currents in the case of rapid shutdown of the magnetic field. In such a case forces equivalent to a pressure of 0.5 bar may occur. To limit the eddy currents the large metallic areas of the shields need to be subdivided.

Design of the outer vessel is almost complete and the call for tender will be issued at the beginning of 2000. Appropriate openings for the ports, domes, and manholes as well as space for supports and supply lines and aspects of assembly, testing, and inspection have been considered.

The use of high-temperature superconductor material is beeing considered for the current leads of the superconducting coils. For economic reasons, the current leads will be cooled only when the magnets are excited, whereas during stand-by they are allowed to warm up. For that reason, thermal ageing tests of several samples of high-temperature superconductor were conducted. Samples were periodically cooled to liquid-nitrogen temperature and warmed to ambient temperature. Although some degradation was observed after several thousand cycles, the samples turned out to be sufficiently robust for application in W7-X .

## 3.3 In-vessel Components

### *3.3.1 Divertor engineering*

To protect the wall of the plasma vessel from the hot plasma and the plasma from wall impurities, all plasma-facing surfaces have to be covered with low-Z material, e.g. carbon or boron carbide. Three different types of surfaces can be distinguished in W7-X: The divertor target plates are hit by hot particles from the plasma and have to withstand high heat loads of up to 10 MW/m². Baffles which influence the neutral particle fluxes and density need to be designed for heat loads of 0.5 MW/m². The inner surface of the plasma vessel is hit by neutral particles and radiation and needs to withstand heat loads of up to 0.1 MW/m². For each of these areas specific components need to be developed. For conditioning the in-vessel components will be baked at a temperature of 150° C.

To remove the neutralised particles from the divertor, vacuum pumps are installed outside the machine. Additionally, cryo-pumps are installed inside the divertor units.

Experience with tokamak divertors indicates that the divertor for W7-X can be designed with due allowance for the special geometry of the magnetic configuration. The W7-X divertor takes advantage of this magnetic configuration which confines the plasma in a natural way. This means that the confinement region is either defined by the separatrix, i.e. the last closed magnetic surface of magnetic islands, or by an ergodised boundary with remnants of islands. Appropriate positioning of target plates relative to the magnetic field lines allows the particle and energy flow from the plasma to be controlled. Investigation of the interaction of the plasma with the divertor is an essential part of the scientific programme of W7-X.

Design of the in-vessel components therefore needs to be flexible for further modifications. The basic installation will be an "open divertor" capable of continuously handling the full power of 10 MW.

### 3.3.2. *Target plates*

With two target plates per divertor unit, a total of twenty target plates will be arranged along the plasma column to cover an area of 22 m². Their exact position and shape were chosen to intercept the particle flow from the plasma along the open flux bundles at the boundary at a maximum distance from the confinement region.

To limit the heat load to below 10 MW/m² the focus area is adjusted to achieve a small incidence angle of 1-3° at the target plates. In addition, the size of the target area must be large enough to allow operation of W7-X throughout the full magnetic configuration within the range of the rotational transform from 5/6 to 5/4.

The 3D-shaped surfaces of the target plates are approximated and composed of five standardised plane elements with dimensions ranging from 55x270 mm² to 55x500 mm². Flat carbon fibre composite (CFC) tiles are brazed or welded to a cooled support structure. Different cooling concepts and material combinations have already been manufactured and successfully tested at a stationary power load of up to 12 MW/m$^2$.

The surface temperature of CFC must be limited to 1200° C. This temperature is determined by the thermal conductivity of the CFC material and cooling structure. So far, titanium zirconium molybdenum (TZM) and copper alloys (CuCrZr and glidcop) have been tested as structural material for the water-cooled support of the tiles. For TZM the thickness of the CFC tiles is limited to 5-6 mm. The better thermal conductivity of the copper alloy would allow the CFC thickness to be increased up to 10 mm, giving a greater safety margin against erosion. The test results of two prototypes using the CFC material SEPN11 agree with thermal calculations. Tests with a third sample using a CFC material from a different source could not confirm the higher thermal conductivity quoted by the manufacturer. Further prototypes were manufactured with four parallel swirl-cooling channels.

The water cooling of each divertor unit is divided into 5 circuits to reduce the diameter of the pipes and allow economic distribution of the cooling water according to the actual heat load. In order to remove a total heating power of 15 MW a water flow of up to 3000 m$^3$/h is required. The pressure in the water cycle was optimised to have sufficient heat transfer in the cooling channels of the support structure and suppress boiling at temperatures of up to 150° C. As a result the water will enter the divertor at a pressure of 24 bar and leave it at 10 bar.

To verify the thermodynamic calculations and get experimental data in the highly turbulent flow regime, a test arrangement reproducing the flow channels of the target elements and a representative manifold for the water distribution was manufactured and tested.

The thermodynamic and hydraulic design of the target elements and the test results are now being discussed with members of the divertor group of TORE SUPRA at CEA, Cadarache. As next step, construction and testing of a prototype target module consisting of 10–15 target elements are planned.

### 3.3.3 *Baffle and wall*

To control the neutral particle flux and avoid back-diffusion of neutralised particles, baffles are installed in front of the target plates. The baffle elements cover a total area of 30 m². The wall of the vessel spans a total area of approx. 150 m². In principle, the baffle plates and wall protection will be based on a similar design. The conventional concept uses flat carbon tiles clamped on a water-cooled structure. To reduce the number of tiles and simplify mounting within the plasma vessel an alternative concept is favoured. Panels with a larger area, integrated cooling circuits, and a surface coating of low-Z material are now under development. With this approach 1,500 elements are sufficient to cover the wall.

Larger prototype panels with integrated water cooling and surface layers of $B_4C$ have been ordered from industry. The coating will be applied by vacuum or atmospheric plasma spray techniques. In a supporting test programme the Materials Research Division of IPP will analyse the physical properties of the plasma-facing surfaces.

Depending on the local requirements and constraints within the vessel and to protect specific areas which may be hit by the beams of the ECR, NBI and ICR heating systems, the final design will apply a combination of these concepts.

### 3.3.4. *Pumping*

Vacuum pumps are required to evacuate the plasma vessel to a level of less than $10^{-8}$ mbar before plasma operation, to pump out neutral particles from the divertor chamber, and to control the density of auxiliary gases injected into the divertor chamber. For that purpose, the pumps must be able to produce the high vacuum and have a high pumping capacity at intermediate pressures. Additional cryo-pumps behind the divertor allow the pumping capacity to be increased during high-density plasma discharges, e.g. during injection of neutral beams or pellets. In such cases particle fluxes of $5x10^{21}$ s$^{-1}$ have to be handled at pressures of about $10^{-3}$ mbar.

Turbomolecular pumps (TMP) and corresponding backing pumps will be connected to the 10 divertors and will continuously provide the basic vacuum. Each pumping set will consist of a TMP with an effective pumping speed of 4200 l/s for $H_2$ backed by a Roots pump with a capacity of 1000 m$^3$/h and a rotary pump with a capacity of 65 m$^3$/h. The rotary pumps and the Roots pumps have already been delivered.

The gas flow from the divertor chamber will be directed to the TMPs by two symmetrically arranged pumping ducts and can be controlled by butterfly valves. The stray field of the W7-X magnets imposes restrictions on the positioning of the TMPs and the routing of the pumping ducts. For that reason, a test programme was run with TMPs from three manufacturers. When a magnetic induction of only 5 mT was applied, the induced eddy currents in the rotating parts already resulted in unacceptable degradation of the pumping capacity and excessive overheating. Eventually, further tests or magnetic screening of the pumps will be necessary.

The cryo-pumps consist of four cryo-panels per divertor and will be positioned between the diagnostic ports. The cryo-pump system will be designed for a total pumping capacity of 150,000 l/s for a duration of 2 hours and is to be recoverable within a short time. Freezing argon onto the cryo-panels or coating them with activated carbon allows helium to be pumped.

### *3.3.5. Mounting of in-vessel components*

Mounting of the in-vessel components at the wall of the plasma vessel was studied in detail. Precise orientation of the target plates with respect to the plasma calls for tolerances of less than 0.5° and radial displacements of below 2 cm. In addition, misalignment of the in-vessel components due to deformations of the plasma vessel by thermal contraction must be avoided. The temperature of the plasma vessel will therefore be stabilised. This is done by a water-cooling circuit on the outside of the vessel wall. The cooling cycle is designed to keep the wall below 60° C and remove up to 300 kW of heat which may be conducted to the wall from the hot in-vessel components. This installation also allows the wall protection to be operated at a temperature of 150° C, which may be favourable for physical reasons.

### *3.3.6. Divertor diagnostics*

The diagnostics required to operate and protect the divertor are designed by the Plasma Diagnostics Division, Berlin. These include facilities for thermography, thermometry, water flow control, and measurement of thermo-currents. Supplementary diagnostics, described in detail in the section W7-X Diagnostics, will be used to provide physical data on the plasma boundary and interacting areas.

Thermographic observation of the target plates is to be done with uncooled bolometer arrays with sensors operating in the micrometer-wavelength region. Such sensors were recently developed. In contrast to ordinary CCD cameras, they allow temperature changes to be detected already at lower temperatures. First experiments with a commercially available infrared camera were conducted in order to examine the spatial and temporal resolution of such uncooled bolometer arrays and check operation at higher temperatures and in a magnetic field.

In particular, operation of the camera in a magnetic field is critical and needs further development of the electronics. At present, the locations of the cameras are being considered in view of the costs of necessary accessories. Further activities focus on data storage and processing in real-time. Hardware and software components considered as candidates using the Windows NT and LINUX PC operating systems will be tested.

To control the cooling water and make the calorimetric measurements, a conceptual design including the architecture of the data acquisition system has been proposed. The technical components of the proposed PROFI bus system will be ordered and tested. This system is regarded as a model for real-time processing of diagnostic data with the possibility of data visualisation.

There are several options for measuring the currents to and the electrical potential of the insulated target plates. The preferred solution is to use the resistance of the cooling-water pipe connection to measure the current to the target module. The conductivity of the cooling water as a resistance parallel to the pipe needs to be considered to correct the measurements. A high-current generator was developed and built to simulate the expected currents to a target module.

## 3.4 Control System

The W7-X experiment will be controlled by a master control system with local controllers for all subsystems such as magnets, cryogenics, heating units, diagnostics, and data acquisition. The local controllers will run automatically according to predefined routines and parameters, which will be set either locally during commissioning and testing or from the master control system during the individual experiment.

W7-X allows plasma discharges with a duration of up to 30 min. A large number of different scientific measurements will therefore be made during one discharge. In order to structure the experiment, plasma discharges will be divided into experimental segments of variable duration. A "segment programme" defines the rules and parameters which determine the state of each unit as far as it is relevant. During each of the segments these rules and parameters of the system will be kept constant.

The segment concept will also be extended to other W7-X operations such as conditioning and calibration of diagnostics. An additional control level will be introduced to manage the sequence of segments during different phases of the experiment.

Programmable Logic Controllers (PLCs) will be used mainly to control those machine components and diagnostic systems which do not require short response times. Segment processing and fast feedback control, which require data processing in real time, will be performed by PCs running the VxWorks operation system. Standard PCs running general-purpose operating systems, e.g. Windows NT, will be used to provide the man-machine interface for commissioning, testing, programming the segments, and supervising and

controlling automatic operations and discharges. Hard wiring will be used for interlocks with high safety relevance. A simple prototype featuring basic functions of the control system was constructed to develop and test the concept and components and identify areas which need further development.

Internet methods, particularly the TCP/IP protocol on Ethernet, are widely used by industry for different control purposes. It is intended to use this type of network also to exchange data between real-time computers and the PLCs on W7-X. Trials showed that data can be successfully exchanged via the Internet between a Siemens S7 PLC and a PC running VxWorks and using the UDP protocol. With UDP on a dedicated fast Ethernet it is possible to exchange data between two PCs under VxWorks with a time-lag of the order of 100 µs only. It is also planned to use this technique for an event-messaging system and periodic distribution of measured data to controllers.

The development of the control system has to take into account the long construction period and lifetime of W7-X and hence react flexibly to the rapid progress in computer technology. To allow easy extension and updating of the system by replacement or addition of components, a mechanism has been developed for installing driver software in VxWorks. Object-oriented software development using the StP computer-aided software engineering tool and the C++ programming language has been started.

Precise timing and synchronisation of all actions on a time scale of microseconds are essential for operation of W7-X. The concept of a Trigger-Timing-Event system with a central clock, a message manager, and signal distribution along glass fibres has been specified. In co-operation with the university of Rostock a prototype unit is to be developed.

### 3.5 W7-X Assembly

An essential feature of W7-X is its modular design, which could be adopted for a later reactor. Basically, the assembly of the cryostat is performed by joining five prefabricated modules to a torus. Each module is composed of two half-modules which are symmetric to each other. The specific arrangement of the coils only allows the modules to be moved radially towards their final positions in the torus.

The concept of the assembly is currently being studied in detail. A paramount necessity for W7-X is to ensure the required accuracy of the magnetic field. As a consequence, an accuracy of the order of 0.1 mm/m has to be achieved for the positions of the individual coils. This requirement calls for precision machining of the interfaces of the coil casings as well as of the supporting structure and for control of the assembly by computer-controlled theodolites.

The small clearance between the coils and the plasma vessel means that the plasma vessel of each half-module has to be divided to allow the coils to be strung across the vessel. A CAD study is being performed to model the mounting sequence and define the optimum size of the plasma vessel segments and thermal insulation.

Specific mounting platforms and handling devices are being designed to assemble the half-modules and modules.

The present assembly sequence is as follows: First the coils of one half-module are pre-mounted and adjusted to the coil support structure, dismantled again, and strung across the plasma vessel. After the coils are again attached to the support structure, the thermal protection is mounted and the coils are electrically connected.

Next, two prefabricated half-modules are joined. Finally, the assembly is lifted into the outer vessel, the cryostat is closed, the ports are welded, and the thermal protection is completed. After a leak test, the divertor and other in-vessel components are installed. Fully equipped and tested modules are transported to their final position on the steel foundation in the experimental hall.

## 4. HEATING SYSTEMS

### 4.1. ECRH

ECRH is the main heating system for start-up and during the initial operation phase of W7-X. ECRH will provide 10 MW of heating power continuously at 140 GHz. The ECRH system is being developed and provided by FZK as a joint project with IPP, IPF Stuttgart, CRPP Lausanne, involving strong industrial participation. The "Projekt Mikrowellen-heizung für W7-X" (PMW) at FZK co-ordinates all engineering and scientific activities in the laboratories and industry.

The microwave power is generated by 10 gyrotrons with 1 MW of output power each. Gyrotrons with the required performance are being developed in Europe, the US, and Russia. The European R&D programme started in 1998 and combines the expertise of European industry and the research laboratories. The design of the first prototype gyrotron was completed. The gyrotron operates with a $TE_{28.8}$ cavity mode converted to the required Gaussian output mode by an advanced quasi-optical converter. The tests of the different components at low RF power showed good agreement with the design.

The gyrotron incorporates a depressed collector for energy recovery which increases the efficiency to approx. 45%. The RF microwave beam is extracted from the gyrotron horizontally through an edge-cooled diamond window. Its excellent heat conduction and low microwave losses make diamond particularly suited to transmission of microwaves.

A first prototype gyrotron (Maquette, see Fig. 3) was built by TTE and delivered to FZK in autumn 1999 for conditioning and tests.

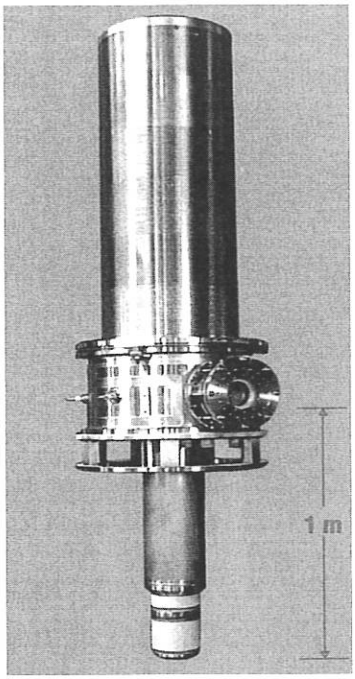


*FIG. 3: First prototype gyrotron, "Maquette".*

The test facility at FZK was upgraded to allow testing of the gyrotron for 3 min at a power of 1 MW. The test stand is also used for stationary tests of auxiliary systems such as the water cooling, the HV installation, a dummy load, and different RF techniques. Although most of these components are prototypes, they are designed for their nominal operation in the final installation at Greifswald. After successful testing of the prototypes series production of these components will be contracted out. The water cooling, high-voltage installation, and power supply for operation of the depressed collector have already been successfully tested. Work on the hardware and software of the protection system will be continued. A breadboard version is ready for test measurements with Maquette.

Testing of the gyrotron is now postponed because the superconducting magnet for it was damaged during transport to FZK and needs major repair.

IPF Stuttgart is responsible for the conceptual and engineering design and supervision of the construction of the transmission system as well as for the ECRH-specific HV system. The conceptual design of the quasi-optical transmission system was completed on schedule and the detailed design phase has started. A full-scale prototype transmission line is being built up at IPF. Major components were fabricated. Low power testing of the mirror components was very promising. All mirrors have to be water-cooled. The finite-element investigations on thermomechanical properties of the mirrors were finalised and an optimum concept with respect to mechanical rigidity under steady-state thermal loading and acceptable fabrication costs was found. First samples of full-sized water-cooled mirrors are under construction. Positive results were also obtained with a self-check system for alignment and positioning of the individual mirrors.

Work on the high-voltage supply for the depressed collector, the cathode heater, and the protection system was continued and a first prototype of the power supply was installed at the FZK test stand and successfully tested.

At IPP, ECRH work concentrated on design of the in-vessel components such as the quasi-optical launcher, imaging mirrors, and the appropriate plasma diagnostics. The different alternatives studied have to consider the special shape of the plasma vessel and the limited space for protection of the first wall.

## 4.2 ICRH

The design of ICRH for W7-X has not yet started. Major interfaces to the machine, the high-voltage power supply, and the building were defined to allow later installation of the ICRH components. As a basis for the application of ICRH, a contract was placed to develop a 3-dimensional ICRH code for the non-axisymmetric stellarator geometry of W7-X.

## 4.3 Neutral Beam Injection

Neutral beam injection is envisaged in W7-X for bulk heating of the plasma in the high-density, high-ß regime. A neutral beam power of up to 20 MW will be delivered by two injector boxes of the ASDEX Upgrade type for pulse lengths of up to 10 seconds. The beam lines will be equipped with RF sources, developed for and recently put into operation on the second injector of ASDEX Upgrade.

In 1999, the first two PINI (including extraction grids and main insulators) were delivered. In addition, the cooling-water pipes between the NBI building and torus hall have been installed. The detailed design of the portholes for stage I/II NBI has been finalised. Some recent modifications have improved beam transmission through the ports, now making it comparable to that in ASDEX Upgrade.

Furthermore agreement has been reached for the design of the tangential ports in order to allow for a later accommodation of high energy neutral beam heating.

# 5. AUXILIARY SYSTEMS

## 5.1 Refrigeration System

Manufacture of the storage vessels for gaseous helium proceeded as scheduled. Liquid-nitrogen and liquid-helium storage tanks with capacities of 30,000 l and 10,000 l were ordered. Alternative thermodynamic studies were performed to supply the approx. 430 cooling circuits of the magnet

system with liquid helium. These concepts will now be evaluated in respect of economy, operation, and assembly.

## 5.2 HV Power Supply

The power requirements of Greifswald Branch of IPP amount to approx. 48 MW and will be provided by the local 20 kV grid and a dedicated 110 kV junction of the Mecklenburg-Vorpommern grid. The ECRH, ICRH, and NBI heating systems will be powered by a DC high voltage. For that purpose, power from the main 110 kV supply will be transformed and rectified to the required DC voltage and distributed by a switchgear to the different users.

The different power requirements of the heating systems call for a modular design of the DC high-voltage power supply. Eight modules are designed for a DC voltage of 65 kV to supply gyrotrons continuously with a current of 50 A. Alternatively, always two units can be connected in series to deliver current pulses of 130 A at a voltage of 130 kV for the NBI injectors.

The two generators for ICRH are supplied by two additional power supply units. These units are designed for a voltage of 32.5 kV and 160 A pulses with a length of 15 s every 3 min. These units can alternatively be connected in series to provide 65 kV, 100A to operate the remaining two gyrotrons continuously. The Thomcast/Siemens consortium will deliver the high-voltage power supply, which uses the advanced pulse step modulation (PSM) technique. This technique uses up to 84 voltage stages of approx. 0.8 kV height and variable pulse length to adjust and control the output voltage.

In the switchgear, the high voltage from the ten power supplies is distributed to the different users, which are connected by tri-axial cables with appropriate damping elements at both ends. To allow for the different switching combinations of the units, polarities and grounding of individual units need to be changed.

## 5.3 Cooling-water System

The power which needs to be removed from the gyrotrons, NBI injectors, and ICRH sources depends mainly on the efficiency of the gyrotrons and will amount to some 28 MW during a pulse length of 30 min. This pulse length far exceeds all relevant time constants of the plasma experiment and hence is sufficient to demonstrate steady-state performance of W7-X. The technical solution consists of two reservoirs of 1200 $m^3$ each which are re-cooled by cooling towers. During long-pulse operation cooling water is circulated from the cold reservoir through the experiment and back to the second reservoir with a temperature rise of up to 15° C. Between the experimental phases the water reservoir is re-cooled at a rate of 5.5 MW. This arrangement allows two full-power pulses of 30 min duration twice a day and pulses of 10 s every 5 min in between. Additional water cooling circuits are provided for the auxiliary systems.

# W7-X DIAGNOSTICS

(Head of Project: Dr. Hans-Jürgen Hartfuß)

**Experimental Division 3**: M. Anton, R. Brakel, M. Endler, S. Fiedler, C. Fuchs, J. Geiger, L. Giannone, P. Grigull, H. Hartfuß, M. Hirsch, R. Jaenicke, M. Kick, S. Klose[1], K. Knauer[1], G. Kühner, K. McCormick, A. Weller, C. Wendlandt[1], A. Werner, E. Würsching

**Experimental Division 4**: J. Baldzuhn, R. Burhenn, R. König

**Plasma Diagnostics Division:** C. Biedermann, D. Hildebrandt, M. Laux, D. Naujoks, R. Radtke, U. Wenzel

**FZ Jülich:** W. Biel, G. Bertschinger, P. Mertens, A. Pospieszczyk, B. Schweer

## 1. OVERVIEW

The work concentrated on the definition of a diagnostics set with sufficient redundancy and complementarity and its proper positioning at the machine. The port design of the 160 ports foreseen considers the needs and demands of the diagnosticians. Search for standardized solutions of the diagnostic electronics and the computer control has been started. The work is documented in the KRONODOC system accessible via the internet and the IPP home page. The following chapters summarize the work of the projects nine subgroups in brief status reports.

## 2. STATUS REPORTS OF SUBGROUPS

### 2.1 Fluctuations

A large number of the proposed diagnostics for W7-X are capable of delivering data on plasma turbulence. The most important amongst them are Langmuir probe arrays, magnetic Mirnov probes, $H_\alpha$ detectors, reflectometry, ECE and SX diagnostics, and some spectroscopic and atomic beam diagnostics. While the individual diagnostics are designed in the specialists groups, the fluctuations subgroup defines the requirements on the background of turbulence theory and proposed possible experimental programs. A catalogue of physics questions has been formulated starting with topics of interest for all types of fusion experiments and ending up with W7-X specific ones. Answers to these questions are important for the description of turbulent transport in edge transport codes which in turn are crucial to understand and to model the edge and divertor physics in W7-X. It is being discussed whether the proposed set of fluctuation diagnostics can provide the experimental information to answer the questions.

### 2.2 Plasma Edge

The subgroup coordinates the development of a large number of diagnostics able to collect information about the polymorphic plasma edge of W7-X. The aim is to get the necessary redundancy and complementarity in information to describe adequately the 3D SOL and the 2D deposition zones at the targets. Again, most of the diagnostics, i.e. Thomson scattering, bolometry, spectroscopic diagnostics are developed in the specialists groups while the Langmuir probes standard edge diagnostics are acquired by this group as well as atomic beam and high resolution divertor spectroscopic methods. The problem to describe the plasma edge in non-axisymmetric stellarators is very complex. Nevertheless, an interplay of various diagnostics at different magnetic field periods but at topologically equivalent positions allows to do it with a certain degree of redundancy if stellarator symmetry is preserved. With the symmetry broken due to misalignement of targets, SOL bifurcation etc. it becomes impossible. This underlines the importance of tools for supervision and control of the SOL symmetry. In the conceptual design of the edge diagnostics it is foreseen that the SOL symmetry is supervised by 2D imaging cameras (thermography, spectroscopy) viewing the targets in each divertor module. Target integrated pop-up probe arrays and various $H_\alpha$ diagnostics will allow for the comparison of different divertor modules. The other edge diagnostics, Thomson scattering, fast reciprocating Langmuir probes, divertor bolometry, SOL and divertor spectroscopy and atomic beam spectroscopy are distributed around the torus according to available ports and space. Full stellarator symmetry supposed, the set-up is rather comprehensive but complementarity as well as redundancy of single module diagnostics is not yet satisfactory. Due to access limitations only little chance is seen to completely overcome the shortcomings but gradual improvement seems possible by sharing ports for different complementary diagnostics.

## 2.3 Microwave Diagnostics

The subgroup develops the diagnostics in the mm-, the sub-mm and the IR wavelength regions. It is foreseen to install a ten-channel IR laser interferometer, a combined single channel submillimeter interfero-polarimeter, an ECE radiometer, and various mm-wave reflectometers. Later extensions of the ECE radiometric systems to correlation radiometers and extremely fast swept reflectometers will especially concentrate on fluctuation measurements. The $CO_2$ laser interferometer works at 10.6 μm which makes refraction negligible. The moderate phase shift requires highly sensitive phase measurements but reduces fringe jump perturbations. The total round trip phase shift through the plasma might be comparable to phase changes from mechanical vibrations, which makes compensation with a two-colour scheme necessary. Long pulse operation requires a robust measurement of the line-integrated density for discharge control purposes. A Cotton-Mouton polarimeter operating at a probing beam frequency of about 1 THz can provide it. An ammonia twin laser system generating also the elliptical modulation necessary for the planned detection scheme is foreseen. The multichannel ECE radiometers will be extremely wideband heterodyne systems. A prototype covering the full temperature profile with 32 channels has already been built up. As a feature, 16 narrow spaced channels can be shifted to any radial position allowing for measurements with maximum radial resolution. Concerning the reflectometers sightlines have been defined both for high field side and low field side launch chosen to complement profile information as obtained by the Li-beam diagnostic. Probably heterodyne reflectometers operating in X-mode polarization will be designed. It has not been decided yet which type of reflectometer will be used, AM, FM CW etc. Because of the progress both in mm-wave technology and reflectometer development, it will be decided as close as possible to the experimental start-up of W7-X.

## 2.4 Charge Exchange Diagnostics

The energy spectrum of plasma ions neutralised by charge exchange will be measured with a number of neutral particle energy analysers to determine the ion temperature and generally the ion energy distribution function especially during NBI and ICRH heating where strong deviations from a Maxwellian are expected. A diagnostic neutral beam injector will be used to increase the neutral particle density allowing for local measurements i.e. the ion temperature profile. Five lines of sight are planned with five individual analyzers for a simultaneous measurement. With long pulse operation this multilocal measurement can be replaced by moving the lines of sight along the beam axis viewing it from nearly perpendicular to the magnetic field. It is planned to operate the analyzers with parallel electric and magnetic fields for a simultaneous measurement of hydrogen and deuterium. The upper energy limit will be in the order of some 100 keV. It is being discussed whether a modification of the extraction grid system of the W7-AS power injectors can meet the requirements of the diagnostic beam injection system especially with respect to smaller beam divergence.

## 2.5 Spectroscopy

The extensive number of spectroscopic diagnostics foreseen can roughly be split into two groups, one mainly dealing with the investigation of the core plasma, the second one concentrating on the plasma edge. For local measurements several active diagnostics will be available on both regimes. A CXRS system with a dedicated diagnostic neutral beam will be employed for the determination of ion temperature, low-Z impurity density, and poloidal and toroidal rotation velocity profiles. The attenuation of the diagnostic neutral beam and the composition of the energy fractions in the beam will be determined experimentally via beam emission spectroscopy. From visible bremsstrahlung observations in a tangential line of sight $Z_{eff}$ will be deduced. For an investigation of particularly the medium and high-Z impurities in the bulk plasma, a number of VUV spectrometers is proposed. A bor, carbon, oxygen monitor and two low resolution SPRED systems, covering the wavelength range from about 10 to 200 nm, will serve as impurity monitors and for transport studies. These are complemented by two high resolution grazing incidence spectrometers allowing for detailed studies in the range from 1 to 250 nm. A high spectral resolution X-ray imaging crystal spectrometer will provide information on impurity content and impurity transport as well as on electron and ion temperatures and on plasma rotation, while a ten-channel Bragg spectrometer fan will be utilized to measure radial density profile evolutions of different ionisation states of various impurity species with high time resolution and sufficient spatial resolution for Abel inversion. The island divertor plasma will spectroscopically be diagnosed mainly in the visible. Initially a number of imaging systems consisting of 2D CCD-cameras equipped with $H_\alpha$ filters will be used to look for possible toroidal asymmetries. Some of these systems will later be equipped with beam splitters and further interference filters for CII and/or CIII and $H_\gamma$ allowing to determine simultaneously the local hydrogen and carbon influx with high spatial resolution and also to derive locally the degree of detachment from the intensity ratio of $H_\alpha/H_\gamma$ across target plates. High spectral and spatial resolution of the visible spectroscopy will give detailed information on the processes at the interaction zones of the islands with the target plates. These will be complemented by active divertor diagnostics like the thermal He-beam and laser induced fluorescence. A large number of video cameras distributed around the machine are proposed mainly for operational purposes, i.e. to get immediate information on plasma position, configuration and possibly interaction with in-vessel components. The total radiated power will be measured by two bolometer arrays probably on the basis of metal resistor detectors. Development of the bolometer electronics and tests of alternative detectors are already in progress.

## 2.6 Thomson Scattering

Three different Thomson scattering systems are being planned for W7-X. For the bulk plasma, as the robust standard diagnostic, a Nd-YAG laser system is foreseen to measure the electron temperature and density profiles. The set-up is planned to deliver profiles in real time to allow for online plasma

monitoring and profile shape event recognition. A second system is especially dedicated to the divertor region. The laser beam will be movable in radial direction to investigate 2D structures in front of the divertor surfaces i.e. island structures in the divertor region. Experimentally the idea is to employ a frequency doubled Nd-YAG laser to avoid interference with the blackbody radiation of the divertor plates. The third system uses a ruby laser. It will be placed in a local minimum of the B-field close to the ECRH deposition planes. The scattering distribution function will be measured with high spectral and spatial resolution. The motivation is to look for small spatial structures as well as for distortions in the electron distribution function. The high resolution system employs CCD-cameras operating in the visible, it is being discussed whether the experimental set-up can be used as well to measure the dye laser excited $H_\alpha$ resonance fluorescence to determine the neutral hydrogen density at the plasma edge.

## 2.7 Soft X-Ray and Electromagnetic Dignostics

The X-ray measurements will basically provide information on plasma equilibrium, MHD instabilities, electron temperature, impurity content, and impurity transport. To achieve images of the 2D X-ray emissivity and hence the magnetic topology, a multi-camera tomography system is proposed installed inside the vacuum vessel. This sets constraints on the usage of detectors and in particular on changing filters. A second conventional flexible camera system is proposed with the possibility to adjust the spectral range by interchangeable energy filters enhancing the sensitivity for particular impurity species to tailor the radial emissivity profile for equilibrium and MHD mode analysis and to derive the electron temperature according to the 2-foil absorption method. In addition pulse height analysis systems are being planned to investigate the X-ray spectra in various energy bands providing necessary data for the interpretation of the radiation profiles obtained with the camera systems. Electromagnetic diagnostics measure the magnetic fields produced by currents inside the plasma. The standard method to do this is to use coils or loops outside the plasma and integrate the induced voltage to obtain the magnetic flux through the coil. Various types of coil arrangements like Rogowski coils, diamagnetic loop, saddle coils, flux loops, and poloidal magnetic field coils exist to measure different aspects of the plasma current distribution such as total current, diamagnetic current, or dipole moment of the parallel currents. The whole set of measurements will be used for equilibrium identification. In addition Mirnov coils will be installed to investigate instabilities. Challenges due to properties of W7-X are the reduced parallel currents and the planned long-time discharges which require electronic integration of extremely small signals. The most severe restrictions are imposed by the limited space available inside the vacuum vessel.

## 2.8 Heavy Ion Beam Probe

The heavy ion beam probe is a unique diagnostic to measure the local plasma potential. On the basis of 3D orbit calculations, the port geometry of the beam injection and detector ports has been determined for a primary beam species of $Cs^+$ ions with 3 MeV energy. An optimization with respect to best access, minimum necessary beam energy, and maximum detectable plasma region has been performed. Three ports at W7-X are modified to meet the demands. An alternative use of the accelarator for basic research is being discussed.

## 2.9 Neutron Diagnostics

W7-X deuterium plasmas are estimated to generate $10^{12}$ to $10^{16}$ neutrons per second depending on the heating scenarios allowing to evaluate information on plasma parameters like ion velocity distribution, deuterium density as well as MHD activity and the thermal reaction fractional contribution in the neutron emission rate and the energy distribution. The time dependent total reaction yield will be measured with various neutron counters and time integrated with an activation system. Time-of-flight spectrometry will be used to evaluate the central ion temperature, high energy tails, and thermal reaction fractions. A fast profile camera is planned to measure neutron emission profiles. Provisions are suggested for measurements of gamma radiation and charge fusion products.

# 3 DATA ACQUISITION AND CONTROL

The operation of a diagnostic system requires an exchange of information between a variety of logic units amongst which the specific components of an individual diagnostic, the data acquisition system and the central machine control system are the most important ones. Strongly supported by the groups responsible for experiment control and data acquisition, discussion started to define the individual requirements to these logic units for each diagnostic as a first step towards the design of the interfaces. The control signals between the units including their properties with respect to speed and security will have to be defined in the next step. An important point in the discussion is, how responsibilities should be distributed amongst the diagnosticians, the control, and data acquisition groups. Since W7-X will be operated in continuous mode, all diagnostic systems must be able to acquire and to store data continuously. A common clock will be used to synchronize data taking and provide time stamps for data samples. The complete history of all acquired data and control parameters will be stored in an appropriate central data server. A significant effort is necessary to reduce the streams of data at the sources to a relevant portion. The strategy is to fraction the data streams by multiple buffering into time intervals having physical significance and to decide by pattern recognition methods which intervals to keep or discard. The pattern recognition possibilities shall be used too for advanced feedback facilities. In order to provide an overview of the discharge history as well as a possiblity for data base searches, a continuous but strongly reduced stream of data will be stored independently of the above mentioned selection procedure. This reduced stream is intended as the basis for on-line monitoring of the experiments for the general user. The latter is viewed at as being principally remote which has consequences for the possibilities of participating in the experiment planning, monitoring and off-line data analysis.

# WENDELSTEIN 7-AS

(Head of Project: Dr. Rolf Jaenicke)

Members of the W7-AS group: see section "Divisions and Groups, Experimental Plasma Physics Division 3".

## 1. OVERVIEW

The experiments in W7-AS with 10 control coils, which were installed during 1998 as the first step to the future island divertor, were concluded. The effectiveness of the control coils could be demonstrated in various important fields:

- The possibility of increasing the plasma radius was verified. The compensation of the natural islands in the case of iota = 1/2 through the control coils and thereby the extension of the undisturbed flux surfaces up to the limiter allow for the first time a direct comparison of the energy content at equal plasma radius between iota = 1/2 and iota = 1/3. As a result, a better extrapolation is possible to the conditions in W7-X.
- Measurements with the poloidal Langmuir probe array showed that while ramping the control coil current the footprints of the islands behaved as expected from vacuum field calculations.
- By means of the control coils the ratio of perpendicular to parallel transport within an island could be changed by a factor of 2.
- The high recycling conditions achieved in the first experimental campaign with its very open "divertor structure" showed that there are good prospects for a large range of conditions for successful studies of a closed island divertor in the second experimental campaign.

In the middle of August 1999 the experiments on W7-AS were shut down as planned and the machine was opened. This was done to carry out the second step of the project "Divertor Experiment at W7-AS", which involves the installation of divertor modules, titanium getter pumps and divertor diagnostics. It will be completed at the end of June 2000. With this divertor a better density control is expected as well as a reduced impurity content and the ability to control larger heating power, that can lead to higher $\beta$ values and a higher density limit.

Attainment of higher $\beta$ values is also the reason, why the four counter injectors of the neutral injection heating system will be converted into co-injectors, so that after re-starting eight injectors are at disposal which inject all in the same direction tangentially to the magnetic field. Considering the decisive role of the radial electrical field for the neoclassical transport, a radial injector is added to the machine. This permits both to modify the radial electrical field inside the plasma and measure - as a diagnostic injector - the radial electrical field in the plasma centre.

A new H-mode window was found at iota = 5/9, which is marked by for distinctive transitions and better confinement times. With a new high spatial resolution Ruby Thomson scattering system, unexpectedly steep density gradients at the edge during the H-mode were measured.

The ECRH and ECCD experiments mainly concentrated on the phase space interaction of electrons with high power ECRH. In particular, different launch scenarios and non-linear effects were investigated.

With the double-loop antenna better fitting to the plasma surface significantly higher power could be coupled to the plasma. With ICRH minority heating, the energy of an ECRH plasma could be increased from 10 to 15 kJ. With ICRH alone, a plasma with 10 kJ was achieved.

## 2. EXPERIMENTAL AND THEORETICAL RESULTS

### 2.1 Boundary Layer Studies

#### *2.1.1 Effects of the new control coils*

In preparation for divertor operation starting next year, a set of 10 control coils was installed inside the machine, giving ample control on critical aspects of the island geometry, albeit still using the set of 10 inboard sector limiters instead of the real divertor.

First tests with the control coils proved their ability to influence the plasma edge. Vacuum field predictions of effective plasma radius changes as a function of the control coil currents were roughly validated via the $W_{dia} \sim a_{eff}^2$ scaling (Fig. 1).

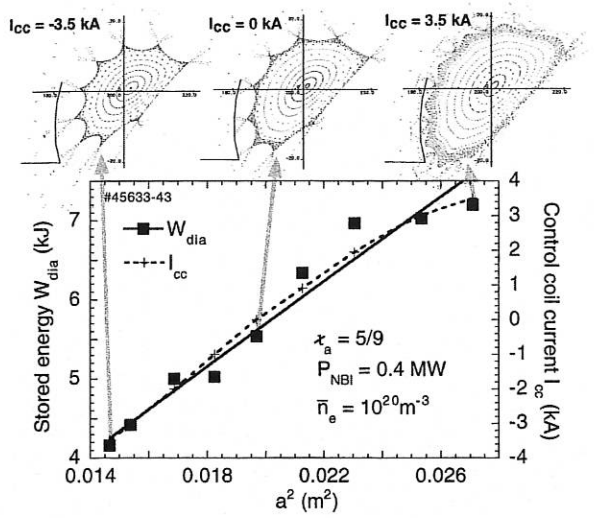


*FIG. 1: Stored energy $W_{dia}$ versus the square of the plasma minor radius a. The latter was varied by the control coil currents $I_{cc}$.*

The ability to vary the plasma radius via the control coils is also clearly visible in the radial electron temperature profiles (plotted as a function of frequency) measured by the ECE diagnostic (Fig. 2a). If particle and momentum transport are assumed to be governed by parallel classical convection with sound speed $c_s$ and perpendicular anomalous diffusion described by a diffusion coefficient D, then the parallel and perpendicular transport time scales can be roughly estimated as $\tau_{\parallel} = L_c/c_s$ and $\tau\perp = 2r_i^2 / D$, with $r_i$ being the island radius, $L_c = R\pi/\Delta\iota_i$ the field line connection length measured from the stagnation point to the target, and $\Delta\iota_i$ the internal rotational transform within an island. With the control coils it was possible to change the ratio of parallel to cross-field transport $\tau_{\parallel} / \tau_{\perp} \sim L_c / r_i^2$ by a factor of 1.8 by increasing the connection length $L_c$ (averaged over the strike point region) from 60 m to 110 m by reducing the control coil current from $I_{cc}$ = -3.5 kA to 0 kA at a fixed X-point height of 3 cm above the inner limiters. The longer $L_c$ resulted, as required for the proper functioning of the island divertor, in a broadening of the power deposition profile (Fig. 2b), and a widening of the $H_\alpha$ emission profiles (not shown) by a factor of 1.6±0.1 and ~1.3 respectively.

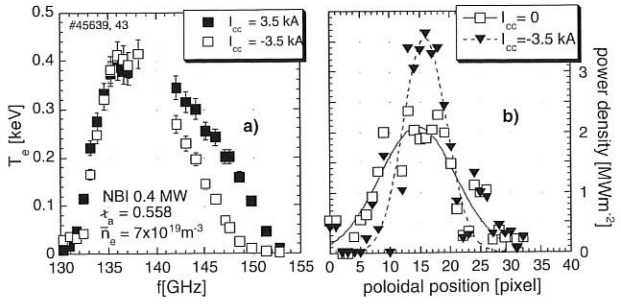


*FIG. 2: a) Radial temperature profiles from ECE at the two extreme control coil currents, and b) broadening of the power deposition (from IR camera viewing an inboard limiter) with increasing connection lengths.*

### 2.1.2 *A new H-mode operational range*

In W7-AS, the occurrence of the quiescent H-mode (H*) is restricted to narrow ranges of the rotational transform. In addition to the already known windows at the edge rotational transforms $\iota_a \approx 0.48$ and 0.52, a new H*-mode range was found in the vicinity of $\iota_a \approx 0.56$, where the configuration is bounded by large magnetic islands of symmetry $n/m$ = 5/9 (Fig. 3). The three windows have in common that the edge region inside the separatrix, which is relevant for transport barrier formation, is free of low-order rationals.

In NBI (0.4 MW) heated discharges with density ramps, the L–H* transition occurs at line-averaged densities $n_e^{thr} \geq 10^{20}m^{-3}$. The gain in the energy confinement time $\tau_E$ within the H* phases is maximum for the high $\iota$ window (up to $\tau_E^{H*}/\tau_E^{ISS95} \approx 2$). Threshold densities as well as $\tau_E$ enhancements in ECRH (140 GHz) discharges are generally lower.

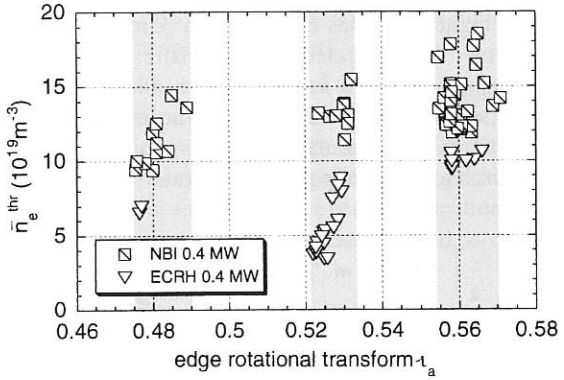


*FIG. 3: Threshold densities for transition to the quiescent H-mode (H*) for NBI and ECR (140 GHz) heated discharges with density ramps. Outside the shaded ranges, discharges stayed at the L-mode or showed dithering and/or ELMy phases in some cases.*

In contrast to tokamaks, the threshold densities increase with heating power, $n_e^{thr} \propto P_h$ (and not the reverse!), for both NBI and ECR heated discharges. The L-H* transitions show well-known signatures indicating rapid establishment of a negative radial electric field and formation of an edge transport barrier extending to about 3 cm inside the separatrix. At fixed heating power, threshold $n_e$ and $T_e$ values measured at about 2 cm inside the separatrix lie approximately on a $T_e n_e$ = *const.* curve. In general, the H* phases are preceded by dynamic phenomena (dithering, ELMs). In contrast to these latter scenarios, which could be stably maintained over many confinement times, H* phases are generally transient: the improved particle confinement leads to a loss of density control, rapidly increasing impurity radiation (mainly from carbon), and subsequent radiative collapse (H*-mode induced radiative density limit).

### 2.1.3 *Edge plasma conditions for boundary island configurations at $\iota_a$ ~5/9*

Plasma-wall interactions are minimized within a divertor when $T_{ed}$ at the target plate falls to values well below 10 eV. This is consonant with attaining high upstream separatrix

densities $n_{e_s}$ and still higher target plate densities $n_{ed}$. The values and relationships among these quantities as a function of heating power have been studied in a preliminary sense using the inner sector limiters, in preparation for the upcoming divertor phase.

Density ramp discharges for $\iota_a \sim 5/9$ at $P_{nbi} \sim 0.4$ MW invariably effect a transition into H* long before $n_{e_s}$ has reached a level consistent with effective divertor operation. Moreover, $n_{e_s}$ decreases at the transition, and the core plasma generally proceeds towards radiation collapse – rendering ELM-free plasmas suitable for neither steady-state core confinement nor acceptable divertor conditions.

Increasing the heating power $P_h$ not only leads to an increase in $n_e^{thr}$ but also in $n_{e_s}$. An example is the comparative behaviour of $n_{e_s}$ vs. the line-averaged density $n_e$ for two levels of $P_{ecrh}$. We find: $n_{es}(10^{19}\ m^{-3}) \approx 0.083\ n_e + 0.33$ ($n_e \leq 8 \times 10^{19}\ m^{-3}$, 0.4 MW) and $n_{es} \approx 0.15\ n_e + 0.6$ ($n_e \leq 10^{20}\ m^{-3}$, 0.8 MW). For $P_{ecrh} \sim 0.8$ MW, due to ELMing activity at higher densities ($n_e > 10^{20}\ m^{-3}$), $n_{es}$ intermittently drops below the indicated characteristic. Nevertheless, whereas $n_{es}$ ($\sim 2 \times 10^{19}\ m^{-3}$) for $P_{ecrh} \sim 0.8$MW and $n_e \sim 10^{20}\ m^{-3}$ is still far below that predicted necessary by EMC3 calculations to consummate divertor detachment, such ELMing discharges are of potential interest:

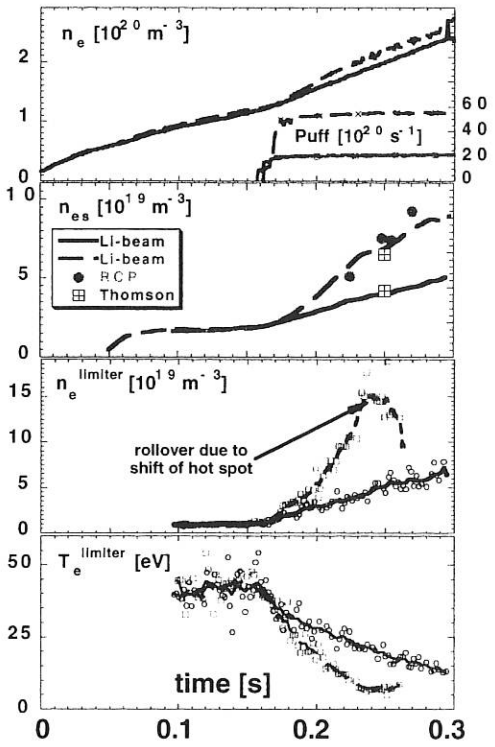


*FIG 4: $n_e$ for two discharges (#47128, 47129) with gas programme as indicated. $n_{es}$ from Li beam (traces), RCP (dots), and edge Thomson (squares). $n_e^{lim}$ and $T_e^{lim}$ at lower limiter from a Langmuir probe. $P_{nbi}$ = 2MW, $P_{abs} \sim 1.8$MW. Electron fuelling rate from NBI is ~2.5 x $10^{20}$ $s^{-1}$. $H^o$->$D^+$.*

They may afford the possibility of avoiding core impurity accumulation and a possible density limit predicted on radiation collapse of the core.

To maximize $n_{e_s}$ it is essential to suppress the H-mode completely, which at $P_{nbi} \sim 2$ MW is the case. Figure 4 depicts features of two density-ramp discharges with the difference being that the 2nd discharge (#47129) had a still stronger gas puff – about 20 times higher than the beam fuelling rate. The consequence of the heavy puff is to enhance significantly $n_{e_s}$ for otherwise the same line density. $n_{e_s}$ approaching 9 x $10^{19}$ $m^{-3}$ is achieved for $n_e \sim 2.5 \times 10^{20}\ m^{-3}$. At the limiter $n_e^{lim}$ exceeds 1.5 x $10^{20}$ $m^{-3}$, with $T_e < 10$ eV. $n_e^{lim}$ follows the characteristic $n_e^{lim} \sim n_{es}^2$, which is weaker than that expected from the 2-point model ($n_e^{lim} \sim n_{es}^3$) for high recycling. The peak density actually achieved cannot be determined since the interaction zone shifted away from the Langmuir probe at higher $n_e$ (verified by $H_\alpha$), causing the rollover in $n_e^{lim}$ manifest in Fig. 4.

## 2.2. Transport and Confinement

### 2.2.1 *Physics of the density limit in the W7-AS stellarator*

Density limit discharges in the W7-AS stellarator, with constant line-integrated density and a duration of up to 2 seconds, were studied at three values of the toroidal magnetic field ( B = 0.8, 1.25 and 2.5 T ). The central factor governing the physics of the density limit in stellarators was demonstrated to be the decreasing net power to the plasma when the radiated power density profile exceeds that of the deposited power density. The peaking of the electron density under these conditions further accelerated the process. In discharges with B = 2.5 T, simulations of the centrally peaked radiation power density profiles could be shown to be due to peaked impurity density profiles which is supported by transport coefficients devived from Laser blow-off measurements. These discharges had the electron density profile form found in the improved confinement H-NBI mode on W7-AS. A comparison of ECRH, NBI and combined ECRH and NBI heating highlights the need to control impurity sources and choose electron densities well below the density limit in order that steady-state operation can be attempted in discharges without ELM's.

A simple model of bulk radiation predicted that the limiting density should depend on the square root of the heating power and this was experimentally confirmed. The magnetic field scaling of the limiting density found experimentally can be recovered when the magnetic field scaling of the thermal conductivity is included in this simple model. The power law fit of $n_e$ with the volume - averaged absorbed power and magnetic field for density limit discharges in W7-AS is shown in Fig. 5.

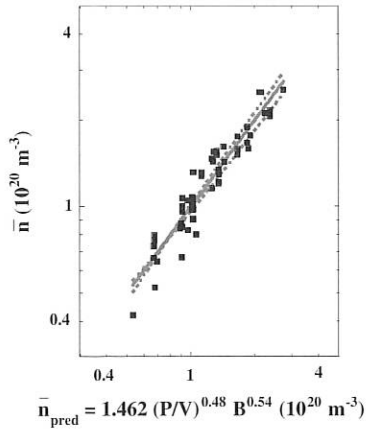


*FIG. 5*

### 2.2.2 *Particle transport studies*

Previously, radially peaked density profiles were found in ECRH discharges in W7-AS. Changes in the central particle source were not significant and do not explain the density peaking. This is evidence for inward particle convection.

A new experiment campaign was carried out in order to further study the peaked density profiles. The ECRH deposition position was scanned from the plasma centre towards the edge. The peaking increases continuously as the deposition position is moved radially outwards. There is no evidence of a critical value of the deposition position close to which the density peaking would be especially sensitive. The plasma density and the ECRH power were varied in order to find parameter dependences of the density peaking. The density profile peaking parameter was found to decrease with increasing heating power. No clear density dependence was found. Strong gas puffing or the connected higher edge density prevents the formation of the peaked profiles. This effect was revealed by an experiment with three different density plateaus (see Fig. 6). The dependence of the density peaking on the gas puff is similar to the reheat effect observed in CHS.

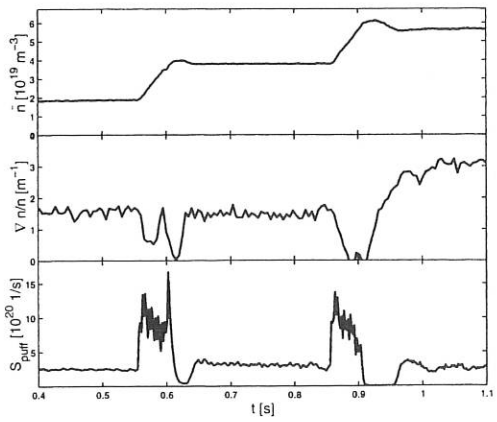


*FIG. 6 The line averaged density (upper frame), the average peaking parameter, n'/n (middle frame) and the total particle source from the gas puff $S_{puff}$ (lower frame) in discharge #46282. The peaking parameter drops rapidly after gas puffing has been started and increases after the gas puffing has been ended.*

### 2.2.3 *Impurity transport*

The derived impurity diffusion coefficients in W7-AS were found to be large in the plasma centre and rather small at the plasma periphery for ECR heated plasmas. The latter determine the impurity influx and consequently the time constant for approaching equilibrium density profiles, being consistent with the observed slow increase of intrinsic impurity radiation (e.g. chlorine) during the discharge on the assumption of a constant impurity source at the plasma edge. In order to confirm the derived transport coefficients at high density and exclude a possible effect of increasing impurity sources with time due to the thermal load to inboard tiles, the transport behaviour of fluorine was investigated in an identical discharge but with a constant external fluorine influx. A similar increase of fluorine radiation during the pulse duration was observed, supporting the earlier statement that transport rather than variations in the impurity source is responsible for the radiation increase. Also the soft-X-ray radiation profiles were fairly well simulated with the experimental transport coefficients.

Furthermore, the dependence of impurity transport on the toroidal magnetic field strength was studied in NBI heated discharges by means of transport analysis of aluminium injection experiments. Investigations at toroidal magnetic field of 1.25 tesla and 2.5 tesla revealed indications of higher diffusion coefficient values at smaller field strengths than expected from theory.

### 2.2.4 *Confinement bifurcation by the bootstrap current*

Confinement in ECR-heated discharges in W7-AS can be well described by a model which assumes enhanced electron energy transport in the presence of rational surfaces and a reduction of enhanced transport with increasing magnetic shear. The model, originally derived from experiments with inductive net current control, has now been applied to scenarios without external loop voltage ("true" stellarator operation) where the plasma current equals the bootstrap current. This introduces an additional degree of freedom, leading to a confinement bifurcation for identical external control parameters. Depending on the initial conditions, the close coupling of transport, bootstrap current and rotational transform profile may shift from unfavourable vacuum field values with densely spaced rational surfaces upwards into the next resonance-free region (high-confinement branch) or not (low-confinement branch).

The basic features of this prediction could be demonstrated experimentally at a rotational transform of the vacuum field of 0.45, with an inductively driven current being applied in the start-up phase as the bifurcation parameter (B = 2.5 T, $P_{ECRH}$ = 400 kW). When the external loop voltage is switched off the plasma current evolves freely according to the L/R time and to temporal changes in confinement. At a critical initial current between 1.5 and 2 kA bifurcation occurs to final states of low ($W_{dia}$ = 3.3 kJ and $I_{BS}$ = 1.0 kA) or high confinement ($W_{dia}$ = 7.5 kJ, $I_{BS}$ = 8.0 kA). The experimental plasma profiles of the bifurcated steady states are in rather good agreement with those calculated from the model (Fig. 7).

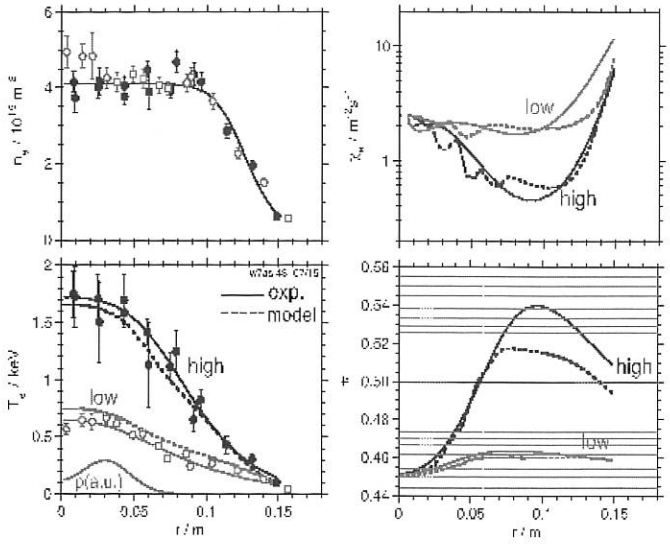


*FIG. 7: Radial profiles for the low and high-confinement states. Dashed lines: model. Solid lines and data points: from Thomson scattering ($\chi_e$ from power balance, $\iota$ from bootstrap current normalized to plasma current). The assumed power density profile is indicated. Horizontal lines: rational $\iota$-values up to m = 20.*

### 2.2.5 *Dependence of transport on $\iota$*

With regard to W7-X, which will operate at a rotational transform close to 1, a favourable dependence of the energy confinement time on $\iota$ is indicated by the W7-AS energy confinement time scaling ($\propto \iota^{0.3}$). In order to elucidate the origin of the dependence in more detail, local transport coefficients were derived for both optimum confinement close to $\iota$ = 1/2 and 1/3 in ECR-heated discharges (B = 2.5 T, $P_{ECF}$ = 400 kW, $n_e(0) = 4.7 \times 10^{19}$ m$^{-3}$, $a_p \approx 16$ cm). The particle diffusion coefficients, as measured by gas-modulation experiments, and the impurity diffusion coefficients, as measured by analysis of aluminum injection experiments, show no clear difference within their available accuracy. The heat diffusivity $\chi_e$, as derived from power balance analysis, is similar in the outer region of the plasma, where transport is assumed to be anomalous (r > 10 cm, deviations arise from variations in the plasma aperture and uncertainties in the gradient region). Despite of large experimental scatter in $\chi_e$ even for comparable discharges, there seems to be evidence of a reduction of the heat diffusivity in the central part of the plasma (r < 8 cm) of approximately 20 % for the case of $\iota$ = 1/2 compared with $\iota$ = 1/3. The corresponding increase in electron temperature is restricted to the central region and should not substantially contribute to the total plasma energy. This is consistent with the small enhancement of the diamagnetic energy for $\iota$ = 1/2 compared with 1/3 of the order of 10 %, half of it being due to slight differences in density and heating power. Code calculations for the two cases in order to prove the consistency of the observed difference in the central radial profiles of $\chi_e$ with neoclassical predictions are the next step in the ongoing investigations.

## 2.3 Ion Cyclotron Resonance Heating

### 2.3.1 *Ion cyclotron resonance heating (ICRH)*

During the 1999 experimental campaign the heating performance of the high-field side double-strap antenna was investigated. This antenna had been installed during the preceding torus opening and replaced the broad antenna. It differed from the broad antenna by a better fit to the three-dimensional plasma contour and by a discontinuous distribution of the poloidal antenna currents.

Due to the better fit the coupling efficiency of the double strap antenna was about twice that of the broad antenna; thus the maximum launched RF power also doubled and reached 1 MW. The heating efficiencies were comparable for the heating schemes: minority hydrogen in deuterium, hydrogen in deuterium mode conversion and second-harmonic hydrogen. The increase in the bolometric radiation with launched RF power was also comparable. The wall recycling, however, was considerably stronger, particularly for second-harmonic heating, so that density control was not possible in such discharges. It can thus be concluded that for high-field-side launch and good fit of the antenna to the plasma and a boronized plasma vessel careful toroidal shaping of the poloidal RF currents - as was done with the broad antenna - is not necessary for good antenna performance.

At high RF powers a decrease of the efficiency of hydrogen minority heating was observed. This was probably due to enhanced particle loss as indicated by the lost-particle analyzer and indirectly confirmed by the observed saturation of the hydrogen tail temperature.

A new heating scenario reminiscent of magnetic beach heating was investigated. The magnetic configuration was chosen such that the field was highest in front of the antenna and decreased toroidally. The generator frequency was chosen such that the resonance for hydrogen was located on the low-field side outside the plasma but entered the plasma at a different toroidal angle due to the decreasing magnetic field. Only if the hydrogen concentration was such that the two ion hybrid layer was located in the bulk plasma ($n_H/n_e \approx$ 20 – 40 %), was a fast hydrogen tail observed. It is believed that since the group velocity perpendicular to the two-ion hybrid layer approaches zero, a wave propagating along the layer is mode-converted either into an ion Bernstein wave that damps on electrons or, if the layer crosses the cyclotron resonance, a slow wave that damps on the resonant ions. This is experimentally observed: decreasing the magnetic mirror ratio had little effect on the overall heating efficiency, but changed the temperature ratio of electrons to ions in favour of the electrons since ion Bernstein wave damping becomes dominant. For the standard magnetic configuration, where the hydrogen resonance nowhere entered the plasma, no fast hydrogen was observed.

### 2.3.2 *ICRF wall-conditioning experiments*

Conditioning in the presence of a strong magnetic field is mandatory for W7-X. ICRF-assisted wall conditioning and coating (ICC) has recently been established at the Tore Supra and TEXTOR tokamaks. Experiments have been started at

W7-AS to investigate the potential of ICC in a stellarator. The magnetic field was operated up to B = 1.25 T at $\iota = 0.4$ with pulse lengths ranging from steady state at B ≤ 0.3 T to 5 s at 1.25 T. ICRF was applied by the two poloidal strap antennas, A1 with a Faraday screen (74 MHz, pulse length between 3 min at P ≤ 12 kW and 2 s at P = 120 kW), A2 without (37 MHz, P ≤ 2 kW). The working gas was helium at a pressure from $3 \cdot 10^{-5}$ to $3 \cdot 10^{-3}$mbar. Breakdown was possible only with A2, but after breakdown the discharges could be sustained and heated by A1.

The electron density profiles of the ICRF discharges, measured by multichannel interferometry, were centrally peaked and symmetric with respect to the minor radius. The mean density (Fig. 8) strongly increases with ICRF power, moderately increases with the gas pressure, and is rather insensitive to B. The electron temperature measured by a Langmuir probe near the last closed magnetic surface ranged from 15 to 30 eV, increasing with power. Mass spectroscopy indicates that the amount of desorbed and pumped hydrogen isotopes increases with the power density, $P_{ICRF}/p_{He}$, saturating at about P = 50 kW (also Fig. 8). This dependence is reciprocal to the tokamak results and its significance has to be checked in another campaign. The effect on stellarator performance was comparable for both 9 min He-ICC (3 x 3 minutes, $P_{ICRF}$ = 12 kW) and He-GDC. After conditioning density control was significantly improved for both ECRF and NBI heated discharges. This is attributed to enhanced wall pumping.

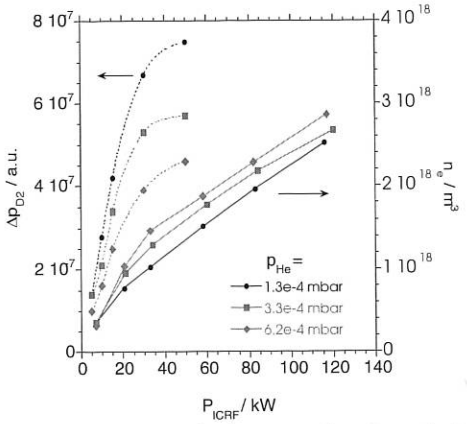


*FIG. 8: Line-averaged electron density of the ICRF plasma and increase of the D2 partial pressure after 10 s ICRF pulses as a function of ICRF power at different He pressures (B = 0.4 T).*

## 2.4 Electron Cyclotron Resonance Heating

The ECRH and ECCD experiments mainly concentrated on the phase space interaction of electrons with high-power ECRH. In particular, different launch scenarios and nonlinear effects were investigated.

### *2.4.1 Experiments on ECRH heating*

To investigate the influence of the electron distribution function on the stellarator confinement, high-field launch and low-field launch were compared for different magnetic field configurations. Two 140 GHz beams with up to 0.8 MW power in the second harmonic X-mode (X2) polarisation were launched from the low-field side, which couples to the thermal electrons, and from the high-field side with preferred coupling to high-energetic electrons. For the high-field launch a strong increase of the suprathermal electron population was observed by the vertical ECE diagnostic compared with the standard low-field launch scenario. In the "standard" magnetic configuration with local magnetic minimum and trapped particles at the ECRH launch position, the central confinement could be improved by high-field launch, as shown in Fig. 9. This can be explained by an enhanced radial electric field driven by ECRH-generated suprathermal trapped electrons. Consistently, in the "maximum B" configuration with few trapped particles at the ECRH launch position, the high-field launch is less advantageous than the low-field launch.

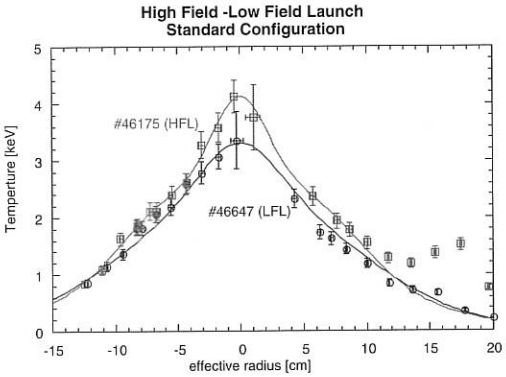


*FIG. 9: Electron temperature profiles of a low-field launch (LFL) and high-field launch (HFL) heated ECRH plasma in the "standard" configuration with trapped particles at the ECRH power deposition zone. The second peak at the right plasma edge is due to suprathermal emission from the plasma centre and does not represent the edge temperature.*

### *2.4.2 Nonlinear absorption*

At high-power ECRH flux densities the validity conditions for the quasilinear description of the EC absorption may be violated and as a result the optical depth is reduced. This was investigated by transmission measurements. Two 140 GHz beams with maximum power of 0.4 MW each and with second-harmonic extraordinary (X2-mode) polarisation were launched from the low-field side at different toroidal positions into the target plasma with central densities $2.5 \times 10^{19}$ m$^{-3}$ and $4.5 \times 10^{19}$ m$^{-3}$. The beams were modulated linearly in power from 0.01 to 0.4 MW with a phase shift of 180° between each other. This made sure that the total absorbed power and thus the electron temperature remained constant, while the local power flux density was varied between 8 and 320 MW/m$^2$ (spot size 4 cm). The transmitted power was measured by a pick-up wave guide at the torus inner wall. To achieve a measurable amount of non-absorbed power, the EC resonance was shifted towards the plasma edge, where the optical depth was about 3. Since for ordinary polarisation (O2-mode) the absorption was low, it was

ensured that the input polarisation was completely X2-mode. Nevertheless, at the high density the transmitted power could not be reduced to zero, although in this case the plasma should be optically thick. Since the transmitted power was linearly increased with the input power, conversion from X2- to O2-mode by density fluctuations is assumed to explain the results.

For the lower density this effect was much less and the transmitted power is mainly dominated by the optical depth of the plasma. Here the transmitted power nonlinearly increases with the input power as shown in Fig 10. As expected the optical thickness is thus reduced. The results are used to test codes for the nonlinear EC absorption which are currently under development.

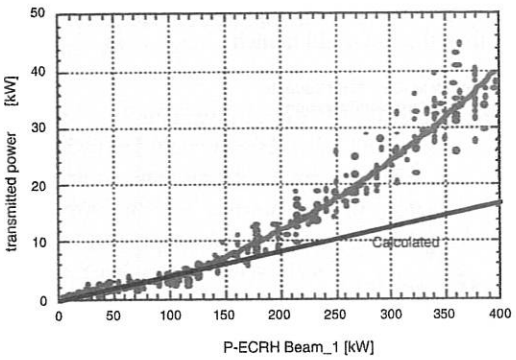


*FIG. 10: Non-absorbed ECRH power versus input power of one beam. The straight line is the expected linear power transmission from ray-tracing calculation.*

### *2.4.3 High power EC current drive experiments*

In the experiments described here, 2nd harmonic X-modes at 140 GHz (corresponding to B = < 2.5 T) with a power level of up to 1.3 MW (3 gyrotrons) were launched. For the "standard" configuration, a significant amount of trapped particles exists in the ECRH launching plane. By increasing the current in the coils at the "elliptical" plane, a "maximum-B" scenario without trapped particles in the ECRH launching plane can be realised. No direct access to the ECCD densities is experimentally available, and estimates from the current balance must rely on accurate calculation of both the bootstrap and the inductive current densities, which depend on the $n_e$, $T_e$ and $Z_{eff}$ profiles. In addition, an estimate of the ECCD density from linear theory is obtained from the adjoint approach with trapped particles included[1] (implemented in the ray tracing code) and compared with the current balance. ECCD currents of up to 20 kA are obtained from the current balance of bootstrap ($I_{bt}$) and ohmic currents ($I_{OH}$), i.e. $I_{ECCD} + I_{bt}+I_{OH} = 0$, in the net-current-free discharges. For the "standard" configuration at low density ($n_e = 2.5\ 10^{19}\ m^{-3}$), the launching-angle scan yields significantly smaller ECCD currents from the current balance than the linear prediction; (see Annual Report 1998). Especially for co-ECCD, the "experimentally" observed current was reduced by a factor of more than 2. At higher density ($n_e = 6\ 10^{19}\ m^{-3}$), however, fairly good agreement between the current balance and the linear prediction was found. These results were confirmed by density scans at fixed launching angles ($phi_{inj} = + 13°$ co- and $-13°$ ctr-ECCD). For an equivalent density scan in a "maximum-B" configuration (without trapped electrons in the launching plane), where the linear theory predicts a 50 % higher ECCD efficiency, at low density the EC-driven current from the current balance is increased by that factor, but the discrepancy between the experimental value and linear prediction remains. At high density good agreement was again found. For very low densities ($n_e = 1\ 10^{19}\ m^{-3}$), however, the evaluation is affected by a fairly strong uncertainty of the $Z_{eff}$ values.

The reduced ECCD efficiency at low densities cannot be explained by the nonlinear Fokker-Planck simulations with the "convective" power loss model (see 2.7.5 W7-AS Theory). The assumption of a kinetic instability driven by the strong gradient (with respect to $v_{parallel}$) of the distribution function close to the loss-cone boundary (see Fig. 12, Section 2.7.5) needs further investigation.

## 2.5 Neutral beam injection

### *2.5.1 Deposition profiles*

Experiments on measuring the deposition profile of the heating power via modulation techniques have been continued. At low power (400 kW), the measured deposition power agrees reasonably with the theoretical expectation (FAFNER code). At higher power (800 kW, either one continuous beam and one modulated beam or one ECRH gyrotron continuous and one beam modulated), there are characteristic deviations from theory which are not yet understood. A cause of the deviation may be the effect on fast-ion orbits of Global Alfvén Eigenmodes (GAEs) which are observed in phase with the modulated beam.

### *2.5.2 Plasma ignition solely by NBI*

Ignition and build-up of a plasma in W7-AS by NBI alone has been reexamined. In this campaign of experiments some efforts were undertaken to reduce the starting neutral gas pressure in the torus. Consequently, the plasma has been ignited solely by NBI within a time constant of 50 to 100 ms and built up to quite respectable parameters (5 kJ). More experiments are planned in the future in order to optimize the method for a reliable and reproducible means for plasma build-up.

## 2.6. Stability and Fluctuations

### *2.6.1 Stability with net toroidal currents*

Recent design activities on compact stellarator devices that utilize the bootstrap current to create sufficent total rotational transform have initiated studies with significant toroidal plasma currents in W7-AS in order to assess operational limits imposed by current driven instabilities. Previous experiments in W7-A with ohmic heating showed that large tearing modes causing major disruptions could be avoided in

[1] M. Romé et al., Plas. Phys. Contr. Fusion 40 (1998) 511

the presence of a modest external rotational transform provided by the helical windings[2]. This effect was attributed to the improved positional stability and the shift of the relevant rational surface away from the steep current gradient region. The OH transformer system of W7-AS was used to drive toroidal currents under various heating conditions (ECRH or NBI, combined ECRH and NBI). The external rotational transform was varied in the accessible range $0.3 \leq \iota_{ext} \leq 0.57$, in order to involve different low order rational surfaces at different levels of toroidal current. The most significant effects are associated with the rational surface $\iota = 1/2$, where disruption-like events frequently prevent the edge rotational transform to be raised above $\iota(a) = 1/2$ with currents exceeding about 10 kA at 2.5 T ($\iota_{ext} \leq 0.4$, $\iota_{ext}/\iota_{tot}(a) \leq 0.65$). In the phase preceding the thermal collapse (2,1)-tearing modes are identified by various diagnostics. The magnetic perturbations reach

$$\tilde{B}_\theta / B_0 \big|_{r=a} > 1 \cdot 10^{-3},$$

their radial extent covers up to 1/3 of the plasma radius, and effects of mode locking are frequently observed. Even at higher external rotational transform ($\iota_{ext} > 0.5$) tearing mode activity and partial energy and current collapses are observed. However, the effects are not as severe as in the $\iota = 1/2$ case, and the discharges are only transiently affected. The experimentally observed stability behaviour is consistent with predictions as assessed by a delta-prime code (in cylindrical approximation). This analysis also yields estimates of the saturated mode amplitudes and island widths which are in rough agreement with the experimental data. The fact that the stability behaviour found in W7-AS, where the ohmic heating power can be neglected, is different to the W7-A case with ohmic heating can only be explained by broader current density profiles due to different power deposition profiles and the increases contribution of the bootstrap current in W7-AS.

### 2.6.2 *Plasma edge fluctuations and transport*

The radial particle and energy fluxes induced by correlated fluctuations of the plasma density, temperature, and poloidal electric field ("electrostatic fluctuations") in the edge plasma of toroidal confinement devices have been considered as a significant contribution to or even the main cause of the anomalous transport derived from radial density and temperature profiles. This idea has been confirmed, at least for the particle transport in most devices, by direct comparison of the radial particle flux across the last closed magnetic surface (LCMS), calculated from fluctuations of the ion saturation current, and the poloidal gradient of the floating potential, with the global particle confinement time. In W7-AS, fast-swept Langmuir probe measurements had given information on the relation between the electron temperature, density and electric potential fluctuations in the edge plasma (see Annual Report 1997, p. 61-62). This information was combined with ion saturation current and floating potential measurements for a large variety of discharges to create a database of the radial energy flux across the LCMS of W7-AS. For a series of discharges with different plasma density and heating power, energy confinement times were calculated from these fluxes and compared with the global energy confinement times calculated from diamagnetic plasma energy, heating power and radiation losses. Although various uncertainties are introduced into this comparison by the assumptions which had to be made (e. g. the same behaviour of electron temperature fluctuations across the whole edge plasma or extrapolation of local flux measurements to the whole flux surface), the order of magnitude of the energy confinement times calculated in the two different ways are in good agreement. The general tendency of increasing global energy confinement time with increasing plasma density is reproduced by the values calculated from the fluctuation-induced fluxes as well as the confinement degradation with increasing heating power. This is the first time that such a comprehensive comparison between fluctuation-induced fluxes and global confinement time has been made in a stellarator. Nevertheless, the fluctuation measurements still require some improvements to reduce the uncertainties and identify deviations between anomalous and fluctuation-induced transport if these should exist.

## 2.7 W7-AS Theory

### 2.7.1 *Fast equilibrium reconstruction*

Work continued by investigating the possibility of pressure profile reconstruction based on magnetic measurements only. A database of ca. 400 net-toroidal-current-free NEMEC-equilibria of W7-AS was used to analyze a dense set of magnetic point measurements. To avoid false optimism, the simulated measurements were placed just outside the vacuum vessel. A principal component analysis showed that, in general, the average pressure (i.e. the kinetic energy) together with a peaking factor for the profile can be recovered fairly well. However, further details of the profile seem to be beyond the resolution of magnetic diagnostics. If one aims at equilibrium reconstruction, further information has to enter in the form of profile measurements of temperature and/or density. This is especially the case since current density profiles have to be taken into account and are not included in the current database if magnetic measurements are to be utilized in the experiment.

### 2.7.2 *Kinetic energy from magnetic signals*

Installation of the control coils in 1998 for the upcoming divertor experiments forced the fast diamagnetic coil system to move to a different location. On this background, the calculation of the kinetic energy from the diamagnetic coils on the basis of the large-aspect-ratio approximation was revised. A database of ca. 280 NEMEC free-boundary equilibria for which the magnetic signals had been calculated with the Diagno package was investigated. The result of the analysis was cast into new formulas for the fast diamagnetic coil located near the $\phi = 15°$ plane, the slow diamagnetic coil in the $\phi = 36°$ plane, and the signal arising from 2 saddle coils measuring the vertical field component generated by the Pfirsch-Schlueter currents. The new signals show generally

[2] W7-A Team, Nuclear Fusion 20 (1980) 1093

good agreement for pure ECRH discharges. For discharges with NBI the signal derived from the saddle coils is higher for lower densities, which could indicate an anisotropic pressure component from the parallel NBI.

### 2.7.3 *EMC3/EIRENE code*

Code development: The EMC3 code has been benchmarked with the B2 code, the main purpose being a comparison of the two completely different algorithms used to solve the plasma fluid equations, namely a Monte Carlo technique and a finite-difference method. The island SOL geometry is simplified by a 2D slab model, the particle source is approximated by an exponential decay function. In a first step the energy equations for ions and electrons are solved for $T_e$ and $T_i$ with a 200 kW power flux through the separatrix and a constant density of 2 x $10^{13}$ $cm^{-3}$, then the particle and momentum balance equations are solved for $n_e$ and $v_{||}$ with the temperature profiles given by the solution of the first step. The results are compared in Fig. 11, showing an excellent agreement of the relevant plasma parameter profiles.

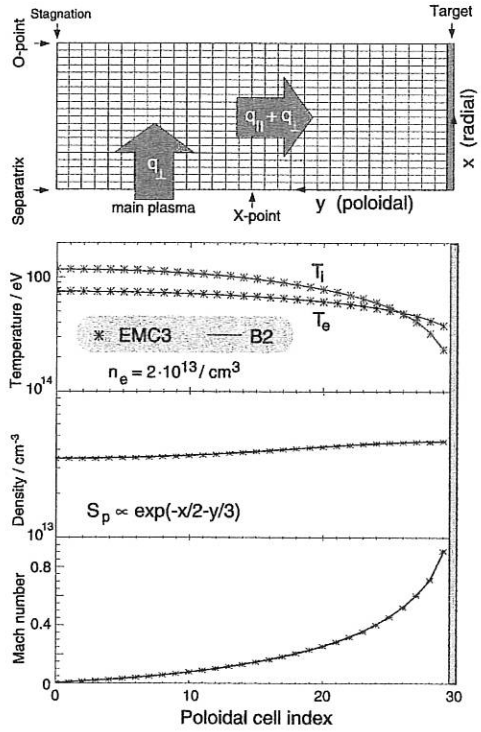


*FIG. 11: Comparison of the EMC3 and B2 Codes on a 2D slab model of the island SOL.*

Code application: Both the small field line pitch and small island size of island divertors imply a higher weight of the cross-field transport with respect to comparable tokamaks. Major consequences, clearly evidenced by a comparison of EMC3 simulations for the SOL geometry of W7-AS with the predictions of the two-point model, are:

- drop of the upstream temperature due to ⊥ heat transport,
- momentum loss even at low densities due to ⊥ particle transport,
- smooth transition from low to high recycling conditions.

A further consequence is a broadening of the power deposition profiles on the targets.

### 2.7.4 *Effect of 3-D geometry on mode structure*

In axisymmetric plasmas, a characteristic feature of modes in the MHD Alfven continuum is that they become singular at a resonant magnetic surface. The theory of continuum modes was extended to the general nonaxisymmetric case and a singularity was recovered. It was found that the form of the singularity close to the singular layer is qualitatively the same as in the axisymmetric case, namely a power law, $d^{\sigma}$, at the distance d to the singular layer, and with an imaginary value of $\sigma$. This corresponds to an oscillatory singularity. In special cases the oscillatory singularity is replaced by a logarithmic one. This result endures, provided the nonaxisymmetry of the configuration is not too large. The opposite case needs further analysis (in collaboration with J. Tataronis, University of Wisconsin, Madison).

### 2.7.5 *Bounce-averaged Fokker-Planck code*

The bounce-averaged Fokker-Planck code (FPTM) is reformulated in a fully relativistic form. In order to provide a consistent interface with ray-tracing codes (a new one is needed for W7-X) to describe the ECRH absorption as well as the electron cyclotron emission (ECE) also for non-Maxwellian distributions, this relativistic formulation is needed. This work is not yet finished (WTZ collaboration with N. Marushchenko, Kharkov).

### 2.7.6 *FPTM modelling of high power ECCD discharges*

The high-power ECCD scenarios with highly localized power deposition close to the axis are analyzed with the FPTM code. The radial energy transport is formulated in convective form by the grad B drift of suprathermal ripple-trapped electrons generated by the ECRH. For these discharges in the lmfp regime, both the "diffusive" neoclassical transport (1/ν regime) and the "convective" Monte Carlo simulation are confirmed by the experimental findings.[3]

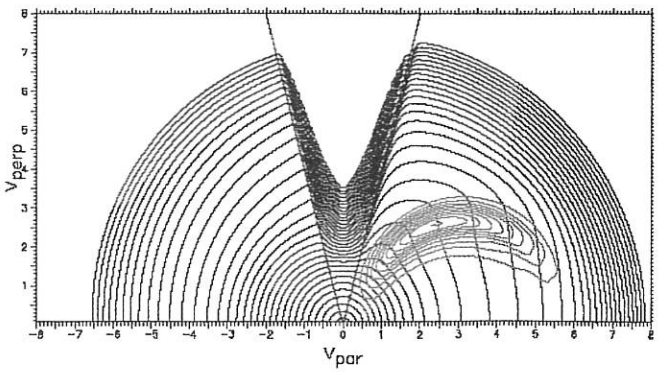


*FIG. 12: Contour levels of the electron distribution function in the ECRH launching plane from Fokker-Planck modelling, and contour levels of the quasi linear diffusion coefficient, $Q_{\perp}$, from ray-tracing: $n_e = 2.5\ 10^{19}\ m^{-3}$, $T_e = 3$ keV and 50 W/cm³ absorbed power density.*

[3] Maassberg et al., Phys. Plasma 7 (2000) 295.

In the simulation of Fig.12, the collisional power transfer to the ions as well as radiative losses are small, and the "energy sink" in the loss-cone is very close to the absorbed power density (corresponding to 1.2 MW ECRH power). The steep gradients in the electron distribution function drive the strong collisional power flux from the heating zone into the loss-cone. Nonlinear absorption effects are negligible for this scenario. With this "convective" loss-cone modelling, the ECCD efficiency slightly increases with power. Furthermore, the electrical conductivity is nearly unaffected (WTZ collaboration with N. Marushchenko, Kharkov).

### 2.7.7 *Kinetic stability analysis of distribution functions*

The complete dielectric tensor for arbitrary distribution functions (given numerically on a cylindrical velocity space grid) was implemented in a nonrelativistic formulation and tested. Using the Cauchy root-finding algorithm for the dispersion relation together with mode tracing in k-space provides the main numerical tools for kinetic stability analysis of distribution functions. A preliminary stability analysis of a high power ECCD scenario with strongly positive gradients at the loss cone boundary (with respect to $v_{parallel}$) yields marginal stability even in the nonrelativistic case. For these scenarios, a relativistic formulation of the dielectric tensor in the limit of small $k_\perp$ with respect to the gyro-radius is needed (proposed WTZ collaboration with E. Suvorov, Nizhny Novgorod).

### 2.7.8 *Estimation of polarization currents in "electron-root" scenarios*

The transient evolution of the central $T_e$ profile in "electron-root" discharges after switch-off of gyrotrons was analyzed. The electron power balance equation with purely neoclassical transport coefficients was integrated, and the radial electric field profile was modelled to fit the experimental $T_e$ profile. Within the "electron-root" region the strongly positive $E_r$ decays with a time constant well below 1 ms (there is no damping in the electron power balance). Estimating from the $E_r$ decay the radial polarization current (in an axisymmetric approximation) leads to electron particle fluxes which are well consistent with the ripple-trapped suprathermal fluxes calculated by the 5D Monte Carlo simulation. This result confirms the essential role of the ECRH-driven particle fluxes for establishing the "electron-root" feature at W7-AS (in collaboration with S. Murakami, NIFS, Japan).

## 3 DIAGNOSTIC DEVELOPMENT

### 3.1 Ruby Thomson Scattering System with High Spatial Resolution

The new Thomson scattering diagnostic with enhanced spatial resolution for plasma edge and gradient investigation on the high-field side in the triangular plane is in operation. The detection system combines a self-developed Littrow-type spectrometer and an intensified CCD camera. Depending on the installed diffraction grating (600 or 1800 lines/mm), a total wavelength range of 80 nm (suitable for plasma edge investigations) or 320 nm (suitable for gradient investigations) can be surveyed. Absolute sensitivity calibration for the system is implemented with Raman scattered light (723.8 nm) by means of hydrogen gas filled in the vacuum vessel. Thomson profiles in the centre and low-field region of the plasma were still determined by means of 15 interference filter polychromators, already in operation for years. Complete spatial electron density and temperature profiles can therefore be derived.

The measured profiles are in good agreement with results from other profile diagnostics (time-resolved Nd:YAG Thomson scattering, ECE), but the new system offers a higher spatial resolution (up to 4 mm). Because of this improvement, steep gradients in the electron density profile during "H-mode"-like discharge phases could be detected (Fig. 13). Due to modifications of the NBI heating equipment of W7-AS, the interference filter polychromators have to be replaced by a space saving CCD-based system in 2000.

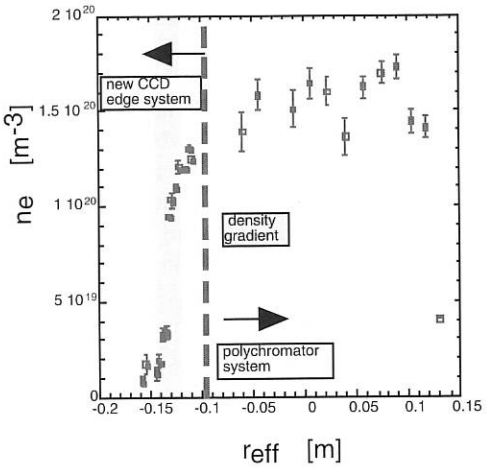


*FIG. 13: Electron density profile with steep gradient during an "H-mode" discharge. Measured by the ruby Thomson scattering system.*

### 3.2 High-resolution Extreme-bandwidth ECE Radiometer

Broadband multichannel heterodyne radiometers have now been established for many years as a standard diagnostic tool for time and space-resolved electron temperature measurements. Technical improvement especially in mm-wave mixer design now allows for extreme broadband mixers with an instantaneous RF-input and IF-output bandwidth of more than 40 GHz. Such a mixer was used to develop 48 channel ECE radiometer for W7-AS covering the full 2nd harmonic ECE spectrum at 2.5 T, which ranges from 120 to 160 GHz. The IF and filter bank parts of the system are formally as realized in many other systems, but, in contrast, the IF-amplifiers and filters used cover the frequency range to 40 GHz, being twice as wide as existing systems. As a novel feature a second down-conversion step with variable local oscillator frequency was included. In this part of the radiometer, 16 additional channels are generated with high space/frequency resolution and with narrow channel separation. The position of these additional channels in the

ECE spectrum and the corresponding electron temperature profile respectively is variable and can be shifted from the centre to the edge, depending on the experimental requirements, e.g. for ECRH power deposition profile analysis or steep temperature gradient investigations during H-mode discharges.

## 3.3 Development of an ECE Imaging System

To get a deeper insight in the physics of plasma turbulence, especially temperature fluctuations here, it is essential to have two-dimensional information about the fluctuating structures, their size, and velocity fields. For the two-dimensional characterization of temperature fluctuations in the core of the W7-AS plasma an ECE imaging system is being developed. As a first step an array of four poloidal sightlines is planned with eight radial channels along each sightline.

The mm-wave detector array acting as the front end of a multichannel heterodyne radiometer consists of four channels, each comprising an antenna, a mixer, filters, and the on-chip local oscillator power distribution. This high-frequency part is being developed in collaboration with TU Darmstadt. All components are fully integrated on a single of 48 $mm^2$ substrate. The array will be illuminated by the electron cyclotron emission (ECE) using Gaussian beam optics with a lens and an elliptical mirror. Simulations showed that the use of a substrate lens is necessary to realize the desired nonoverlapping Gaussian beams in the plasma core. The detector array and the lens will be placed outside the vessel, the mirror inside the vessel.

An alternative approach is being installed which uses four conventional, separated mm-wave mixers, allowing preliminary experiments using the same intermediate frequency filter banks as the final design.

## 3.4 Measurements and Simulations of Electron Bernstein Wave Emission

A new diagnostic based on radiometry of mode-converted thermal emission of electron Bernstein waves (EBWs), to measure the electron temperature profile at densities higher than the ECE cut off, is under development at W7-AS.

The key feature is that EBWs propagate without upper density limit. Although they cannot leave the plasma directly, they can be detected after conversion into electromagnetic waves, polarized at first in extraordinary (X) and finally in ordinary (O) mode (so-called BXO process). In order for XO conversion to occur, the sightline has to form oblique "optimal angles" with respect to the magnetic field and plasma cutoff layer, polarization of the detected O-mode therefore being elliptical.

Special attention was devoted to the new requirements arising with respect to traditional ECE radiometry. First, a quarter-wave phase shifter is necessary to convert the polarization from elliptical to linear, in the broad frequency range f = 60 – 90 GHz. After comparison of several devices, a waveguide with elliptical cross-section satisfies best the diagnostic requirements. Secondly, to convert the experimental spectra into temperature profiles, it is necessary to reconstruct the complicated mode-converted ray-paths in the plasma. For this purpose, a new 3D ray-tracing code for EBWs in full stellarator geometry was developed (Fig.14, top). Good agreement was found between simulations and measurements performed within a temporary experimental set-up (Fig.14, bottom) using an ECRH antenna as receiving antenna. At the moment a dedicated antenna for EBW diagnostics, optimized by means of ray-tracing calculations, is under construction.

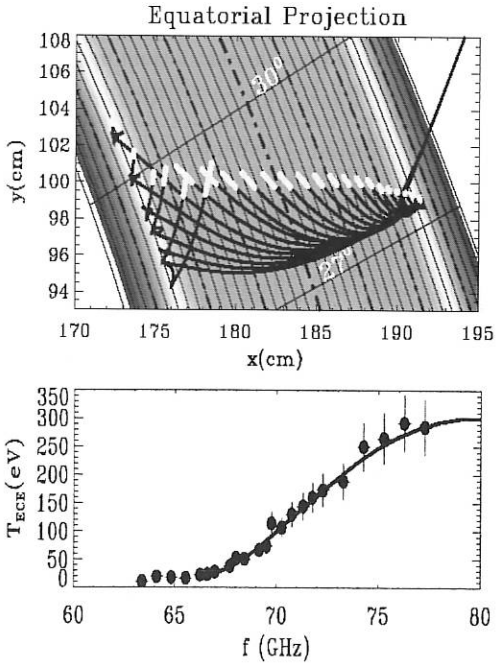


*Fig. 14: EBWs ray tracing for B = 2.4 T and n = 1.7 $10^{14}$ $cm^{-3}$ at centre, f = 67-9 GHz with step 1 GHz. The grey scale refers to density making evident the overdense plasma core. The parts of the rays where the signals originate are also shown (top). Experimental (circles) and simulated (solid line) EBE spectrum, shot 45077 (bottom).*

## 3.5 Detection of Fast Ion Losses with a Scintillator Base Probe

A new probe, based on the concept of the alpha particle loss diagnostic in TFTR, was used to measure fast ion losses in W7-AS. This probe, which is capable of resolving fast ion losses in pitch angle and gyroradius, consists of an aperture system and a scintillator plate behind. In principle, the detector is a magnetic spectrometer, i. e. the gyrating fast ions have to pass a pinhole followed by a slit before they strike the scintillator plate. The subsequently emitted light is detected by an optical system equipped with a CCD camera for sufficient spatial resolution and, additionally, with 15 photomultipliers for sufficient temporal resolution. A new feature of this probe is simultaneous detection of both co- and counter-moving ions, which was achieved by integrating two aperture systems into one casing and with a scintillator layout with two separate domains. Between these domains of sedimented ZnS and the glass substrate of the scintillator plate a thin Cr layer was applied, also well separated into two domains, which allows measurement of the ion loss current

necessary for absolute calibration of the loss rates. The probe was designed for detection of ions with pitch angles between 15° and 85° and for gyroradii, derived from the full kinetic energy, between 5 mm to 50 mm. This new diagnostic was first become operational in March 1999. Fast-ion losses were detected in many discharges under various plasma conditions. The main results were obtained from discharges with neutral beam injection, where perpendicular and tangential injection was studied by utilizing diagnostic and heating beams, and from ICR-heated discharges, where the second-harmonic, minority, and the so-called *magnetic-beach* heating scenarios were applied. The observed loss rates can be explained in terms of the fast ion confinement properties of the magnetic field configuration and in terms of slowing-down processes of the fast ions. Additionally, effects of H-mode transitions and interaction between particles and MHD instabilities on fast-ion losses are found, including losses during tearing modes and intermittent Alfvén eigenmodes.

### 3.6 Magnetic Equilibrium Diagnostics

Four coils placed at a poloidal circumference of W7-AS were used to measure the poloidal magnetic flux induced by the toroidal plasma current distribution. Linear combinations of the four raw signals are formed which can be related to moments of the current density distribution. The sum is proportional to the total current. Other linear combinations reflect the dipole moment and a second moment of the current distribution which is formally analogous to the moment of inertia of a planar mass distribution. Measured signals were compared with the magnetic flux calculated from current distributions obtained from neoclassical theory and experimental profile data.

### 3.7 PC-controlled Bolometer Amplifiers

Bolometer amplifiers with remote control operation and in-situ calibration of the bolometer foils were developed. A 16-channel 16-bit 100-kHz ADC with 8 DIO lines for setting gains and controlling the measurement and calibration function of each board was used. Prior to each measurement, the Wheatstone bridge of the bolometer foil is balanced. A first stage amplification of 40 allows a noise level of $3mV_{pp}$ at the output for an amplification factor of 1000 to be achieved. A proposal to reduce the noise level further by a factor of 3 and so approach the thermal noise of the bolometer meander resistors is currently being investigated. With this noise level, the operation of bolometers with beryllium filters could be extended beyond the present 2 µm thickness currently in operation on W7-AS. This possibility would be of particular interest in discharges where high neutron fluxes prevent operation of conventional soft X-ray diodes.

Data acquisition and control of the bolometer amplifiers with a PC using Windows NT 4.0 and LabView 5.1 are currently being prepared for evaluation on W7-AS. A test of data streaming to disk of 16 channels for 30 s was successful. Of particular interest will be the performance of the Bittware 16-bit 32-channel ADC with integrated DSP (Analog Devices 21060 40 MHz 120 Mflops), which is presently being put into operation.

### 3.8 Divertor Diagnostics for W7-AS

The primary plasma quantities and associated diagnostic systems being developed for the divertors consist of: a) $T_e$ and $I_{sat}$ at the target plates from arrays of Langmuir probes, four rows each in an up-down module pair, with nine probes per row yielding a poloidal spatial resolution of 7.5 mm for two adjacent rows ($\delta t \sim 2ms$). b) 2D power flux to the same up-down module pair from two IR cameras ($\delta r \sim 3$ mm, $\delta t \geq 2$ ms); c) particle flux to these modules via 2D $H_\alpha$ CCD cameras ($\delta r \sim 1$ mm, $\delta t \sim 16$ ms); d) carbon flux from one target plate via a 2D CII CCD camera ($\delta r \sim 1$ mm, $\delta t \sim 16$ ms); e) mapping of regions with $T_e < 2$ eV (divertor detachment) via the ratio of $H_\gamma/H_\alpha$, with $H_\gamma$ being monitored at one divertor via a 2D CCD camera; f) $T_e$ and $I_{sat}$ along a line extending from the target plate towards the core plasma by means of a reciprocating Langmuir probe. h) $T_e$ and $n_e$ along a similar chord, derived using a thermal helium beam in conjunction with a spectrometer viewing characteristic lines along the beam; i) plasma radiation in a poloidal plane intersecting one divertor via three bolometer cameras arranged as: 12 channels looking through the target plate into the core plasma, 20 channels opposite and viewing the same cross section, 8 channels parallel to the target plates; j) integral power flux to the target plates via 100 thermocouples covering the target plates of six modules, with two thermocouples each for the remaining four modules; h) five gauges in the main vessel and four behind the target plates to measure the neutral pressure.

## 4 MACHINE OPERATION AND TECHNICAL ACTIVITIES OF W7-AS

### 4.1 Main Activities of W7-AS

In 1999, the W7-AS experiment was operational for about 3500 pulses mainly at 2.5 T. In August, the torus was opened for installing the divertor modules and the necessary divertor diagnostics. Other in-vessel components have to be modified to make room for the rather large divertor modules, and the ICRH antenna had to be removed.

Preparations for installing a divertor in W7-AS began in 1995. Ten divertor modules at the top and bottom of the plasma close to the "elliptic" symmetry planes of the configuration will replace the two old top-bottom limiters. The topology is similar to the W7-X divertors; details of the geometry were optimized by methods similar to those applied to the W7-X divertor. Peak power densities under worst conditions of 15 $MW/m^2$ are expected. Inertia cooling of the CFC target plates and graphite baffles will be sufficient for the relatively short heating pulses of W7-AS even at high heating power. Getter pumps with Mo-Ti filaments similar to those used in the former ASDEX divertor will be placed behind the baffle plates.

Each divertor module consists of two parts. One part bears a toroidal row of target tiles and a poloidally adjacent row of baffle plates. The other part bears a row of baffle plates and houses the getter pump behind the baffle plates. 11 helically

wound filaments of Mo-Ti sublimator wire are connected in parallel by two copper bars extending in the toroidal direction. While the filaments are directly heated by electric current, Ti is sublimated from the wires and deposited on corrugated aluminium plates surrounding the sublimators. An original divertor getter module was technically tested in a vacuum tank. The lifetime of the filaments will probably be sufficient for all the divertor discharges to be performed if brittling is avoided by proper operation. The pumping speed is limited by the relatively narrow entrance slit. The value measured for cold molecular hydrogen would be marginally sufficient for density control, but higher values are expected with plasma operation.

Many target tiles are instrumented with Langmuir probes or thermocouples. In two modules there are 4 arrays of 9 flush probes each for electron density and temperature profile measurements. About 100 thermocouples will permit measurement of the heat load distribution on the target plates.

Meanwhile, about one-third of all components have been installed inside the discharge vessel and completion of the assembly is expected in summer 2000.

## 4.2 140 GHz ECRH System

During the experimental campaign, a third 140 GHz gyrotron was installed. Therefore, at the end up to 1.5 MW 140 GHz ECRH power was available. After machine shut down the repaired new technology 140 GHz, 0.8 MW gyrotron with voltage depression was brought again into operation. Inside the vacuum vessel a grooved graphite reflector was installed at the inner wall of the torus for the high field launch experiments. It provides a 90° polarisation rotation of second harmonic ordinary wave, which is only weekly absorbed at the usual electron temperatures. The reflected extraordinary wave is then fully absorbed at the EC-resonance.

## 4.3 Neutral beam injection

### *4.3.1 Radial injector*

The preparations for installing an additional radial injector are well advanced. In order to allow beam injection close to perpendicular (for generation of an electric field via fast ion orbit losses), a porthole was modified. Due to the restricted cross-section of this port, a transmitted neutral power of 500 kW only is expected from two ion sources (cf. 750 kW standard). Both sources (of the new circular RF type) were conditioned to full power. The new support structure for the injector box was installed. Further installation work is in progress.

### *4.3.2 Additional co-injector*

Change-over of the former East injector to its new position (North-East) and new orientation is largely completed. The revised injector box is assembled, mounted on the new support, and connected to the W7-AS torus. The control and supply connections to the box are installed. Still outstanding are installation of the four ion sources (Periplasmatrons) and their connection to the high-voltage multifilament cables. It is expected that the co-injector will be available in time for the re-start of W7-AS in early summer.

# STELLARATOR THEORY

(Prof. Dr. Jürgen Nührenberg)

X. Bonnin, M. Borchardt, M. Drevlak, S. Gori, R. Hatzky, R. Kleiber, A. Könies, H. Leyh, P. Merkel, A. Mutzke, C. Nührenberg, J. Nührenberg, J. Riemann, R. Schneider R. Zille.

Guests: A. Boozer,[1] B. Braams,[2] M. Isaev,[3] R. Ishizaki,[4] M. Isobe,[4] R. Kanno,[4] M. Mikhailov,[3] M. Nadeem,[5] N. Nakajima,[4] S. Nishimura,[4] S. Okamura,[4] M. Persson,[5] D. Reiter,[6] A. Runow[7] V. D. Shafranov[3]

## 1. INTRODUCTION

In 1999, the work of the Stellarator Theory Division Physics Group was concentrated on widening the scope of the theoretical work /645, 646/ at the Greifswald Branch Institute and on further development of the stellarator concept /281, 431, 225/, notably for quasi-axisymmetric /469, 630, 677/ and quasi-isodynamic configurations. /93, 645/.

## 2. CONFIGURATION STUDIES

It was shown that quasi-axially symmetric finite-$\beta$ stellarators can simultaneously exhibit good collisionless $\alpha$-particle confinement and ballooning-stability properties. An example of a configuration with 3 periods, aspect ratio $\approx 6$, and $\langle\beta\rangle = 0.035$ is shown in Fig. 1.

## 3. EQUILIBRIUM CALCULATIONS WITH ISLANDS

In collaboration with the theory division at PPPL (D. Monticello, A. Reiman) improvements were made to the PIES code. In particular, the graphics capabilities were extended and the code was ported to SUPER-UX (NEC). Sections of the code critical to performance were optimized for greater efficiency on this platform.

The revised code was used in fixed boundary calculations of equilibria of the HELIAS class. Capitalizing on the increased vector power available, these calculations were taken to very large numbers of iterations (several $10^2$), resulting in a high degree of convergence (changes consistently smaller than $10^{-4}$ between iterations). Special attention was paid to the evolution of islands at finite $\beta$. In several computations it was observed that large islands occurring at the beginning of the computation diminish to very small size after a sufficiently large number of iterations. An example is shown in Fig. 2.

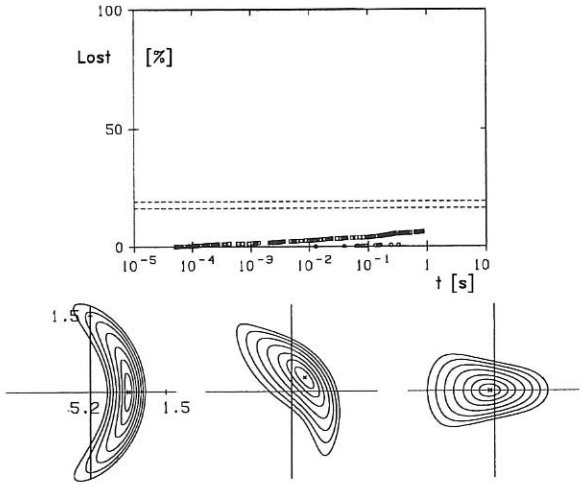


*FIG. 1: Top part: Collisionless $\alpha$-particle losses in the configuration shown in the bottom part as a function of the time of flight. Particles are started at $s_{\mathrm{start}} = 0.0625$ (○) and $s_{\mathrm{start}} = 0.24$ (□) ($\approx$ 1/4 and 1/2 of the plasma radius); the dashed lines show the fractions of reflected particles; each symbol indicates the loss of one particle. Bottom part: Flux surface cross-sections of this quasi-axisymmetric stellarator. Shown are sections at the beginning, quarter of and half a period.*

*FIG. 2: Poincaré plot of the magnetic field in a W7-X type equilibrium at $\langle\beta\rangle = 5\%$. In contrast to the design configuration, which avoids this resonance, $\iota = 5/5$ is located inside the plasma volume.*

A new iteration technique was explored, blending the new current density with that from the previous iteration instead of blending the magnetic fields. This technique was shown to avoid the initial growth of islands and to arrive at the final solution more rapidly.

## 4. IDEAL MHD STABILITY

In 1999, applications of the CAS3D stability code to (i) existing stellarator experiments (W7–AS at IPP Garching /222, 223, 224, 763/, LHD at NIFS Toki[8], and CHS

[1] Columbia U., [2] NYU, [3] Kurchatov I., [4] NIFS
[5] Chalmers U., [6] U. Düsseldorf, [7] FZJ

[8] Chen *et al.*, Phys. Plasmas **6** (1999) 1562

at NIFS Nagoya[9]), to (ii) stellarator experiments in the construction phase (W7-X at IPP Greifswald /221/), and to (iii) stellarator experiments in the design phase (QAS at PPPL /676, 245, 244 675, 677, 630/ and HSR at IPP Garching /280/) set the tone in ideal MHD work and helped to continue the collaborations with PPPL and NIFS. CAS3D proved to be a versatile MHD stability tool for straight cylindrical, straight helical, 2D, and 3D plasma configurations, and helped to deepen understanding of the ideal MHD spectrum, gap formation, and gap modes, i.e. GAEs, $\beta$-induced AEs, geometry-induced AEs, with both even and odd parity. Figure 3 shows that the cylindrical GAEs have their 3D analog. In the W7-AS case shown here, the required flatness of the continuum frequency minimum results from a helicity-induced and, therefore, stellarator-type coupling.

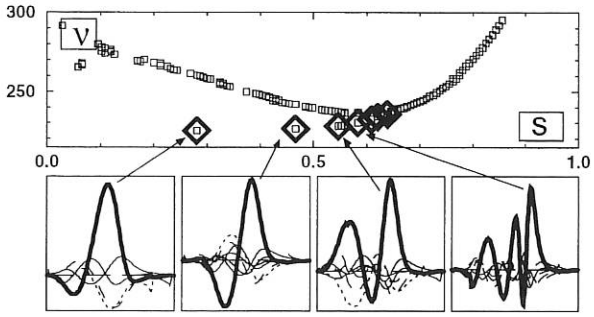


*FIG. 3: CAS3D for W7-AS #41618 (frequencies [kHz] versus normalized flux-label in the upper frame; normal-displacement harmonics in the lower frames; compare /222/): The Sturmian discrete Alfvén spectrum (◇; number of radial nodes in the perturbation harmonics increases with the frequency) clusters from below at the minimum of the corresponding Alfvén continuum branch (□).*

## 5. MHD STABILITY WITH KINETIC EFFECTS

The recent observations of Alfvén wave excitations in stellarator geometry and their successful description by the global MHD stability code CAS3D, have raised the question of destabilization of such modes by a fast-particle population. A linearized drift kinetic equation has been solved in three dimensions for electromagnetic perturbations where the radial drifts have been neglected. Therefore the flux surface is a constant of the particle motion and approximates the drift surface given by a constant second adiabatic invariant. This approximation is in particular suitable in the W7-X case. A propagator technique developed by Brunner and Vaclavik is used to perform the integration of the particle orbits, and the integration along the particle trajectory is approximated by an integration along a field line. The perturbed pressure can easily be expressed in terms of the perturbed distribution function. Then, a generalized energy integral can be obtained from the force balance equation if MHD-like perturbations are assumed. As the perturbed pressure depends on the mode frequency $\omega$ itself, the associated eigenvalue problem becomes complex and nonlinear. The relevant matrix elements have to be calculated by performing a fivefold integration. The numerical implementation of the theory has been started.

[9] collaboration N. Nakajima (NIFS), C. Nührenberg

## 6. ION-TEMPERATURE-GRADIENT-DRIVEN (ITG) INSTABILITIES

ITG instabilities are now commonly held responsible for turbulence giving rise to anomalous ion heat transport in the core of tokamaks. ITG turbulence could become the dominant mechanism of W7-X as collisional transport has been optimized in this stellarator. Therefore, in collaboration with CRPP, a non linear global gyrokinetic simulation code for W7-X is being developed /501, 502/. Although the most realistic physical choice, global non linear calculations are numerically very demanding concerning the numerical methods and computational effort. Even for the geometrically easy configuration of a $\theta$-pinch, which was investigated here, the achieved numerical results in the saturation phase are not yet satisfactory. Although the underlying set of gyrokinetic equations is energy-conserving, energy conservation is lost in the saturation phase. Figure 4 shows a particularly pronounced example. The reason seems not to be a convergence problem of particle number but to be associated with the gyro-averaging.

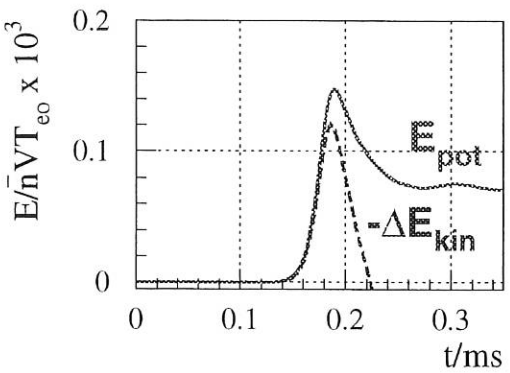


*FIG. 4: Potential energy (solid line) and kinetic energy (dashed line) as a function of time for a non linear $\theta$-pinch calculation of 33,554,432 tracers.*

## 7. DRIFT WAVES IN STELLARATORS

The code for calculating global linear resistive electrostatic drift instabilities in general geometry [1] was applied to a sequence of VMEC-generated $\ell$=2-stellarator equilibria (the major radius was used as the sequence parameter) in which the aspect-ratio per topological period (5 field period) and the $\iota$-profile remain fixed. In this sequence unstable modes near the outer boundary (see the figure for a typical mode spectrum) were found whose growth rates diminish if the

[1] Kleiber, R.: Proc. of the 25th EPS Conf. Control. Fusion and Plasma Phys., Prague 1998, 1753-1756

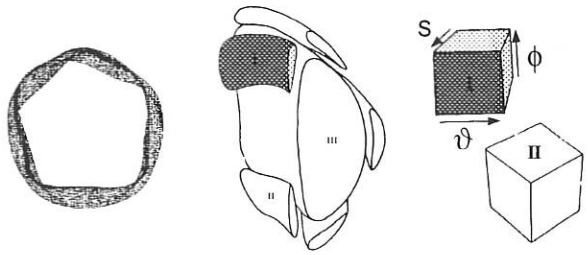


*FIG. 6: Island flux tube in real space and magnetic coordinates.*

sequence parameter is decreased. Also, the spatial structure of the modes is not correlated with the normal curvature but appears (at least for the straight stellarator) to be determined by the metric component $g^{s\theta}$, which is connected to the local shear /558/.

Application of this code to purely curvature-driven modes in stellarator configurations was also started. For tests a simple tokamak model was employed to establish the relation between the global eigenmodes and the modes from a ballooning analysis of the equations.

The above sequence of stellarator equilibria was also used to derive flux tubes with imprinted stellarator geometry. These were utilized in turbulence calculations with the DALF3 nonlinear code developed by B.Scott.

In collaboration with M.Nadeem and M.Persson, their previous studies of drift waves in stellarators, which are based on the ballooning formalism, are being extended to a more complete set of equations and applied to W7-X.

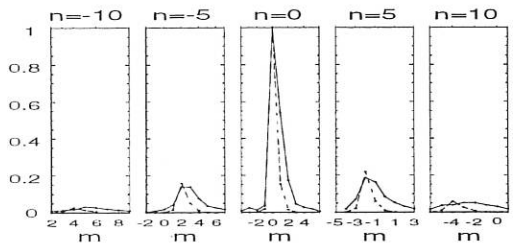


*FIG. 5: Fourier spectra of modes with phase factor $M_P = 651, N_P = -277$ in $\ell$=2-stellarator equilibria with major radii $R = 80, 20$ (dashed, solid lines); m and n the Fourier indices relative to those of the phase factor.*

## 8. PLASMA EDGE THEORY

For the W7-X stellarator a divertor is planned that uses the existing island topology of the magnetic field, where configurations with and without strong stochastic effects are possible. Comparison of stellarator and tokamak results /117, 25, 45, 46, 69, 85, 87, 142, 162, 183, 213, 215, 228, 250, 259, 277, 314/ shows the latter case to be of particular interest. For this situation a 3D SOL transport code (BoRiS, abbrev. authors) is under development /22/ to solve the strongly anisotropic transport equations in magnetic coordinates, thus taking account of full 3D geometry. This ansatz allows standard discretization methods with higher-order schemes retaining full geometric flexibility. BoRiS is based on the same plasma fluid approach as used for B2-Eirene, and experience from 2D SOL modelling can be directly adapted, including extension to multi-fluid formulation and coupling with neutral transport models.

With the magnetic coordinates chosen and stochastic effects being assumed to be negligible, the entire computational domain can be described as a conjunction of unique coordinate cubes (see Fig. 6 ), each of them corresponding to a different region of the original plasma. The general design of the code enables local grid refinement by indirect addressing of the computational cells, which are assumed to be convex polyhedrons.

The equations to be considered are obtained from the original multi-fluid Braginskii equations. These equations can be written in magnetic coordinates $(s, \theta, \phi)$ by introducing the representation of the elementary differential operator $\vec{\nabla}$ with respect to the left-handed orthogonal system $\vec{B}$, $\vec{\nabla}s$, $\vec{\nabla}s \times \vec{B}$ ($\|$, $\perp_1$, $\perp_2$ respectively).

In a first step the anisotropic Laplace equation for the electron temperature $T_e$ was solved for several situations serving as a test case for the general concept. Subsequently, this scheme was generalized by involving the ion temperature $T_i$ and coupling with $T_e$.

The equations are integrated applying Gauss', theorem and discretized with the finite-volume (FV) method, leading to a system of non linear equations. Upon linearization the Jacobian is determined numerically and the system is solved via a Newton method, i.e. by approximating the total flux balance for each cell successively, using a direct sparse matrix solver. Intermediate point properties are derived from grid point properties by an interpolation scheme capable of considering up to 3rd order neighbours, thus resulting in different computational molecules to be used.

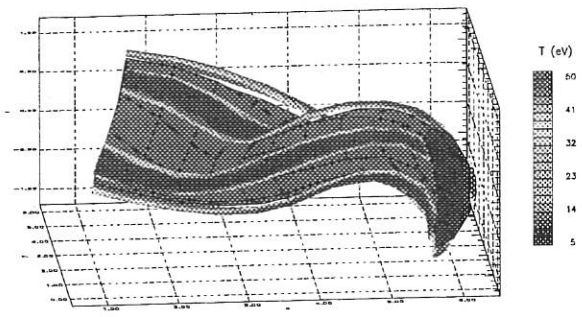


*FIG. 7: One period of a W7-X plasma in real space.*

Figure 7 shows one period of a W7-X plasma with the five flux tubes winding around the core. The shading indicates the temperature on the outermost radial grid position $s = 0.95$. This result is obtained either by modelling a single flux tube in a $10 \times 10 \times 50$ grid $(s, \theta, \phi)$ or by following five separate flux tubes over one period in a $5 \times (10 \times 10 \times 10)$ grid taking advantage of the five fold periodicity.

Specific areas of interest for the numerical development are upwind schemes, optimization introducing other solvers, esp. matrix-free methods (collaboration with UEDGE group), and parallelization.

# STELLARATOR SYSTEMS STUDIES

(Head of Project: Dr. Horst Wobig)

T. Amano*, C.D. Beidler, E. Harmeyer, F. Herrnegger, O. Jandl**, A. Kendl, J. Kisslinger, I.N. Sidorenko, E. Strumberger, H. Wobig

*Guest from NIFS, Japan, ** MF Division

## 1. OVERVIEW

A great part of the activity was related to the magnet system of a Helias reactor and to the adaption of various blanket concepts, which have been developed for tokamaks. Physics studies were focussed on plasma equilibrium, MHD-stability, neoclassical transport, confinement of alpha-particles and anomalous transport induced by drift waves. First steps were also undertaken to explore the 4- and 3-period Helias configurations.

## 2. WENDELSTEIN 7X STUDIES

In 1999 several computations were carried out for the Wendelstein 7-X project. The maximum magnetic field on the superconductors and the stray field in the vicinity of the machine were calculated. For the test arrangement at Euratom Association CEA-DAPNIA in Saclay, where the manufactured W 7-X coils will be tested, some calculations were done, e.g. the magnetic stray fields and the inductance matrix. The forces on the coils during a fast deloading phase were also considered. Furthermore, the magnetic field on the conductors for the different load cases of the W7-X-Demo-Coil was recalculated in detail in order to interpret the measured data collected during the test phase in 1999 in the TOSKA test arrangement in Karlsruhe. The results of all these computations are stored at an ftp-site, which is accessible to the members of the working groups for the Wendelstein 7-X device. Further computations were made with respect to the optimisation of the vacuum vessel.

## 3. HELIAS REACTOR STUDIES

Investigations on a Helias Reactor (HSR) were continued. Particular attention was devoted to the structural analysis of the coil system, the alpha-particle behaviour, the plasma drift waves, the design of the blanket elements, and the energy balance in such a device. The results of the investigations were presented at the EPS Conference in Maastricht, at the Jahrestagung Kerntechnik in Karlsruhe, at the 12th Stellarator Workshop in Madison, Wisconsin, and at the 15th Conference on Computational Mechanics in Nectiny, Czech Republic.

### 3.1 Coil system of HSR

The cross-section of the HSR modular coils, which are an upgrade of the Wendelstein 7-X system, has been modified. In this new version, called HSR-D, the winding pack of the five different coil types was subdivided into 8 pancakes and arranged trapezoidally over the coil cross-section, as shown in Fig.1.

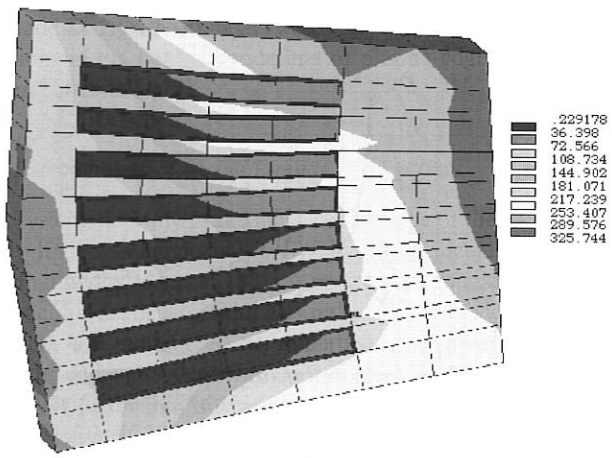


*Fig. 1: Coil cross-section of the HSR-D configuration: The 8 pancakes of the winding pack and the surrounding coil housing are shown. The radial stainless steel webs between the pancakes are subjected to maximum equivalent stress values of 290 MPa in this cross-section, far below the limits.*

This arrangement serves to diminish the current density at the location of maximum magnetic field and to stiffen the coil winding pack. As a result of this geometry the maximum magnetic field could be reduced to 10 T, while the field at the magnetic axis is 5 T. Thus NbTi-technology at a coolant temperature of 1.8 K can be applied. In the configuration HSR-D, the 8 pancakes of the coil winding pack contain 18 x 2 = 36 turns per pancake. The coil pancakes are

embedded in the coil housing with a layer of epoxy inbetween. Finite element computations were done for coil 1 of the HSR-D configuration in its own magnetic field. The 8 pancakes of the winding pack were subdivided into 3072 elements, surrounded by 7680 elements of the epoxy layer, and 8352 elements of the coil housing, resulting in a total number of 19104 elements with 21504 nodes for one coil. The epoxy layer between the pancakes of the winding pack and the coil housing was modelled such that the expected nonlinear behaviour of the arrangement is approximated. The results of these computations, as shown in Fig. 1, indicate that the radial webs of stainless steel between the pancakes are not overloaded. Furthermore, the maximum compression stress values of the winding pack in HSR-D are lower than in the former HSR-B configuration.

## 3.2 Blanket in HSR

The dimensions of the Helias reactor are mainly determined by the need to accommodate a breeding blanket and a shield. In the narrowest region on the inboard side the distance between plasma surface and coil casing is 1.5 m, which leaves a gap of 1.3 m for blanket and shield. In other places around the torus the gap is wider, reaching as much as 2 m. In the frame of the NET-ITER activity, several blanket concepts have been developed and one of the goals in Helias reactor studies was to transfer these concepts to the Helias reactor and to make a critical assessment of the advantages and disadvantages of the various concepts. The options in the Helias reactor are:

- Helium-cooled solid breeder blanket (HCPB)
- Water-cooled Li-Pb blanket (WCLL)

The implications of these concepts on the Helias reactor have been investigated and the procedure of maintenance has been analysed.

## 3.3 Alpha-particle orbits in a Helias reactor

It is shown that in the equilibrium magnetic field of the Helias configuration with <beta> = 5% and without perturbations all trapped particles form only poloidally passing bananas. The banana center orbits are closed inside the plasma column, which provides absolute confinement of trapped particles. Due to electromagnetic perturbations the poloidal drift can be suppressed and superbanana orbits can appear in the configuration as a result of the poloidal trapping of the banana orbit center. The poloidal size of superbanana orbits depends on the poloidal mode number m, while the deviation from the original orbit and the width of the superbanana in the radial direction depend on the radial profile and amplitude of the perturbations. If the perturbation does not go to zero on the plasma edge, particles with such orbits can be easily lost. The effect of electric perturbation is strongly selective in particle energy, which can be useful for helium ash removal. Electrostatic perturbations with a maximum value 30 V/cm, which is less then 1/5 of the ambipolar electric field, do not effect trapped hot alpha-particles, slightly change the trajectory of cold alpha-particles, and significantly perturb orbits of "ash" alpha-particles. The same effect can be expected for thermal deuterium and tritium particles. The influence of time independent magnetic perturbation does not depend on particle energy.

Applying the mapping technique, the long-term confinement of circulating alpha-particles has been analysed. Since under time-dependent perturbations the energy of particles is not conserved, resonant phenomena can arise and anomalous losses of particles can occur due to the effect of Arnold diffusion.

## 3.4 Drift waves in Helias configurations

The implications of Helias magnetic field geometry for drift wave stability and plasma edge turbulence have been studied by linear and nonlinear simulations in local field-aligned models of the metric. Three-dimensional electromagnetic fluid and gyrofluid drift-Alfvén turbulence codes have been applied to the equilibrium of Wendelstein 7-X and other non-axisymmetric model geometries in close collaboration with the Tokamak Theory Division. By variation of the configuration or flux tube alignement it has been found that the local metric has significant influence on instability and transport in stellarators. In cold-ion fluid models local shear contributes as the principal damping mechanism in low-global-shear stellarators. For a series of finite beta HSR equilibria, the reduction of unfavourable helical normal curvature with increasing beta was shown to result in less unstable linear ion-temperature-gradient driven gyrokinetic modes.

## 3.5 Low Aspect Ratio Helias Configurations

The magnetic field properties of the high iota version with 4 field periods (Fig. 2) is most similar to the current configuration. Fig. 3 shows Poincare' plots of an equilibrium of this configuration with <beta> = 4%.

The configuration currently considered for the Helias reactor is similar to the Wendelstein 7-X configuration and has five field periods and an aspect ratio of 11. A lower aspect ratio would allow one to reduce the major radius of the reactor and/or to enlarge the space between plasma and coils needed for blanket and shield. One way to lower the aspect ratio is to reduce the number of field periods. An easy procedure to get a configuration similar to W7-X is to take the coil description of W7-X in angle co-ordinates, reduce the major radius so that the coil size is unchanged, and arrange the toroidal coil system with the desired number of field periods. The main difference of the magnetic fields obtained this way is:

- the rotational transform is reduced because it is nearly constant per field period,
- the ratio of the helical field component to the axi-symmetric $B_{01}$ component is also reduced because the $B_{01}$ component increases with the reduction of the plasma aspect ratio,
- the magnetic well is deepened.

Following this procedure two configurations with 4 and one with 3 periods have been derived.

First calculations of the neoclassical transport coefficient $\varepsilon_{eff}$ show for the case with 4 periods values of less then 1% in the core region and an increase to about 1.5% towards the edge; in the case with 3 periods $\varepsilon_{eff}$ in the core is about 1.5% increasing towards the edge to 3.7%. The increase of $\varepsilon_{eff}$ towards the edge has the advantage of counteracting the formation of hollow density profiles.

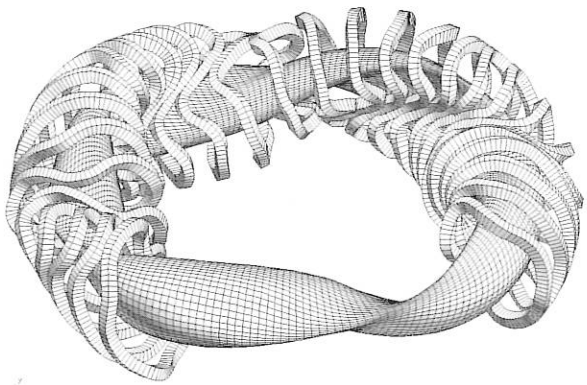

*Fig. 2: Coil system and magnetic surface of a 4-period Helias configuration*

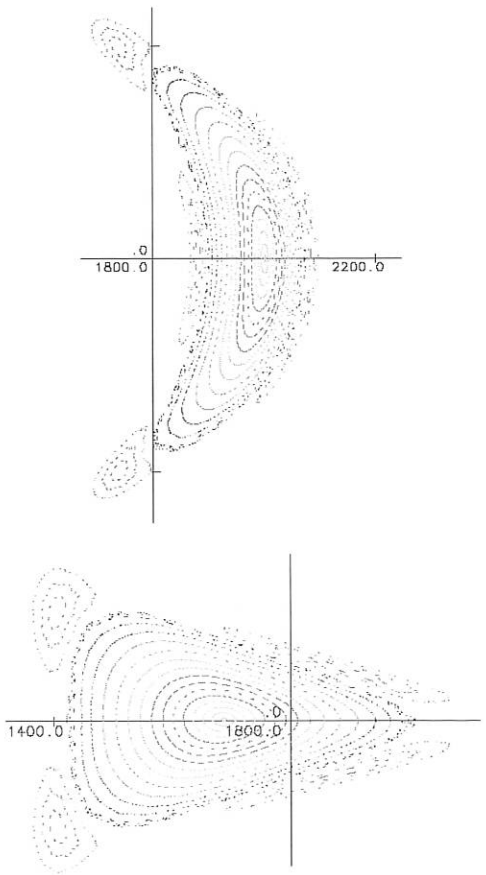


*Fig. 3: Poincaré plots of the 4-period configuration and $\iota_a$ = 4/4 at the symmetric planes (<β> = 4%).*

TABLE I. Main data of the Helias configurations with variou aspect ratios (δU/U = magnetic well, M = number of fiel periods)

| M | R[m] | a[m] | R/a | $\iota_o$ | $\iota_a$ | δU/U |
|---|---|---|---|---|---|---|
| 3 | 15 | 2.26 | 6.6 | 0.63 | 3/4 | 4% |
| 4 | 18 | 2.12 | 8.5 | 0.83 | 4/4 | 2.5% |
| 5 | 18 | 2.10 | 8.5 | 0.69 | 4/5 | 1% |
| 5 | 22 | 2.05 | 10.7 | 0.87 | 5/5 | 0.7% |

The disadvantage of the low aspect ratio configurations is th larger ratio of magnetic field strength on the coils to th average field strength on the magnetic axis due to the lowe coil aspect ratio leading to larger forces on the coils. If the fiel strength on the coils is a limiting value, a reduction of the fiel strength in the plasma region results. However, if the lov aspect ratio configurations would allow stable operations witl higher beta values, this disadvantage can be compensated. A second possibility for compensation is an increase of th plasma volume.

Configurations with a lower number of field periods relative t the current Helias reactor would allow one to reduce the majc radius to 18 m (4 periods) or 15 m (3 periods) if stabl operation at high beta (4 to 5%) is possible and th confinement of the α-particles sufficient.

## 3.6 Adaption of TOTAL_P code for interactive modelling of transport phenomena

The interactive transport code TOTAL_P (Toroidal Transport Analysis Linkage) with graphical interface is being further developed and applied to predict plasma parameters in the Helias reactor. The report IPP III/246 gives a manual for using this code package and describes the underlying physical models. The three-dimensional nature of the stellarator equilibria are taken into account. The transport equations solved in TOTAL_P are the time-dependent one-dimensional density and energy continuity equations with source terms. The particle diffusion fluxes and the thermal energy fluxes are written as a sum of neoclassical and anomalous fluxes. The particle source consists of the sources by pellet injection, recycling gas puffing neutrals, neutral beam injection, deletion of fuel Deuterium and Tritium and creation of He ions for D, T burning plasmas. The electron density is obtained from the charge neutrality condition. To describe the neoclassical diffusion flux, we follow Beidler's formulation of the neoclassical transport in stellarators. The radial electric field is determined from the ambipolar diffusion condition. A typical result for the Helias reactor with major radius R = 22 m, minor radius a = 1.8 m, average beta = 3.6%, beta(0) = 11% are shown in the Figures for electron density, temperatures and the fusion output. The simulation runs for 200 seconds physical time.

# IEA IMPLEMENTING AGREEMENT
## for Cooperation in Development of the Stellarator Concept

### 1. OBJECTIVES OF THE AGREEMENT

The objective of the Implementing Agreement, first concluded in 1985, is to "improve the physics base of the Stellarator concept and to enhance the effectiveness and productivity of research and development efforts relating to the Stellarator concept by strengthening co-operation among Agency member countries". To achieve this, it was agreed to exchange information, conduct workshops, exchange scientists, do joint theoretical, design and system studies, coordinate experimental programmes in selected areas, exchange computer codes, and perform joint experiments. In 1995 the Agreement was extended until June 2000. The contracting parties are EURATOM, the U.S. DoE, Japan, and Australia. In September 1994, Russia became an Associate Contracting Party.

### 2. STATUS OF THE AGREEMENT

In 1999, there were two meetings of the Executive Committee. The 27$^{th}$ meeting was held at Maastricht, The Netherlands, on June 15, in conjunction with the 26$^{th}$ European Physical Society Conference on Controlled Fusion and Plasma Physics from June 14 to 18. F. Wagner from IPP was introduced as a new member of the committee. H. Wobig participated as alternate. All members agreed on the extension of the Stellarator Implementing Agreement for 5 years (expiry date is July 2000). Other main points were the status of experiments, association of the Ukraine to the IEA Implementing Agreement, increased collaboration on new devices, and forthcoming meetings. The need for a reactor study on stellarators including comparison with the tokamak line was pointed out.

The 28$^{th}$ meeting was held at Madison, USA, on September 28 in conjunction with the 12$^{th}$ Int. Stellarator Conference. From IPP, H. Wobig and J. Nührenberg participated as alternates. The committee approved the statement of Japan on extending the LIME programme to the next year and adding two new programmes relating to plasma-wall interaction and fusion materials technology in two years. It was suggested that a special session on stellarator power reactors will be organized during the next Toki Conference in January, 2000.

### 3. REPORT ON 1999 ACTIVITIES

In 1999, 29 physicists participated in the exchange of scientists.

During his stay from January 11 to 25, D. Darrow from Princeton designed a diagnostic probe for analysis of fast ion losses in W 7-AS. This probe was successfully operated during the following experimental campaign at W 7-AS. The visit of D. Darrow from April 26 to May 7 served to discuss the initial measurements, and, in particular, define and perform an experimental programme concerning different issues relating to confinement of fast ions in W 7-AS. The previous work of D. Darrow on these topics at TFTR and CHS and his activity for W 7-AS have led to fast realization of this diagnostics and important results obtained in W 7-AS. K. Watanabe from NIFS Toki continued the definition of an international local transport stellarator database with U. Stroth from January 23 to February 27. E. Solano from Austin discussed coupled systems of particle and energy balance equations with H. Maassberg for 4 weeks in January. M. Bitter from Princeton participated in W 7-AS operation in the field of spectroscopy and discussed X-ray diagnostics for W 7-X in February. T. Morisaki and A. Takayama from NIFS Toki were concerned with edge neutral calculation and modelling during their 5-week stays in spring. A. Mase from the University of Tsukuba had an exchange of views on microwave diagnostics, especially imaging systems, with H.-J. Hartfuss during his short visit in February. Staying for 4 weeks in March, K. Kondo from the University of Kyoto measured the plasma radiation in the soft X-ray region by means of the W 7-AS grazing incidence spectrometer. K. Yamasaki from NIFS Toki held discussions on NEMEC and MFBE codes with H. Wobig for two days in March. The visit of S. Hamaguchi from NIFS Toki was concerned with analogous transport issues on helical devices and stellarators (23.3. – 27.3.). R. Boivin from MIT Cambridge was interested in AXUV diodes and bolometry during his short visit from June 9 to 11. J. Lyon from ORNL stayed for 7 days in June to discuss continuation of co-operation on stellarator research. K. Tanaka from NIFS Toki is the responsible scientist for interferometry at LHD. On the occasion of the EPS conference in Maastricht he visited IPP from June 20 to 27 and gave a

talk on density profile measurements and transport investigations at LHD. His visit was also devoted to intensifying contact between the W 7-AS/X and LHD microwave diagnostic groups. J. Tataronis from the University of Wisconsin investigated Alfvén modes-singular behaviour for one month in July. During his visit from July 12 to 18 P. Morrison from Austin gave a talk on transport barriers in toroidal systems and had several discussions on this issue with the experts at IPP. He is an expert in Hamiltonian flows and mapping techniques and the purpose of his stay was to apply these techniques to the issue of anomalous transport in stellarators and tokamaks. The purpose of a 3-day visit of K. Ida from NIFS Toki in autumn was technical coordination concerning a fast system for Charge Exchange Recombination Spectroscopy. This system is being developed in cooperation between NIFS and IPP as part of the LIME scientific programme of the Japanese government. The spectroscopic system will be first tested and employed on W 7-AS, later on LHD. Mr. Hanatani from the University of Kyoto has developed a code which computes neoclassical transport and bootstrap currents in tokamaks and stellarators. In particular, his interest during his stay from October 18 to 29 was to apply this theory to bootstrap currents in the Helias configuration (WENDELSTEIN 7-X and the stellarator reactor). The long-term collaboration with S. Murakami from NIFS will be continued. In the past, S. Murakami applied his Monte Carlo code both to the description of the ECRH-driven electron fluxes ("electron root" scenarios) at W 7-AS and to confinement of fast ions generated by ICRH. The "electron root" results were presented at the IAEA conference in Yokohama (1998) as well as in a paper in Phys. Plasmas (Dec. 1999). The future development of these Monte Carlo simulations and further collaboration were discussed during his visit from December 11, 1999, to January 31, 2000.

U. Stroth held a seminar talk and discussed possible research projects with UCLA/UCSD and Caltech Lab. to be adopted at Kiel University, during a short visit to San Diego from February 20 to 27. H. Wobig participated in the 3rd Symposium on Current Trends in International Fusion Research – review and assessment – in Washington from March 8 to 12. L. Giannone visited NIFS Toki from March 18 to April 1 to discuss possible collaboration on density limit investigations. During April 12 to 14 V. Erckmann and G. Cattanei attended the 13th Trop. Conference on Applications of Radio Frequency Power to Plasmas in Annapolis/Maryland. U. Stroth and J. Bleuel stayed at Portland for 3 days in April to participate in a European Transport Task Workshop and discuss the role of the radial electric field for confinement in W 7-AS. F. Sardei and Y. Feng attended the 7th Plasma Edge Theory Conference at NIFS Toki in October. From October 4 to 8 Ch. Fuchs and V. Erckmann visited Oh-arai to participate in the IAEA Technical Committee Meeting on ECRH Physics and Technology for Fusion Devices and in the 11th Joint Workshop on Electron Cyclotron Emission and ECRH. A. Werner attended the 6th IAEA Technical Committee Meeting on Energetic Particles in Magnetic Confinement Systems at Naka, Toki, from October 12 to 14. D. Hartmann participated in a Technical Committee Meeting on Steady State Operation at Fukuoka from October 25 to 29.

## 4. CONFERENCES AND WORKSHOPS

In 1999, the 12th Int. Stellarator Conference took place at Madison/USA from September 27 to October 1. From IPP 13 scientists participated in the Conference.

# Divisions and Groups

# THE SCIENTIFIC DIVISIONS OF IPP

**Experimental Plasma Physics Division 1**
Director: Prof. M. Kaufmann

ASDEX Upgrade (Divertor Tokamak)
- operation of ASDEX Upgrade
- investigation of ITER plasma boundary in a reactor-relevant divertor
- advanced tokamak studies
- investigation of energy transport, MHD stability, beta limit, density limit and disruptions

JET collaboration
- operation of special discharge scenarios at JET
- collaboration in pellet injection physics
- preparation of scientific work on JET under EFDA

**Experimental Plasma Physics Division 2**
Director: Prof. H. Zohm

ASDEX Upgrade
- analyses of MHD stability of ASDEX Upgrade discharges
- active control of MHD instabilities using ECRH
- effect of MHD instabilities on core plasma parameters

ITER
- scaling of the abovementioned topics to reactor-grade plasmas

JET
- contribution to Task Forces S1 (conventional scenarii) and M (MHD)

**Experimental Plasma Physics Division 3**
Director: Prof. F. Wagner

WENDELSTEIN 7-AS (Advanced Stellarator)
- stellarator with improved magnetic characteristics

Experiment-orientated stellarator Theory
- interpretation of stellarator experiments

Stellarator power plant system studies
- development of the HELIAS power plant concept

Preparation of the WENDELSTEIN 7-X diagnostics
Preparation of ECRH for WENDELSTEIN 7-X
Development of Greifswald site

**Experimental Plasma Physics Division 4**
Director: Prof. K. Behringer

Experimental and theoretical investigations of plasma boundary and divertor physics, impurity transport, chemical impurity production and plasma radiation in ASDEX Upgrade and WENDELSTEIN 7-AS
- spectroscopic diagnostics on ASDEX Upgrade
- spectroscopic diagnostics on WENDELSTEIN 7-AS
- laboratory experiments at the University of Augsburg, Experimental Plasma Physics

**WENDELSTEIN 7-X Construction**
Director: Dr. M. Wanner

WENDELSTEIN 7-X R&D programme
WENDELSTEIN 7-X Construction
- engineering, construction and installation of the WENDELSTEIN 7-X device incl. plasma heating and in-vessel components
- project control and quality management

**Stellarator Theory Division**
Director: Prof. J. Nührenberg

General stellarator theory
- Further development of the stellarator concept and computational as well as analytical methods to investigate equilibrium, stability and transport problems in three-dimensional toroidal configurations.

Plasma edge physics
- Theoretical work on 3D plasma edge physics

**Tokamak Physics**
Director: Prof. K. Lackner

General tokamak physics
- experiment-oriented theoretical work for the design and interpretation of tokamak experiments

Plasma edge physics
- experimental and theoretical work on plasma edge physics

Nonlinear plasma dynamics
- numerical simulation of turbulent transport and MHD reconnection phenomena

ITER collaboration
MHD stability
- linear and nonlinear investigations of MHD stability in conventional and advanced tokamak scenarios
- influence of fast particles

**Surface Physics Division**
Directors: Prof. V. Dose, Prof. J. Küppers

Surface physics
- atomistic characterization of surfaces

Plasma-wall interactions (analytical)
- interactions of atoms, ions and electrons with solid surfaces
- wall fluxes in the boundary layer of plasma devices
- limiter and wall analyses

Plasma-wall interaction (preparative) (see also Technology Division)
- preparation and characterization of thin-film coatings for plasma devices

Data analysis
- application of Bayesian techniques to experimental data

**Technology Division**
Director: Prof. R. Wilhelm

Neutral injection
- development and construction of the injection systems for WENDELSTEIN 7-AS, ASDEX Upgrade and WENDELSTEIN 7-X
- implementation of injection experiments

Electron cyclotron resonance heating
- construction and operation of an ECRH system for ASDEX Upgrade

Ion cyclotron resonance heating
- preparation and implementation of ICRH experiments for WENDELSTEIN 7-AS, ASDEX Upgrade and WENDELSTEIN 7-X

Plasma technology (see also Surface Physics Division)
- development, characterization and modelling of low-pressure plasma processes for thin-film formation

**Plasma Diagnostics Division**
Director: Prof. G. Fussmann

Edge plasma physics
- experimental and theoretical work relating to fusion devices

Plasma generator PSI-1
- basic plasma physics
- plasma interaction with solid surfaces
- development and testing of plasma diagnostics

Electron Beam Ion Trap (EBIT)
- production of highly charged ions
- X-ray spectroscopy and atomic physics measurements

UHV laboratory, arc physics, ITER collaboration

**Materials Research Division**
Director: Prof. H. Bolt

Characterization of fusion relevant properties of plasma facing materials; Development and qualification of plasma facing materials for present fusion devices, esp. ASDEX Upgrade, WENDELSTEIN 7-X;
Design and development of materials for plasma facing applications in fusion reactors.

# EXPERIMENTAL PLASMA PHYSICS DIVISION 1

(Prof. Dr. Michael Kaufmann)

The activities of division E1 are concentrated on the ASDEX Upgrade related work and are reported in section "ASDEX Upgrade Project".

The division E1 comprises

1. Three diagnostic groups
   a. pellet injection, bolometer, neutral gas, neutron measurements, HXR, mass spectrometer
   b. He measurements, ECE, microwave reflectometry and fluctuations, SABA, charge exchange, LENA, DCN interferometer, calorimetry, Langmuir probes, Li-beam diagnostics, manipulators
   c. electromagnetic measurements, plasma control, MSE, halo current measurements

   which are responsible for the development of plasma diagnostics as well as for plasma physics exploitation.

2. Three machine groups
   a. operation
   b. mechanical design
   c. assembly,

   which are concerned with the operation and engineering developments of the tokamak experiment ASDEX Upgrade and its peripheral installation.

3. Two computer groups
   a. real-time control of the ASDEX Upgrade plasma,
   b. data acquisition and data evaluation.

These groups are supported by 3 workshops: mechanical, electrical, and electronical.

Divison E1 is also devoted to collaboratin on JET and to continue studies for ITER.

# EXPERIMENTAL PLASMA PHYSICS DIVISON 2

(Prof. Dr. Hartmut Zohm)

Department E2 investigates the magnetohydrodynamic stability of ASDEX Upgrade discharges. In addition to the pure analysis of instabilities, their effect on the reduction of the tokamak operational space is examined. In collaboration with the ASDEX Upgrade ECRH group, strategies are being developed which will increase the operational space via the active control of instabilities.

For these purposes, E2 operates the following diagnostics on ASDEX Upgrade:

- The classical MHD-Diagnostic Mirnov and SXR and the use of fast ECE (in collaboration with E1). Along with the installation of Hardware, methods of improved data analysis are investigated, like for example the direct comparison with results from MHD-codes (in collaboration with TOK).
- Thomson scattering for the determination of the core plasma parameters $T_e$ and $n_e$. In addition, the set-up of this diagnostic allows to determine the average charge state $Z_{eff}$ via measurement of the Bremsstrahlung emission.

Scientific staff: A. Gude, B. Kurzan, A. Letsch (Diploma student), M. Maraschek, J. Meskat (PhD Student), R. Monk, H.D. Murmann, A. Mück (Diploma student), K.H. Steuer, H. Zohm

Diploma and PhD students are part of the collaboration with IPF, Stuttgart University.

Technical staff: J. Hausmann, K. Huber, G. Jones, J. Krippner, U. Ortner

# EXPERIMENTAL PLASMA PHYSICS DIVISION 3 (W7-AS)

(Prof. Dr. Friedrich Wagner)

The W7-AS group comprises Experimental Plasma Physics Division 3. The work is fully reported in the section "STELLARATOR Project", of which the members are as follows:

*Experimental Plasma Physics Division 3*

T. Amano[11], M. Anton, S. Bäumel[23], T. Baloui[5, 23], N. Basse[1], C. Beidler, M. Bitter[21], J. Bleuel[22], R. Brakel, H. Callaghan[2], G. Cattanei, D. Darrow[21], D. Dorst, H. Ehmler[22], A. Elsner, M. Endler, K. Engelhardt, V. Erckmann, Y. Feng, S. Fiedler, N. Franz[24], C. Fuchs[22], F. Gadelmeier[22], U. Gasparino, J. Geiger, L. Giannone, P. Grigull, O. Grulke[6, 23], H. Hacker, S. Hamaguchi[11], K. Hanatani[13], E. Harmeyer, H.J. Hartfuß, F. Herrnegger, M. Hirsch, E. Holzhauer[7], J.K. Hübner[5], K. Itoh[11], S.-I. Itoh[12], R. Jaenicke, F. Karger, A. Kendl[23], M. Kick, A. Kislyakov[15], J. Kisslinger, T. Klinger[4], S. Klose[22], J. Knauer, G. Kocsis[9], J.P. Koponen[8], H. Kroiss, G. Kühner, A. Kus, H. Laqua, L. Ledl[23], R. Liu, L. Lubyako[17], H. Maaßberg, N. Marushchenko[19], A. Mase[14], K. McCormick, G. Michel, T. Morisaki[11], P. Morrison[21], S. Murakami[11], S. Niedner[6, 23], M.G. Pacco-Duechs, G. Petravich[9], S. Reimbold[5, 23], M. Rodriguez[3], M. Romé[10], N. Ruhs, N. Rust[22], J. Saffert, M. Saffman[1], A. Salat, E. Sallander[18], J. Sallander[18, 20], F. Sardei, A. Shishkin[19], M. Schubert[23], V. Sergeev[16], I. Sidorenko[22], T. Stoeferle[24], U. Stroth, E. Suvorov[17], K. Tanaka[11], A. Takayama[11], J. A. Tataronis[20], H. Thomsen[4, 23], F. Volpe[23], F. Wagner, H. Walter[22], K. Watanabe[11], A. Weller, Chr. Wendland[22], A. Werner[22], E. Würsching, W. Xu[7, 22], D. Zimmermann, M. Zippe, S. Zoletnik[9]

1) Guest from RISOE, Roskilde (Denmark)
2) Guest from University of Cork (Eire)
3) Guest from University Darmstadt (Germany)
4) Guest from EMAU Greifwald (Germany)
5) Guest from IAP/University Heidelberg (Germany)
6) Guest from University of Kiel (Germany)
7) Guest from IPF Stuttgart (Germany)
8) Guest from University of Helsinki, Espoo (Helsinki)
9) Guest from KFKI Research Inst., Budapest (Hungary)
10) Guest from University Milano (Italy)
11) Guest from NIFS, Nagoya (Japan)
12) Guest from RIAM, Kyushu (Japan)
13) Guest from Kyoto University (Japan)
14) Guest from Tsukuba University (Japan)
15) Guest from IOFFE Institute, St. Petersburg (Russia)
16) Guest from TUAP, St. Petersburg (Russia)
17) Guest from IAP Nizhny Novgorod (Russia)
18) Guest from RIT Stockholm (Sweden)
19) Guest from IPT-NSC Kharkov (Ukraine)
20) Guest from Univ. of Wisconsin (USA)
21) Guest from PPPL (USA)
22) Postdocs
23) Doctoral fellow
24) Undergraduate

*Technical Team W7-AS:*

G. Abele, P. Ahlrep, J. Ahmels, S. Bartsch, W. Bendak, M. Bergbauer, P. Böhm, J. Bömerl, K.H. Brumm, H. Czich, S. Eder, A. Eschlwech, A. Fohr, M. Fusseder, H. Greve, G. Grünwald, J. Hofner, H. Holitzner, F. Hollmann, H. Ibbach, E. Katzmarek, K.H. Knauer, F. Kunkel, D. Lingen, J. Littwin, U. Neumann, R. Neuner, F. Noke, F. Offenbächer, I. Ott, V. Otte, J. Prechtl, R. Puff, F. Purps, S. Radau, S. Ravichandran, T. Richert, H. Rixner, L. Schmid, H. Scholz, P. Schötz, S. Schraub, R. Semler, R. Singer, H. Speer, B. Stajminger, H.-J. Stresau, M. Steffen, H. Volkenandt, K.H. Wagner, H. Wolf, Chr. Wöstmann, G. Zangl, W.v. Zeppelin, R. Zille, Do. Zimmermann

*Experimental Plasma Physics Division – Reactor Studies*

C. Beidler, E. Harmeyer, F. Herrnegger, J. Kisslinger, I. Ott, H. Wobig, R. Zille

*Experimental Plasma Physics Division 4*

J. Baldzuhn, K. Behringer, R. Burhenn, R. König A. Weghorn

*ECRH (Electr. Cycl. Resonance Heating):*

W. Kasparek, L. Empacher, W. Förster, G. Gantenbein, P.G. Schüller, K. Schwörer (IPF Stuttgart)
L. Lubyako, E. Suvorov (IAP Nizhny Novgorod)

*ICRH (Ion Cycl. Resonance Heating):*

W. Becker, F. Braun, H. Faugel, D.A. Hartmann, F. Hofmeister, J.M. Noterdaeme, F. Wesner (Technology Division)

*NBI (Neutral Beam Injection):*

W. Ertl, W. Ott, F.-P. Penningsfeld, F. Probst, R. Riedl, W. Schärich, E. Speth, R. Süß, (Technology Division),

*Plasma Surface Interaction Group:*

R. Behrisch, V. Dose, U. Langer, J. Roth, E. Taglauer

*Plasmadiagnostics (Berlin)*

D. Hildebrandt, D. Naujoks

*Computer Centre:*

S. Heinzel, H. Lederer, A. Schott

*Central Technical Services:*

D. Arz, B. Brucker, H. Eixenberger, Th. Franke, E. Grois, F. Gresser, R. Kutzner, W. Melchior, J. Perchermeier, J. Stadlbauer, K. Voigt, G. Wenzel

# EXPERIMENTAL PLASMA PHYSICS DIVISION 4

(Head of Division: Prof. Dr. Kurt Behringer)

Experimental Plasma Physics Division 4 (E4) consists of the ASDEX Upgrade, W 7-AS and ITER Diagnostics groups. This work is described in the ASDEX Upgrade and W 7-AS project reports. For ITER Diagnostics, activities had waned and are just restarting. Experimental Plasma Physics at the University of Augsburg is closely linked to E4, allowing physics students to participate in IPP's scientific programme or do basic research at Augsburg. Recent results are given under University Contributions to IPP Programme.

ASDEX Upgrade: I. Altmann, D. Bolshukhin, R. Dux, W. Engelhardt, J. Gafert, A. Geier, A. Kallenbach, B. Plaum, R. Pugno, R. Neu, H. Meister, K. Schmidtman, W. Ullrich, M. Zarrabian. W 7-AS: J. Baldzuhn, R. Burhenn, R. König Augsburg: U. Fantz, B. Heger, H. Paulin, ITER Diagnostics: H. Salzmann. Technical Staff: G. Daube, M. Hien, J. Fink, G. Schmitt, A. Weghorn. Diplomanden: A. Lotter, T. Madeira, S. Meir, A. Kottmair, P. Starke, B. Waldmann, D. Wünderlich.

Co-operation: IPP Berlin, JET, KFA Jülich, TU München, University of Strathclyde (Scotland), Stuttgart University.

The E4 scientific programme deals with plasma boundary and divertor physics, with impurity transport and plasma radiation, and with low- and high-Z wall materials. Mainly spectroscopic diagnostics and analysis methods are being used in E4. Recent topics in ASDEX Upgrade were divertor plasma parameters, radiative cooling and chemical carbon erosion. Impurity transport at the H-mode edge is being studied from silicon soft X-ray radiation. As an alternative to carbon, partially tungsten-covered walls and neoclassical high-Z transport are being investigated. The interest in W 7-AS is focused on measurements of electric fields, neoclassical impurity transport, impurity pellet injection and magnetic field structures. Spectroscopic diagnostics for W7-X are also being developed.

Spectroscopic measurements of line or continuum intensities as well as molecular band radiation (see Augsburg University contribution) require interpretation on the basis of atomic physics and radiative transfer. To have access to the most up-to-date results, E4 is part of the ADAS international co-operation. Even for atomic hydrogen, electron excitation rate coefficients are not very well known and new, improved data have become available at the end of 1999 [1]. These are very important, since hydrogen line intensities or line ratios are routinely being used for divertor diagnostics. Figures 1 and 2 show results of collisional-radiative calculations using the new theory and comparisons with experimental results from ASDEX Upgrade edge and divertor. Measurements in microwave plasmas are also shown. The agreement of theory and ex-periment is very good for $H_\alpha/H_\gamma$ line ratios, while $H_\alpha/H_\beta$ appears to be somewhat underestimated. Density mesurements by means of $H_\alpha/H_\gamma$ line ratios now have a much safer basis.

[1] Anderson H, Ballance C P, Badnell N R and Summers H P, An R-matrix with pseudo-states approach to electron impact excitation of HI for diagnostic applications in fusion plasmas, submitted to J. Phys. B: At. Mol. Opt. Phys., 1999

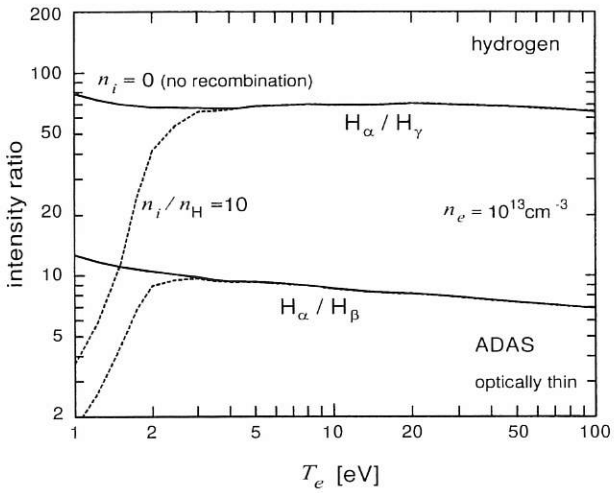


*FIG. 1: Calculated hydrogen line ratios with new rate coefficients as a function of electron temperature.*

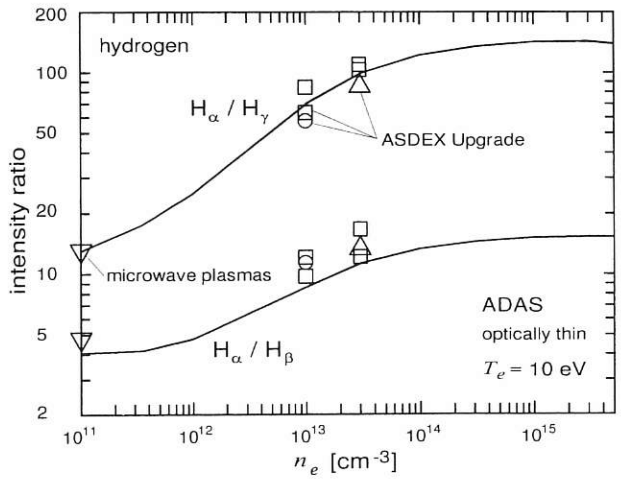


*FIG. 2: Calculated hydrogen line ratios with new rate coefficients as a function of $n_e$. Results for ASDEX Upgrade edge and divertor plasmas and microwave plasmas are also shown.*

# WENDELSTEIN 7-X Construction

(Dr. Manfred Wanner)

*W7-X Construction Division*
*Engineering Team:* I. Bojko, J. Boscary, T. Bräuer, R. Bünde, J.-H. Feist, H. Greuner, H. Grote, B. Hein, F.-W. Hoffmann, H. Laqua, M. Nagel, H. Niedermeyer, M. Pieger-Frey, J. Reich, H. Renner, T. Rummel, J. Sapper, J. Schacht, F. Schauer, F. Schneider, H. Schneider, R. Schönecker, I. Schoenewolf, A. Spring, M. Wanner, L. Wegener, F. Werner

*Technical Team:* H. Bau, A. Benndorf, H.-J. Bramow, R. Brockmann, A. Brückner, M. Czerwinski, M. Fricke, F. Füllenbach, W. Gardebrecht, J. Glagla, M. Gottschewsky, A. Hölting, U. Kamionka, E. Köster, C. Kopplin, K. Lang, T. Mönnich, I. Müller, F. Nankemann, A. Opitz, M. Pietsch, S. Pingel, R. Rieck, U. Schultz, K.-U. Seidler, F. Starke, O. Volzke, I. Wald, A. Wölk

The W7-X Construction Division was supported by

*Technology Division (NBI, ICRH)*: E. Speth, B. Heinemann, S. Obermayer, W. Ott, F.-P. Penningsfeld, R. Riedl, W. Schärich, K. Wittenbecher, D. Hartmann, F. Wesner

*Experimental Division E3 (ECRH):* R. Brakel, V. Erckmann, F. Hollmann, H. Laqua, G. Michel

*Plasma Diagnostics Division Berlin:* K. Gallowski, D. Hildebrandt, M. Laux, D. Rüter, J. Sachtleben

*Materials Research Division:* O. Jandl, S. Koetterl, M. Rehm

*Central Technical Services (ZTE)*: D. Arz, W. Bitter, H. Eixenberger, R. Holzthüm, N. Jaksic, F. Kerl, B. Mendelevitch, K. Pfefferle, J. Simon-Weidner, B. Sombach, J. Tretter, M. Weißgerber, F. Ascher, S. Geißler, H. Pirsch, J. Stadlbauer, A.E. Maier

*Forschungszentrum Karlsruhe FZK (IHM, IMF I, ITP, PMW)*: A. Arnold, E. Borie, G. Dammertz, M. Darweschsad, S. Fink, G. Friesinger, P. Grundel, R. Heidinger, R. Heller, W. Herz, H. Hunger, S. Illy, M. Klenk, P. Komarek, H.-R. Kunkel, M. Kuntze, W. Leonhardt, W. Maurer, I. Meyer, G. Neffe, G. Noether, S. Nold, B. Piosczyk, G. Schleinkofer, M. Schmid, R. Spörl, M. Suesser, M. Thumm, A. Ulbricht, R. Vincon, A. Weis, F. Wuechner, G. Zahn

*Institut für Plasmaforschung (IPF) Stuttgart*: L. Empacher, W. Förster, G. Gantenbein, W. Kasparek, G.A. Müller, P.G. Schüller, W. Xu, H. Zohm

# STELLARATOR THEORY DIVISION

(Prof. Dr. Jürgen Nührenberg)

The activity of the Stellarator Theory Division is concentrated on further development of the stellarator concept and numerical as well as analytical methods to investigate equilibrium, stability and transport problems in three-dimensional toroidal configurations.

The relevant team is:
X. Bonnin, M. Borchardt, M. Drevlak, S. Gori, R. Hatzky, R. Kleiber, A. Könies, H. Leyh, P. Merkel, A. Mutzke, C. Nührenberg, J. Riemann, R. Schneider, R. Zille.

# TOKAMAK PHYSICS

(Head of Project: Prof. Dr. Karl Lackner)

Most of the scientific work of this division is carried out in close collaboration with experiments and reported in the respective sections on the projects: ASDEX–Upgrade, JET, ITER. This concerns, in particular, all applied studies on MHD instabilities, modelling of scrape-off layer and divertor plasmas, and the analysis of transport properties. The contributions described here concern therefore model developments in the stage prior to specific applications, basic plasma physics issues, or parts of theory (in particular turbulent transport) where the comparison with experiments is still in the qualitative rather than quantitative phase.

Head: K. Lackner, Deputy: M. Brambilla
R. Arslanbekov, G. Becker, A. Bergmann, R. Bilato, D. Biskamp, K. Borrass, M. Brambilla, K. Büchl, A. Carlson, A. Celani, D. Correa-Restrepo, D. Coster, D. Düchs, W. Feneberg, S. Günter, K. Hallatschek, V. Igochine, B. Janauschek, F. Jenko, O. Kardaun, J. Kim, R. Kochergov, L. Lengyel, D. Lortz, P. Martin, R. Meyer-Spasche, W.-C. Müller, J. Neuhauser, G. Pautasso, A. Peeters, S. Pinches, E. Poli, W. Sandmann, S. Schade, R. Schneider, W. Schneider, E. Schwarz, J. Schweinzer, B. Scott, G. Spiess, E. Strumberger, G. Tardini, H. Tasso, C. Tichmann, A. Teo, M. Weinlich, R. Wunderlich, H.-P. Zehrfeld, A. Zeiler

Guests: C.V. Atanasiu, Institute for Atomic Physics, Romania H. Bürbaumer, Technical University of Vienna, J. F. Drake, University of Maryland, S. Egorov, State Technical University, St. Petersburg, J.H. Han, Korea Basic Science Institute, Korea, U. Holzmüller, University of Innsbruck, P. Lalousis, IESL.FORTH, Heraklion, P. McCarthy, University College, Cork, V. Rozhansky, State Technical University, St. Petersburg, Samuli Saarelma, Helsinki University of Technology, G.N. Throumoulopoulos, University of Ioannina, N. Tsois, Demokritos, Athens, A. Ushakov, State Technical University, St. Petersburg, I. Veselova, State Technical University, St. Petersburg, S. Voskoboynikov, State Technical University, St. Petersburg, H. Weitzner, Courant Institute of Mathematical Sciences, Q. Yu, Institute of Plasma Physics, Hefei, China

## 1. APPLIED THEORY OF TOROIDAL CONFINEMENT

Plasmas are fluids of, in general, high Reynolds or Rayleigh number and are hence prone to develop various kinds of turbulence, where one distinguishes mainly between small-scale and large-scale turbulence. The former is typical of low-$\beta$ sheared systems, such as in tokamaks, while the latter occurs in high-$\beta$ plasmas, e.g. in the solar wind.

### 1.1 Transport

The studies reported here focus on the cool edge region of tokamak discharges, where a fluid description is adequate.

#### *1.1.1 Electromagnetic ion-temperature-gradient-driven (ITG) turbulence*

D. Biskamp, K. Hallatschek, A. Zeiler, W.- C. Müller

The numerical simulations are based on three-dimensional simulations of the electromagnetic Braginskii equations in a toroidal flux-tube domain, treated in the local (= Boussinesq) approximation. It is found that, contrary to linear theory, where electromagnetic effects tend to increase the wavelength of the unstable modes and hence seem to indicate an increase of transport, nonlinear turbulence exhibits a strong reduction of the transport in relation to the electrostatic limit. The reason for this behaviour is linked to the saturation mechanism of the ITG mode. Instabilities driven by unfavourable curvature on the torus outside form radial streamers, *i.e.* an alternating pattern of radial flows in the inward and the outward directions. It is the breakup of this sheared flows by secondary instabilities which controls the saturation of the instability and ultimately the transport level. In the electrostatic limit of the ITG instability, the secondary instability is the Kelvin-Helmholtz mode, which destroys the radial streamers generated by the linear instability. In the electromagnetic regime the radial streamers drag along the toroidal magnetic field, thus producing a radial magnetic field which alternates sign in the poloidal direction. The reconnection of this magnetic field breaks the radial streamers apart more efficiently than the Kelvin-Helmholtz mode, leading to a lower transport level. It is thus found that electrostatic and electromagnetic turbulence follow fundamentally different nonlinear dynamics, such that an estimate of the transport based on the linear properties of the ITG mode has to fail.

#### *1.1.2 Nonlocal edge transport*

D. Biskamp, K. Hallatschek, A. Zeiler, W.- C. Müller

At the plasma edge, temperature gradients may be very steep, so that the profile scale length $L_T$ becomes comparable to a typical turbulent wavelength $k_0^{-1}$ and the local approximation breaks down. A newly developed nonlocal electrostatic code was used to study the turbulence behaviour in this region, in particular the transition between ITG turbulence located on the hotter inner side of the edge plasma and resistive ballooning turbulence in the cool outermost plasma region. It was found that, by increasing the nonlocality parameter $(L_T k_0)^{-1}$ above unity, the

turbulent transport is reduced to a small fraction of the value in a local system. For the ITG mode, the turbulence quench is primarily due to a decrease of the linear growth rate, while for the ballooning mode a novel inherently nonlocal saturation mechanism was identified: nonlocal modification of the linear eigenmodes, which leads to enhanced nonlinear production of harmonics and sub-harmonics, such that saturation occurs at a smaller amplitude.

### *1.1.3 Electron–temperature–gradient–driven turbulence*

F. Jenko

It is widely believed that two instabilities are responsible for the anomalous (turbulence-induced) transport in the core of fusion plasmas, namely ion-temperature-gradient-driven (ITG) and trapped-electron-driven modes. However, in recent years there has been increasing evidence that this ''standard model'' of core turbulence is incomplete. Particularly, the behaviour of internal transport barriers (ITBs) in advanced tokamak discharges cannot be understood without introducing additional microinstabilities such as the electron-temperature-gradient-driven (ETG) mode. This mode exists on extremely short length and time scales and is therefore hard to detect experimentally. Nevertheless, in some cases one can observe a clear signature of ETG-induced electron heat transport: the local electron temperature gradient is close to the critical value above which the ETG mode is destabilized. Quasilinear theories and nonlinear models exploiting similarities between ETG and ITG turbulence fail to predict this kind of behaviour. Therefore, we explored collisionless ETG turbulence via direct nonlinear simulations with the GENE gyrokinetic electromagnetic code. Somewhat surprisingly, and unlike the analogous case of ITG turbulence, we find that the turbulent electron heat transport is significantly underpredicted by the quasilinear estimate. This oberservation is directly linked to the presence of radially highly elongated vortices (''streamers'') which lead to very effective radial transport. The simulations indicate ETG-induced turbulent transport can be high enough to force the electron temperature gradient towards its critical value in a wide region of parameter space. Because of its small spatial and temporal scales, ETG turbulence is able to exist even in a large poloidal shear flow environment and therefore sets a lower limit on the electron heat transport within an ITB. Moreover, ETG turbulence is likely to be also relevant to other regimes in fusion experiments.

### *1.1.4 Electromagnetic gyrofluid turbulence in realistic tokamak geometry*

B. Scott

The basic outline of the model is equal treatment of the electron and ion fluids, with proper kinetic dissipation mechanisms for each. Additionally, comparisons with simpler fluid models have shown the importance, especially for the ions, of keeping the perpendicular and parallel temperatures as separate variables, since the collisions are too weak to keep the temperature isotropic. In most regimes of interest the perpendicular ion temperature is the largest of the normalized fluctuating variables - but the electron dynamics at finite plasma beta is still very important in a synergistic way, helping to drive the system to a strong turbulence level. Physics tests involving a hierarchy of fluid models have shown that resistive ballooning can be ruled out as an important physical mechanism for edge turbulence. We started with the linear instabilities and then followed their development through the saturation phase and into fully developed turbulence. The various effects in the vorticity equation were directly measured, with the result that magnetic curvature, which is decisive for linear modes, becomes subdominant in the turbulent regime as the self-advection of small-scale flows takes over. The physics is drift-wave-like, with the curvature acting as a catalyst and the perpendicular ion temperature adding the ITG physics to form the overall situation. We achieve adequate success in comparison with experiment only when using globally consistent magnetic flux surface geometry from an actual Grad-Shafranov equilibrium, even qualitatively. In the simple S-$\alpha$ model, ideal ballooning physics is overvalued for edge turbulence, and the streamer formation regime for the ETG turbulence is actually undervalued. With all the effects brought in by finite aspect ratio and magnetic shear and shaping accurately modelled, we find trends of transport with radial position and temperature are well reproduced in L-mode by the gyrofluid model. The H-mode is apparently the result of nonlocal physics, part of which results from the neoclassical equilibrium electric field. Results from our local models have been promising, but actual capture of an L-to-H transition will require incorporation of the profile changes in a self-consistent way.

### *1.1.5 Guiding centre simulation of wide-orbit neoclassical transport in ASDEX Upgrade*

A. Bergmann

Although turbulent transport is often dominant in tokamak plasmas, it is important to know the level of neoclassical transport, e.g. if turbulent transport is reduced by an internal transport barrier. Also, neoclassical effects such as bootstrap current and polarization current can be important. However, the standard neoclassical theory is not valid for a plasma with wide banana orbits, particularly in the central plasma around the axis. Therefore, the HAGIS guiding centre code was augmented by a module for calculating the effect of pitch angle scattering on the ion motion employing a Monte Carlo representation of the Fokker Planck collision term. The code was validated by benchmarking against standard neoclassical theory for an equilibrium with circular cross-section. Calculations of ion energy transport in a discharge of ASDEX Upgrade with enhanced inverse shear and internal transport barrier were performed. The transport is strongly reduced in the central region $r < 0.3$ to a level of a few times the Pfirsch Schlüter transport.

### *1.1.6 Neoclassical transport at high poloidal Mach number*

W. Feneberg

Neoclassical transport in a tokamak was studied by solving a gyrokinetic equation including poloidal flow. In the absence of an outside momentum source, the driving force within the bulk plasma is the radial temperature gradient only. Besides the well-known neoclassical solution with small flow, there is also a solution with poloidal Mach numbers between two and three.

## 1.2 MHD

### *1.2.1 TM tearing mode code*

Q. Yu

Modelling the recent experiments showing stabilization of neoclassical tearing modes (NTMs) using electron cyclotron current drive (ECCD) has required modification and extension of the TM code. This entailed including a description of the effects of the ECCD as well as including the effects of the 2D fast electron transport parallel and perpendicular to the field. The experimental observations that various modes of different helicities are affected by each other also prompted development into extending the model to make it describe an increased number of modes with different helicities.

### *1.2.2 Linear MHD eigenmodes with fluid rotation*

E. Strumberger

In order to investigate quantitatively the influence of differential plasma rotation on double tearing modes, the CASTOR code was extended by adding the terms of toroidal rotation and viscosity to the equations for the perturbed quantities. As a first step, parallel viscosity for the motion along the field lines is used for the perturbed viscous force. First computations confirm the damping of the double tearing mode with increasing differential rotation.

### *1.2.3 Tearing mode stability for parameter for arbitrary plasma shapes*

C. Atanasiu

Code developments were made in the calculation of the tearing mode stability parameter, $\Delta'$, for diverted tokamak configurations. They enable the influence of plasma parameters, such as aspect ratio, ellipticity, and triangularity, as well as the location of the wall on $\Delta'$ to be calculated.

## 1.3 RF Physics

M. Brambilla

A subroutine which calculates the profiles of RF-driven current from the power deposition and electric field patterns of waves in the ion cyclotron range of frequencies has been added to the TORIC full-wave toroidal code. The model is based on the 'adjoint' solution of the Fokker-Planck equation developed by Fisch and Karney and takes into account the effects of toroidal trapping. The routine is capable of distinguishing between current drive by ion Bernstein waves (Landau damping only, relatively low efficiency) and by the fast wave (Landau and transit time damping, higher efficiency).

Beam tracing is employed to compute propagation and absorption of EC waves. The wave beam is described by means of a central ray and a set of parameters connected with the curvature of the wave front and the amplitude profile. Analytic solutions in an inhomogeneous magnetized plasma have been obtained for perpendicular propagation in a slab geometry. A code has been written which allows one to calculate EC wave propagation, absorption, and current drive in a tokamak geometry. The first results obtained for ASDEX Upgrade and RTO/RC ITER configurations show that the diffractive broadening of the beam can significantly modify the profiles of power absorption and driven current with respect to the geometrical-optics prediction.

## 1.4 Edge Physics

D. Coster, H. Bürbaumer

To prepare incorporation of mesh refinement, a version of the B2 code with cell-centred velocities (as opposed to the original staggered grid version) has been developed in collaboration with the University of Vienna.

# 2. GENERAL PLASMA THEORY

## 2.1 Basic MHD Theory

### *2.1.1 Magnetohydrodynamic (MHD) Turbulence*

D. Biskamp, K. Hallatschek, A. Zeiler, W.- C. Müller

Since it is difficult to generate MHD turbulence in laboratory experiments, numerical simulation is particularly important. 3D freely decaying MHD tubulence was investigated numerically in a periodic box using for the first time a spatial resolution of $512^3$ collocation points. The decay of the energy of the turbulent fluctuations, $E = E^K + E^M$ , is governed by the conservation of the magnetic helicity and the rapid decay of the energy ratio $\Gamma = E^K/E^M$. A simple theoretical model is proposed which predicts the asymptotic decay laws $E \sim t^{-1/2}, \Gamma \sim t^{-1}$, in good agreement with the behaviour observed in the simulations, invalidating previous theoretical and numerical results. The spatial scaling properties of isotropic MHD turbulence indicate that the turbulence does not follow the previously favoured Iroshnikov-Kraichnan phenomenology, which predicts the energy spectrum $E_k \sim k^{-3/2}$. Instead one finds a clear Kolmogorov spectrum $\sim k^{-5/3}$. The scaling exponents of the structure functions are well described by a modified She-Leveque model corresponding to basic Kolmogorov scaling of the fluctuation amplitudes and a sheet-like character of the dissipative eddies. Hence cross-field eddy-like motions, much as in hydrodynamic turbulence, are more important than the parallel dynamics, the interaction of Alfven waves.

### *2.1.2 Relaxed Plasma-Vacuum Systems*

D. Lortz, G. O. Spies

Taylor's theory of relaxed toroidal plasmas (states of lowest energy compatible with given total magnetic helicity and toroidal magnetic flux) is extended to include a vacuum region between the plasma and the wall. Perhaps the most remarkable property of relaxed states is a surface current in the plasma-vacuum interface.

### *2.1.3 Dipolar Magnetic Equilibria with Gravitation and Flow*

H. Tasso, G. N. Throumoulopoulos

Previous solutions by Krasheninnikov et al. are extended to the case of stationary equilibria with gravitation and incompressible flows. This is made possible by assuming a "dipole ansatz" in spherical coordinates in the generalized elliptic equation previously derived by Tasso and Throumoulopoulos.

### *2.1.4 Resistive MHD equilibria with flow*

H. Tasso, G. N. Throumoulopoulos

For a Spitzer resistivity it can be shown by expansions around the magnetic axis that the flow cannot lie in the magnetic surfaces. If the conductivity is taken as a function of the magnetic surface and the distance to the axis of symmetry, but with an overall plausible profile, several classes of solutions with incompressible flows aligned with the magnetic field can be constructed.

### *2.1.5 Balooning Stability of MHD Equilibria with Bootstrap Current*

H. P. Zehrfeld

Prior to a stability analysis in the presence of bootstrap currents is a consistent calculation of the equilibrium. Such advanced equilibrium calculations have been performed and the results have been subjected to stability analyses with respect to ballooning and peeling modes using the GARBO and GATO stability codes. It is found that the bootstrap current can drive the peeling mode unstable and that the instability also has a ballooning component. The combination of these two modes provide a possible explanation for the ELM phenomenon.

### *2.1.6 Dissipative Magnetohydrodynamic Equilibria with Compressible Fluid Flow*

H. P. Zehrfeld

Considering the dissipative equilibrium state of a toroidally confined axisymmetric plasma as that of a compressible Newtonian fluid with scalar viscosity, resistivity and thermal conductivity a closed set of partial differential equations for eight scalar functions providing a complete description of the equilibrium was established and solved. Suitable Neumann and Dirichlet boundary conditions to be imposed on the solutions are discussed in detail. It is shown that due to taking into account the compressibility of the plasma the coupled vorticity-stream function problem of hydrodynamics does not apply and no-slip boundary conditions for the poloidal and toroidal velocities can be satisfied.

## 2.2 Development of Basic Physics Models and Computational Tools

### *2.2.1 Combined Maxwell and Kinetic Gyrocentre Nonlinear Theory*

D. Correa-Restrepo

Work is in progress with the aim of deriving a consistent system of kinetic and Maxwell equations for gyrocentres, i.e. for guiding centres in the presence of low-frequency, short-wavelength electromagnetic field fluctuations. Use is to be made of a variational Lagrangian formalism which describes both the gyrocentres and the Maxwell fields, and which directly yields local conservation laws for electric charge and energy, together with charge, current, and energy flux densities. The usual complications of having to transform the kinetic and Maxwell equations from the particle to the gyrocentre phase space are thus avoided.

### *2.2.2 Preservation of Properties Differential Equations by Difference Schemes*

R. Meyer-Spasche

In search of difference schemes which preserve, at moderate size of the time step, all important properties of a given differential equation, we investigated exactness, stability properties, and symplecticity of various schemes. Some of these results give new insights into the nature of Runge-Kutta schemes.

### *2.2.3 Statistical Program to fit Catastrophe-type Response Functions*

O. Kardaun

The FORTRAN-90 catastrophe-fitting program, CATA2, has been streamlined and its portability increased. The NAG04 routine for constrained nonlinear optimization has been replaced by our own stochastic optimization routine and the PVM complex message-passing package on T3E and a workstation cluster was circumvented by a vectorized single-processor version on NEC SX5.

# SURFACE PHYSICS DIVISION

(Prof. Dr. Dr. h.c. Volker Dose

Prof. Dr. Jürgen Küppers)

The Surface Physics Division is organised in three groups. Contributions to the "Plasma-Facing Components" project constitute the work of the Plasma-Wall Interaction group. This concerns experiments in collaboration with fusion machines as well as more fundamental laboratory studies including work within Sonderforschungsbereich 338. The latter concentrates on adsorption at solid surfaces and integrates work at the Munich Universities and the Max Planck Institutes MPQ and IPP. The second group, working on properties of low-temperature plasmas, their diagnostics and application to thin film deposition, is run as a joint venture with IPP's Technology Division, and its work is being reported in a separate section entitled "Plasma Technology". The third group, Data Analysis, aims at interpreting experimental data from our own work as well as from other divisions employing Bayesian probability theory.

Head: V. Dose, Deputy Head: E. Taglauer

Scientific Staff:

A. Alimov[4], R. Behrisch, R. Beikler[2], M. Donath, W. Eckstein, K. Ertl, R. Fischer, P. Goldstraß[2], A. Golan[5], S. Günter[6], K. Hanson[7], Ch. Hopf[2], W. Jacob, H. Kang[2], A. von Keudell, K. Klages[2], A. Kohl[2], H. Knözinger[16], K. Krieger, B. Landkammer[2], U. Langer[1], Ch. Linsmeier, J. Luthin[2], C. Lutterloh[1], Ch. Math[2], M. Meier[2], V. Milosavljevic[8], S.T. Nakagawa[9], P. Pecher[1], R. Preuss, V. Prozesky[10], B. Racine[11], G. Rangelov, N. Reinecke[2], J. Roth, K. Schmid[2], Th. Schwarz-Selinger[2], V. Shulga[12], G. Staudenmaier, A. Steltenpohl[2], A. Stevens[13], S. Suga[14], A. Tabasso[1], U. von Toussaint[2], S. Vasquez-Borucki[2], G. Venus, G. van Wyk[15].

Technical Staff:

S. Bassen, L. Beck, M. Ben Hamdane, H. Friedrich, Ch. Fritsch, K. Gehringer, R. Hippele, W. Hohlenburger, A. Holzer, E. Huber, E. Hürzeler, St. Lindig, P. Matern, J. Mauermair, W. Ottenberger, B. Plöckl, M. Roppelt, J. Schäftner, A. Schlamp, H. Schmidl, I. Zeising.

1 Post Doc
2 Doctoral Candidate
3 Undergraduate Student

Guests:

4 Institue of Physical Chemistry, Moscow, Russia
5 American University, Washington, USA
6 Synchrotron Trieste, Italy
7 Los Alamos National Laboratory, Los Alamos, USA
8 University Beograd, Yugoslavia
9 Okayama University of Science, Okayama, Japan
10 National Accelerator Centre, Faure, South Africa
11 University Amiens, France
12 Moscow Lomonossov University, Russia
13 TU Eindhoven, NL
14 University Osaka, Japan
15 University of the Free State, Bloemfontein, South Africa

Collaboration with:

16 Ludwig-Maximilians-Universität, Munich, Germany

# 1. PLASMA-WALL INTERACTION

## 1.1 Multi-element Wall Materials

### *1.1.1 Surface Reactions of Beryllium with Carbon*

Surface reactions of evaporated carbon on a metallic beryllium single crystal (0001) were investigated in situ by means of X-ray photoelectron spectroscopy (XPS) and Rutherford backscattering spectrometry (RBS). After cleaning (oxygen as sole impurity below 0.1 %) different amounts of carbon were deposited at room temperature. The resulting films were successively heated to temperatures between 473 K and 873 K and analyzed after each 100 K step. The as-deposited films consist of $Be_2C$ at the beryllium/carbon interface and of a mixture of graphitic and disordered carbon on top. At elevated temperatures carbidization takes place between 473 K and 673 K and leads to a homogeneous layer of $Be_2C$ on top of the beryllium. The $Be_2C$ bulk photoelectron energies are found to be 282.7 eV for C 1s and 113.0 eV for Be 1s.

### *1.1.2 Carbon Films and Carbide Formation on Tungsten*

The reaction of carbon films on tungsten substrates was investigated by means of X-ray photoelectron spectroscopy (XPS). Gold substrates were also used to afford a comparison with a non-reactive metal. After deposition XPS analysis showed two different chemical states of unreacted carbon. The gold surface did not react with C after all annealing steps up to 1170 K and no changes in the C 1s intensity were observed. The two C 1s states initially observed in the spectra converged into one peak with increasing annealing temperatures. The tungsten samples were annealed up to temperatures of 1270 K. XPS analysis showed stepwise formation of two different carbide phases. At 970 K the C 1s photoelectron peak was shifted towards lower binding energies. After annealing at 1270 K a second shift occurred, indicating WC and $W_2C$ formation. Above 870 K the C concentration of the surface distinctly decreased with increasing annealing temperatures.

### *1.1.3 Energy Distributions of Sputtered Species*

The dynamic Monte Carlo program TRIDYN was modified for effective use on a parallel computer. This version was used to calculate energy distributions of backscattered projectiles and sputtered species versus the incident fluence. The distributions are reconstructed from their moments by the maximum-entropy method to determine the distributions over 5 decades. The targets of pure Cu, $Cu_{0.5}W_{0.5}$, and $Ni_{0.9}W_{0.1}$ were bombarded with Ar at normal incidence in the energy range from 60 to 1030 eV. The computed spectra are in qualitative agreement with experimental data (University of Kaiserslautern).

### *1.1.4 Rutherford Backscattering from Layered Structures*

Rutherford backscattering spectra were calculated by means of a parallel version of the Monte Carlo program TRIM.SP for 0.5 and 1 MeV He impinging normal to a target consisting of about 100 nm Au on Si. The calculated energy distributions are compared with experimental distributions and with those calculated by SIMNRA including double scattering. The contributions of plural scattering to the distributions are determined.

## 1.2 Hydrogen Inventory in Plasma-Facing Materials

### *1.2.1 Hydrogen Isotope Analyses*

During analysis of the hydrogen isotopes in samples from the vessel walls of fusion experiments some hydrogen is released by the analyzing ion beam. Depending on the ion beam density profile an algebraic formula was derived for the fluence dependence of the release. Fitting this formula to the measured values both allows extrapolation of the measured amount to zero analyzing fluence and provides information on the current density profile in the analyzing ion beam.

### *1.2.2 Deuterium Retention and Lattice Damage in Pure and C-irradiated Tungsten*

Deuterium retention and damage formation in a pure single crystal of tungsten, as well as deuterium implantation in a tungsten single crystal preimplanted with carbon were investigated. Ion energies of 10 and 100 keV $D^+$ and 40 keV $C^+$ were used and deuterium profiles were obtained from nuclear reaction analysis (NRA). Information on the type of defects created by the D irradiation were obtained by RBS/channelling, measuring the energy dependence of the dechannelling parameter $\chi$. The results suggest that there are at least two types of ion-induced defects responsible for the trapping of deuterium: (i) cavities localized in the implantation zone and (ii) dislocations which are distributed from the surface to a depth of 1-2 µm and which capture deuterium diffusing beyond the implantation zone. After heating up to 900 K cavities are not observed and the W crystal contains dislocations alone. Upon preimplantation with carbon ions the deuterium retention is strongly influenced if the range of the deuterium ions is confined within the carbon-modified surface layer. The total D retention is smaller in the carbon-preimplanted tungsten sample than in the pure W crystal and depth profiling shows that deuterium is only retained within the range distribution without diffusion beyond the carbon-modified surface layer. If the D ions are implanted at depths larger than the carbon-modified layer thickness, diffusion beyond the ion range occurs as in pure tungsten.

## 1.3 Ion Beam Analysis

### *1.3.1 Round-robin Experiment*

In order to compare all techniques applied to analyze the hydrogen isotopes in wall samples of fusion experiments, a set of equal amorphous deuterated carbon layers was distributed for quantitative analysis to 6 different laboratories and universities in Germany, where different analyzing techniques were applied. The measured absolute amounts agree within 30 %. The experiments showed the critical points in the different

measuring techniques. If due attention is paid to these, absolute measurement within 10 % uncertainty should be achievable.

### *1.3.2 Sputtering by High-energy Ions*

For ion beam analysis, high-energy ions in the MeV range are used for Rutherford backscattering (RBS), particle-induced X-ray emission (PIXE), and elastic recoil detection (ERD). Interaction of these projectiles with the sample may introduce errors in the surface analysis. However, there is not much information on erosion by MeV ion beams. Interaction of 10 MeV Si ions with thin (10 – 80 nm) Cr films on a silicon substrate was investigated at different angles of incidence. The layer thickness was measured by PIXE, induced by the 10 MeV Si primary ion beam. The experimental sputtering yields were compared with TRIM.SP calculations. For 10 and 35 nm layers the experimental yield was smaller than the TRIM.SP results, whereas for the 80 nm film the experimental yield was roughly one order of magnitude larger than the calculated number. The results of the thin Cr films may be dominated by carbon buildup or surface oxides. Similar results as for the 80 nm film were reported for Au on C.

## 1.4. Sniffer Probe Measurements at W7-AS.

### *1.4.1 Hydrogen Inventory*

The sniffer probe at the W7-AS stellarator has been reactivated during the spring and summer measurement campaign and has been routinely operated to measure the ion fluxes in and near the plasma edge as well as to determine the composition of the neutral gas and also the hydrogen isotope ratio. This allowed the hydrogen inventory of W7-AS to be investigated in detail. Figure 1 shows the temporal development of the H/D isotope

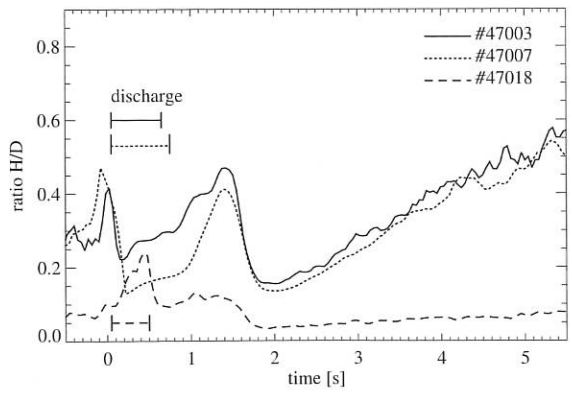


*Figure 1: Hydrogen isotope ratio H/D of the neutral gas in the edge region of W7-AS during and after various discharges: before (#47003) and after (#47007) He glow discharge cleaning and after boronization (#47018).*

ratio during and after three discharges in deuterium. Between the shots #47003 and #47007 a glow discharge in helium was performed and between shots #47007 and #47018 boronization in a mixture of 10% deuterated diborane and 90% helium was carried out.

Comparison of discharges #47003 and #47007 shows that the glow discharge in helium has a clear influence on the isotope ratio during the plasma discharge. The H/D ratio is reduced by a factor of about 1.8. Nevertheless, the hydrogen inventory of the machine itself remains unchanged as the ratio approaches a value of about 0.6 after both discharges. After boronization the measured hydrogen ratio is even higher during the discharge owing to the different discharge conditions. On the other hand,

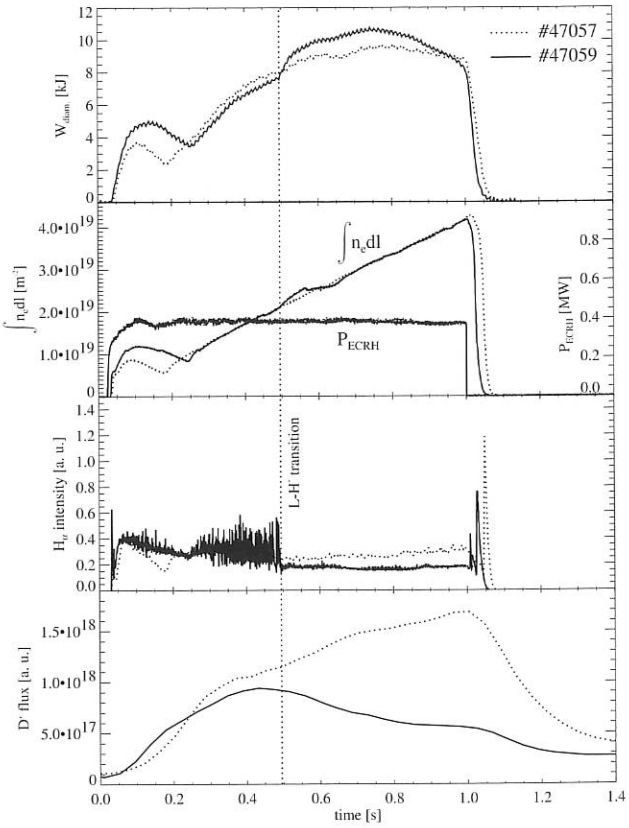


*Figure 2: Comparison of two discharges without (#47057) and with (#47059) L-H* transition. The sniffer probe signal (lowest panel) shows an early and drastic reduction of the D+ flux in the plasma edge in connection with the H-mode.*

as a result of the wall coating the hydrogen inventory of the machine itself has clearly changed as the isotope ratio is reduced to about 0.1. This effect remains visible for about two days (approx. 100 discharges). A further detailed analysis of the hydrogen balance shows that more than 90% of the puffed gas goes to the walls and only less than 10% into the plasma. Moreover, this behavior is independent of the discharge type and heating scenario. After the discharge a significant rise of the hydrogen neutral gas pressures is observed. This is due to outgassing of the walls and loss of ionization processes and the associated pumping capability of the plasma.

### *1.4.2 H-mode Transition*

During various H-mode discharges in W7-AS the temporal development of the hydrogen and deuterium fluxes in the plasma edge was studied with the sniffer probe. Figure 2 shows

the time traces of some discharge parameters for two similar discharges, #47057 and #47059, with deuterium gas puffing and ECR heating. In discharge #47059 a L-H* transition occurs at about 500 ms, which is expressed in the increase of the diamagnetic energy and the sharp change of the $H_\alpha$ intensity. Moreover, the L-H* transition in W7-AS generally shows well-known features, e.g. steepening of the density profile in the region of the separatrix.

The lowermost time traces in Fig. 2 display the development of the $D^+$ flux in the plasma edge of these discharges. For discharge #47057 (without H-mode) the measured $D^+$ flux roughly follows the evolution of the line-integrated electron density. In the case of discharge #47059 (with H-mode) a drastic decrease of the $D^+$ flux is observed, whereas the reduction of the deuterium flux already occurs prior to the transition. This fact confirms the assumption that the steepening of the density profiles starts at the outermost edge of the plasma. Moreover, sniffer probe measurements in the plasma edge could possibly identify a precursor for the L-H* transition. For this purpose it is necessary to improve the temporal resolution by experimental or mathematical means. A further analysis of the hydrogen neutral gases shows a distinct change of the hydrogen isotope ratio during the transition. This observation is in agreement with the change in the particle fluxes onto the targets and can also be seen in the reduced $H_\alpha$ signals from the limiters.

## 2. SURFACE SCIENCE

The co-operation of the Surface Science group within the Sonderforschungsbereich (SFB 338: Adsorption on Solid Surfaces) is continuing. Recent contributions include investigations of the composition and structure of alloy surfaces, the kinetics of surface faceting and properties of model catalysts. Additionally, the magnetic properties of thin-film systems are being studied.

### *2.1 SFB 338*

The composition and structure of alloy surfaces can differ from the corresponding bulk properties due to segregation and relaxation effects. Low-energy ion scattering (LEIS) is suitable for probing the topmost atomic arrangement of alloys by providing mass and layer sensitivity at the same time. The (100) surface of the ordered alloy CuAu and amorphous Ni and Al were studied by low-energy $Ne^+$ and $Na^+$ ion scattering. The interpretation of the experimental results is supported by numerical simulations using the MARLOWE code. In the CuAu system a certain geometry was found to be very sensitive to Au present in the 2nd layer, the amount of which is expected to be rather low. Experiments concerning the return to equilibrium after perturbation by preferential sputtering confirm segregation of Au to the 1st layer.
Comparison with MARLOWE results also allows one to study variations in the ion yields arising from neutralization effects. Ion survival probabilities are estimated for Ni and Al, by trajectory analysis, resulting in excellent agreement between calculated and measured energy spectra as shown in Figure 3.

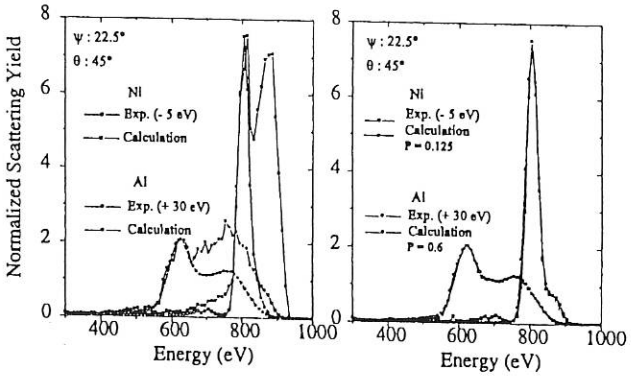


*Figure 3: Comparison of experimental and calculated yields without (left panel) and including (right panel) neutralization effects. The experimental resolution of 22 eV has been taken into account in the latter case.*

Faceting of the vicinal Cu(115) and Cu(119) surfaces due to oxygen adsorption was further studied by scanning tunneling microscopy (STM). Both surfaces reconstruct into three different facet types characterized by energetically favoured Cu-O-Cu chains On oxygen-saturated surfaces (exposure between 100 L and 1000 L) the facet size is determined by formation kinetics. This facet size varies between 1 nm and 100 nm; ist dependence on temperature and oxygen partial pressure can be formally described by equations derived from nucleation and growth mechanisms. Experiments with lower oxygen exposure (10 L to 20 L) show details of the initial growth process. First small (100) facets are formed along the step edges which grow and define the final facet size. Further experiments were made to give information about the facet stability.

The investigation of model catalysts for $SiO_2$-supported Rh and the effect of the promoter $VO_x$ on $Rh/SiO_2$-systems was continued. Using the rhodium signal intensity information and the binding energy shift of the XPS (X-ray photoelectron spectroscopy) Rh $3d_{5/2}$ signal, it was possible to describe the growth of rhodium clusters on $Rh/SiO_2/Mo$ and $Rh/VO_x/SiO_2/Mo$ model catalysts as a function of temperature. The final cluster sizes derived from these methods are consistently about 1 nm on $Rh/SiO_2/Mo$ and about 2 nm on $Rh/VO_x/SiO_2/Mo$ after heating these systems from room temperature to 873K in UHV. In contrast to powder catalyst systems prepared by wet impregnation and thermal treatment in air, it was possible to exclude the influence of rhodium compounds, which are known to have a large effect on the sintering process, and to model the agglomeration behaviour of rhodium metal.
First experiments with a new reactor system for catalytic reactions on small-area model catalysts at atmospheric pressure were conducted with success. The reactions of CO and $O_2$ over Pt foil and CO and $H_2$ over Rh foil showed the expected product distribution measured by a quadrupole mass spectrometer (QMS). Further investigations of the catalytic performance of $VO_x$ promoted and unpromoted $Rh/SiO_2/Si(100)$ model catalysts are in progress.

### 2.2 *Surface magnetism*

The magnetic order in ultrathin films critically depends on a variety of film parameters. To correlate the magnetic properties and the underlying spin-dependent electronic structure is a challenging task, which we approach experimentally by spin-resolved electron spectroscopies. The combination of spin-resolved inverse photoemission (IPE) and spin-polarized secondary electron emission (SPSEE) enables us to monitor the spin-dependent electronic states and the magnetization at surfaces and in ultra-thin films. Co (hcp) and Fe (bbc) films on W (110) were investigated with respect to their electronic surface states and their magnetic order. Spin-dependent surface states were identified at both surfaces, Co (0001) and Fe (110), and described within the theoretical framework of the one-step model of IPE. The role of these surface states for the surface magnetic order is still being discussed.
How sensitive the magnetic order of a film can depend on surface conditions is shown in Fig. 4. A reversible, adsorbate-induced magnetic reorientation transition is observed in Fe (110) films. While the directions of easy magnetization in bulk Fe are along ⟨100⟩, ultra-thin films of Fe on W (110) exhibit in-plane magnetization along the $[1\,\bar{1}\,0]$ direction. At t = 0 the clean surface of a 20-ML thick Fe film is magnetized along $[1\,\bar{1}\,0]$. After 200 min under ultra-high vacuum conditions ($p \approx 1 \times 10^{-10}$ mbar, UHV) the magnetization M has switched to [001] by adsorption of residual gas. Electron bombardment (E = 2.5 keV) again leads to a rotation of the magnetization due to electron-stimulated desorption of the adsorbates.

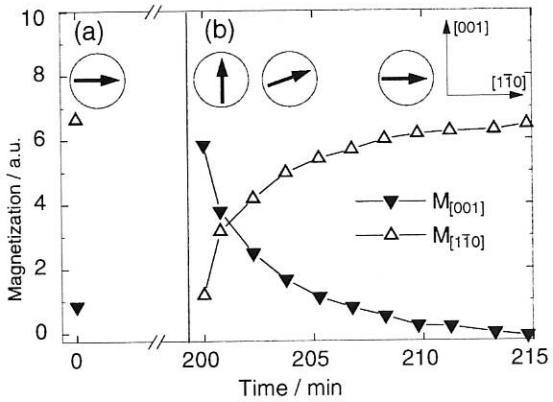


*Figure 4: Adsorbate induced magnetic reorientation transition of iron films on W (110).*
*(a) as prepared, (b) after 200 min in UHV, followed by electron-bombardment (see text for details).*

Spin-resolved appearance potential spectroscopy (APS) was applied to study the magnetic properties of Co in different crystal structures and chemical environments. The APS results of hcp-like films on W (110) show characteristic changes compared with fcc-like films on Cu (001), which are well described by changes in the spin-dependent local density of states. The element sensitivity of APS was used to study $Fe_xCo_{1-x}$ alloy films on Cu (001). The structural transitions from fcc to bcc and back to fcc with increasing x is reflected by reduced element-specific spin-asymmetry signals in APS. The results are in agreement with independent magnetic and structural measurements.

## 3. DATA ANALYSIS

Robust inference of physical quantities from new data is often hampered by finite resolution and deterioration by noise. Analysis of data is improved if all relevant knowledge previously gathered is exploited. Bayesian probability theory provides a general and consistent frame for combining various kinds of information.

Energy confinement data from various stellarators has been used to determine a scaling relation which allows for differences in the transport behaviour of heliotron/torsatrons and shearless stellarators. In order to do so each machine was assigned its own scaling constant. The scaling parameters themselves were evaluated by employing Bayesian probability theory. Each stellarator line showed similar scaling constants, which indicated similar transport behaviour among the devices of the respective line. However, since the scaling constant of the heliotron/torsatron line was a factor of 1.5 smaller than that of the advanced stellarator line, the latter branch promises better confinement for the same set of parameters (density, magnetic field, etc.).
The electron energy distribution function (EEDF) is essential for modelling the performance of fusion and process plasmas, like chemical reactions, growth processes in thin-film deposition, surface treatment, and wall erosion and material migration in fusion experiments. Determination of the EEDF from optical measurements of spectral line intensities is superior to conventional methods such as Langmuir probes since direct contact with inevitable deterioration of the plasma is avoided. For the first time the EEDF in electron-cyclotron resonance heated low-pressure helium plasmas was reconstructed form-free from 8 helium spectral line intensities. Quantitative spectral analysis often relies on being able to subtract from the data the contribution from the background. A general probabilistic model for estimating background contributions to measured spectra is developed on the defining characteristics, namely that the background is smoother than the signal. Our technique is demonstrated on particle-induced X-ray emission (PIXE) spectra and Auger emission spectra, which are prominent examples of complex background contributions.
PIXE is a routinely used, well-established diagnostic for trace element detection and quantification of wall material in ASDEX Upgrade. Reconstruction of the depth distribution of the detected elements is achieved by simultaneous evaluation of measurements with different incident angles of the ion beam on the probe. Like previously reconstructed depth profiles from Rutherford backscattering spectroscopy (RBS), the ill-conditioned inverse problem is solved with the powerful tool of Bayesian probability theory. The new technique was demonstrated in reconstruction of depth profiles of layered Si-Nb-Cr samples and of trace elements.

# MATERIALS RESEARCH DIVISION

(Prof. Dr. Dr. Hans-Harald Bolt)

In magnetic fusion devices the plasma-facing materials are subjected to complex loading conditions. In addition, the response of the materials to this environment can have a strong influence on the plasma performance of the fusion device. From the plasma a flow of ions and neutral atoms reaches the surfaces surrounding the plasma. The incident particles can lead to erosion processes on the material surfaces. Radiation from the plasma as well as the incident particles cause energy deposition on the surface of the plasma-facing component. The resulting thermomechanical loading of materials and components can limit the lifetime of the component. Excessive heat loads during operation lead to immediate destruction by melting or fracture. Furthermore, the materials can also adsorb and absorb hydrogen isotopes and eventually release fractions of the stored gas under thermal loading. This can influence the particle balance during plasma operation of the device. In addition to these fluctuations, the more resident inventory of hydrogen isotopes in a fusion device is strongly dependent on the selection of materials and should be minimized. The intense neutron irradiation of the plasma-facing materials in a fusion reactor causes nuclear activation of materials and also damage to materials, which results in degradation of dimensional stability and physical and mechanical properties. Plasma-facing materials have to be developed and optimized in order to meet these requirements as far as possible.
Since progress in plasma physics has paved the way towards the use of fusion as energy source, the issues relating to the development of materials for fusion applications are requiring intense effort. This entails clarification of the loading mechanisms in fusion devices and the response of materials to these loading conditions, as a basis for the development and qualification of suitable materials.
To contribute to this field the Materials Research Division of IPP was newly founded in 1999. The aim of this division is to characterize and develop materials for plasma-facing components of fusion devices. The work is complementary and closely linked to the activities of the Surface Physics Division of IPP. In the Materials Research Division the following work has been newly initiated: Materials characterization involving of metallography and scanning electron microscopy for morphological examinations, elemental analysis (EDX) and structural analyses (EBSD) as well as measurement of the thermal diffusivity of materials; thin-film synthesis allowing plasma-assisted deposition of films relevant to fusion applications together with the full
range of process analytical instruments; development work on thick low-Z coatings; numerical analyses of the thermomechanical behaviour of plasma-facing compounds and components, including micromechanical modelling.
Since most of the work is directly relevant to the application of materials in fusion devices, the major portion of the work is described in the report of the "Plasma-Facing Materials and Components" project. Numerical analyses which contribute to the design and evaluation of components for W7-X are mentioned in the "W7-X Construction" report. The generic work aimed at the development of innovative materials for fusion reactors and clarification of basic damaging mechanisms of materials is described in this section.

Staff

M. Balden, O. Jandl, F. Koch, S. Kötterl, S. Lindig, H. Maier, K. Marx, S. Picarle[3], M. Rehm, Y. Takamura[1], D. Valenza[2], J.-H. You

1 Guest from Univ. of Tokyo
2 Doctoral Candidate
3 Undergraduate Candidate

## 1. $AL_2O_3$ COATINGS FOR HYDROGEN PERMEATION BARRIER APPLICATIONS

In a fusion power plant operating with a deuterium-tritium mixture, the on-site tritium inventory is of concern with respect to radiological safety. Since hydrogen isotope diffusion into and through metals is a phenomenon which cannot in general be completely suppressed by the choice of a specific metal or alloy, the problem of controlling tritium migration within the facility arises. Furthermore, current design studies of nuclear fusion power plants intend to reduce the radioactive waste problem by employing special low-activation materials,e.g. reduced-activation steel alloys or vanadium-based materials

such as V4Cr4Ti. In the latter case, the problem of tritium handling is aggravated by the fact that the hydrogen isotope solubility and diffusivity are very high as compared with stainless steel.

Surface coating with thin films acting as diffusion barriers is a promising approach for handling this hydrogen isotope permeation problem. For such an application of thin coatings, however, the deposited films have to comply with severe requirements. Since in many materials diffusion is governed by grain boundaries and other imperfections, high-quality dense films without significant void fractions or impurity contents are required. For this reason, films deposited with the filtered vacuum arc method are under investigation here: A vacuum arc discharge on a solid aluminium cathode produces an aluminium plasma, and together with oxygen added from a gas inlet an $Al_2O_3$ coating is deposited onto the substrate. The controllable kinetic energy of the incident particles facilitates deposition of dense films. The arc discharge, however, also produces droplets of molten material, which would significantly reduce the performance of the films as permeation barriers if they were incorporated into the coating. A very effective method of avoiding this drawback is to prevent the droplets from reaching the substrate by employing a 90° magnetic toroidal filter system. On the laboratory scale, a substantial decrease of droplet contamination of the coatings can be achieved by this method while sustaining high deposition rates. With this setup, a variety of metallic and non-metallic materials can be coated with $Al_2O_3$ at temperatures of up to 700° C.

Since the deposited film is generated from an ionized plasma, the application of a bias voltage allows one to control the energy of the incident particles. By varying this energy and the substrate temperature, the microstructure of the deposited coatings can be controlled. The permeation barrier performance of these coatings will subsequently be investigated in a hydrogen permeation measurement setup, which is now under construction.

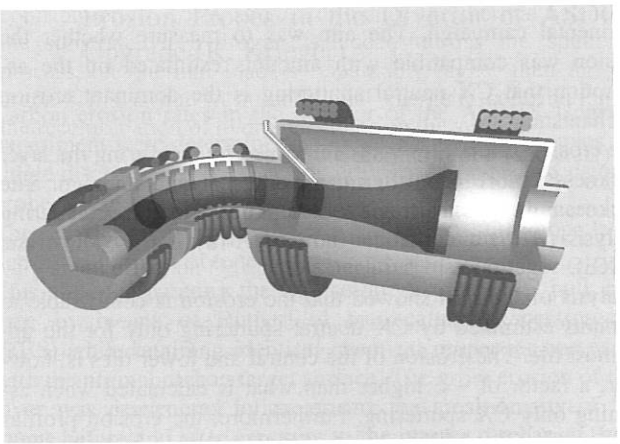

*FIG. 1: Vacuum arc facility with toroidal filter assembly. An aluminium plasma is generated from the aluminium cathode (left) and magnetically guided through a 90° bend. After adding oxygen is added from the gas inlet (centre), the plasma is shaped by the main vessel field coils and deposited onto the substrate (right).*

## 2. METHODOLOGY FOR ANALYSIS OF THE THERMOMECHANICAL BEHAVIOUR OF COMPOSITE MATERIALS

Composite materials are known for their high strength and stiffness under elevated temperatures as well as their benign crack propagation and fracture behaviour. Carbon-fibre-reinforced carbon composites (C-C composites) are being applied as plasma-facing materials and the potential of SiC-SiC composites for application in fusion reactors is under investigation.

For the design and optimisation it is indispensable to be able to predict theoretically the mechanical properties of composite materials. In order to gain expertise in this field, a study on the solid mechanics of composite materials was conducted which is to be the basis of further modelling efforts. Two different kinds of composites, ceramic matrix (CMC) and metal matrix composites (MMC), were investigated. The thermo-elastic properties, such as stiffness tensor and thermal expansion matrix, were analytically formulated by using the Eshelby tensor or micromechanical models. In parallel, mathematical approximation methods (asymptotic and numerical homogenisation) were studied.

The physically non linear behaviour of CMCs on the one hand and MMCs on the other needs a different methodology. The macroscopically non linear behaviour of CMCs, which is caused by microscopic energy dissipation processes, e.g. damage (crack initiation and propagation, interfacial debonding) or friction at interfaces, was modelled analytically. Technically relevant parameters which have to be derived from this are the linear elastic limit, ultimate tensile strength, and permanent strain. For analysis we used mainly fracture mechanical methods, Weibull statistics, and shear-lag analysis. Some macroscopic constitutive laws based on micromechanics were revisited for their validity in this respect. As input parameters for these analyses the material parameters, such as adhesion strength and frictional resistance of interfaces, have to be determined. To this end the theoretical modelling and the necessary experimental equipment were assessed. To determine the gross damage of a composite material a failure criterion under multiaxial loading conditions has to be established. For this purpose the applicability of Puck's model was studied.

## 3. STRUCTURE AND PROPERTIES OF MATERIALS

In addition to metallography and optical light microscopy, a scanning electron microscope was installed (Philips XL30 ESEM). Special features of this SEM are the variable-pressure operation allowing also investigations on electrically non-conducting surfaces without additional surface preparation, energy dispersive x-ray analysis (EDX) for measurements of the elemental composition of specimens, and electron backscatter diffraction imaging (EBSD) for analysis of local crystal structures with high spatial resolution (>1 μm).

For measurement of the thermal diffusivity a laser flash apparatus was installed (Netzsch LFA 427). Measure-ments can be performed up to 1600° C.

# PLASMA-FACING MATERIALS AND COMPONENTS

(Heads of Project: H. Bolt, J. Roth)

Plasma-material interaction studies are a major field of scientific activity at IPP. This work is focused on plasma-wall interaction studies in fusion devices (e.g. ASDEX Upgrade, JET), laboratory investigations of plasma-induced erosion processes, and other surface processes. Complementarily to this field, the operation conditions of fusion devices increasingly require specific material developments aimed at tailoring material properties to the specific operational conditions. The "Plasma-Facing Materials and Components" project has been initiated to tie the aspects of plasma-material interaction studies and materials characterization and development together and direct this work towards the application of plasma-facing materials in ASDEX Upgrade and W7-X. This project also includes well-defined longer-term aspects concerning the development of new materials.
Further basic underlying scientific work being done beyond the scope of this project, e.g. on basic surface process studies or the development of barrier films, is reported in the respective sections of the scientific divisions concerned.
Since the specific tasks of this project were initiated during the period of the report, rather the outline of the work than detailed results are described in the following. Some work carried out in 1999 before this project was initiated can now be allocated to this context. The respective results are therefore described here.
The tasks of the project are:

- plasma-wall interaction and plasma-facing materials for ASDEX Upgrade
- low-Z coatings for the first wall of W7-X
- doped carbon materials with improved erosion resistance

## 1. PLASMA-WALL INTERACTION AND PLASMA-FACING MATERIALS FOR ASDEX UPGRADE

### 1.1 Erosion of Tungsten-coated Samples in the Whole Vessel Wall of ASDEX Upgrade (A. Tabasso)

A critical issue for future fusion devices such as ITER is the choice of the material for the first wall of the main chamber. Tungsten is considered as a candidate material because, besides its high-energy threshold for sputtering, it does not suffer from chemical sputtering such as, for example, carbon does. It is therefore of interest to quantify and understand whether the erosion mechanisms are due only to charge exchange (CX) neutrals or also to ion sputtering. Because of the relatively low flux density of particles impacting on the first wall, respective measurements are only possible using long-term samples exposed for a full experimental campaign. ASDEX Upgrade plans to cover the heat shield of the inner main chamber wall with tungsten-coated graphite tiles. As a first step, four test tiles were installed at different poloidal positions in the same toroidal sector of the heat shield and removed after a full experimental campaign. The aim was to measure whether the erosion was compatible with amounts estimated on the assumption that CX neutral sputtering is the dominant erosion mechanism.
The erosion of the tiles was determined by measuring the layer thickness before and after the experimental campaign. The thickness was measured by both Rutherford backscattering analysis (RBS) and particle-induced X-ray emission analysis (PIXE).
Analysis of the tiles showed that the erosion is comparable to amounts estimated by CX neutral sputtering only for the uppermost tile. The erosion of the central and lower tiles is, however, a factor of ~ 5 higher than what is calculated when assuming only CX sputtering. Furthermore, the erosion profiles of these three tiles show marked toroidal asymmetry that can only be explained by assuming a shadowing effect of the neighbouring tiles. This, together with erosion incompatible with the CX flux expectations, points to the fact that the erosion of the W-coated tiles must be ion-dominated. The erosion results for the upper tile and for shadowed regions are close to the values expected from CX sputtering.
If the measured W erosion is scaled to full W tile coverage of the heat shield, a total W release of $\sim 1.7 \times 10^{17}$ atoms/s is calculated. This implies a ratio W/D $\sim 4\ 10^{-5}$, assuming a penetra-

tion probability of 1 and a particle residence time of ~0.1 s, which represents an upper limit.
The ion erosion may be due either to the plasma being in a limiter phase at start-up or to the vicinity of the magnetic separatrix to the wall or to a combination of the two effects. The results indicate that, provided the geometry remains the same, it is possible with a W heat shield to reduce the W influx further by keeping the plasma column further away from the tiles, especially in the lower part of the wall.

## 1.2 Development of Tungsten Coatings for the First Wall (H. Maier)

The applicability of tungsten as a plasma-facing material in the main chamber of ASDEX Upgrade has been investigated with encouraging results. The provision of large surface areas of the first wall with tungsten coatings is therefore currently being prepared. Applying high-Z materials in the main chamber is aimed at substantially decreasing plasma contamination by impurity production at the first wall. To achieve this goal, specific requirements have to be met. For this purpose, techniques for coating graphite tiles with thin tungsten films of the order of several μm have to be developed, yielding dense films and full coverage of the graphite surfaces. Other requirements are low contents of light impurites such as oxygen and carbon, and good adhesion properties of the films.
Since this project involves large surface areas and a correspondingly large number of graphite tiles to be coated, industrial-scale manufacturing capabilities are required. For this reason, co-operation with the Fraunhofer Institut für Elektronenstrahl- und Plasmatechnik was initiated to fabricate test specimens, which will be analyzed at IPP with respect to the required properties. A comparative study of different coating techniques such as magnetron sputtering and plasma ion deposition will also involve other industrial cooperation partners.

## 1.3 Erosion Probes in the Divertor of ASDEX Upgrade (K. Krieger)

Carbon erosion rates in the divertor of the ASDEX Upgrade experiment were determined by exposing graphite samples for single discharges at the outer divertor strike point area using a probe manipulator system.
The samples were covered with a 50-100 nm $^{13}C$ isotope layer deposited from an isotope-clean RF methane discharge.
This allows separating the $^{13}C$ isotope from the $^{12}C$ bulk isotope by means of Rutherford backscattering spectroscopy (RBS) while retaining identical chemical properties compared with the normal carbon target surface. The gross erosion of this layer was determined by measuring the areal density of $^{13}C$ atoms before and after exposure to the plasma discharge. From the energy spectrum of the backscattered ions the depth distribution of the carbon isotope fractions was derived by means of maximum-entropy deconvolution. The $^{13}C$ areal density and in addition the amount of redeposited $^{12}C$ on top of the $^{13}C$ layer were obtained by integration over the respective depth profiles.
At low values of the impacting hydrogen ion flux ($\Gamma_D \leq 10^{22}\,m^{-2}\,s^{-1}$) the original $^{13}C$ layer was found to be uniformly eroded without redeposition of foreign material.
Significant erosion of the $^{13}C$ layer was also found on samples exposed at high ion flux values ($\Gamma_D \geq 10^{23}\,m^{-2}\,s^{-1}$), but in addition the eroded $^{13}C$ layer was found to be completely covered by deposited $^{12}C$ with a thickness of up to 200 nm. Therefore, the observed erosion of $^{13}C$ represents in this case only the lower limit of gross carbon erosion.
Since the probes were exposed to discharges with long stationary phases in which the particle flux and the plasma temperature at the probe position were kept at a constant level, erosion yields $Y$ could be determined from the ratio of carbon erosion fluence and impacting hydrogen isotope fluence according to $Y(E, \Gamma_D) = \int \Gamma_C\, dt \,/\, \int \Gamma_D\, dt$.

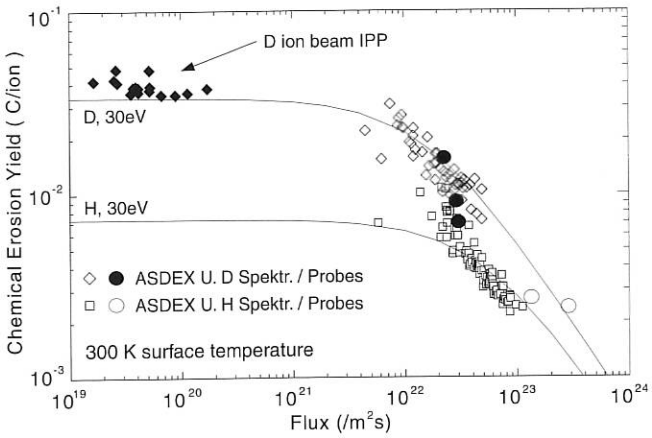


*FIG. 1: Comparison of chemical erosion yields of carbon obtained by different experimental methods.*

Figure 1 shows the directly measured erosion yields together with the spectroscopically determined yields, low-flux ion beam data, and the semiempirical model by Roth, Pacher, and Garcia-Rosales. Probe results and spectroscopic results agree well for hydrogen and for deuterium. At very high fluxes the probe erosion data indicate, however, a less pronounced decrease of the erosion yield than predicted by the model.

## 1.4 Deuterium Inventories in the Lyra Divertor of ASDEX Upgrade (H. Maier)

Since the summer of 1997 ASDEX Upgrade has been operated with the Lyra divertor arrangement. To investigate the critical issue of permanent hydrogen isotope retention, a nuclear reaction ion beam analysis of the near-surface deuterium content of this divertor configuration was performed and compared with previous results from Divertor I.
As nearly all components of the Lyra divertor possess curved, non-flat surfaces, a new manipulator system designed for handling complete large tiles (see Annual Report 1998, Surface Physics Division) was employed for this purpose. The sample translation and rotation possible with this device ensured normal incidence of the ion beam on the surface element under investigation without the necessity of cutting a large number of small samples from the respective modules.
Deuterium inventory profiles for the inner and outer target module are displayed in Figure 2. Several important results were obtained: In contrast to the Divertor I configuration, the data yield high deuterium inventories in the high-flux area of

both, the inner and outer target module. This indicates that codeposition of deuterium occurs in both divertor legs of the Lyra configuration, while in Divertor I the outboard side was dominated by erosion. This difference can be understood by comparing averaged electron temperatures in the two configurations.

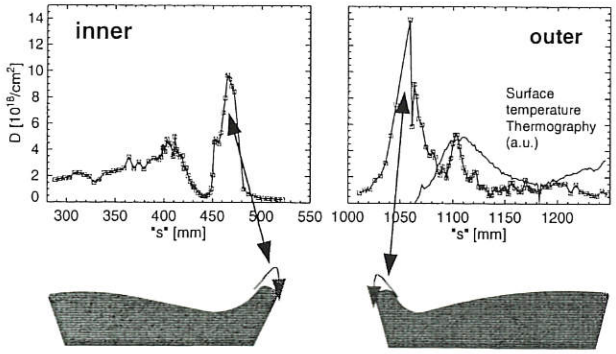


*FIG. 2: D inventories along the surfaces of the target modules of the Lyra divertor. Also shown is an averaged surface temperature profile of the outer module in arbitrary units to indicate the strike location of the plasma fan. The lower part of the figure shows the shapes of these modules. The arrows indicate that the maxima are located at the rounded edges.*

Another striking feature of the results is the observation of large amounts of deuterium at the rounded edges of both target modules. These locations are not subject to high particle fluxes directly from the plasma fan. This indicates that the mechanism at work here is not direct codeposition of deuterium with carbon impurities from the plasma, as is usually assumed for the strike locations.

## 2. LOW-Z COATINGS FOR THE FIRST WALL OF W7-X (S. Kötterl)

For the W7-X first-wall concept with actively cooled stainless-steel panels as plasma-facing components, coatings of materials with low atomic number, in particular boron carbide ($B_4C$) layers, are being developed in order to avoid accumulation of high-Z impurities in the plasma during steady-state operation. The use of thick $B_4C$ coatings on large areas of the first wall would allow a considerably simplified first-wall design compared with a design with clamped graphite tiles. Also $B_4C$ coatings lead to a reduction of the chemical erosion of the plasma-facing material and enhanced plasma performance due to oxygen gettering by the boron.
Characterization of plasma-sprayed $B_4C$ coatings has been started with regard to their structure and in terms of their fusion-relevant properties (composition and impurities, thermal conductivity, erosion behaviour, adhesion and cohesion, thermomechanical behaviour). Data obtained from this work will be needed to assess the actual application of plasma-sprayed $B_4C$ as plasma-facing material.

## 3. DOPED CARBON MATERIALS WITH IMPROVED EROSION RESISTANCE (M. Balden)

### 3.1 Temperature Dependence of the Chemical Erosion of Graphite and Silicon under Deuterium Impact

The temperature dependences of the erosion yields for graphite and silicon under D ion bombardment were determined by the weight loss method in the energy range between 20 eV and 300 eV at temperatures of up to 1100 K. For C, the temperature of the maximum of the chemical erosion ($T_{max}$) increases with ion energy from below 600 K for 20 eV to above 850 K for 300 eV. Also for Si a temperature dependence of the erosion yield was observed: $T_{max}$ for Si is decreased for all investigated ion impact energies by about 250 K compared with graphite. The erosion yields of Si are about one order of magnitude smaller than those of graphite for most temperatures and ion impact energies. At room temperature the yields for C and Si are about 4% and 0.3% for 20 eV impact energy, respectively.
Production of chemical erosion species was observed mass spectroscopically: Methane and silane production was observed for C and Si, respectively. Chemical erosion yields for C obtained by weight loss measurements always exceed yields measured mass spectrometrically by a factor of about two. Collector experiments show that a fraction of the eroded particles sticks to walls and, therefore, reduces the yield measured by mass spectrometry. With Si targets, deposited layers were also found for ion impact energies below the threshold for physical sputtering.

### 3.2 Erosion Behaviour of Carbide-doped Graphites

In co-operation with CEIT, San Sebastian, a series of carbon materials doped with different amounts of $B_4C$, SiC, TiC, VC, WC, and ZrC were produced, starting from a mixture of mesophase carbon powder (grain size: 0.5–4 µm) and carbide powders with a grain size around 1µm. The graphitization was performed at temperatures above 2300 K. Of all carbide dopants investigated, VC shows the highest catalytic effect on graphitization. Prior to the ongoing erosion experiments, the materials were characterized in respect of density, porosity, degree of graphitization, thermal conductivity and anisotropy factor, mechanical properties, and dopant distribution in the bulk and on machined surfaces.
The influence of the dopant distribution in bulk on the enrichment of the dopant at the surface during erosion is to be found by determining the fluence dependence of the erosion yield. Furthermore it will be attempted to identify the influence of the different dopant elements on the chemical erosion processes. Emphasis will be placed on the low-temperature, low-ion-energy regime of the chemical erosion.

# TECHNOLOGY DIVISION

(Prof. Dr. Rolf Wilhelm)

The Technology Divison of IPP is concerned with the technical development and operation of the three plasma heating and current drive systems - Neutral Beam Injection (NBI), Ion Cyclotron Heating (ICRH), and Electron Cyclotron Heating (ECRH) - for the ASDEX Upgrade tokamak (NBI, ICRH, and ECRH) and W7-AS stellarator (NBI and ICRH) experiments. Additional tasks are the planning and development of heating systems (NBI, ICRH) for the W7-X project in Greifswald and the development of a negative ion NBI system on the basis of RF-driven plasma sources (in cooperation with CEA Cadarache).
For more detailed information please refer to respective sections of this report. This section presents some additional information on specific technical developments and theoretical work.

## 1. NEUTRAL INJECTION HEATING

NI Group

### 1.1 Development of a RF Negative Ion Source

NBI systems based on RF plasma sources have a mechanical and electrical design intrinsically simpler than systems with conventional arc discharge sources. Especially for long-pulse systems ion sources without filaments could be of significant advantage due to reduced maintenance and costs. A large-area RF source for negative ion based long-pulse systems is therefore being investigated at IPP in cooperation with CEA Cadarache.
In 1999 mainly experiments with a new source were conducted, and for the first time from a large RF source $H^-$ current densities were extracted which are comparable to those from conventional arc sources.
The new source (type VI) has the RF coil wound around an alumina cylinder attached to the back of a bucket chamber, which provides magnetic confinement for the source plasma (Fig. 1). The design of the source is well suited to extrapolation to larger extraction areas and long-pulse operation. Reliable operation has already been demonstrated up to 150 kW of RF power and in the low-pressure range (<0.5 Pa) indispensable for negative ion extraction systems.
In a first step the filter field configuration was optimized. Measurements with an RF-compensated Langmuir probe show that the filter field reduces - as in arc sources - the high electron temperature in the "driver" region (ca. 15 eV) to about 1 eV in the region close to the extraction grid. The low temperature is essential to avoid destruction of the $H^-$ ions.
The source has been operated without Cs seeding ("Volume Production Mode") and with Cs seeding ("Surface Production Mode"). By "Volume Production" $H^-$ current densities of up to 10 mA/cm² can be achieved by addition of argon to the working gas ($H_2$) (Fig. 2). This improvement by the addition of argon in an uncesiated source is remarkably reproducible and avoids the difficulties of source operation with caesium. Krypton and xenon admixtures have also been used, but the resulting increase in $H^-$ current density was much less than with argon. It has been argued that only argon can improve $H^-$ production via the volume process because argon has metastable states with energies very close to those of vibrational states of $H_2$ molecules.

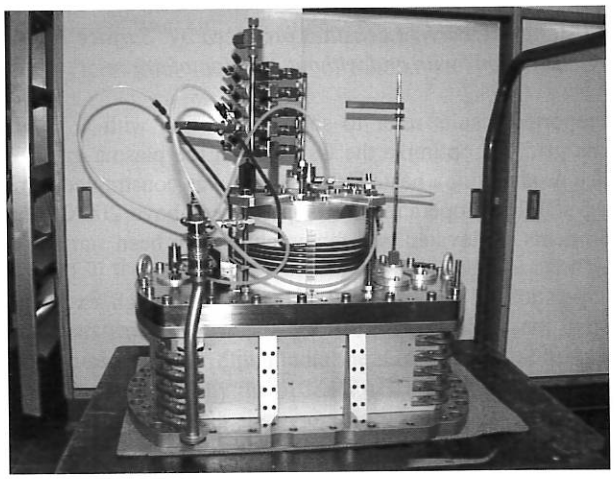

*FIG. 1: TypeVI RF source with external RF coil*

With caesium seeding of the source the $H^-$ current density approached 10 mA/cm² (Fig. 3). The best performance of the source is achieved by addition of argon into the cesiated source (Fig. 3). Up to 15 mA/cm² can be extracted by application of high RF power. (For negative ion beam systems a current density of around 30 mA/cm² is envisaged.)

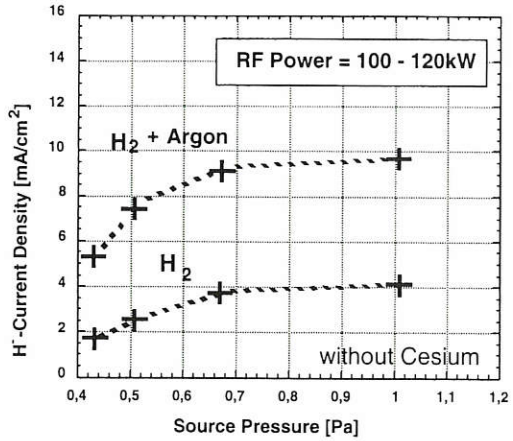


*FIG. 2: Effect of argon admixture on "Volume Production" of H⁻ current densities.*

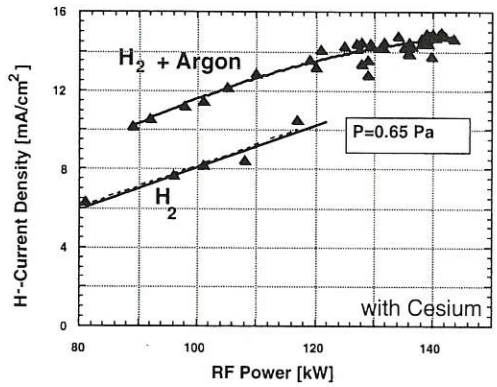


*FIG. 3: H⁻ current densities produced by "Surface Production" with and without addition of argon.*

The reported results refer to source operation with a "cold" plasma grid. To optimize the Cs layer on the plasma grid for surface production, a heated plasma grid was constructed, providing stabilized operation at temperatures above 200°C, and experiments at elevated grid temperature have been started on the Batman testbed.
For operation of negative RF ion sources at high extracted negative ion currents the large teststand in L6 was modified during 1999. Extraction experiments with a large-area extraction system are scheduled in 2000.

## 2. ION CYCLOTRON RESONANCE HEATING

ICRH Group

Further information on ICRH and experimental results can be found in the ASDEX Upgrade and W7-AS sections.

### 2.1 Ferrite Matching System

With 3-dB hybrids stable high-power operation of ICRH was achieved at ASDEX Upgrade. But plasma variations still result in reflections and reduced heating power due to the slow mechanical stub tuners used for matching. To obtain faster methods, a stub tuner system using premagnetized ferrites to control the electrical length of tuners was tested on the ICRH testbed and at ASDEX Upgrade. It was developed for Doublet III-D and loaned to IPP for the tests.
Although this system specifically designed for D III-D is not applicable to ASDEX Upgrade, the suitability of ferrite technology for fast-matching systems and the high-power handling capability of the ferrite striplines used were proved; fast load variations simulated by firing a spark gap could be matched within 2 ms. But some disadvantages of the chosen double stub and feedforward control principles were also seen.
Complementary calculations showed that with trombone-stub combinations using ferrites these disadvantages can be avoided and an elegant principle for the two-dimensional feedback task becomes possible: Two independent control loops can be used, the first varying the trombone length so that the second can reach matching by adjusting the stub length. Such a system is to be applied on ASDEX Upgrade /424/.

## 3. ECRH ON ASDEX UPGRADE

ECRH Group (AUG)
(in cooperation with IPF Stuttgart)

Information on the ECRH system and experimental results can be found in the ASDEX Upgrade section of this report.

### 3.1 Electron Cyclotron Current Drive with the Fundamental Frequency X-mode Launched from the Low-field Side

The electron cyclotron resonance layer in a tokamak, $\omega = \omega_c(r)$, is not accessible to the extraordinary wave from the low-field side, because it is shielded by a cutoff layer. However, an X-mode launched at a nonzero toroidal angle propagates at the cutoff parallel to the magnetic field and has circular polarization. It can therefore interact efficiently with electrons via the Doppler-shifted relativistic resonance. The condition that resonant electrons in velocity space exist leads to a maximum local density of $\omega_p^2/\omega_c^2 < 1 - (1-N_\parallel^2)^{0.5}$ at which such absorption is possible, where $N_\parallel$ is the parallel refractive index of the wave (typically $\omega_p^2/\omega_c^2 < 0.3$). With increasing density the energy for the resonant electrons increases, too, requiring a higher-temperature plasma for sufficient absorption. In low-density plasmas the driven current can be many times higher than that driven by the second harmonic X-mode or the fundamental O-mode. But, as their absorption increases with temperature, the difference in efficiency is much less pronounced at high temperatures /376/.

# PLASMA TECHNOLOGY

(Prof. Dr. Dr. h.c. Volker Dose

Prof. Dr. Rolf Wilhelm)

The Plasma Technology group is concerned with three tasks: Surface coatings are produced by means of plasma chemical vapour deposition (PCVD) for special applications, mainly in fusion plasma devices. New or improved PCVD procedures or devices are being developed for this purpose. The scientific part of the activity involves the use of plasma, plasma edge, and thin-film diagnostics in order to correlate the discharge parameters with the properties of the resulting coatings and improve understanding of the basic mechanisms of plasma deposition. The third goal is modelling of the deposition process which allows the discharge conditions to be adjusted in a predictable way in order to optimise a desired property of the growing film.

In 1999, the main activities were investigation of deposition of hydrogenated carbon films due to neutral radicals, quantitative characterisation of a neutral beam source for atomic hydrogen and hydrocarbon radicals, and construction of a new experiment to study the surface mechanisms of hydrocarbon radicals and atomic hydrogen.

V. Dose (Division Head)[2], C. Hopf[1, 4], W. Jacob[1], G. Kerkloh until (30.03.99)[2, 5], A. von Keudell[1], B. Landkammer[1, 4], P. Pecher[3], T. Schwarz-Selinger[1, 4], S. Vasquez-Borucki[1, 4], R. Wilhelm (Division Head)[2], M. Meier[1, 4], B. Racine[6], A. Stevens[7].

1. Surface Physics Division
2. Technology Division
3. Postdoc
4. PhD Student
5. Technical Staff
6. Guest from Univ. of Amiens
7. Guest from Techn. Univ. of Eindhoven

## 1. THIN-FILM DEPOSITION AND EROSION

Understanding and quantification of the interaction of hydrocarbon radicals with surfaces are important for describing carbon transport and re-deposition in fusion devices. The surface loss probabilities of hydrocarbon radicals were, therefore, investigated in low-temperature plasmas using a variety of hydrocarbon source gases. The surface loss probability $\beta$ corresponds to the sum of the probability of effective sticking and the probability of the reaction to a non-reactive volatile product at the surface. This quantity was measured by the cavity technique: radicals from a remote plasma source enter a small cavity via an entrance slit and lead to film deposition on the inside surfaces. Comparison of the measured deposition profiles with model calculations allows the surface loss probabilities to be deduced.

A set of three $\beta$ values is sufficient to interpret all experimental data for different hydrocarbon source gases and cavity geometries. These $\beta$ values are $\beta_1 = 0.80$, $\beta_2 = 0.35$, and $\beta_3 = 10^{-2}$. They correspond to different hydrocarbon radicals and can be explained by the different states of hybridisation of the hydrocarbon growth precursors.

## 2. DEVELOPMENT AND CHARACTERIZATION OF A RADICAL BEAM SOURCE

To allow the interaction of hydrocarbon radicals with surfaces and the synergistic interaction between different radicals to be studied quantitatively, a particle beam source was developed which is capable of producing thermal beams of neutral hydrocarbon radicals. The radicals are produced in a resistively

heated tungsten capillary as a result of thermal dissociation at the hot walls of the capillary. Using $H_2$ or azomethane $N_2(CH_3)_2$ as precursor gases one can produce a flux of atomic hydrogen or methyl radicals ($CH_3$), respectively. Fluxes of about $3\times10^{15}$ H atoms $cm^{-2}$ $s^{-1}$ and of $3\times10^{14}$ $CH_3$ radicals $cm^{-2}s^{-1}$ at a distance of 46 mm from the capillary are achieved. The $CH_3$ radical flux produced with azomethane is thereby about one order of magnitude higher than that achievable with methane as precursor gas. The angular distribution of the emitted radical flux is measured by ionisation threshold mass spectrometry in a dedicated set-up in which the mass spectrometer can be rotated around the exit orifice of the capillary. The angular distribution of atomic hydrogen was additionally determined by a new technique using erosion of an amorphous hydrogenated carbon film as a probe: a hydrocarbon film is exposed to the atomic hydrogen beam. The local etch rate on the planar probe can be converted into an absolute H flux on the basis of the known exposure time and the known erosion yield for atomic hydrogen. The resulting etch profile, representing the angular distribution of the emitted species, is shown in Fig. 1. The experimental results are in excellent agreement with a theoretical model describing beam formation in a hot capillary.

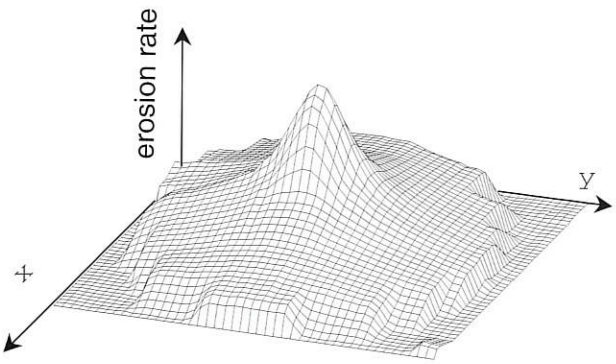


*Figure 1: 2-dimensional erosion profile of an amorphous hydrogenated carbon layer exposed to a beam of atomic hydrogen at a surface temperature of 650 K. The peak in the centre is due to the beam formation in the capillary. The circular-shaped plateau is determined by the mask used in the substrate holder.*

## 3. BASIC STUDIES OF THIN FILM DEPOSITION PROCESSES

To study the surface mechanisms of hydrocarbon radicals and atomic hydrogen, a new UHV chamber was set up. This chamber is equipped with two independent radical sources of the type described in Sect. 2. The growth or etch rate during exposure of a sample to the radical beams can be measured by in-situ real-time ellipsometry. The chemical composition of the surface is measured by in-situ real-time infrared spectroscopy.

A sticking coefficient of $1\times10^{-4}$ for $CH_3$ on a hydrogen saturated amorphous hydrogenated carbon film was determined. This result suggests that $CH_3$ is a very inefficient precursor for the formation of the thick deposits, found in the divertor region of fusion experiments, in particular in the JET Mark II divertor. However, since $CH_3$ can survive many wall collision due to its low surface reactivity, it is a conceivable precursor for hydrocarbon film formation in very remote regions of present-day fusion experiments.

During simultaneous interaction of a $CH_3$ beam and an atomic hydrogen beam with the surface of an amorphous hydrogenated carbon film the sticking coefficient of $CH_3$ increases by two orders of magnitude to $1\times10^{-2}$. The hydrogen induced sticking of methyl radicals is explained by the creation of free surface bonds due to hydrogen abstraction. Incoming methyl radicals can attach themselves to these free surface bonds. This represents the first experimental verification and quantification of this growth synergism. It also illustrates further that the description of the hydrocarbon re-deposition in fusion experiments requires not only knowledge of the sticking coefficients of individual hydrocarbon radicals, but also knowledge about existing synergisms or mutual inhibition among the reactive species.

# PLASMA DIAGNOSTICS DIVISION

(Head of Division: Prof. Dr. G. Fussmann)

The Plasma Diagnostics Division contributes to various WENDELSTEIN 7-X activities (conceptual studies and experimental testing of diagnostic components) and participates in the ASDEX Upgrade and WENDELSTEIN 7-AS fusion experiments at Garching. The results of these efforts are described in the sections dealing with the respective projects. Additional work comprises experimental and theoretical investigations in Berlin. The topics covered are: PSI plasma generator, UHV laboratory, electron beam ion trap (EBIT) experiment, and studies of edge physics problems. Only these activities are treated in this part of the report.

P. Bachmann, C. Biedermann, W. Bohmeyer, T. Fuchs, D. Hildebrandt, B. Jüttner[1], H. Kastelewicz[1], P. Kornejew, M. Laux, D. Naujoks, R. Radtke, H.D. Reiner, J. Sachtleben, A. Stareprawo, D. Sünder, K. Uludag, U. Wenzel.

1 Humboldt-University, Berlin

## 1. PSI PLASMA GENERATOR

A major topic of investigation was spectroscopic measurements of the drift velocity and diffusion coefficient of impurity ions. After a short xenon gas pulse was injected into an argon discharge, the radiation of the ionized xenon atoms was measured as a function of time at different positions in the plasma generator. From the analysis of the data the streaming velocity was determined to be $u_z = 1150$ m/s. Modelling of the broadening of the intensity profiles resulted in $D_{\parallel} = 60$ m$^2$/s for the parallel diffusion coefficient. This value for $D_{\parallel}$ is consistent with the classical one. By combining the particle transport studies with the results from Langmuir probe measurements it was also possible to determine the $D_{\perp}$ coefficient. Diffusion across the magnetic field lines can be best described if $D_{\perp} \approx 0.1$ m$^2$/s, a value also close to classical diffusion. The drift velocity and the temperature of the impurity ions were measured by laser-induced fluorescence in another experiment. The results revealed that there is continuous energy transfer from the electrons to the ions along the roughly 2-m-long drift region. This fact, together with the observed streaming velocity, suggests that the electron-ion relaxation time in the PSI plasma generator is about 1.5 ms.

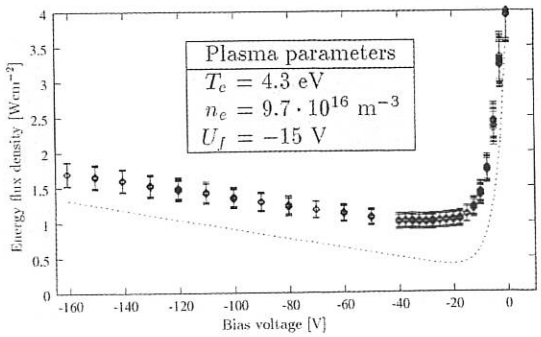


*FIG. 1: Heat flux to the sensor as a function of the bias voltage. The data points are from the present experiment. The broken curve represents the predictions from a theoretical model corresponding to the conditions of the experiment.*

Development of a new sensor for direct measurement of the heat flux is almost complete. The heat flux sensor is water cooled and its diameter is 6 mm. Operation and testing of the sensor started with discharges in deuterium. Figure 1 is an example showing the heat flux as a function of the bias voltage. The plasma parameters (electron temperature and electron density, floating potential) were obtained from a double probe placed in the vicinity of the sensor. By relating the measured heat flux to predicted values one can infer the sheath transmission factor from the experimental data.

## 2. ELECTRON BEAM ION TRAP (EBIT)

The radiative cooling rates for high-ionization species of krypton (C-like $Kr^{30+}$ to He-like $Kr^{34+}$) could be measured. The fractional abundances of the ions in EBIT were tuned to approach the ionization balance of a plasma at a temperature of 4.7 keV. By distinguishing between different radiation channels, 17 specific electron-ion interactions could be resolved in the spectroscopic analysis, including contributions from bremsstrahlung, radiative recombination, dielectronic recombination, and line radiation following electron-impact excitation. The dominant contribution to the cooling rate is made by the L-shell spectra of krypton (n = 3-2, n = 4-2, ... X rays), which produce more than 75 % of the total radiation loss. In Fig. 2, the experimental total cooling rate is compared to the values predicted by two different models. The difference between measurement and indicates that the power lost through the L-shell radiation of krypton is underestimated in the theoretical treatment.

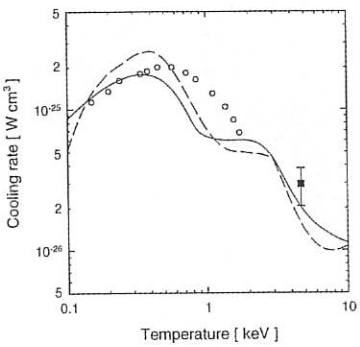


*FIG. 2: Radiative cooling rate for krypton as a function of the electron temperature. The curves represent two different theoretical calculations. The data points below about 2 keV are from a tokamak experiment. The result at 4.7 keV is from the present EBIT experiment.*

During 1999, a new grazing-incidence spectrometer was implemented at the EBIT facility for spectroscopy in the extreme ultraviolet spectral region. The wavelength range

covered by the spectrometer extends from about 10 Å to about 1000 Å. The spectrometer was employed to record spectra for low and medium charge states of tungsten ranging from Ag-like $W^{27+}$ to Ni-like $W^{46+}$. The short-wavelength spectrum from such ionization states was recently observed in ASDEX Upgrade, but it is not well understood because of the blending of hundreds or thousands of spectral lines forming narrow emission bands. Figure 3 shows five EBIT spectra observed in the 45-70 Å region. Each spectrum represents a particular ion population in EBIT corresponding to the electron-beam energy indicated in the figure. At the highest electron-beam energy (3.0 keV), the emission lines originate from Zn-like $W^{44+}$ and Cu-like $W^{45+}$. With decreasing beam energy, the ion population in EBIT is shifted to lower charge states. The spectra at 2.1 and 1.7 keV show lines representing transitions in Ge-like $W^{42+}$ and Kr-like $W^{38+}$, respectively. For the beam energies 1.4 and 1.1 keV, where the trap inventory is dominated by Mo-like $W^{32+}$ and Pd-like $W^{28+}$, respectively, a drastic change in the emission spectrum is observed: a narrow band is emitted and its centre shifts towards shorter wavelengths as the charge state decreases. Theoretical analysis of these results is in progress and will be reported in a separate paper.

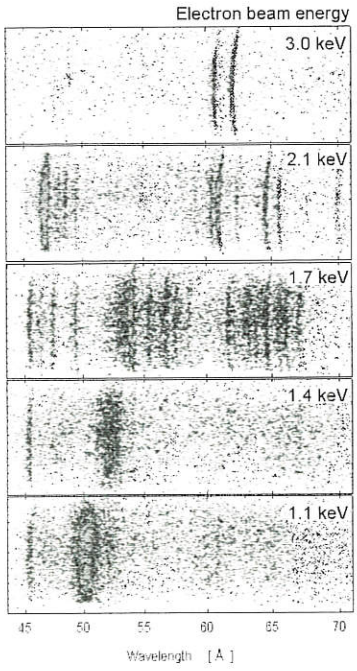


*FIG. 3: Spectra of highly charged tungsten ions in the extreme ultraviolet.*

## 3. THE UHV LABORATORY

In the UHV laboratory, the composition of tungsten and carbon-based coatings was analyzed after exposing a suitable substrate sample to the SOL plasma of TEXTOR-94. The sample consisted of fine-grained graphite covered with a 300 nm thick tungsten layer. Part of the sample was furnished with an additional 200 nm thick a-C:H film deposited on the tungsten layer. The sample exhibits significant differences in impurity deposition, depending on the structure of the surface. Analysis of the tungsten-coated surface revealed that a mixed material layer (C plus W) is formed during plasma exposure. Carbon deposits could be detected in this layer at depths of up to 400 nm. On top of the mixed material layer a tungsten concentration of about 30 % was measured. Different from this result is the situation for the a-C:H film. Here, the formation of a 200 nm thick carbon layer is observed. The amount of carbon deposited on the a-C:H film is about twice as large as in the mixed-material layer. In addition to exposure of samples to the plasma of TEXTOR-94, laboratory investigations were carried out to determine how the processes of diffusion and ion implantation can effect the elemental composition of multi-layer coatings. Carbon ion bombardment and annealing of suitable samples were employed in these measurements. From the analysis it was found that carbon can in fact diffuse into the tungsten substrate, provided the temperature of the sample is above 1000 K. However, the diffusion process is associated with formation of tungsten carbide ($W_2C$), which, in turn, is not present in the mixed-material layer. Thus, one can infer that temperature-dependent diffusion or penetration following carbon ion bombardment cannot contribute to the mixed-material formation. Instead, it is more likely that erosion and prompt redeposition are the decisive processes producing the mixed-material layers.

## 4. THEORY AND MODELLING

There were three main items in the theory and plasma modelling groups' activities:

(i) Bifurcation of temperature in edge plasmas. The energy balance of the boundary layer plasma was analyzed in limiter tokamaks and axisymmetric devices. Bifurcation in limiter tokamaks occurs if the heat flux from the core plasma exceeds a critical value, which, in turn, is smallest if the plasma is homogeneous in the poloidal direction. For a given heat flux beyond the critical value, the bifurcation phenomena are less pronounced when the sheath transmission factor at the limiter is increased. In axisymmetric devices, the maximum temperatures increase with rising axial influx and reduced sheath factor.

(ii) Sheath super-heat transmission due to redeposition of thermally emitted material. A new code (BPHI-3D) has been developed to analyze the plasma-surface interaction in 3-D geometry. The code uses Monte Carlo methods, full kinetic treatment of the plasma and impurity ions, Boltzmann/guiding-centre electrons, and a particle-in-cell time-independent Poisson solver. The code was used to explain the hot spot or super brilliance events as observed at TEXTOR-94 and Tore Supra. It was shown that, under certain plasma conditions, near-surface ionization of emitted material causes excess-heat flow to the surface which initiates a rapid increase of the surface temperature.

(iii) Modelling of the plasma in the PSI plasma generator. B2- EIRENE modelling calculations were made for discharges in deuterium. The calculations can reproduce the plasma characteristics very well at radial positions where the plasma is produced in the generator. Major discrepancies between experiment and code predictions exist for the central region and the anode shadow. Here, a more realistic transport model and inclusion of ion kinetic methods are required.

# GARCHING COMPUTER CENTRE (RZG)

(Head: Stefan Heinzel)

RZG traditionally provides supercomputing power and archival services for IPP and other Max Planck Institutes throughout Germany. Besides operation of the systems, application support is given to Max Planck Institutes with high-end computing needs in fusion research, materials science, astrophysics, and other fields. Large amounts of experimental data from the fusion devices of IPP (ASDEX Upgrade, Wendelstein 7-AS, and, later, Wendelstein 7-X), satellite data of MPI of Extraterrestrial Physics (MPE) at the Garching site, and data from supercomputer simulations are administered and stored with high lifetimes. In addition, RZG provides network and standard services for IPP and part of the other MPIs at the Garching site.
Since 1998, the new experiment data acquisition software development group for the new Wendelstein 7-X fusion experiment and the current ASDEX Upgrade fusion experiment operates as part of RZG.

A. Altbauer, G. Bacmeister, J. Cox, R. Dohmen, K. Desinger, S. Gross, A. Hackl, R. Hamberger, S. Heinzel, C. Hennig*, K. Lehnberger, H. Lederer, R. Mühlberger, W. Nagel, M. Panea-Doblado, P. Pflüger, F. Pirker, A. Porter-Sborowski, H. Reuter, H.-G. Schätzko, J. Schmidt, A. Schott, H. Schürmann*, K. v. Sengbusch, H. Soenke, U. Schwenn, R. Tisma, I. Weidl, V. Weinert

Data Acquisition Group:

P. Heimann, J. Maier, S. Valet*, M. Zilker

* IPP Greifswald

## 1. MAJOR HARDWARE CHANGES

In order to close the gap between the massively parallel Cray T3E system (with 816 processors, 102 GB main memory and a peak performance of 0.49 Tflop/s) for highly scalable parallel applications and the comparatively low performance of single RISC processors for non-parallel codes, a vector system with high single processor performance was installed: a NEC SX-5 system with 3 processors and 12 GB of main memory (first system in Europe), which replaced the NEC SX-4B interim system. The SGI Origin 2000 systems of MPI of Astronomy and RZG were integrated into one system and upgraded to a total of 16 processors and 6 GB of main memory.

## 2. DATA MANAGEMENT

### 2.1 Developments in Multiple-resident AFS

New features in commercially available standard AFS software required new designs in the internal organization of the extension of migrating MR-AFS. MR-AFS is used at RZG for comfortable, fault-tolerant automatic tape storage and retrieval of large amounts of experimental data. Maintenance and development of the MR-AFS software is done at RZG /246, 681/.

### 2.2 A new archival and backup system

Concerning mass storage of data, a basic distinction is made between experiment-type data sets with requirements for long-time conservation and short-lifetime data of the backup type which are replaced by new versions at short intervals. For the second type, the backup data, not MR-AFS is used, but the so-called "arc" software which had been developed at RZG for the most common system platforms. However, in order to better support backups for the growing number of Windows NT platforms especially at external sites like IPP Greifswald, RZG has started to introduce the commercially available product ADSM from IBM. A basic ADSM server environment has been implemented at RZG which consists of a server machine (IBM RS6000) to which 4 tape drives (STK 9840 "Eagle") are attached, these being served by the Grau/EMASS robot system and tape silo. In the meantime regular backups of Win NT systems of IPP Greifswald and RZG are routinely taking place, as well as backups of the AFS user volumes in parallel to the conventional "arc" backups. Prototype backups for different UNIX systems are in progress. For improvement of data security against physical damage, negotiations with the Leibniz Rechenzentrum München have started to implement cross-wise generation of a second tape copy: For selected ADSM data, a second tape copy of RZG data shall be stored at LRZ in

downtown Munich, a second tape copy of LRZ data shall be stored at RZG in Garching.

# 3. DEVELOPMENT FOR HIGH-END PARALLEL COMPUTING

Application development and support for high-end parallel computing is of increasing importance for both disciplines already established in this field such as plasma physics, materials science, and astrophysics, and new disciplines in this field, especially from biosciences /173, 588/. Outstanding projects to support new developments in close collaboration with the respective scientists are described in detail.

## 3.1 Fusion Research

### *3.1.1 Turbulence code*

The KINEM Fortran code to study the effect of kinetic drift wave turbulences on anomalous transport phenomena had reached its limits of applicability since the treatment of ion dynamics was being carried out only in 3D based on a fluid model. This treatment had to be improved to the level of the highly precise calculation of the electron dynamics with a five-dimensional distribution function. A first approach aimed at improving an existing parallel code of the University of Maryland in a collaboration for massively parallel usage. A study of the implemented code structure revealed, however, that there was little chance to achieve high scalability for large problem sizes with acceptable programming effort. A new own parallel code, GENE (Gyrokinetic Electromagnetic Numerical Experiment) was therefore developed for the five-dimensional ion treatment plus the additional treatment of extra features, and combined with the precise electron treatment. The new GENE code shows excellent parallel performance and is well suited for the treatment of very large systems which exceed the capabilities of the current T3E system with 100 GB memory by one order of magnitude.

### *3.1.2 Plasma edge transport*

The new EMC3 parallel 3D Monte Carlo code for study of plasma transport in edge regions allows solution of Navier-Stokes-like fluid equations especially for protons and electrons which allow fluid approaches.

For particles not suited to diffusion or fluid approaches like neutral atoms or molecules the kinetic Boltzmann equations can be solved with the 3D EIRENE code of FZ Jülich.

To integrate the two separate codes into one new parallel code, a combined effort by the authors of the two codes and RZG is being made. In a first step, extensive memory usage of both codes had to be reduced by implementing a dynamic memory usage scheme. A common problem description structure and data handling structure for both codes is under development by the authors as a prerequisite for code coupling and parallelisation of the interface.

## 3.2 Materials Sciences

### *3.2.1 Electronic structure calculations*

The full-potential Linearized Augmented Plane Wave (FP-LAPW ) method plays an important role for electronic structure calculations in materials research. As only sequential code implementations exist so far, this method could not be applied to large problems for which the resources of a massively parallel computer are required. The WIEN 97 sequential code package consists mainly of 3 different parts: LAPW0 computes the total potential from the total electron density as input; LAPW1 sets up the Hamilton and overlap matrix, calculates eigenvalues and eigenvectors for Schroedinger´s equation, and is the most cpu-consuming part; LAPW2 computes the Fermi energy and the expansions of the electronic charge densities.

All three parts have been parallelized for efficient usage on Cray T3E /232, 428, 429/. For a matrix of rank 7000 up to 128 processors may be efficiently used for a single k point (par. efficiency (64) = 0.9, par. efficiency (128) = 0.7). For typically 4-20 k points the complete package offers the additional possibility of trivial parallel processing within LAPW1 and thus scalability up to 512 processors. This new MPP version shows significant advantages over the sequential, highly vectorizable code version /590/.

### *3.2.2 Development of the wave function*

The Dyn5d sequential code solves the Schroedinger equation and calculates the development of the wave function in time.

For larger problems a parallel version is required. In a first step a Fortran 90 version of the Fortran 77 code was generated. In this version the FFTs were parallelized for the first two spatial dimensions. To enhance the scalability the third dimension was additionally parallelized (Legendre transformation). Two different approaches were compared: 1. domain decomposition, local transformations of the partial vectors per processor followed by global summation to complete the vectors, and 2. domain decomposition, provision of complete vectors per processor via get operations with global summations being unnecessary. This second approach proved advantageous. An overall parallel efficiency of 0.73 on 128 processors and of 0.66 on 256 processors could be achieved. By application to larger problem sizes the efficiency will be further improved.

## 3.3 Astrophysics

For solution of thermonuclear combustion processes in stars which can be dealt with a hydrodynamic approach the PROMETHEUS parallel code was used as solver. More complex scenarios which require dynamic adaptable resolution, can be solved by the Adaptive Mesh Refinement (AMR) procedure, within which solvers like PROMETHEUS or HERAKLES may be used.

The project to implement a parallel AMR version is being carried out in several phases. In phase 1 the basic concept and its realization for a simple data set was carried out. For the first time steps a static implementation for a one-dimensional data set was done. The derived grids with different resolutions were evenly distributed over the available processors. In phase 2 all program parts were included and applied to a more complex (two-dimensional) data set. The number of time steps and the number of adaptation levels were increased. Further parallelization work was required within previously unused program parts. The implementation work in phase 2 should cover the applicability of a three-dimensional data set.

Planned phase 3 includes dynamic load balancing, optimization, and eventually implementation of dynamic memory management, if required.

### 3.4 Biochemistry

For biological structure determination by electron microscopy a procedure for pattern recognition is used for vastly automatic detection whether a certain organelle type is present within a cell. As this procedure is extremely cpu time intensive, but well suited to parallelization, a concept for the parallelizing strategy was developed and advice given for usage of adequate library routines. The code implementation was carried out by the user and shows good parallel performance.

### 3.5 Psychiatry

By repetitive Transcranial Magnetic Stimulation (rTMS) brain regions are stimulated by a magnetic field varying in time which is generated by an arbitrarily shaped coil. The aim is to determine the rTMS induced currents. For large data sets the chosen numerical approach could not be carried out any more on a single processor.

As a first step the distribution of the electrical conductivity has to be derived from the magnetic resonance scan data. The resulting magnetic field is calculated from the coil parameters within the relevant object volume. After discretizing the object space and the Maxwell equations along the cells the electric field has to be determined by solution of the system of linear equations, and furthermore the current density distribution by means of the electrical conductivity distribution. The solution concept of the user requires solution of a system of linear equations of type Ax=B for an extremely sparse matrix A (occupation density $10^{-5}$) of rank $10^{6}$. No sequential source code was available as previous usage was on a personal computer with program formulations by means of the Mathematica package. Tests with sequential solvers revealed the bad conditioning of the input matrix. An alternative approach was developed that avoids handling of extremely large sparse asymmetric matrices. A relaxation procedure for solution of Maxwell´s equations was developed which requires significantly less main memory and cpu time so that no parallel computer is required.

## 4. VECTOR COMPUTING

With the installation of a 3-processor NEC SX-5 vector system which replaced the NEC SX-4B interim system, support for code migration especially in the fields of data format representation and library routines was necessary, due to the combination of change of hardware, introduction of new compilers, and its restriction to pure IEEE format.

## 5. MULTIMEDIA

### 5.1 Visualization

The different confinement properties of alpha particles in a tokamak, an l=2 stellarator and in the Wendelstein7-X optimized stellarator were simulated on the Cray T3E system by a Guiding Centre code, visualized with the AVS 3D graphics software. The animations were converted to Mpeg-1 movies, which were shown out of PowerPoint presentations on various occasions such as an IAEA Technical Meeting 99 /649/ and the IPP Summer University 99 /711/.

### 5.2 Video Conferencing

For simultaneous meetings of the Wissenschaftliche Leitung distributed between Garching and Greifswald, the PictureTel systems have been accepted and are in regular use, as is the case for group meetings with smaller systems. For desktop communication only the NetMeeting software has been used so far. The requirements for simultaneous sessions in the IPP auditorium and the Greifswald auditorium are more complicated. The video and audio system based on the MBone tools turned out to be too complex and unreliable, whereas the PowerPoint conference mode was accepted by most of the lecturers and the audience /712/. First presentations of outsourced commercial solutions are due at the end of January 2000.

## 6. DEVELOPMENTS IN NETWORKING

New network infrastructure was implemented at IPP. The goal was to use a cabling structure that can easily be adapted to future technologies. The data network realized was therefore based on the concept of a "collapsed backbone", consisting of redundantly implemented switches at a few central locations which connect to all end points via adequate techniques based on copper or fibre lines. This structure has significant advantages over standard "structured cabling" (EN 50173 from 1995), such as fewer sources of problems (fewer components), more flexible choice of network techniques, no bandwidth bottlenecks, and a single point of management. The employed Switched-Ethernet family at 10/100/1000 Mbps (with Gigabit Ethernet at the backbone) relies on the same well-established protocol and the existing infrastructure is easily integrated /485/.

## 7. PILOT PROJECTS FOR THE NEXT GENERATION GERMAN SCIENCE NETWORK

So-called Gigabit Testbeds (GTB), funded by the German government, were implemented to run pilot projects for the next-generation German science network (G-WiN). In the testbed between Munich, Erlangen, and Berlin, RZG contributes to all 4 funded projects in the area of visual supercomputing and metacomputing /589/. After installation of the GTB backbones, the end-to-end connections had to be established and the performance of components had to be tuned, especially in the area of protocol switching from ATM OC12 to HIPPI. Finally the Cray T3E systems at RZG and Konrad-Zuse-Zentrum (ZIB) in Berlin could be connected with a bandwidth of 30 MByte/s over the GTB for large data packets (>= 512 kB). The connections of visualization workstations at RZG, ZIB, Fritz Haber Institute (Berlin), and Albert Einstein Institute (Potsdam) to the T3E systems achieved similar data rates as the performance of the HIPPI interfaces of the T3E systems seem to be the rate limiting factors /591/.

## 8. DATA ACQUISITION AND DATA BASES FOR PLASMA FUSION EXPERIMENTS

A new group was established to concentrate the development of data acquisition, data management, and data analysis systems for the fusion experiments at IPP. The primary task of this group will be to design and develop the data acquisition environment for the newly built W7-X stellarator in Greifswald. An additional task is the cooperation with the ASDEX Upgrade data management team in future developments for the tokamak experiment /9, 334, 377/. A new design is necessary since W7-X will be operated in continuous mode, in contrast to ASDEX-Upgrade and earlier experiments that were run in discharge mode.

### 8.1 Design Principles

As most promising approach for the software design an object-oriented concept has been chosen. To guide the development process the "Software Through Pictures" design tool based on UML has been selected for the system design. As programming languages C++ and Java will be used. The decision on operating systems and hardware will be postponed as long as possible in order to benefit from future developments.

### 8.2 Data Storage

The data will be archived in an object-oriented data base. For storage of data the following set of classes is proposed: diagnostic, data stream, and data box. The data base chosen is Objectivity, which can be configured for several servers and allows storage of objects in parallel data streams. The daily amount of data to be archived is expected to be of the order of several hundred Gigabytes. To understand the principles and study the possibilities of Objectivity several ASDEX Upgrade data files were transferred to the object data base.

### 8.3 Time

Since chronology is so important in a continuously operating system, all collected data will be marked by a timestamp. The global system time is distributed in a star-like network from a central timer system. Every diagnostic system is equipped with a local timer for measurements of timestamps and delays. Timestamps can be sampled in a local time-to-digital converter with the same sample frequencies as the data-producing components. The hardware for the local timer was defined and will be developed by the control group of W7-X. The highest resolution of the local clock was chosen to be preliminarily 10 ns.

### 8.4 Monitoring

Continuous operation of the experiment also requires monitoring of several important signals from the experimental control system as well as from diagnostic subsystems. Every system user should be able to sign on to various monitor signals for observation of the plasma behaviour. A publisher-subscriber model was implemented with the "Java Message Queue" library and the "Java Naming and Directory Services" to investigate the possibilities of these methods.

### 8.5 Data Reduction

Diagnostic systems with high data rates and a large number of channels must be designed to reduce data before archiving. Reduction is mainly done on physics analysis or by event-dependent change on sample rate. When necessary, reduction can be done in parallel by multiple cpus. The Siemens HPCLine-computers will be investigated for these tasks, with a four node system using the Linux and Solaris operating systems. In a next step the driver for the data acquisition boards must be developed.

### 8.6 Prototype

A prototype data acquisition system for a few diagnostics was proposed and will be built for testing these concepts. The first diagnostic will be a simple bolometer diagnostic consisting of a 16-channel ADC with sample rates of several kHz per channel in a Compact PCI Crate. The second diagnostic is a HPCLine-computer hosting 2 ADC's with PCI interface and 2 MHz sample rate. A large amount of data in W7-X will be produced by numerous video and CCD cameras. To investigate how this mass of data can be handled in the experimental environment a third typical video diagnostic will be incorporated. The sampled data will be stored in the Objectivity data base.

# CENTRAL TECHNICAL SERVICES

(Dr.-Ing. Harald Rapp)

The Central Technical Services (ZTE) of Max-Planck-Institut für Plasmaphysik support the experimental divisions with the design, development and construction of experimental components and diagnostic equipment. They also run all kinds of utilities for facility and experiment operation. The staff at Garching comprises approximately 155 workers, technicians and engineers plus 20 apprentices. At Greifswald a branch site of IPP for the Wendelstein 7-X stellarator is under construction. The site development group will later form the Greifswald Technical Services Department as part of ZTE with a work force of 60. For recruitment of personnel to Greifswald the staff at Garching is still being continuously reduced. More ambitious technical tasks at both the ASDEX-Upgrade and Wendelstein 7-X experiments call for restructuring of the staff and reinforcement of qualified technicians and professionals.

## 1. MECHANICAL DESIGN AND CALCULATION (J. Simon-Weidner)

The department designs, calculates and develops experimental devices. It also cares for the CAD system of IPP at all sites. Most effort was devoted to design and construction work for W7-X. Critical points were space and stress problems with the coils, the plasma vessel and the cryostat. The relocation of the W7-X staff to Greifswald called for a more intensive assistance service for CAD and EPD systems.

## 2. ELECTRONICS DEVELOPMENT (D. Arz)

The department develops analogue and digital electronic equipment, including fast voltage switching and control devices for plasma heating systems. Major effort went into contributions to design of the control system for W7-X. The reliability and further use of high-power switching tubes became a subject of concern.

## 3. MATERIALS TECHNOLOGY (J. Perchermeier, since February)

The department was reduced by transferring the materials testing group to a new scientific division. It still offers technical services for functional surface treatment, galvanic technique, UHV plasma welding and vacuum testing, optical spectroscopy, chemical processing including boronization and plastics technology. Difficult vacuum quality checks of the demo cryostat of W7-X and repair work were important tasks.

## 4. EXPERIMENTAL POWER SUPPLY (M. Huart, since July)

The department's task is to provide the electric power supply for the experiments. It consists of the High Current group and the High DC Voltage group. The Flywheel Generator group will join later. The call for tender of a 120 MVA 4-quadrant rectifier was completed. It will provide redundancy for the ASDEX Upgrade magnet coil supply. Replacement of the Hg rectifiers was prepared. Two HVDC modules 140 kV/50 A were commissioned. The design of an overvoltage protection system for the HC rectifiers was further developped. Problems with fuses of rectifier branches are being investigated. Problems with digital controllers in use with 4Q rectifiers still continue. A major challenge were studies on parallelling of the 10 kV bus of generators #3 and #4 in order to enable optimum power and energy sharing between generators.

## 5. FACILITY OPERATION (W.R. McGlaun)

The department is charged with planning and supervising facility installations such as electric supply, heating and airing systems and cooling equipment. It also still runs the flywheel generators. Repair of the rotor of generator #2 has been initiated. Renewal of the building equipment was continued in close collaboration with the civil engineering department. The electrical power supply for a neighbouring institute was provided. The contract for electrical energy supply was renewed after a country-wide call for tender and yielded a cost reduction of 40%.

## 6. WORKSHOPS (M. Keiner)

The department was subjected to a major decrease in manpower. Effective task sharing between IPP and commercial workshops has therefore become more important. Quality assurance, work routing, coordination and planning remain the domain of ZTE services. Apprentice training for electronic craftsmen is running successfully. Approximately 240 apprentices have been trained in 38 years.

## 7. GREIFSWALD SITE DEVELOPMENT GROUP (G.Pfeiffer)

In 1999 most of the buildings of the Greifswald branch institute of IPP were completed. Part of the installations for power supply was commissioned. The time and budget schedule is well within plan. The office and laboratory equipment was delivered. The staff increased to 20. Three apprentice mechanics started their training. The DC high voltage supply for plasma heating of the Wendelstein 7-X stellarator experiment was ordered. All personnel will move into the new buildings in April 2000.

# ADMINISTRATION

## PERSONNEL DEPARTMENT

The personnel department is responsible for administrative matters relating to personnel. The personnel figures of the institute for 1999 were as follows:

| | |
|---|---|
| Total personnel (including Greifswald and Berlin) | 1016 |
| Scientists | 290 |
| Technicians | 454 |
| Directorate and Staff Representative Council | 29 |
| General Services | 44 |
| Administration | 81 |
| Other personnel | 118 |
| | 31.12.99 |

## CONTRACTS AND PURCHASING DEPARTMENT

The contracts and purchasing department is responsible for placing survey and follow-up of all contracts and orders placed by IPP. In 1999, approximately 9.800 orders were made. They include complex contracts, many of which were signed after European-wide calls for tender. Furthermore, all export and import formalities are handled within this department: about 210 international and European shipments were carried out in 1999.

## FINANCE AND ACCOUNTING DEPARTMENT

The finance and accounting department is responsible for the financial planning and all financial transactions and fiscal matters of IPP.

| | |
|---|---|
| Total expenses in 1999: | 275,0 MDM |
| These expenses were financed as follows: | |
| Federal Republic of Germany through Federal Ministry of Education, Science, Research and Technology (BMBF) | 145,4 MDM |
| Bavaria | 9,2 MDM |
| Berlin | 0,9 MDM |
| Mecklenburg-Vorpommern | 35,6 MDM |
| EURATOM | 52,2 MDM |
| Other income | 31,7 MDM |
| | 29.02.00 |

## SITE AND BUILDINGS DEPARTMENT

The site and buildings department is in charge of planning, construction, structural alteration and reconditioning of buildings and main service facilities. Building maintenance is also provided for the neighbouring Max Planck Institutes of Astrophysics and Extraterrestrial Physics, the European Southern Observatory and Greifswald.

## SOCIAL DEPARTMENT

The social department gives assistance to employees seeking housing, provides accommodation for guests in IPP residences, and runs the transport pool, bus and cleaning services.

These departments are reporting directly to the heads of administration Garching/Greifswald.

## LEGAL AND PATENT DEPARTMENT

The legal and patent department works out and controls co-operation contracts with German and foreign universities and research institutes.

Concerning patent matters it attends to patent applications and supervision and licensing of patents in co-operation with Garching Innovation GmbH, a subsidiary of the Max Planck Society. In 1999 the division supervised 95 patents and similar rights.

## AUDITING DEPARTMENT

The Auditing department is responsible for the auditing of workflow and proceedings within the administration of IPP with respect to their commercial efficiency and their compliance with regulations. The single tasks are defined in an auditing plan, which is drawn up every year according to the directives of the management of IPP.

## ORGANISATION DEPARTMENT

The Organisation Department is mainly dealing with data processing within the administration. It co-ordinates and develops on the one hand the SAP-Equipment, the Outsourcing-DP-Centre and the SAP-Users of the entire institute, on the other hand the about 100 PC-Users, their workstations, software and the network of the administration in order to meet the requirements of the IPP-Administration. The Organisation Department is the first level helpdesk for the above mentioned systems. In addition, it is responsible for organisational means like e.g. form and charts, organisation-manuals and phonebook

## CONTROLLING W7-X

This department is responsible for the planning, controlling and co-ordination of the W7-X construction in Greifswald.

These departments are reporting directly to the managing director.

# Publications

# Publications and Conference Reports


1. *Anton, M., J. Geiger, R. Jaenicke, W7-AS Team and ECRH Group:* Toroidal Current Densities Viewed by Magnetic Diagnostics at W7-AS. In: Proc. 26th EPS Conf. Control. Fusion and Plasma Phys., Maastricht 1999, (Eds.) B.Schweer, G.Van Oost, E.Vietzke. ECA 23J. Europ. Phys. Soc., Geneva 1999, 1461-1464.

2. *Arndt, S., P. Merkel, D.A. Monticello* and A. Reiman*:* Finite-β Equilibria for Wendelstein 7-X Configurations Using the Princeton Iterative Equilibrium Solver Code. Physics of Plasmas **6**, 1246-1252 (1999).

3. *Bachmann, P. and D. Sünder:* One-Dimensional Multifluid Plasma Models. Part 1: Fundamentals. Journal of Plasma Physics **61**, 645-667 (1999).

4. *Balden, M.:* Overview on the Effects of Dopants on Chemical Erosion and RES of Carbon-Based Materials. Physica Scripta **T81**, 64-69 (1999).

5. *Balden, M., M. Mayer and J. Roth:* Co-Deposition of Deuterium with Silicon Doped Carbon. Journal of Nuclear Materials **266-269**, 440-445 (1999).

6. *Bäumel, S., M. Rodriguez* and H.-J. Hartfuß:* ECE Imaging Development at W7-AS. In: Proc. 26th EPS Conf. Control. Fusion and Plasma Phys., Maastricht 1999, (Eds.) B.Schweer, G.Van Oost, E.Vietzke. ECA 23J. Europ. Phys. Soc., Geneva 1999, 1581-1584.

7. *Becker, G.:* Strong Impact of Neutrals on Anomalous Inward Drift and Width of Steep Gradient Zone. Nuclear Fusion **39**, 95-106 (1999).

8. *Becker, G.:* Study of Radiation Limits in Fusion Reactor Scenarios. Nuclear Fusion **39**, 937-948 (1999).

9. *Behler K., H. Blank, A. Buhler, R. Drube, H. Friedrich, K. Förster, K. Hallatschek, P. Heimann, F. Hertweck, J. Maier, R. Merkel, M.-G. Pacco-Düchs, G. Raupp, H. Reuter, U. Schneider-Maxon, R. Tisma, M. Zilker and ASDEX Upgrade Team:* Review of the ASDEX Upgrade Data Acquisition Environment - Present Operation and Future Requirements. Fusion Engineering and Design **43**, 247-258 (1999).

10. *Behringer, K. and U. Fantz*:* Some Basic Physics Results for Plasma Spectroscopy and Modelling. Contributions to Plasma Physics **39**, 411-425 (1999).

11. *Behrisch R., W. von der Linden*, U. von Toussaint and D. Grambole*:* Surface Layer Destruction during Ion Beam Analysis. Nuclear Instruments and Methods in Physics Research B **155**, 440-446 (1999).

12. *Beidler, C.D., F. Herrnegger, J. Kisslinger, H. Wobig and A.V. Zolutkhin:* Guiding Center Studies of Collisionless α-Particles in a Helias Configuration. Problems of Atomic Science and Technology. Series: Plasma Physics, Issues **1**(1), **2**(2), 35-37 (1999).

13. *Berger, E., W. von der Linden*, V. Dose, M. Jacobi* and A.W. Koch*:* Reconstruction of Surfaces from Phase-Shifting Speckle Interferometry: Bayesian Approach. Applied Optics **38**, 4997-5003 (1999).

14. *Biedermann, C., T. Fuchs, P. Liebisch, R. Radtke, E. Behar* and R. Doron*:* X-Ray-Spectroscopic Measurements of Dielectronic Recombination of Highly Charged Krypton Ions. Physica Scripta **T80**, 303-304 (1999).

15. *Bilato*, R. and M. Brambilla:* Radio Frequency CD by LH Waves in the Reversed Field Experiment. In: Proc. 13th Top. Conf. Radio Frequency Power in Plasmas, Annapolis,MD 1999, (Eds.) S.Bernabei, F.Paoletti. AIP Conf. Proc. 485, AIP Press, Melville,NY 1999, 202-210.

16. *Biskamp, D. and W.-C. Müller:* Decay Laws for Three-Dimensional Magnetohydrodynamic Turbulence. Physical Review Letters **83**, 2195-2199 (1999).

17. *Biskamp, D. and W.-C. Müller:* New Developments in MHD Turbulence Theory (I). In: Interrelation between Plasma Experiments in Laboratory and Space, Kreuth 1999, (Ed.) MPI für Extraterrestr. Physik, Garching 1999, 2.4.

18. *Biskamp, D., E. Schwarz, A. Zeiler, A. Celani* and J.F. Drake*:* Electron Magnetohydrodynamic Turbulence. Physics of Plasmas **6**, 751-758 (1999).

19. *Bleuel, J., M. Endler and W7-AS Team:* The Contribution of Edge Fluctuations to Anomalous Transport in W7-AS. In: Proc. 26th EPS Conf. Control. Fusion and Plasma Phys., Maastricht 1999, (Eds.) B.Schweer, G.Van Oost, E.Vietzke. ECA 23J. Europ. Phys. Soc., Geneva 1999, 61-64.

20. *Bolt, H., F. Koch, J.L. Rodet*, D. Karpov* and S. Menzel*:* $Al_2O_3$ Coatings Deposited by Vacuum Arc with Different Filtering Methods - Characterization of High Temperature Properties. Surface and Coatings Technology **116-119**, 956-962 (1999).

21. *Bolt, H., J. Linke*, H.J. Penkalla* and E. Tarret*:* Emission of Solid Particles from Carbon Materials under Pulsed Surface Heat Loads. Physica Scripta **T81**, 94-97 (1999).

22. *Borchardt, M., A. Mutzke, J. Nührenberg, J. Riemann, R. Schneider and S. Weber:* Towards a 3-D Plasma Fluid Modelling for the W7-X Divertor. In: Proc. 26th EPS Conf. Control. Fusion and Plasma Phys., Maastricht 1999, (Eds.) B.Schweer, G.Van Oost, E.Vietzke. ECA 23J. Europ. Phys. Soc., Geneva 1999, 1501-1504.

23. *Borrass, K., J. Schweinzer, J. Lingertat* and ASDEX Upgrade Team:* Scaling of the Separatrix to Pedestal Density Ratio in ASDEX Upgrade H Modes. Nuclear Fusion **39**, 843-847 (1999).

24. *Bosch, H.-S., J.C. Fuchs, J. Gafert, G. Haas, A. Herrmann, A. Kallenbach, M. Kaufmann, J. Neuhauser, F. Ryter, R. Schneider, J. Schweinzer, W. Ullrich, U. Wenzel, G.C. Vlases*, L.D. Horton*, G.F. Matthews*, ASDEX Upgrade Team and JET Divertor Physics Topic Group*:* Effect of Divertor Geometry on Boundary and Core Plasma Performance in ASDEX Upgrade and JET. Plasma Physics and Controlled Fusion **41**, A401-A408 (1999).

25. *Bosch, H.-S., W. Ullrich, A. Bard, D.P. Coster, G. Haas, A. Kallenbach, J. Neuhauser, R. Schneider and ASDEX Upgrade Team:* Noble Gas Exhaust with a Strongly Baffled Divertor in ASDEX Upgrade. Journal of Nuclear Materials **266-269**, 462-466 (1999).

26. *Bosia*, G. and M. Brambilla:* Performance of a Multi-Section ICRF Array for a RTO/RC ITER. In: Proc. 13th Top. Conf. Radio Frequency Power in Plasmas, Annapolis,MD 1999, (Eds.) S.Bernabei, F.Paoletti. AIP Conf. Proc. 485, AIP Press, Melville,NY 1999, 445-448.

27. *Brakel, R. and W7-AS Team:* The Dependence of Confinement on Rotational Transform and Magnetic Shear in Wendelstein 7-AS. Stellarator News **61**, 13-15 (1999), http://www.ornl.gov/fed/stelnews.

28. *Brambilla, M.:* A Comparison of the Order Reduction Algorithm with the Finite Larmor Radius Model for the Simulation of Ion Cyclotron Waves in Toroidal Plasmas. In: Proc. 13th Top. Conf. Radio Frequency Power in Plasmas, Annapolis,MD 1999, (Eds.) S.Bernabei, F.Paoletti. AIP Conf. Proc. 485, AIP Press, Melville,NY 1999, 325-332.

29. *Brambilla, M.:* The High-Frequency Constitutive Relation of Axisymmetric Toroidal Plasmas. Plasma Physics and Controlled Fusion **41**, 775-800 (1999).

30. *Brambilla, M.:* Numerical Simulation of Ion Cyclotron Waves in Tokamak Plasmas. Plasma Physics and Controlled Fusion **41**, 1-34 (1999).

31. *Brañas*, B., M. Hirsch, J. Sánchez* and V. Zhuravlev*:* Geometrical Optics Interpretation of the Phase Runaway in Microwave Reflectometry. Review of Scientific Instruments **70**, 1025-1029 (1999).

32. *Brandenburg, R., J. Schweinzer, S. Fiedler, F. Aumayr* and H.P. Winter*:* Modelling of Fast Neutral Li Beams for Fusion Edge Plasma Diagnostics. Plasma Physics and Controlled Fusion **41**, 471-484 (1999).

33. *Burhenn, R., A. Weller, W7-AS Team and NI Group:* Derivation of Local Impurity Transport Quantities from Soft-x Radiation Evolution during Tracer Injection at W7-AS. Review of Scientific Instruments **70**, 603-607 (1999).

34. *Buuron*, A., F. Koch, M. Nöthe* and H. Bolt:* Diagnostics and Modelling of a Hollow Cathode Arc Deposition Plasma. Surface and Coatings Technology **116-119**, 755-765 (1999).

35. *Callaghan*, H.P., P. McCarthy and J. Geiger:* Fast Equilibrium Interpretation on the W7-AS Stellarator Using Function Parameterization. Nuclear Fusion **39**, 509-523 (1999).

36. *Campbell, D.J., H.J. de Blank*, O. Gruber, T.C. Hender*, J. Jacquinot*, F.W. Perkins*, M.L. Watkins* and M. Zabiego*:* Report on the 5th Europ. Fusion Phys. Workshop, Sesimbra 1997. Plasma Physics and Controlled Fusion **41**, 133-158 (1999).

37. *Carlson, A. and A. Bergmann:* Effects of Temperature Gradients and Sheath Power Transmission on Langmuir Probes. Journal of Nuclear Materials **266-269**, 1020-1022 (1999).

38. *Carreras*, B.A., B. Van Milligen*, C. Hidalgo*, R. Balbin*, E. Sanchez*, I. Garcia-Cortes*, M.A. Pedrosa*, J. Bleuel and M. Endler:* Self-Similarity Properties of the Probability Distribution Function of Turbulence-Induced Particle Fluxes at the Plasma Edge. Physical Review Letters **83**, 3653-3656 (1999).

39. *Carreras*, B.A., B. Van Milligen*, M.A. Pedrosa*, R. Balbin*, C. Hidalgo*, D.E. Newman*, E. Sanchez*, R. Bravenec*, G. McKee*, I. Garcia-Cortes*, J. Bleuel, M. Endler, C. Ricardi*, S. Davies*, G.F. Matthews*, E. Martines* and V. Antoni*:* Experimental Evidence of Long-Range Correlations and Self-Similarity in Plasma Fluctuations. Physics of Plasmas **6**, 1885-1892 (1999).

40. *Cattanei, G. and W7-AS Team:* Folded Lisitano Coil. In: Proc. 13th Top. Conf. Radio Frequency Power in Plasmas, Annapolis,MD 1999, (Eds.) S.Bernabei, F.Paoletti. AIP Conf. Proc. 485, AIP Press, Melville,NY 1999, 421-424.

41. *Celani*, A. and D. Biskamp:* Bridge Relations in Navier-Stokes Turbulence. Europhysics Letters **46**, 332-338 (1999).

42. *Coelho*, R., M. Maraschek, H. Zohm and F. Serra*:* Mirnov Signal Reconstruction from Numerical Simulations of Toroidally Coupled Tearing Modes. In: Proc. 26th EPS Conf. Control. Fusion and Plasma Phys., Maastricht 1999, (Eds.) B.Schweer, G.Van Oost, E.Vietzke. ECA 23J. Europ. Phys. Soc., Geneva 1999, 1265-2268.

43. *Connor*, J.W., P. Buratti*, J.G. Cordey*, C. Hidalgo*, A. Jacchia*, U. Stroth and W. Suttrop:* EU-US Workshop on Transport in Fusion Plasmas. Plasma Physics and Controlled Fusion **41**, 693-707 (1999).

44. *Correa-Restrepo, D.:* Resistive Ballooning Modes near the Edge of Toroidal Configurations. Physics of Plasmas **6**, 530-540 (1999).

45. *Coster, D.P, K. Borrass, R. Schneider and ASDEX Upgrade Team:* B2-EIRENE Modelling of the Density Limit on ASDEX Upgrade. Journal of Nuclear Materials **266-269**, 804-808 (1999).

46. *Coster, D.P., A. Kallenbach, M. Kaufmann, R. Schneider and ASDEX Upgrade Team:* Towards a Better Understanding of Power Loading and Carbon Radiation in the Divertor. In: Proc. 26th EPS Conf. Control. Fusion and Plasma Phys., Maastricht 1999, (Eds.) B.Schweer, G.Van Oost, E.Vietzke. ECA 23J. Europ. Phys. Soc., Geneva 1999, 1517-1520.

47. *DeKock*, L., C. Walker*, E. Coccorese*, A.E. Costley*, M. Dremin*, J. Gernhardt, I. Senda*, T. Shoji*, J. Leuer*, R. Snider*, P. McCarthy, A. Portone*, P. Stott* and K. Young*:* Design of the Magnetic Diagnostic for ITER. Review of Scientific Instruments **70**, 452-457 (1999).

48. *Dinger*, A., C. Lutterloh*, J. Biener* and J. Küppers:* Hydrogen Atom Reactions with Graphite Island Edges on Pt(111) Surfaces: Hydrogenation through Eley-Rideal and Hot-Atom Processes. Surface Science **421**, 17-26 (1999).

49. *Dinger*, A., C. Lutterloh*, J. Biener* and J. Küppers:* Reactions of Gaseous H Atoms with Propylene Oxide Monolayers Adsorbed on Graphite Covered Pt(111) Surfaces. Surface Science **421**, 44-52 (1999).

50. *Dinger*, A., C. Lutterloh*, J. Biener* and J. Küppers:* Reactions of Hydrogen Atoms with Acetone Monolayers Adsorbed on Graphite Monolayer Covered Pt (111) Surfaces. Surface Science **437**, 116-124 (1999).

51. *Dinger*, A., C. Lutterloh* and J. Küppers:* Kinetics of D Abstraction with H Atoms from the Monodeuteride Phase on Si (100) Surfaces. Chemical Physics Letters **311**, 202-208 (1999).

52. *Donath, M.:* Magnetic Order and Electronic Structure in Thin Films. Journal of Physics: Condensed Matters **11**, 9421-9436 (1999).

53. *Donath, M.:* Spin Polarized Electron Studies of Low-Dimensional Magnetic Systems. Australian Journal of Physics **52**, 579-593 (1999).

54. *Dose, V. and W. von der Linden*:* Outlier Tolerant Parameter Estimation. In: Maximum Entropy and Bayesian Methods, (Eds.) W.v.d.Linden, V.Dose, R.Fischer, R.Preuss. Kluwer Acad. Publ., Dordrecht 1999, 47-56.

55. *Drüsedau*, T.P., T. Bock*, T.M. John*, F. Klabunde* and W. Eckstein:* Energy Transfer into Growing Film during Sputter Deposition: An Investigation by Calorimetric Measurements and Monte Carlo Simulations. Journal of Vacuum Science and Technology A **17**, 2896-2905 (1999).

56. *Dux, R., A.G. Peeters, A. Gude, A. Kallenbach, R. Neu and ASDEX Upgrade Team:* Z-Dependence of the Core Impurity Transport. Nuclear Fusion **39**, 1509-1522 (1999).

57. *Dux, R., A.G. Peeters, A. Kallenbach, R. Neu and ASDEX Upgrade Team:* Z-Dependence of Central Particle Transport in ASDEX Upgrade H Mode Discharges. In: Proc. 26th EPS Conf. Control. Fusion and Plasma Phys., Maastricht 1999, (Eds.) B.Schweer, G.van Ost, E.Vietzke. ECA 23J. Europ. Phys. Soc., Geneva 1999, 1409-1412.

58. *Eckstein, W., R. Dohmen, H. Friedrich and F. Hertweck:* Dependence of Energy Distributions of Sputtered and Reflected Atoms on Incident Fluence. Nuclear Instruments and Methods in Physics Research B **153**, 345-349 (1999).

59. *Eckstein, W. and M. Mayer:* Rutherford Backscattering from Layered Structures beyond the Single Scattering Model. Nuclear Instruments and Methods in Physics Research B **153**, 337-344 (1999).

60. *Eckstein, W., V.I. Shulga* and J. Roth:* Carbon Implantation into Tungsten at Elevated Temperatures. Nuclear Instruments and Methods in Physics Research B **153**, 415-421 (1999).

61. *Egorov*, S., G. Pautasso, K. Büchl, J.C. Fuchs, O. Gruber, R.S. Lang, M. Maraschek, V. Mertens, I. Perchermeier and ASDEX Upgrade Team:* A New Pellet Injection System for Softening of Disruption Loads on ASDEX Upgrade. In: Proc. 26th EPS Conf. Control. Fusion and Plasma Phys., Maastricht 1999, (Eds.) B.Schweer, G.Van Oost, E.Vietzke. ECA 23J. Europ. Phys. Soc., Geneva 1999, 1425-1428.

62. *Elevant*, T., B. Wolle* and A. Weller:* Proposed Neutron Diagnostics for Wendelstein 7-X Stellarator. Review of Scientific Instruments **70**, 1185-1189 (1999).

63. *Endler, M.:* Measurements of Anomalous Transport in Tokamaks and Stellarators. In: Interrelation between Plasma Experiments in Laboratory and Space, Kreuth 1999, (Ed.) MPI für Extraterrestr. Physik, Garching 1999, 2.6.

64. *Endler, M.:* The Poloidal Variation of the Radial Transport due to Electrostatic Fluctuations in Toroidal Magnetic Confinement Experiments. Plasma Physics and Controlled Fusion **41**, 1431-1440 (1999).

65. *Endler, M.:* Turbulent SOL Transport in Stellarators and Tokamaks. Journal of Nuclear Materials **266-269**, 84-90 (1999).

66. *Erckmann, V., G. Dammertz*, D. Dorst, L. Empacher*, W. Förster*, G. Gantenbein*, T. Geist, W. Kasparek*, H.P. Laqua, G.A. Müller*, M. Thumm*, M. Weißgerber, H. Wobig, W7-X Team, W7-AS Team, W7-X Team (FZ Karlsruhe)* and W7-X Team (IPF Stuttgart)*:* ECRH and ECCD with High Power Gyrotrons at the Stellarators W7-AS and W7-X. IEEE Transactions on Plasma Science **27**, 538-546 (1999).

67. *Erckmann, V., G. Dammertz*, W. Kasparek*, H.P. Laqua, H. Maaßberg, M. Thumm*, W7-X Team, W7-AS Team, W7-X Team (FZ Karlsruhe)* and W7-X Team (IPF Stuttgart)*:* ECRH and ECCD at W7-AS, Prospects for W7-X Radio Frequency Power in Plasmas. In: Proc. 13th Top. Conf. Radio Frequency Power in Plasmas, Annapolis,MD 1999, (Eds.) S.Bernabei, F.Paoletti. AIP Conf. Proc. 485, AIP Press, Melville,NY 1999, 229-236.

68. *Erckmann, V., H. Maaßberg, W7-AS Team and ECRH Group:* Recent Results with ECRH and ECCD on the W7-AS Stellarator. Stellarator News **61**, 22-24 (1999), http://www.ornl.gov/fed/stelnews.

69. *Fantz*, U., K. Behringer, D.P. Coster, R. Schneider, D. Reiter* and ASDEX Upgrade Team:* Molecular Enhanced Recombination in the Divertor of ASDEX Upgrade. In: Proc. 26th EPS Conf. Control. Fusion and Plasma Phys., Maastricht 1999, (Eds.) B.Schweer, G.Van Oost, E.Vietzke. ECA 23J. Europ. Phys. Soc., Geneva 1999, 1549-1552.

70. *Fantz*, U., K. Behringer, J. Gafert, D.P. Coster and ASDEX Upgrade Team:* Optical Emission Measurements of $H_2$- and $D_2$-Molecules in the Divertor Region of ASDEX Upgrade. Journal of Nuclear Materials **266-269**, 490-494 (1999).

71. *Federici*, G., R.A. Anderl*, P. Andrew*, J.N. Brooks*, R.A. Causey*, J.P. Coad*, D. Cowgill*, R.P. Doerner*, A.A. Haasz*, G. Janeschitz*, W. Jacob, G.R. Longhurst*, R. Nygren*, A.T. Peacock*, M.A. Pick*, V. Philipps*, J. Roth, C.H. Skinner* and W.R. Wampler:* In-Vessel Tritium Retention and Removal in ITER. Journal of Nuclear Materials **266-269**, 14-29 (1999).

72. *Feist J.-H. and M. Wanner:* Status of the WENDELSTEIN 7-X Experiment. Stellarator News **61**, 6-8 (1999), http://www.ornl.gov/fed/stelnews.

73. *Feng, Y., J. Kisslinger and F. Sardei:* Transport Characteristics Related to the Island Divertor Geometry of W7-AS. In: Proc. 26th EPS Conf. Control. Fusion and Plasma Phys., Maastricht 1999, (Eds.) B.Schweer, G.Van Oost, E.Vietzke. ECA 23J. Europ. Phys. Soc., Geneva 1999, 1465-1468.

74. *Feng, Y., F. Sardei, P. Grigull, G. Herre and W7-AS Team:* Drift Effects in W7-AS Limiter and Island Divertor Configurations. Journal of Nuclear Materials **266-269**, 928-933 (1999).

75. *Feng, Y., F. Sardei, P. Grigull and J. Kisslinger:* Island Divertor Studies for W7-AS. Stellarator News **61**, 34-36 (1999), http://www.ornl.gov/fed/stelnews.

76. *Feng, Y., F. Sardei and J. Kisslinger:* 3D Fluid Modelling of the Edge Plasma by Means of a Monte Carlo Technique. Journal of Nuclear Materials **266-269**, 812-818 (1999).

77. *Fenstermacher*, M.E., N. Jalufka*, W.H. Meyer*, D.G. Nilson*, J. Gafert, J. Hogan*, C.J. Lasnier*, A.W. Leonard*, R.A. Pitts*, G. Porter* and DIII-D Team*:* Evolution of 2D Visible and VUV Divertor Emission Profiles during DIII-D H-Mode Detachment Transitions. In: Proc. 26th EPS Conf. Control. Fusion and Plasma Phys., Maastricht 1999, (Eds.) B.Schweer, G.Van Ost, E.Vietzke. ECA 23J. Europ. Phys. Soc., Geneva 1999, 1197-1200.

78. *Fiedler, S., R. Brandenburg, J. Baldzuhn, K. McCormick, F. Aumayr*, J. Schweinzer, H.P. Winter*, W7-AS Team and ASDEX Upgrade Team:* Edge Plasma Diagnostics on W7-AS and ASDEX-Upgrade Using Fast Li Beams. Journal of Nuclear Materials **266-269**, 1279-1284 (1999).

79. *Fischer, R. and V. Dose:* Electron Energy Distribution Reconstruction in Low-Pressure Helium Plasmas from Optical Measurements. Plasma Physics and Controlled Fusion **41**, 1109-1123 (1999).

80. *Fischer, R., W. Jacob, W. von der Linden* and V. Dose:* Bayesian Reconstruction of Electron Energy Distributions from Emission Line Intensities. In: Maximum Entropy and Bayesian Methods, (Eds.) W.v.d.Linden, V.Dose, R.Fischer, R.Preuss. Kluwer Acad. Publ., Dordrecht 1999, 99-106.

81. *Franzen, P., W. Kraus, O. Vollmer, B. Heinemann, R. Riedl, E. Speth and A. Stäbler:* Spectroscopic Determination of the Species Distribution and the Divergence of the ASDEX Upgrade Neutral Beam Injection System. In: Proc. 26th EPS Conf. Control. Fusion and Plasma Phys., Maastricht 1999, (Eds.) B.Schweer, G.Van Oost, E.Vietzke. ECA 23J. Europ. Phys. Soc., Geneva 1999, 1557-1560.

82. *Fuchs, C., J. Geiger, H.-J. Hartfuß, H. Maaßberg and W7-AS Team:* ECRH Absorption and Shafranov Shift in the "Electron Root" Feature at the W7-AS Stellarator. In: Proc. 26th EPS Conf. Control. Fusion and Plasma Phys., Maastricht 1999, (Eds.) B.Schweer, G.Van Oost, E.Vietzke. ECA 23J. Europ. Phys. Soc., Geneva 1999, 1469-1472.

83. *Fuchs, C. and H.-J. Hartfuß:* Line Integrated Density Measurements Based on Cotton-Mouton Polarimetry. Review of Scientific Instruments **70**, 722-725 (1999).

84. *Fuchs, C. and H.-J. Hartfuß:* Polarimetric Line Density Measurements on W7-AS Using the Cotton-Mouton Effect. Stellarator News **61**, 19-21 (1999), http://www.ornl.gov/fed/stelnews.

85. *Fuchs, J.C., K.-F. Mast, D.P. Coster, A. Herrmann, R. Schneider and ASDEX Upgrade Team:* Variation of Radiation Profiles with Plasma Parameters in ASDEX Upgrade. In: Proc. 26th EPS Conf. Control. Fusion and Plasma Phys., Maastricht 1999, (Eds.) B.Schweer, G.Van Oost, E.Vietzke. ECA 23J. Europ. Phys. Soc., Geneva 1999, 1385-1388.

86. *Fußmann, G., C. Biedermann and R. Radtke:* EBIT: An Electron Beam Ion Source for the Production and Confinement of Hihgly Charged Atoms. In: Advanced Technologies Based on Wave and Beam Generated Plasmas, (Eds.) H.Schlüter, A.Shivarova. NATO ASI Series 3: High Technology 67, Kluwer Acad. Publ. 1999, 429-468.

87. *Gafert, J., K. Behringer, D.P. Coster, C. Dorn, A. Kallenbach, R. Schneider, U. Schumacher* and ASDEX Upgrade Team:* Spectroscopic Investigation of the Dynamics of Ions and Neutrals in the ASDEX Upgrade Divertor II. Journal of Nuclear Materials **266-269**, 365-369 (1999).

88. *Gafert, J., K. Büchl, M.E. Fenstermacher*, W.H. Meyer* and ASDEX Upgrade Team:* Reconstruction of Two-Dimensional Emissivity Distributions in the ASDEX Upgrade LYRA-Divertor from TV-CCD Data. In: Proc. 26th EPS Conf. Control. Fusion and Plasma Phys., Maastricht 1999, (Eds.) B.Schweer, G.van Ost, E.Vietzke. ECA 23J. Europ. Phys. Soc., Geneva 1999, 1577-1580.

89. *Gasparino, U., J. Geiger, S.V. Kasilov*, H. Maaßberg, N. Marushchenko*, S. Murakami* and M. Romé*:* Fokker-Planck Estimation of Electron Distribution Functions for High Power ECCD at W7-AS. In: Proc. 26th EPS Conf. Control. Fusion and Plasma Phys., Maastricht 1999, (Eds.) B.Schweer, G.Van Oost, E.Vietzke. ECA 23J. Europ. Phys. Soc., Geneva 1999, 1569-1572.

90. *Geier, A., K. Asmussen, A. Bard, R. Neu and K. Krieger:* A Sublimation Probe for the Injection of High-Z Impurities into Fusion Devices. Review of Scientific Instruments **70**, 63-67 (1999).

91. *Giannone, L., R. Burhenn, P. Grigull, U. Stroth, R. Brakel, R. Dux, A. Elsner, S. Fiedler, G. Kühner, F.-P. Penningsfeld, G. Pereverzev, F. Wagner, A. Weller, C. Wendland, NBI Team and W7-AS Team:* Radiation Measurements and Modelling of the Density Limit on the W7-AS Stellarator. Journal of Nuclear Materials **266-269**, 507-512 (1999).

92. *Goldstraß, P., W. Eckstein and C. Linsmeier:* Erosion of Beryllium and Deposition of Carbon and Oxygen due to Bombardment with C+ and CO+ Ions. Journal of Nuclear Materials **266-269**, 581-586 (1999).

93. *Gori, S. and J. Nührenberg:* Quasi-Isodynamic Stellarators with Magnetic Wall and Positive Shear. In: Theory of Fusion Plasmas, (Eds.) J.W.Connor, E.Sindoni, J.Vaclavik. Ed. Compositori, Bologna 1999, 473-489.

94. *Grambole*, D., F. Herrmann*, R. Behrisch and W. Hauffe*:* Hydrogen and Deuterium Depth Profiling in Divertor Tiles of a Fusion Experiment by Micro-ERDA. Nuclear Instruments and Methods in Physics Research B **158**, 647-652 (1999).

95. *Grieger, G.:* Prof. Atsuo Iiyoshi Resigning the Post of Director General of NIFS. Stellarator News **63**, 4 (1999), http://www.ornl.gov/fed/stelnews.

96. *Grigull*, S., R. Behrisch and S. Parascandola*:* Nitrogen Implantation into Carbon: Retention, Release and Target-Erosion Processes. Journal of Nuclear Materials **275**, 158-163 (1999).

97. *Grigull, P., M. Hirsch, K. McCormick, J. Baldzuhn, R. Brakel, S. Fiedler, C. Fuchs, L. Giannone, H.-J. Hartfuß, D. Hildebrandt, J. Kisslinger, R. König, G. Kühner, H. Maaßberg, F. Wagner and W7-AS Team:* H-Mode Phenomenology in W7-AS Configurations Bounded by Magnetic Islands. In: Proc. 26th EPS Conf. Control. Fusion and Plasma Phys., Maastricht 1999, (Eds.) B.Schweer, G.Van Oost, E.Vietzke. ECA 23J. Europ. Phys. Soc., Geneva 1999, 1473-1476.

98. *Grote, H., W. Bohmeyer, P. Kornejew, H.-D. Reiner, G. Fußmann, R. Schlögl*, G. Weinberg* and C.H. Wu*:* Chemical Sputtering Yields of Carbon Based Materials at High Ion Flux Densities. Journal of Nuclear Materials **266-269**, 1059-1064 (1999).

99. *Grote, H., W. Bohmeyer, P. Kornejew, H.-D. Reiner, G. Fußmann, R. Schlögl*, G. Weinberg* and C.H. Wu*:* Flux Dependence of Chemical Sputtering Yields. In: Proc. 4th Int. Workshop Tritium Effects in Plasma Facing Components, Santa Fé,NM, (Ed.) R.A.Causey. Livermore 1999, SAND99-8222, 13-15.

100. *Gruber, O., H.-S. Bosch, S. Günter, A. Herrmann, A. Kallenbach, M. Kaufmann, K. Krieger, K. Lackner, V. Mertens, R. Neu, F. Ryter, J. Schweinzer, A. Stäbler, W. Suttrop, R. Wolf, K. Asmussen, A. Bard, G. Becker, K. Behler, K. Behringer, A. Bergmann, M. Bessenrodt-Weberpals, K. Borrass, B. Braams*, M. Brambilla, R. Brandenburg, F. Braun, H. Brinkschulte, R. Brückner, B. Brüsehaber, K. Büchl, A. Buhler, H.P. Callaghan*, A. Carlson, D.P. Coster, L. Cupido*, S. de Peña Hempel, C. Dorn, R. Drube, R. Dux, S. Egorov*, W. Engelhardt, H.-U. Fahrbach, U. Fantz*, J.-H. Feist, P. Franzen, J.C. Fuchs, G. Fußmann, J. Gafert, G. Gantenbein*, O. Gehre, A. Geier, J. Gernhardt, E. Gubanka, A. Gude, G. Haas, K. Hallatschek, D.A. Hartmann, B. Heinemann, G. Herppich, W. Herrmann, F. Hofmeister, E. Holzhauer*, D. Jacobi, M. Kakoulidis*, N. Karakatsanis*, O.J.W.F. Kardaun, A. Khutoretski*, H. Kollotzek, S. Kötterl, W. Kraus, B. Kurzan, G. Kyriakakis*, P.T. Lang, R.S. Lang, M. Laux, L.L. Lengyel, F. Leuterer, A. Lorenz, H. Maier, M. Manso*, M. Maraschek, M. Markoulaki*, K.-F. Mast, P. McCarthy, D. Meisel, H. Meister, R. Merkel, J. Meskat*, H.W. Müller, M. Münich, H. Murmann, B. Napiontek, A.G. Peeters, G. Pereverzev, S.D. Pinches, G. Raupp, K. Reinmüller, R. Riedl, V. Rohde, H. Röhr, J. Roth, H. Salzmann, W. Sandmann, H.-B. Schilling, D. Schlögl, K. Schmidtmann, H. Schneider, R. Schneider, W. Schneider, G. Schramm, S. Schweizer, R.R. Schwörer, B.D. Scott, U. Seidel, F. Serra*, S. Sesnic, C. Sihler, A. Silva*, E. Speth, K.-H. Steuer, J. Stober, B. Streibl, A. Thoma, W. Treutterer, M. Troppmann, N. Tsois*, W. Ullrich, M. Ulrich, P. Varela*, H. Verbeek, O. Vollmer, H. Wedler, M. Weinlich, U. Wenzel, F. Wesner, R. Wunderlich, N. Xantopoulos*, Q. Yu*, D. Zasche, T. Zehetbauer, H.-P. Zehrfeld, H. Zohm and M. Zouhar:* Overview on ASDEX Upgrade Results. Nuclear Fusion **39**, 1321-1336 (1999).

101. *Gruber, O., R. Wolf, R. Dux, C. Fuchs, S. Günter, A. Kallenbach, K. Lackner, M. Maraschek, P. McCarthy, H. Meister, G. Pereverzev, F. Ryter, J. Schweinzer, U. Seidel, S. Sesnic, A. Stäbler, J. Stober and ASDEX Upgrade Team:* Stationary H-Mode Discharges with Internal Transport Barrier on ASDEX Upgrade. Physical Review Letters **83**, 1787-1798 (1999).

102. *Grulke, O., T. Klinger* and A. Piel*:* Experimental Study of the Dynamics of Conditionally Averaged Structures in Weakly Developed Electrostatic Turbulence. Physics of Plasmas **6**, 788-796 (1999).

103. *Grulke, O., C. Lechte*, F. Greiner*, T. Klinger* and A. Piel*:* Experimental Characterization of Large-Scale Structures in the Turbulent States of a Toroidal Plasma Device. In: Interrelation between Plasma Experiments in Laboratory and Space, Kreuth 1999, (Ed.) MPI für Extraterrestr. Physik, Garching 1999, 3.4.

104. *Gude, A., S. Günter, S. Sesnic and ASDEX Upgrade Team:* Comparison of Fishbones and Fishbone-Like Frequency Changes of the Neoclassical Tearing Mode at ASDEX Upgrade. In: Proc. 26th EPS Conf. Control. Fusion and Plasma Phys., Maastricht 1999, (Eds.) B.Schweer, G.Van Oost, E.Vietzke. ECA 23J. Europ. Phys. Soc., Geneva 1999, 1381-1384.

105. *Gude, A., S. Günter, S. Sesnic and ASDEX Upgrade Team:* Seed Island of Neoclassical Tearing Modes at ASDEX Upgrade. Nuclear Fusion **39**, 127-131 (1999).

106. *Günter, S., A. Gude, H.R. Koslowski*, M. Maraschek, S.D. Pinches, S. Sesnic, Q. Yu* and ASDEX Upgrade Team*: MHD Phenomena at ASDEX Upgrade and TEXTOR. Nuclear Fusion **39**, 1793-1805 (1999).

107. *Günter, S., A. Gude, K. Lackner, M. Maraschek, S.D. Pinches, S. Sesnic, R. Wolf and ASDEX Upgrade Team:* The Influence of Fishbones on the Background Plasma. Nuclear Fusion **39**, 1535-1539 (1999).

108. *Günter, S., A. Gude, M. Maraschek, Q. Yu* and ASDEX Upgrade Team:* Influence of Neoclassical Tearing Modes on Energy Confinement. Plasma Physics and Controlled Fusion **41**, 767-774 (1999).

109. *Günter, S., G. Giruzzi*, A. Gude, R.J. LaHaye*, K. Lackner, M. Maraschek, S. Schade, S. Sesnic, R. Wolf, Q. Yu*, H. Zohm and ASDEX Upgrade Team:* MHD Modes in Regular and Reversed Shear Scenarios and Possibilites for their Control through Current Drive. Plasma Physics and Controlled Fusion **41**, B231-B241 (1999).

110. *Günter, S. and A. Könies:* Diagnostics of Dense Plasmas from the Profile of Hydrogen Spectral Lines in the Presence of a Magnetic Field. Journal of Quantitative Spectroscopy & Radiative Transfer **62**, 425-431 (1999).

111. *Haas, G., R. Maingi*, J. Neuhauser, ASDEX Upgrade Team and DIII-D Team*:* Dynamic Hydrogen Retention in the Walls of the Tokamaks ASDEX Upgrade and DIII-D. Journal of Nuclear Materials **266-269**, 1065-1071 (1999).

112. *Hallatschek, K.:* A Tearing Mode Model for Cascades of High-Frequency Modes. Physics of Plasmas **6**, 2495-2502 (1999).

113. *Harmeyer, E., F. Herrnegger, O. Jandl, J. Kisslinger and H. Wobig:* On the Coil Support Structure of a Stellarator Fusion Reactor. In: Proc. Jahrestagung Kerntechnik, Karlsruhe 1999, (Ed.) Dt. Atomforum e.V. INFORUM Verl., Bonn 1999, 561-564.

114. *Häse, M., M. Hirsch and H.-J. Hartfuß:* Temperature Fluctuations and their Correlation with Density Fluctuations in W7-AS. Review of Scientific Instruments **70**, 1014-1017 (1999).

115. *Hashimoto*, M., S.T. Nakagawa*, S. Nakano*, H. Ogiso*, M. Iwaki* and W. Eckstein:* Theoretical Analysis of the Embedded Layer Formed by High-Energy Au Implantation into Si (I). In: Proc. Symp. 66th Annual Conf. of Japan Electro-Chemical Society, Ionic, Tokyo, 65-68 (1999).

116. *Heikkinen*, J.A., T.P. Kiviniemi*, A.G. Peeters, T. Kurki-Suonio* and S.K. Sipilä*:* L-H Transport Barrier Formation: Neoclassical Simulation and Comparison with Tokamak Experiments. In: Proc. 26th EPS Conf. on Control. Fusion and Plasma Phys., Maastricht 1999, (Eds.) B.Schweer, G.Van Oost, E.Vietzke. ECA 23J. Europ. Phys. Soc., Geneva 1999, 1645-1648.

117. *Herre, G., P. Grigull and R. Schneider:* B2-EIRENE Code Modelling of an Island Divertor. Journal of Nuclear Materials **266-269**, 1015-1019 (1999).

118. *Herrmann, A., J.C. Fuchs, V. Rohde, M. Laux, K.-F. Mast and ASDEX Upgrade Team:* Heat Flux and Radiation Losses for Different Divertor Geometries in ASDEX Upgrade. In: Proc. 26th EPS Conf. on Control. Fusion and Plasma Phys., Maastricht 1999, (Eds.) B.Schweer, G.Van Oost, E.Vietzke. ECA 23J. Europ. Phys. Soc., Geneva 1999, 1505-1508.

119. *Herrmann, A., J.C. Fuchs, V. Rohde, M. Weinlich and ASDEX Upgrade Team:* Heat Flux Distribution in the Divertor-II of ASDEX Upgrade. Journal of Nuclear Materials **266-269**, 291-295 (1999).

120. *Heyn*, M.F., S.V. Kasilov*, W. Kernbichler*, H. Maaßberg, M. Romé*, U. Gasparino and N. Marushchenko*:* Nonlinear Absorption of 2nd Harmonic X-Mode ECRH at W7-AS Stellarator. In: Proc. 26th EPS Conf. Control. Fusion and Plasma Phys., Maastricht 1999, (Eds.) B.Schweer, G.Van Oost, E.Vietzke. ECA 23J. Europ. Phys. Soc., Geneva 1999, 1625-1628.

121. *Hildebrandt, D., M. Akbi, B. Jüttner and W. Schneider:* Deuterium Trapping in Divertor Tiles of ASDEX-Upgrade. Journal of Nuclear Materials **266-269**, 532-537 (1999).

122. *Hildebrandt, D., M. Akbi, B. Jüttner and W. Schneider:* Influence of Surface Roughness on the Deuterium Inventory of ASDEX-Upgrade Divertor Tiles. In: Proc. 4th Int. Workshop Tritium Effects in Plasma Facing Components, Santa Fé,NM, (Ed.) R.A.Causey. Livermore 1999, SAND99-8222, 35-36.

123. *Hildebrandt, D., H. Grote, W. Schneider, P. Wienhold* and J. von Seggern*:* Observation of Non-Uniform Erosion and Deposition Phenomena on Graphite after Plasma Exposure. Physica Scripta **T81**, 25-30, 1999.

124. *Hillis*, D.L., L. Hogan*, M. von Hellermann*, J. Ehrenberg*, L.D. Horton*, R. König, P. Morgan*, G. Saibene* and M.R. Wade*:* Noble Gas Impurity Balance and Exhaust Model for DIII-D and JET. Journal of Nuclear Materials **266-269**, 1084-1090 (1999).

125. *Hirsch, M., E. Holzhauer* and B. Kurzan:* Doppler Reflectometry for the Investigation of Poloidally Propagating Density Perturbations. In: Contributions 4th Reflectometry Workshop, Cadarache 1999, (Ed.) F.Clairet. EUR-CEA-FC-1674. CEA, Cadarache 1999, ohne Pag.

126. *Hirsch, M., M. Kick, H. Maaßberg, U. Stroth and W7-AS Team:* Bifurcations of Neoclassical and Turbulent Transport in W7-AS. Stellarator News **61**, 16-19 (1999), http://www.ornl.gov/fed/stelnews.

127. *Hopf, C., K. Letourneur*, W. Jacob, T. Schwarz-Selinger and A. von Keudell:* Surface Loss Probabilities of the Dominant Neutral Precursors for Film Growth in Methane and Acetylene Discharges. Applied Physics Letters **74**, 3800-3802 (1999).

128. *Horton*, L.D., J.P. Christiansen*, J. Lingertat*, C.F. Maggi*, V. Mertens, O. Pogutse*, G. Saibene*, R. Sartori*, J. Stober, W. Suttrop, JET Team* and ASDEX Upgrade Team:* Performance near Operational Boundaries. Plasma Physics and Controlled Fusion **41**, B329-B341 (1999).

129. *Itoh. S.-I. and K. Itoh:* Statistical Theory of Subcritically-Excited Strong Turbulence in Inhomogeneous Plasmas I. Journal of the Physical Society of Japan **68**, 1891-1905 (1999).

130. *Itoh, S.-I. and K. Itoh:* Statistical Theory of Subcritically-Excited Strong Turbulence in Inhomogeneous Plasmas II. Journal of the Physical Society of Japan **68**, 2611-2625 (1999).

131. *Jacob, W., B. Landkammer and C.H. Wu*:* Removal of Codeposited Layers by ECR Discharge Cleaning. Journal of Nuclear Materials **266-269**, 552-556 (1999).

132. *Jaksic, N. and J. Simon-Weidner:* Nonlinear Global-Local Finite Element Analysis of a Future Plasma Fusion Experiment. Computers and Structures **72**, 209-231 (1999).

133. *Jandl, O. and E. Harmeyer:* Structural Analysis of Stellarator Fusion Reactor Coils. In: Proc. 15th Int. Conf. on Computational Mechanics '99, Nectiny 1999, 133-140.

134. *Janeschitz*, G., G.W. Pacher*, Yu. Igitkhanov*, H.D. Pacher*, S.D. Pinches, O. Pogutse* and M. Sugihara*:* L-H Transition in Tokamak Plasmas: 1.5-D Simulations. Journal of Nuclear Materials **266-269**, 843-849 (1999).

135. *Jenko, F.:* (3+2)D Vlasov Simulation of Electron Drift Turbulence. In: Proc. 26th EPS Conf. on Control. Fusion and Plasma Phys., Maastricht 1999, (Eds.) B.Schweer, G.Van Oost, E.Vietzke. ECA 23J. Europ. Phys. Soc., Geneva 1999, 1417-1420.

136. *Jenko, F. and B.D. Scott:* Numerical Computation of Collisionless Drift Alfvén Turbulence. Physics of Plasmas **6**, 2705-2713 (1999).

137. *Jenko, F. and B.D. Scott:* Numerical Computation of Collisionless Drift Wave Turbulence. Physics of Plasmas **6**, 2418-2424 (1999).

138. *Jüttner B.:* Instabilities of Prebreakdown Currents in Vacuum II: The Nature of the Emission Sites. Journal of Physics D **32**, 2544-2551 (1999).

139. *Jüttner, B.:* Nanosecond Displacement Times of Arc Cathode Spots in Vacuum. IEEE Transactions on Plasma Science **27,** 836-844 (1999).

140. *Jüttner B., M. Lindmayer* and G. Düning*:* Instabilities of Prebreakdown Currents in Vacuum I: Late Breakdowns. Journal of Physics D **32**, 2537-2543 (1999).

141. *Kallenbach, A., A. Bard, A. Carlson, R. Dux and ASDEX Upgrade Team:* Chemical Erosion of Carbon in the Divertor of ASDEX Upgrade. Physica Scripta **T81**, 43-47 (1999).

142. *Kallenbach, A., A. Bard, D.P. Coster, R. Dux, J.C. Fuchs, J. Gafert, A. Herrmann, R. Schneider and ASDEX Upgrade Team:* New Results on Carbon Release and Transport in ASDEX Upgrade. Journal of Nuclear Materials **266-269**, 343-347 (1999).

143. *Kallenbach, A., D.P. Coster, J.C. Fuchs, H.Y. Guo*, G. Haas, A. Herrmann, L.D. Horton, L.C. Ingesson*, C.F. Maggi*, G.F. Matthews*, R. Monk, J. Neuhauser, F. Ryter, J. Schweinzer, J. Stober, W. Suttrop, ASDEX Upgrade Team and JET Team*:* Closed Divertor Operation in ASDEX Upgrade and JET. Plasma Physics and Controlled Fusion **41**, B177-B189 (1999).

144. *Kallenbach, A., M. Kaufmann, D.P. Coster, J.C. Fuchs, A. Herrmann, J. Neuhauser, R. Schneider, K. Borrass, H.-S. Bosch, A. Carlson, J. Gafert, K. Lackner, K. Schmidtmann, J. Schweinzer, W. Suttrop, U. Wenzel and ASDEX Upgrade Team:* Scrape-off Layer Radiation and Heat Load to the ASDEX Upgrade LYRA Divertor. Nuclear Fusion **39**, 901-917 (1999).

145. *Kammler*, Th. and J. Küppers:* Interaction of H Atoms with Cu (111) Surfaces: Adsorption, Absorption, and Abstraction. Journal of Chemical Physics **111**, 8115-8123 (1999).

146. *Kappel*, M. and J. Küppers:* Ripening of Subsurface Amorphous C Clusters Formed by Low Energy He Ion Bombardment of Graphite. Surface Science **440**, 387-397 (1999).

147. *Kardaun, O.J.W.F.:* Interval Estimation of Global {H-Mode} Energy Confinement in ITER. Plasma Physics and Controlled Fusion **41**, 429-469 (1999).

148. *Kazunori*, M., W. Jacob and J. Roth:* Erosion Behavior of Soft, Amorphous Deuterated Carbon Films by Heat in Air and under Vacuum. Journal of Nuclear Materials **264**, 56-70 (1999).

149. *Kendl, A. and H. Wobig:* Geometric Effects on Drift Wave Stability in Advanced Stellarators. Physics of Plasmas **6**, 4714-4721 (1999).

150. *Keudell, A. von and J.R. Abelson*:* Direct Insertion of $SiH_3$ Radicals into Strained Si-Si Surface Bonds during Plasma Deposition of Hydrogenated Amorphous Silicon Films. Physical Review B **59**, 5791-5798 (1999).

151. *Keudell, A. von and J.R. Abelson*:* Thermally Induced Changes in the Hydrogen Microstructure of a-Si:H. Japanese Journal of Applied Physics **38**, 4002-4006 (1999).

152. *Keudell, A. von, C. Hopf, T. Schwarz-Selinger and W. Jacob:* Surface Loss Probabilities of Hydrocarbon Radicals on Amorphous Hydrogenated Carbon Film Surfaces: Consequences for the Formation of Re-Deposited Layers in Fusion Experiments. Nuclear Fusion **39**, 1451-1462 (1999).

153. *Kick, M., H. Maaßberg, M. Anton, J. Baldzuhn, M. Endler, C. Görner, M. Hirsch, A. Weller, S. Zoletnik* and W7-AS Team:* Electric Field and Transport in W7-AS. Plasma Physics and Controlled Fusion **41**, A549-A559 (1999).

154. *weggefallen*

155. *Kocsis*, G., J.S. Bakos*, R. Burhenn, B. Kardon*, S. Kalvin*, L. Ledl*, G. Mank*, G. Petravich*, A. Pospieszczyk* and S. Zoletnik*:* On the Fluctuation of Line Radiation Emitted during Aluminium Micro-Pellet Ablation in Magnetized Plasmas. Plasma Physics and Controlled Fusion **41**, 881-898 (1999).

156. *Kohl, A., E. Taglauer and H. Knözinger*:* Morphology and Surface Reactions of $Rh/VO_x/SiO_2$ Model Catalysts. Physica Status Solidi **173**, 85-91 (1999).

157. *Koponen*, J.P.T., T. Geist, H.-J. Hartfuß, H. Laqua, U. Stroth, C. Wendland, E. Würsching, ECRH Group and W7-AS Team:* Evidence for Convective Inward Particle Transport in W7-AS. In: Proc. 26th EPS Conf. Control. Fusion and Plasma Phys., Maastricht 1999, (Eds.) B.Schweer, G.Van Oost, E.Vietzke. ECA 23J. Europ. Phys. Soc., Geneva 1999, 1641-1644.

158. *Kornejew, P., W. Bohmeyer and H.-D. Reiner:* Measurements of Chemical Erosion in the Plasmagenerator PSI-1. Physica Scripta **T81**, 40-42 (1999).

159. *Krieger, K., H. Maier, D. Grambole*, D. Schleußner, P. Franzen and ASDEX Upgrade Team:* Hydrogen Isotope Inventories in Plasma Facing Components of ASDEX Upgrade. In: Proc. of the 17th IAEA Fusion Energy Conference, Yokohama 1998, IAEA, Vienna 1999, 1317-1320.

160. *Krieger, K., H. Maier, R. Neu and ASDEX Upgrade Team:* Conclusions about the Use of Tungsten in the Divertor of ASDEX Upgrade. Journal of Nuclear Materials **266-269**, 207-216 (1999).

161. *Krieger, K., U. von Toussaint and ASDEX Upgrade Team:* Direct Measurement of Carbon Erosion Rates in the Divertor of ASDEX Upgrade. In: Proc. 26th EPS Conf. Control. Fusion and Plasma Phys., Maastricht 1999, (Eds.) B.Schweer, G.Van Oost, E.Vietzke. ECA 23J. Europ. Phys. Soc., Geneva 1999, 1529-1532.

162. *Kukushkin*, A.S., H.D. Pacher*, G. Janeschitz*, D.P. Coster, D. Reiter* and R. Schneider:* Divertor Performance in Reduced-Technical-Objective/Reduced-Cost ITER. In: Proc. 26th EPS Conf. Control. Fusion and Plasma Phys., Maastricht 1999, (Eds.) B.Schweer, G.Van Oost, E.Vietzke. ECA 23J. Europ. Phys. Soc., Geneva 1999, 1545-1548.

163. *Kumazawa*, R., T. Mutoh*, T. Seki*, K. Saito*, F. Shimpo*, G. Nomura*, T. Ido*, T. Watari*, G. Cattanei and Y. Zhao*:* A Liquid Impedance Matching System for Ion Cyclotron Heating. In: Proc. 13th Top. Conf. on Radio Frequency Power in Plasmas, Annapolis,MD 1999, (Eds.) S.Bernabei, F.Paoletti. AIP Conf. Proc. 485, AIP Press, Melville,NY 1999, 441-444.

164. *Kumazawa*, R., T. Mutoh*, T. Seki*, F. Shimpo*, G. Nomura*, T. Ido*, T. Watari*, J.-M. Noterdaeme and Y. Zhao*:* Liquid Stub Tuner for Ion Cyclotron Heating. Review of Scientific Instruments **70**, 2665-2673 (1999).

165. *Kumazawa*, R., T. Mutoh*, T. Seki*, F. Shimpo*, G. Nomura*, T. Ido*, T. Watari*, J.-M. Noterdaeme and Y. Zhao*:* Steady State Test at High RF Voltage on Transmission System for Ion Cyclotron Heating. Journal of Plasma and Fusion Research **75**, 842-853 (1999).

166. *Küstner*, M., W. Eckstein, E. Hechtl* and J. Roth:* Angular Dependence of the Sputtering Yield of Rough Beryllium Surfaces. Journal of Nuclear Materials **265**, 22-27 (1999).

167. *Lalousis*, P., R. Schneider and L.L. Lengyel: E x B* Type Drifts in Vapour Layers Evolving over Vaporizing Surfaces Subjected to Hot Plasmas. In: Proc. 26th EPS Conf. Control. Fusion and Plasma Phys., Maastricht 1999, (Eds.) B.Schweer, G.Van Oost, E.Vietzke. ECA 23J. Europ. Phys. Soc., Geneva 1999, 1261-1264.

168. *Landkammer, B., A. von Keudell and W. Jacob:* Erosion of Thin Hydrogenated Carbon Films in Oxygen, Oxygen/Hydrogen and Water Plasmas. Journal of Nuclear Materials **264**, 48-55 (1999).

169. *Lang, P.T., J. Gafert, O. Gruber, M. Kaufmann, A. Lorenz, M. Maraschek, V. Mertens, J. Neuhauser, H. Salzmann and ASDEX Upgrade Team:* Accessibility of High Density H-Mode Operation by HFS Pellet Refuelling. In: Proc. 26th EPS Conf. on Control. Fusion and Plasma Phys., Maastricht 1999, (Eds.) B.Schweer, G.Van Oost, E.Vietzke. ECA 23J. Europ. Phys. Soc., Geneva 1999, 1389-1392.

170. *Laqua, H.P., V. Erckmann, H. Maaßberg, W7-AS Team and ECRH Group:* Advanced High Power ECRH Launch Scenarios at the W7-AS Stellarator. In: Proc. 26th EPS Conf. Control. Fusion and Plasma Phys., Maastricht 1999, (Eds.) B.Schweer, G.Van Oost, E.Vietzke. ECA 23J. Europ. Phys. Soc., Geneva 1999, 1573-1576.

171. *Laqua, H.P., W7-AS Team and ECRH Group:* Electron Bernstein Wave Heating and Emission via the OXB Process at W7-AS. Plasma Physics and Controlled Fusion **41**, A273-A284 (1999).

172. *Laqua, H.P., W7-AS Team and ECRH Group:* Electron Bernstein Wave Heating and Emission via the OXB Process on W7-AS. Stellarator News **61**, 25-30 (1999), http://www.ornl.gov/fed/stelnews.

173. *Lederer, H.:* Höchstleistungsrechnen für die Grundlagenforschung in der Max-Planck-Gesellschaft. In: HPSC 99, Bonn 1999, Höchstleistungsrechnen in der Bundesrepublik Deutschland, (Eds.) R.Krahl, G.Wolf. Projektträger des BMBF für Informationstechnik, DLR, Berlin 1999, 9-12.

174. *Ledl*, L., R. Burhenn, V.Yu. Sergeev*, S. Egorov*, B.V. Kuteev*, L.L. Lengyel, S. Skokov*, F. Wagner, W7-AS Team, ECRH Group and NBI Group:* Carbon Pellet Injection Experiments at the Stellarator W7-AS. In: Proc. 26th EPS Conf. Control. Fusion and Plasma Phys., Maastricht 1999, (Eds.) B.Schweer, G.Van Oost, E.Vietzke. ECA 23J. Europ. Phys. Soc., Geneva 1999, 1477-1480.

175. *Lengyel, L.L, K. Büchl, G. Pautasso, L. Ledl*, A. Ushakov*, S. Kalvin* and G. Veres*:* Modelling of Impurity Pellet Ablation in ASDEX Upgrade (Neon) and Wendelstein W7-AS (Carbon) by Means of a Radiative ('Killer') Pellet Code. Nuclear Fusion **39**, 791-813 (1999).

176. *Leonard*, A.W., A. Herrmann, K. Itami*, J. Lingertat*, A. Loarte*, T.H. Osborne*, W. Suttrop, ITER Divertor Modeling and Database Expert Group* and ITER Divertor Physics Expert Group*:* The Impact of ELMs on the ITER Divertor. Journal of Nuclear Materials **266-269**, 109-117 (1999).

177. *Leuterer, F., S. Günter, R. Wolf, M. Beckmann, O. Gruber, K. Lackner, M. Maraschek, P. McCarthy, H. Meister, G. Pereverzev, H. Salzmann, J. Schweinzer, W. Suttrop and ASDEX Upgrade Team:* Simultaneous Attainment of High Electron and Ion Temperatures in ITB-Discharges with ECCD on ASDEX Upgrade. In: Proc. 26th EPS Conf. Control. Fusion and Plasma Phys., Maastricht 1999, (Eds.) B.Schweer, G.Van Oost, E.Vietzke. ECA 23J. Europ. Phys. Soc., Geneva 1999, 1821-1824.

178. *Linden*, W. von der, V. Dose, R. Fischer and R. Preuss (Eds.):* Maximum Entropy and Bayesian Methods. Kluwer Acad. Publ., Dordrecht 1999, 360 S.

179. *Linden*, W. von der, V. Dose, J. Padayachee* and V. Prozesky*:* Signal and Background Separation. Physical Review E **59**, 6527-6534 (1999).

180. *Linden*, W. von der, R. Preuss and V. Dose:* The Prior Predictive Value. In: Maximum Entropy and Bayesian Methods, (Eds.) W.v.d.Linden, V.Dose, R.Fischer, R.Preuss. Kluwer Acad. Publ., Dordrecht 1999, 319-326.

181. *Lingertat*, J., K. Borrass, G.D. Conway*, M. Gould*, K. Günther*, L.D. Horton, G.F. Matthews*, V. Parail* and G. Saibene*:* Characterisation of ELM Triggered Edge Pressure Cycles in JET. In: Proc. 26th EPS Conf. on Control. Fusion and Plasma Phys., Maastricht 1999, (Eds.) B.Schweer, G.Van Oost, E.Vietzke. ECA 23J. Europ. Phys. Soc., Geneva 1999, 261-264.

182. *Loarte*, A., H.-S. Bosch, A.V. Chankin*, S. Clement*, A. Herrmann, D. Hill*, K. Itami*, J. Lingertat*, B. Lipschultz*, K. McCormick, R. Monk, G. Porter*, M. Shimada* and M. Sugihara*:* Multi-Machine Scaling of the Divertor Peak Heat Flux and Width for L-Mode and H-Mode Discharges. Journal of Nuclear Materials **266-269**, 587-592 (1999).

183. *Loarte*, A., A.S. Kukushkin*, H.D. Pacher*, D.P. Coster, R. Schneider, N. Asakura*, K. Itami*, B. LaBombard*, B. Lipschultz*, C.F. Maggi*, R. Monk, G. Porter*, M. Shimada*, M. Sugihara* and J. Terry*:* Comparison of B2-EIRENE Calculations with Multi-Machine Experimental Measurements. Journal of Nuclear Materials **266-269**, 1123-1128 (1999).

184. *Logatchev*, A.A., V.P. Afanasev*, S.M. Shkolnik*, H. Pursch and B. Jüttner:* The Behavior of Vacuum Arc Discharges on Hydrogen Impregnated Electrodes. IEEE Transactions on Plasma Science **27**, 894-900 (1999).

185. *Maaßberg, H., C.D. Beidler and E.E. Simmet:* Density Control Problems in Large Stellarators with Neoclassical Transport. Plasma Physics and Controlled Fusion **41**, 1135-1153 (1999).

186. *Maggi*, C.F., G.D. Conway*, G. Corrigan*, N.C. Hawkes*, L.D. Horton, R. Monk, G. Saibene*, J. Spence* and M. von Hellermann*:* Effect of $D_2$ Fuelling Location in JET MkII GAs Box Divertor Discharges. In: Proc. 26th EPS Conf. on Control. Fusion and Plasma Phys., Maastricht 1999, (Eds.) B.Schweer, G.Van Oost, E.Vietzke. ECA 23J. Europ. Phys. Soc., Geneva 1999, 201-204.

187. *Maggi*, C.F., R. Monk, L.D. Horton, K. Borrass, G. Corrigan*, L.C. Ingesson*, R. König, G. Saibene*, R.J. Smith*, M.F. Stamp*, A. Taroni* and M. von Hellermann*:* The Isotope Effect on the L Mode Density Limit in JET Hydrogen, Deuterium and Tritium Divertor Plasmas. Nuclear Fusion **39**, 979-991 (1999).

188. *Maier, H., K. Krieger, M. Balden, J. Roth and ASDEX Upgrade Team:* Erosion and Deposition in the ASDEX Upgrade Tungsten Divertor Experiment. Journal of Nuclear Materials **266-269**, 1003-1008 (1999).

189. *Maier, H., K. Krieger, A. Tabasso, S. Lindig, V. Rohde, J. Roth and ASDEX Upgrade Team:* Deuterium Inventories in Different Divertor Configurations of ASDEX Upgrade. In: Proc. 26th EPS Conf. Control. Fusion and Plasma Phys., Maastricht 1999, (Eds.) B.Schweer, G.Van Oost, E.Vietzke. ECA 23J. Europ. Phys. Soc., Geneva 1999, 1509-1512 (1999).

190. *Maier J., M.-G. Pacco-Düchs, I. Precht, C. Tichmann and F. Hertweck:* Data Files and their Interdependences: a Data Base for the Tokamak Fusion Experiment ASDEX Upgrade. Fusion Engineering and Design **43**, 451-456 (1999).

191. *Manso*, M., F. Serra*, P. Varela*, J. Santos*, A. Silva*, S. Vergamota*, F. Silva*, I. Nunes*, R. Wolf, M. Maraschek, W. Suttrop and ASDEX Upgrade Team:* Study of the Interplay between the Core and Edge Regions in ITB Plasmas Using Microwave Reflectometry on ASDEX Upgrade. In: Proc. 26th EPS Conf. on Control. Fusion and Plasma Phys., Maastricht 1999, (Eds.) B.Schweer, G.Van Oost, E.Vietzke. ECA 23J. Europ. Phys. Soc., Geneva 1999, 41-44.

192. *Mantsinen*, M., L.-G. Eriksson*, V.P. Bathnagar*, G. Cottrell*, A. Gondhalekar*, C. Gormezano*, R. König, P. Lomas*, E. Righi*, F.G. Rimini*, A.C.C. Sips*, D.F.H. Start*, F.X. Söldner*, D. Testa*, B. Tubbing* and K.-D. Zastrow*:* Analysis of Bulk Ion Heating with ICRH in JET High-Performance Plasmas. Plasma Physics and Controlled Fusion **41**, 843-865 (1999).

193. *Maraschek, M., S. Günter, R. Wolf and ASDEX Upgrade Team:* Neoclassical Tearing Modes in Advanced Scenarios in ASDEX Upgrade. In: Proc. 26th EPS Conf. on Control. Fusion and Plasma Phys., Maastricht 1999, (Eds.) B.Schweer, G.Van Oost, E.Vietzke. ECA 23J. Europ. Phys. Soc., Geneva 1999, 1393-1396.

194. *Maraschek, M., S. Günter, H. Zohm and ASDEX Upgrade Team:* Collisionality Dependence of the Neoclassical Tearing Mode in ASDEX Upgrade. Plasma Physics and Controlled Fusion **41**, L1-L8 (1999).

195. *Marushchenko*, N., V. Erckmann, U. Gasparino, S. Kasilov*, H. Maaßberg, S. Murakami* and W7-AS Team:* W7-AS: Suprathermal Effects Driven by High Power ECRH. Problems of Atomic Science and Technology. Series: Plasma Physics, Issues **1**(1), **2**(2), 57-59 (1999).

196. *Maruyama*, K., W. Jacob and J. Roth:* Erosion Behavior of Soft Amorphous, Deuterated Carbon Films by Heat Treatment in Air and under Vacuum. Journal of Nuclear Materials **264**, 56-70 (1999).

197. *Mayer, M.:* SIMNRA, a Simulation Program for the Analysis of NRA, RBS and ERDA. In: Proc. 15th Int. Conf. on Application of Accelerators in Research and Industry, Denton,TX 1998, (Eds.) J.L.Duggan, I.L.Morgan. AIP Press, Melville,NY 1999, 541-544.

198. *Mayer, M., R. Behrisch, P. Andrew*, J.P. Coad* and A.T. Peacock*:* Transport and Redeposition of Eroded Material in JET. Physica Scripta **T81**, 13-18 (1999).

199. *Mayer, M., R. Behrisch, K. Plamann, P. Andrew*, J.P. Coad* and A.T. Peacock*:* Wall Erosion and Material Transport to the Mark I Carbon Divertor of JET. Journal of Nuclear Materials **266-269**, 604-610 (1999).

200. *McCormick, K., N. Asakura*, H.-S. Bosch, S. Davies*, S. Fielding*, K. Itami*, H. Kawashima*, B. LaBombard*, B. Lipschultz*, A. Loarte*, R. Monk, G. Porter*, J. Schweinzer, M. Shimada* and M. Sugihara*:* ITER Edge Database Investigations of the SOL Width. Journal of Nuclear Materials **266-269**, 99-108 (1999).

201. *McCormick, K., P. Grigull, J. Baldzuhn, Y. Feng, S. Fiedler, L. Giannone, H.-J. Hartfuß, A. Herrmann, D. Hildebrandt, M. Hirsch, J. Kisslinger, J.P. Knauer, G. Kühner, R. König, D. Naujoks, F.-P. Penningsfeld, J. Sallander, F. Sardei, H. Wobig and W7-AS Team:* Core-Edge Studies with Boundary Island Configurations on the W7-AS Stellarator. Plasma Physics and Controlled Fusion **41**, B285-B304 (1999).

202. *Mertens, V., K. Borrass, J. Gafert, M. Kaufmann, M. Laux, H. Murmann, J. Neuhauser, H. Salzmann, J. Schweinzer and ASDEX Upgrade Team:* Scalings of Density Characteristics near the Greenwald Limit in ASDEX Upgrade H-Mode Discharges. In: Proc. 26th EPS Conf. on Control. Fusion and Plasma Phys., Maastricht 1999, (Eds.) B.Schweer, G.Van Oost, E.Vietzke. ECA 23J. Europ. Phys. Soc., Geneva 1999, 1397-1400.

203. *Meyer-Spasche, R. (Ed.):* Pattern Formation in Viscous Flows. Birkhäuser Verl., Boston 1999, 224 S.

204. *Michel, G. and M. Thumm*:* Spectral Domain Techniques for Field Pattern Analysis and Synthesis. Surveys on Mathematics for Industry **8**, 259-270 (1999).

205. *Milch, I.:* Fusionsbrennstoff warm eingepackt. HGF-Jahresheft 2000, 42-43 (1999).

206. *Mousel*, T., W. Eckstein and H. Gnaser*:* Energy Spectra of Sputtered Species under Sub-keV Ion Bombardment: Experiments and Computer Simulations. Nuclear Instruments and Methods in Physics Research B **152**, 36-48 (1999).

207. *Müller, H.W., K. Büchl, M. Kaufmann, P.T. Lang, R.S. Lang, A. Lorenz, M. Maraschek, V. Mertens, J. Neuhauser and ASDEX Upgrade Team:* High-β Plasmoid Drift during Pellet Injection into Tokamaks. Physical Review Letters **83**, 2199-2202 (1999).

208. *Müller, H.W., K. Büchl, M. Kaufmann, P.T. Lang, R.S. Lang, A. Lorenz, V. Mertens, J. Neuhauser and ASDEX Upgrade Team:* High-β Plasmoid Drift during Pellet Injection into Tokamaks. In: Proc. 26th EPS Conf. on Control. Fusion and Plasma Phys., Maastricht 1999, (Eds.) B.Schweer, G.Van Oost, E.Vietzke. ECA 23J. Europ. Phys. Soc., Geneva 1999, 109-112.

209. *Murakami*, S., U. Gasparino, H. Maaßberg, N. Marushchenko*, N. Nakajima*, M. Romé* and M. Okamoto*:* 5D Phase Space Monte-Carlo Simulation of ECRH-Driven Transport of Suprathermal Electrons in Stellarators in Theory of Fusion Plasmas. In: Proc. Joint Varenna-Lausanne Int. Workshop, Varenna 1998, Ed. Compositori, Bologna 1999, 171-184.

210. *Murakami*, S., N. Nakajima*, M. Okamoto* and J. Nührenberg:* Effect of Energetic Ion Loss on ICRF Heating Effeciency and Energy Confinement Time in Heliotrons. Nuclear Fusion **39**, 1165-1173 (1999).

211. *Mutoh*, T., R. Kumazawa*, T. Seki*, F. Shimpo*, G. Nomura*, T. Ido*, T. Watari*, J.-M. Noterdaeme and Y. Zhao*:* Steady State Tests of High Voltage Ceramic Feedthroughs and Co-Axial Transmission Line of ICRF Heating System for the Large Helical Device. Fusion Technology **35**, 297-376 (1999).

212. *Nakagawa*, S.T., S. Nakano*, H. Ogiso*, M. Iwaki*, M. Hashimoto* and W. Eckstein:* Theoretical Analysis of the Embedded Layer Formed by High-Energy Au Implantation into Si (III). In: Proc. 2nd Symp. Accelerator and Related Technology for Application, Tokyo 1999, 73-76.

213. *Naujoks, D., D.P. Coster, H. Kastelewicz and R. Schneider:* Transport of Hydrocarbon Molecules in the Edge Plasma of Fusion Experiments. Journal of Nuclear Materials **266-269**, 360-364 (1999).

214. *Neu, R., F. Ryter, M. Beckmann, R. Brückner, B. Brüsehaber, R. Dux, H.-U. Fahrbach, J.E. Kinsey*, F. Leuterer, G. Pereverzev, J. Schweinzer, J. Stober, W. Suttrop and ASDEX Upgrade Team:* Cold Pulses and Heat Pulses at ASDEX Upgrade. In: Proc. 26th EPS Conf. Control. Fusion and Plasma Phys., Maastricht 1999, (Eds.) B.Schweer, G.van Ost, E.Vietzke. ECA 23J. Europ. Phys. Soc., Geneva 1999, 1413-1416.

215. *Neuhauser, J., D.P. Coster, V. Dose, J.W. Kim, B. Kurzan, H. Murmann, H. Salzmann, R. Schneider, W. Schneider, J. Schweinzer, R. Wunderlich and ASDEX Upgrade Team:* Analysis of High-Resolution ASDEX Upgrade Edge Plasma Profiles. In: Proc. 26th EPS Conf. Control. Fusion and Plasma Phys., Maastricht 1999, (Eds.) B.Schweer, G.Van Oost, E.Vietzke. ECA 23J. Europ. Phys. Soc., Geneva 1999, 1521-1524.

216. *Noterdaeme, J.-M.:* Ion Cyclotron Resonance Frequency Heating on ASDEX Upgrade: an Overview. Problems of Atomic Science and Technology. Series: Plasma Physics, Issues **1**(1), **2**(2), 65-69 (1999).

217. *Noterdaeme, J.-M., M. Brambilla, B. Brüsehaber, R. Dux, H.-U. Fahrbach, ICRF Group and ASDEX Upgrade Team:* ELMs and Sawteeth with ICRF Heating on ASDEX Upgrade. In: Proc. 13th Top. Conf. Radio Frequency Power in Plasmas, Annapolis,MD 1999, (Eds.) S.Bernabei, F.Paoletti. AIP Conf. Proc. 355, AIP Press, Melville,NY 1999, 92-99.

218. *Noterdaeme, J.-M., M. Brambilla, B. Brüsehaber, H.-U. Fahrbach, ICRF Group and ASDEX Upgrade Team:* $^3$He in H, Ion Cyclotron Resonance Frequency Mode Conversion and Minority Heating Experiments in ASDEX Upgrade. In: Proc. 26th EPS Conf. Control. Fusion and Plasma Phys., Maastricht 1999, (Eds.) B.Schweer, G.Van Oost, E.Vietzke. ECA 23J. Europ. Phys. Soc., Geneva 1999, 1561-1564.

219. *Nöthe*, M., A. Buuron*, F. Koch, H.J. Penkalla*, W.P. Rehbach* and H. Bolt:* Characterization of the a-C:H Films with Metal Interlayers and Mixed Interfaces. Surface and Coatings Technology **116-119**, 335-341 (1999).

220. *Nöthe*, M., A. Buuron*, F. Koch, H.J. Penkalla*, W.P. Rehbach* and H. Bolt:* Investigation of the Properties of a-C:H Coatings with Graded Metal Interlayers. Fresenius Journal of Analytical Chemistry **365**, 249-254 (1999).

221. *Nührenberg, C.:* Compressional Ideal Magnetohydrodynamics: Unstable Global Modes, Stable Spectra, and Alfvén Eigenmodes in Wendelstein 7-X Type Equilibria. Physics of Plasmas **6,** 137-147 (1999).

222. *Nührenberg, C.:* Computational Ideal MHD: Alfvén, Sound and Fast Global Modes in W7-AS. Plasma Physics and Controlled Fusion **41**, 1055-1070 (1999).

223. *Nührenberg, C., J. Geiger, C. Goerner and A. Weller:* Computational Study of Alfvén Eigenmodes in W7-AS. In: Theory of Fusion Plasmas, (Eds.) J.W.Connor, E.Sindoni, J.Vaclavik. Ed. Compositori, Bologna 1999, 409-418.

224. *Nührenberg, C., J. Geiger, C. Görner and A. Weller:* Computational Study of Toroidal Alfvén Eigenmodes in W7-AS. Stellarator News **61**, 30-32 (1999), http://www.ornl.gov/fed/stelnews.

225. *Nührenberg, J.:* Quasisymmetries in Toroidal Confinement. Stellarator News **61**, 36-38 (1999), http://www.ornl.gov/fed/stelnews.

226. *Nunes*, L., M. Manso*, P. Varela*, F. Serra*, A. Silva*, F. Silva*, J. Schweinzer, R. Brandenburg, F. Aumayr* and H.P. Winter*:* Density Measurements with Combined Li-Beam Diagnostics and Microwave Reflectometry during Advanced Tokamak Operation on ASDEX Upgrade. In: Proc. 26th EPS Conf. Control. Fusion and Plasma Phys., Maastricht 1999, (Eds.) B.Schweer, G.Van Oost, E.Vietzke. ECA 23J. Europ. Phys. Soc., Geneva 1999, 1633-1636.

227. *Ott, W., C. Fuchs, L. Giannone, J.P.T. Koponen*, F.-P. Penningsfeld, E. Speth, NI Group and NI Team(W7-AS):* Neutral-Beam Deposition Profiles in the W7-AS Stellarator. In: Proc. 26th EPS Conf. Control. Fusion and Plasma Phys., Maastricht 1999, (Eds.) B.Schweer, G.Van Oost, E.Vietzke. ECA 23J. Europ. Phys. Soc., Geneva 1999, 1565-1568.

228. *Pacher*, H.D., A.S. Kukushkin*, D.P. Coster, A. Loarte*, G. Janeschitz*, D. Reiter* and R. Schneider:* Operating Window for High Divertor Radiation in ITER. Journal of Nuclear Materials **266-269**, 1172-1179 (1999).

229. *Padayachee*, J., V. Prozesky*, W. von der Linden*, M.S. Nkwinika* and V. Dose:* Bayesian Pixe Background Subtraction. Nuclear Instruments and Methods in Physics Research B **150**, 129-135 (1999).

230. *Pereverzev, G., O. Gruber, H. Meister, J. Stober, R. Wolf and ASDEX Upgrade Team:* Simulation of ASDEX Upgrade Plasmas with Internal Transport Barrier. In: Proc. 26th EPS Conf. Control. Fusion and Plasma Phys., Maastricht 1999, (Eds.) B.Schweer, G.Van Oost, E.Vietzke. ECA 23J. Europ. Phys. Soc., Geneva 1999, 1429-1432.

231. *Philipps*, V., A. Huber*, H.G. Esser*, A. Pospieszczyk*, B. Schweer*, J. von Seggern*, W. Biel*, G. Mank* and R. Neu:* Operation of TEXTOR-94 with Siliconized Walls. In: Proc. 26th EPS Conf. Control. Fusion and Plasma Phys., Maastricht 1999, (Eds.) B.Schweer, G.van Ost, E.Vietzke. ECA 23J. Europ. Phys. Soc., Geneva 1999, 713-716.

232. *Pichlmeier*, J. and R. Dohmen:* Parallelization of the Full-Potential Plane Wave Code WIEN 97. In: Proc. 5th Europ. SGI/Cray MPP Workshop, Bologna 1999, http://www.cineca.it/mpp-workshop/abstract/rdohmen.htm.

233. *Pinkau, K.:* The ESA Science Programme - A View From Germany. In: Proc. Int. Symp. The History of the ESA, London 1998. ESA SP-436, 135-148 (1999).

234. *Pinkau, K.:* Forschung im freien Staat. In: Wie finden Innovationsprozesse statt? (Eds.) K.Pinkau, C.Stahlberg. Hirzel Verl., Stuttgart 1999, 43-53.

235. *Pinkau, K. and C. Stahlberg (Eds.):* Wie finden Innovationsprozesse statt? Zehn Jahre Karl Heinz Beckurts-Stiftung. Hirzel Verl., Stuttgart 1999, 64 S.

236. *Poli, E., A.G. Peeters, G. Pereverzev and M. Bornatici*:* Gaussian Wave Beam Tracing in Tokamak Plasmas. In: Proc. 26th EPS Conf. on Control. Fusion and Plasma Phys., Maastricht 1999, (Eds.) B.Schweer, G.Van Oost, E.Vietzke. ECA 23J. Europ. Phys. Soc., Geneva 1999, 1553-1556.

237. *Poli, E., G. Pereverzev and A.G. Peeters:* Paraxial Gaussian Wave Beam Propagation in an Anisotropic Inhomogeneous Plasma. Physics of Plasmas **6**, 5-11 (1999).

238. *Porter*, G., S. Davies*, B. LaBombard*, A. Loarte*, K. McCormick, R. Monk, M. Shimada* and M. Sugihara*:* Analysis of Separatrix Plasma Parameters Using Local and Multi-Machine Databases. Journal of Nuclear Materials **266-269**, 917-921 (1999).

239. *Preuss, R., V. Dose and W. von der Linden*:* Dimensionally Exact Form-Free Energy Confinement Scaling in W7-AS. Nuclear Fusion **39**, 849-862 (1999).

240. *Preuss R., V. Dose and W. von der Linden*:* Model Comparison in Plasma Energy Confinement Scaling. In: Maximum Entropy and Bayesian Methods, (Eds.) W.v.d.Linden, V.Dose, R.Fischer, R.Preuss. Kluwer Acad. Publ., Dordrecht 1999, 171-178.

241. *Puri, S.:* Anomalous Inward Particle Convection in Tokamaks. Plasma Physics and Controlled Fusion **41**, L35-L38 (1999).

242. *Raupp, G., K. Behler, R. Neu, W. Treutterer, D. Zasche, T. Zehetbauer and ASDEX Upgrade Team:* Experience from ASDEX Upgrade Discharge Control Management for Long Pulse Operation. Fusion Engineering and Design **43**, 383-391 (1999).

243. *Raupp, G., R. Cole*, K. Lüddecke*, G. Neu, W. Treutterer, D. Zasche, T. Zehetbauer and ASDEX Upgrade Team:* Next Generation Discharge Control System for ASDEX Upgrade. Fusion Engineering and Design **46**, 347-354 (1999).

244. *Redi*, M., C. Nührenberg, W.A. Cooper*, G.Y. Fu*, C. Kessel*, L.P. Ku*, D.A. Monticello*, A. Reiman* and M. Zarnstorff*:* Vertical and Kink Mode Stability Calculations for Current Carrying Quasiaxial Stellarators. In: Proc. 26th EPS Conf. Control. Fusion and Plasma Phys., Maastricht 1999, (Eds.) B.Schweer, G.Van Oost, E.Vietzke. ECA 23J. Europ. Phys. Soc., Geneva 1999, 1693-1696.

245. *Reiman*, A., G.Y. Fu*, S. Hirshman*, L.P. Ku*, D.A. Monticello*, H. Mynick*, M. Redi*, D. Spong*, M. Zarnstorff*, B. Blackwell*, A. Boozer*, W.A. Cooper*, M. Drevlak, R. Goldston*, J. Harris*, M. Isaev*, Z. Lin*, J.F. Lyon*, P. Merkel, M. Mikhailov*, W. Miner*, N. Nakajima*, G. Neilson*, C. Nührenberg, M. Okamoto*, N. Pomphrey*, W. Reiersen*, R. Sanchez*, J. Schmidt*, A. Subbotin*, P. Valanju*, K.Y. Watanabe* and R. White*:* Physics Design of a High-beta Quasi-Axisymmetric Stellarator. Plasma Physics and Controlled Fusion, **41**, B273-B283 (1999).

246. *Reuter, H.:* Hiding HSM Systems from the User. In: Proc. 16th IEEE Symp. on Mass Storage Systems, San Diego,CA 1999, IEEE Computer Soc. Press, Los Alamitos,CA 1999, 215-221.

247. *Rimini*, F.G., P. Andrew*, B. Balet*, J. Bull*, N. Deliyanakis*, H.P.L. De Esch*, L.-G. Eriksson*, C. Gormezano*, C.W. Gowers*, H.Y. Guo*, G.T.A. Huysmans*, T.T.C. Jones*, R. König, M. Lennholm*, P. Lomas*, A. Maas*, M. Mantsinen*, F.B. Marcus*, M. Nave*, V. Parail*, D.F.H. Start*, A. Taroni*, D. Testa* and P. Thomas*:* Combined Heating Experiments in ELM-Free H-Modes in JET. Nuclear Fusion **39**, 1591-1603 (1999).

248. *Rohde, V., R. Neu, R. Dux, T. Härtl, H. Maier, J. Luthin, H.G. Esser*, V. Philipps* and ASDEX Upgrade Team:* Comparison of Boronization and Siliconization in ASDEX Upgrade. In: Proc. 26th EPS Conf. on Control. Fusion and Plasma Phys., Maastricht 1999, (Eds.) B.Schweer, G.Van Oost, E.Vietzke. ECA 23J. Europ. Phys. Soc., Geneva 1999, 1513-1516.

249. *Roth, J.:* Chemical Erosion of Carbon Based Materials in Fusion Devices. Journal of Nuclear Materials **266-269**, 51-57 (1999).

250. *Rozhansky*, V., S. Voskoboynikov*, E. Kovaltsova*, D.P. Coster and R. Schneider:* Modeling of Self-Consistent Electric Fields in Tokamak Edge Plasma with B2.5 Code. In: Proc. 26th EPS Conf. Control. Fusion and Plasma Phys., Maastricht 1999, (Eds.) B.Schweer, G.Van Oost, E.Vietzke. ECA 23J. Europ. Phys. Soc., Geneva 1999, 1749-1752.

251. *Ryter, F., F. Leuterer, M. Beckmann, H. Brinkschulte, R. Brückner, B. Brüsehaber, H.-U. Fahrbach, H. Meister, M. Münich, G. Pereverzev, J. Stober, J. Schweinzer, W. Suttrop and ASDEX Upgrade Team:* Transport Studies with ECRH Power Modulation in ASDEX Upgrade. In: Proc. 26th EPS Conf. Control. Fusion and Plasma Phys., Maastricht 1999, (Eds.) B.Schweer, G.Van Oost, E.Vietzke. ECA 23J. Europ. Phys. Soc., Geneva 1999, 1433-1436.

252. *Saarelma*, S., S. Günter, T. Kurki-Suonio*, M. Maraschek, A. Turnbull* and H.-P. Zehrfeld:* Peeling Mode Stability Studies of ELMs in ASDEX Upgrade. In: Proc. 26th EPS Conf. on Control. Fusion and Plasma Phys., Maastricht 1999, (Eds.) B.Schweer, G.Van Oost, E.Vietzke. ECA 23J. Europ. Phys. Soc., Geneva 1999, 1637-1640.

253. *Saibene*, G., R. Budny*, A.V. Chankin*, G.D. Conway, J.G. Cordey*, K. Guenter*, N.C. Hawkes*, L.D. Horton, J. Lingertat*, C.F. Maggi*, M. Mantsinen*, R. Monk, V. Parail*, F.G. Rimini*, R. Sartori*, J.D. Strachan*, A. Taroni* and M. von Hellermann*:* Comparison of Core and Edge Characteristics of NB and ICRH ELMy H-Modes in JET. In: Proc. 26th EPS Conf. Control. Fusion and Plasma Phys., Maastricht 1999, (Eds.) B.Schweer, G.Van Oost, E.Vietzke. ECA 23J. Europ. Phys. Soc., Geneva 1999, 97-100.

254. *Salat, A. and J.A. Tataronis*:* Radial Dependence of Magnetohydrodynamic Continuum Modes in Axisymmetric Toroidal Geometry. Physics of Plasmas **6**, 3207-3216 (1999).

255. *Schimmel*, Th., Th. Koch*, J. Küppers and M. Lux-Steiner*:* True Atomic Resolution under Ambient Conditions Obtained by Atomic Force Microscopy in the Contact Mode. Applied Physics A **68**, 399-402 (1999).

256. *Schleußner, D., H. Maier, P. Franzen, R. Behrisch, M. Balden, ASDEX Upgrade Team, M. Perl*, W. Knapp* and C. Edelmann*:* Hydrogen Isotope Inventories in the ASDEX Upgrade Tungsten Coated Divertor Tiles. Journal of Nuclear Materials **266-269**, 1296-1302 (1999).

257. *Schleußner, D., D. Rösler*, J. Becker*, W. Knapp*, C. Edelmann*, C. Garcia-Rosales, P. Franzen and R. Behrisch:* Temperature Programmed Desorption from Graphite. Journal of Vacuum Science and Technology A **17**, 2785-2790 (1999).

258. *Schneider, F., F. Gresser and H. Eixenberger:* Zeit-optimaler Regler synchronisiert mit geschalteten Stellern. http://www.rzg.mpg.de/~fns, 7 S. (1999).

259. *Schneider, R., H.-S. Bosch, D.P. Coster, J.C. Fuchs, J. Gafert, G. Haas, A. Herrmann, M. Kaufmann, A. Kallenbach, J. Neuhauser, J. Schweinzer, U. Wenzel and ASDEX Upgrade Team:* Role of Divertor Geometry on Detachment in ASDEX Upgrade. Journal of Nuclear Materials **266-269**, 175-181 (1999).

260. *Schwarz-Selinger, T., A. von Keudell and W. Jacob:* Plasma Chemical Vapor Deposition of Hydrocarbon Films: The Influence of Hydrocarbon Source Gas on the Film Properties. Journal of Applied Physics **86**, 3988-3996 (1999).

261. *Schweinzer, J., K. Borrass, W. Sandmann, ASDEX Upgrade Team and NBI Team:* Separatrix to Pedestal Density Ratio in ASDEX Upgrade H-Modes Comparing DIV-I and DIV-II Operation. In: Proc. 26th EPS Conf. Control. Fusion and Plasma Phys., Maastricht 1999, (Eds.) B.Schweer, G.Van Oost, E.Vietzke. ECA 23J. Europ. Phys. Soc., Geneva 1999, 1637-1640.

262. *Schweinzer, J., R. Brandenburg, I. Bray*, R. Hoekstra*, F. Aumayr*, R.K. Janev* and H.P. Winter*:* Database for Inelastic Collisions of Lithium Atoms with Electrons, Protons, and Multiply Charged Ions. Atomic Data and Nuclear Tables **72**, 239-273 (1999).

263. *Schweinzer, J. W. Sandmann, G. Haas, J. Neuhauser, H. Murmann, H. Salzmann, ASDEX Upgrade Team and NBI Team:* Comparison of Scrape-off Layer Behaviour between DIV-I and DIV-II Operations on ASDEX Upgrade. Journal of Nuclear Materials **266-269**, 934-939 (1999).

264. *Scott, B.D.:* Electromagnetic Gyrofluid Turbulence in Tokamak Edge Geometries. In: Proc. Theory of Fusion Plasmas, Bologna 1998, (Eds.) J.W.Connor, E.Sindoni, J.Vaclavik. Ed. Compositori, Bologna 1999, 359-372.

265. *Shishkin*, A.A., I.N. Sidorenko and H. Wobig:* Dynamic Control of Drift Resonances in HELIAS Configuration. Problems of Atomic Science and Technology. Series: Plasma Physics, Issues **1**(1), **2**(2), 46-48 (1999).

266. *Sidorenko, I.N. and H. Wobig:* Superbanana Orbits in Helias Reactor Caused by the Electromagnetic Perturbations In: Proc. 26th EPS Conf. Control. Fusion and Plasma Phys., Maastricht 1999, (Eds.) B.Schweer, G.Van Oost, E.Vietzke. ECA 23J. Europ. Phys. Soc., Geneva 1999, 1457-1460.

267. *Silva*, A., L. Cupido*, C. Loureiro*, S. Vergamota*, P. Varela*, J. Santos*, M. Manso*, F. Serra*, L. Meneses*, M. Tavares*, I. Nunes*, B. Kurzan, W. Suttrop and V. Grossman*:* New Developments of the ASDEX Upgrade Tokamak Microwave Reflectometer. Fusion Engineering and Design **46**, 389-395 (1999).

268. *Silva*, A., L. Cupido*, M. Manso*, F. Serra*, I. Nunes*, J. Santos*, P. Varela*, S. Vergamota*, L. Meneses*, V. Grossman*, F. Silva*, C. Loureiro*, F. Nunes*, B. Kurzan and W. Suttrop:* Microwave Reflectometry Diagnostic for Density Profile and Fluctuation Measurements on ASDEX Ugprade. Review of Scientific Instruments **70**, 1072-1075 (1999).

269. *Söldner*, F.X., B. Alper*, Yu.F. Baranov*, A. Bickley*, D. Borba*, C.D. Challis*, G.D. Conway, G. Cottrell*, M. de Benedetti*, N. Deliyanakis*, C. Gormezano*, C. Gowers*, C.M. Greenfield*, N.C. Hawkes*, T.C. Hender*, G.T.A. Huysmans*, E. Joffrin*, T.T.C. Jones*, P.T. Lang, X. Litaudon*, P.J. Loma*, A. Maas*, J. Mailloux*, M. Mantsinen*, M. Nave*, V. Parail*, F.G. Rimini*, B. Schunke*, A.C.C. Sips*, P. Smeulders*, M.F. Stamp*, E.J. Strait*, T.J.J. Tala*, M. von Hellermann*, D.J. Ward* and K.-D. Zastrow*:* Optimised Shear Scenario Developement on JET towards Steady-State. In: Proc. 26th EPS Conf. Control. Fusion and Plasma Phys., Maastricht 1999, (Eds.) B.Schweer, G.Van Oost, E.Vietzke. ECA 23J. Europ. Phys. Soc., Geneva 1999, 185-188.

270. *Sorge*, S., S. Günter and G. Röpke*:* On the Consequences of a Realistic Conditional Covariance in MMM-Calculations. Journal of Physics B **32**, 675-681 (1999).

271. *Speth, E., M. Ciric, J.-H. Feist, P. Frank, B. Heinemann, W. Kraus, F. Probst, R. Riedl, R. Trainham*, O. Vollmer and R. Wilhelm:* RF Ion Sources for Fusion Applications: Design, Development and Performance. Fusion Engineering and Design **46**, 383-388 (1999).

272. *Stäbler, A., P. Franzen, O. Gruber, F. Ryter, J. Stober and ASDEX Upgrade Team:* Influence of Beam Heating Deposition Profiles on the Transport of ASDEX Upgrade Plasmas. In: Proc. 26th EPS Conf. Control. Fusion and Plasma Phys., Maastricht 1999, (Eds.) B.Schweer, G.Van Oost, E.Vietzke. ECA 23J. Europ. Phys. Soc., Geneva 1999, 1437-1440.

273. *Stamp*, M.F., D. Elder*, H.Y. Guo*, M. von Hellermann*, L.D. Horton*, R. König, J. Lingertat*, G. McCracken*, A. Meigs*, P. Stangeby* and A. Tabasso:* Experimental Determination of the Contribution of Chemical Sputtering of Carbon on Carbon Core Concentrations. Journal of Nuclear Materials **266-269**, 685-690 (1999).

274. *Steltenpohl, A. and N. Memmel:* Adsorption Site of Oxygen on Pd(111). Surface Science **443**, 13-18 (1999).

275. *Stober, J., O. Gruber, V. Mertens, F. Ryter, W. Suttrop, W. Treutterer and ASDEX Upgrade Team:* Dependence of Confinement and Transport on Triangularity in ASDEX Upgrade. In: Proc. 26th EPS Conf. Control. Fusion and Plasma Phys., Maastricht 1999, (Eds.) B.Schweer, G.Van Oost, E.Vietzke. ECA 23J. Europ. Phys. Soc., Geneva 1999, 1401-1404.

276. *Storm*, J., R.M. Lambert*, N. Memmel, J. Onsgaard* and E. Taglauer:* Catalysis with Monometallic and Bimetallic Films: Trimerization of Acetylene to Benzene on Pd/Ru (001) and (Pd+Au)/Ru (001). Surface Science **436**, 259-268 (1999).

277. *Stotler*, D.P., R.A. Vesey*, D.P. Coster, C.F.F. Carney*, B. LaBombard*, B. Lipschultz*, C.S. Pitcher* and R. Schneider:* Coupled Monte Carlo Neutral-Fluid Plasma Simulation of Alcator C-Mod Divertor Plasma near Detachment. Journal of Nuclear Materials **266-269**, 947-952 (1999).

278. *Stroth, U., T. Geist, J.P.T. Koponen*, H.-J. Hartfuß, P. Zeiler, ECRH Group and W7-AS Team:* Evidence for Convective Inward Particle Transport in a Stellarator. Physical Review Letters **82**, 928-931 (1999).

279. *Strumberger, E.:* The Stochastic Edge Region of W 7-X. Journal of Nuclear Materials **266-269**, 1207-1211 (1999).

280. *Strumberger, E., H. Wobig, J. Kisslinger and C. Nührenberg:* Equilibrium and Stability Properties of a Helias Reactor. In: Proc. 26th EPS Conf. Control. Fusion and Plasma Phys., Maastricht 1999, (Eds.) B.Schweer, G.Van Oost, E.Vietzke. ECA 23J. Europ. Phys. Soc., Geneva 1999, 1485-1488.

281. *Subbotin*, A., W.A. Cooper*, M. Isaev*, M. Mikhailov*, J. Nührenberg and V.D. Shafranov*:* Analytical and Computational Investigations of Improved-Confinement Stellarators. In: Proc. 26th EPS Conf. Control. Fusion and Plasma Phys., Maastricht 1999, (Eds.) B.Schweer, G.Van Oost, E.Vietzke. ECA 23J. Europ. Phys. Soc., Geneva 1999, 1773-1776.

282. *Suttrop, W., O. Gruber, B. Kurzan, H. Murmann, J. Schweinzer, J. Stober, W. Treutterer and ASDEX Upgrade Team:* Effect of Triangularity Variation on Edge Operational Boundaries in ASDEX Upgrade. In: Proc. 26th EPS Conf. Control. Fusion and Plasma Phys., Maastricht 1999, (Eds.) B.Schweer, G.Van Oost, E.Vietzke. ECA 23J. Europ. Phys. Soc., Geneva 1999, 1405-1408.

283. *Suttrop, W., V. Mertens, H. Murmann, J. Neuhauser, J. Schweinzer and ASDEX Upgrade Team:* Operational Limits for High Edge Density {H-Mode} Tokamak Operation. Journal of Nuclear Materials **266-269**, 118-123 (1999).

284. *Suttrop, W., A.G. Peeters, F. Ryter, J. Stober and ASDEX Upgrade Team:* Physics and Scaling of the H-Mode Transition in ASDEX Upgrade. Plasma Physics and Controlled Fusion **41**, A569-A576 (1999).

285. *Svensson*, J., M. von Hellermann* and R. König:* Analysis of JET Charge Exchange Spectra Using Neutral Networks. Plasma Physics and Controlled Fusion **41**, 315-338 (1999).

286. *Tabasso, A., J. Roth, H. Maier*, K. Krieger and ASDEX Upgrade Team:* Studies of Erosion and Redeposition in the Main Chamber Wall of the ASDEX Upgrade Tokamak. In: Proc. 26th EPS Conf. Control. Fusion and Plasma Phys., Maastricht 1999, (Eds.) B.Schweer, G.Van Oost, E.Vietzke. ECA 23J. Europ. Phys. Soc., Geneva 1999, 1533-1536.

287. *Taglauer, E., H. Knözinger* and S. Günther*:* Microprobe Applications for the Characterization of Catalyst Systems. Nuclear Instruments and Methods in Physics Research B **158**, 638-646 (1999).

288. *Taglauer*, A., R. Niessner*, W. von der Linden*, V. Dose, and E. Taglauer:* Trace Metal Detection in Natural Water. In: Maximum Entropy and Bayesian Methods, (Eds.) W.v.d.Linden, V.Dose, R.Fischer, R.Preuss. Kluwer Acad. Publ., Dordrecht 1999, 341-344.

289. *Taglauer, E., A. Steltenpohl, R. Beikler and L. Houssiau*:* Scattered Ion Yields from Bimetallic Crystal Surfaces. Nuclear Instruments and Methods in Physics Research B **157**, 270-273 (1999).

290. *Tasso, H.:* On Lyapunov Stability of Dissipative Mechanical Systems. Physics Letters A **257**, 309-311 (1999).

291. *Thomsen, H., J. Bleuel, M. Endler, A.V. Chankin*, S. Davies*, S.K. Erents*, G.F. Matthews*, W7-AS Team and JET Team*:* On the Parallel Correlation of Electrostatic Fluctuations in the Edge Plasma of W7-AS and JET. In: Proc. 26th EPS Conf. Control. Fusion and Plasma Phys., Maastricht 1999, (Eds.) B.Schweer, G.Van Oost, E.Vietzke. ECA 23J. Europ. Phys. Soc., Geneva 1999, 1541-1544.

292. *Throumoulopoulos*, G.N. and D. Pfirsch:* A Potential Mechanism for the Creation of Reversed-Magnetic-Shear Transport Barriers in Tokamaks. Physics of Plasmas **6**, 3226-3232 (1999).

293. *Throumoulopoulos*, G.N. and H. Tasso:* Ideal Magneto-hydrodynamic Equilibria with Helical Symmetry and Incompressible Flows. Journal of Plasma Physics **62**, 449-459 (1999).

294. *Tichmann, C., G. Pautasso, J.C. Fuchs, K. Lackner, V. Mertens, F.C. Morabito*, W. Schneider and ASDEX Upgrade Team:* Use of a Neural Network for the Prediction of Disruptions on ASDEX Upgrade. In: Proc. 26th EPS Conf. Control. Fusion and Plasma Phys., Maastricht 1999, (Eds.) B.Schweer, G.Van Oost, E.Vietzke. ECA 23J. Europ. Phys. Soc., Geneva 1999, 761-764.

295. *Toussaint, U. von, R. Fischer, K. Krieger and V. Dose:* Depth Profile with Confidence Intervals from Rutherford Backscattering Data. New Journal of Physics **1**, 11.1-11.13 (1999), http://www.njp.org/.

296. *Tsois*, N., C. Dorn, G. Kyriakakis*, M. Markoulaki*, B. Pflug, G. Schramm, P. Theodropoulos*, P. Xantopoulos*, M. Weinlich and ASDEX Upgrade Team:* A Fast Scanning Langmuir Probe System for ASDEX-Upgrade Divertor. Journal of Nuclear Materials **266-269**, 1230-1233 (1999).

297. *Tunklev*, M., P. Breger*, K. Günther*, M. von Hellermann*, R. König and M. O'Mullane*:* Modelling of Passive Charge Exchange Emission and Neutral Background Density Deductions in JET. Plasma Physics and Controlled Fusion **41**, 985-1004 (1999).

298. *Tunklev*, M. P. Breger*, M. von Hellermann* and R. König:* Modelling of Passive Charge Exchange Emission in the Joint European Torus. Review of Scientific Instruments **70**, 933-943 (1999).

299. *Ushakov*, A., L. Ledl*, G. Veres*, R. Burhenn, R. Schneider and L.L. Lengyel:* Simulation of Carbon Pellet Injection and Impurity Cloud Expansion Scenarios in Stellarator W7-AS by Means of a Quasi-Three-Dimensional Pellet Code. In: Proc. 26th EPS Conf. Control. Fusion and Plasma Phys., Maastricht 1999, (Eds.) B.Schweer, G.Van Oost, E.Vietzke. ECA 23J. Europ. Phys. Soc., Geneva 1999, 1481-1484.

300. *Vichev*, R.G., R.H. Petrov*, W. Eckstein, J. Van Humbeeck* and B. Blanpain*:* Oxidation and Preferential Sputtering of a $Cu_{50}Zr_{50}$ Alloy. Applied Surface Science **144-145**, 212-215 (1999).

301. *W7-AS Team:* Overview of W7-AS Results. Stellarator News **61**, 8-13 (1999), http://www.ornl.gov/fed/stelnews.

302. *Wanner, M.:* Das Stellaratorexperiment WENDELSTEIN 7-X, Technische Anforderungen und Projektstatus. In: Jahrestagung Kerntechnik, Karlsruhe 1999, (Ed.) Dt. Atomforum e.V. INFORUM Verl., Bonn 1999, 5-10.

303. *Warrier*, M., S. Jaishankar*, S. Deshpande*, D.P. Coster, R. Schneider, S. Chaturvedi*, R. Srinivasan*, B. Braams* and SST Team*:* Scrape off Layer Modelling Studies for SST-1. Journal of Nuclear Materials **266-269**, 726-731 (1999).

304. *Wehner*, S. and J. Küppers:* Interaction of Gaseous D Atoms with Alkyl Halides Adsorbed on Pt (111), H/Pt (111), and C/Pt (111) Surfaces: Hot-Atom and Eley Rideal Reactions. I. Methyl Bromide. Journal of Chemical Physics **111**, 3209-3217 (1999).

305. *Wehner*, S. and J. Küppers:* Interaction of Gaseous D Atoms with Alkyl Halides Adsorbed on Pt (111), H/Pt (111), and C/Pt (111) Surfaces: Hot-Atom and Eley Rideal Reactions. II. Ethyl Iodide. Journal of Chemical Physics **111**, 3218-3224 (1999).

306. *Wehner*, S. and J. Küppers:* Interaction of Gaseous D Atoms with Alkyl Halides Adsorbed on Pt (111), H/Pt (111), and C/Pt (111) Surfaces: Hot-Atom and Eley Rideal Reactions. III. Isopropyl Iodide. Journal of Chemical Physics **111**, 3225-3232 (1999).

307. *Weitzner*, H. and D. Pfirsch:* Nonperiodicity in Space of the Magnetic Moment Series. Physics of Plasmas **6**, 420-423 (1999).

308. *Weller, A., C. Görner, M. Anton, J. Geiger and C. Nührenberg:* Energetic Particle-Driven Alfvén Instabilities in W7-AS. Stellarator News **61**, 32-33 (1999), http://www.ornl.gov/fed/stelnews.

309. *Weller, A., C. Görner and D. Gonda:* X-Ray Diagnostics on Wendelstein 7-AS. Review of Scientific Instruments **70**, 484-488 (1999).

310. *Wendland, C., U. Gasparino, H. Maaßberg, E.R. Solano and W7-AS Team:* Current Balance Analysis at the W7-AS Stellarator. In: Proc. 26th EPS Conf. Control. Fusion and Plasma Phys., Maastricht 1999, (Eds.) B.Schweer, G.Van Oost, E.Vietzke. ECA 23J. Europ. Phys. Soc., Geneva 1999, 1489-1492.

311. *Wenzel, U., K. Behringer, K. Büchl, A. Herrmann and K. Schmidtmann:* Characterization of the Hydrogen Emission in Divertor II of ASDEX Upgrade. Journal of Nuclear Materials **266-269**, 1252-1256 (1999).

312. *Wenzel, U., K. Behringer, A. Carlson, J. Gafert, B. Napiontek and A. Thoma:* Volume Recombination in Divertor I of ASDEX Upgrade. Nuclear Fusion **39**, 873-882 (1999).

313. *Wenzel, U., A. Carlson, C. Fuchs, H. Kastelewicz and B. Napiontek:* Spectroscopic Study of Divertor Radiation in ASDEX Upgrade at High Density. Plasma Physics and Controlled Fusion **41**, 801-818 (1999).

314. *Wenzel, U., D.P. Coster, A. Kallenbach, H. Kastelewicz, M. Laux, H. Mayer and R. Schneider:* Studies of the Poloidal Temperature Asymmetry in the Scrape-off Layer of ASDEX Upgrade. In: Proc. 26th EPS Conf. Control. Fusion and Plasma Phys., Maastricht 1999, (Eds.) B.Schweer, G.Van Oost, E.Vietzke. ECA 23J. Europ. Phys. Soc., Geneva 1999, 1537-1540.

315. *Werner, A., A. Weller, D.S. Darrow* and W7-AS Team:* Fast-Ion Losses in W7-AS. Stellarator News **65**, 2-7 (1999), http://www.ornl.gov/fed/stelnews.

316. *Whyte*, D.G., J.P. Coad*, P. Franzen and H. Maier:* Similarities in Divertor Erosion/Redeposition and Deuterium Retention Patterns between the Tokamaks ASDEX Upgrade, DIII-D and JET. Nuclear Fusion **39**, 1025-1029 (1999).

317. *Wienhold*, P., H.G. Esser,* D. Hildebrandt, A. Kirschner*, K. Ohya*, V. Phillips*, M. Rubel* and J. von Seggern*:* Investigation of Erosion and Deposition on Wall Components of TEXTOR-94. Physica Scripta **T81**, 19-24 (1999).

318. *Wienhold*, P., H.G. Esser,* D. Hildebrandt, A. Kirschner*, K. Ohya*, V. Phillips*, M. Rubel* and J. von Seggern*:* Investigation of Local Transport and Deposition Efficiency of Reactive Gases Puffed into the Scrape-off Layer of TEXTOR-94. In: Proc. 26th EPS Conf. Control. Fusion and Plasma Phys., Maastricht 1999, (Eds.) B.Schweer, G.Van Oost, E.Vietzke. ECA 23J. Europ. Phys. Soc., Geneva 1999, 705-708.

319. *Wilhelm, R.:* Deposition, Properties and Applications of Carbon-Based Coatings. In: Advanced Technologies Based on Wave and Beam Generated Plasmas, (Eds.) H.Schlüter, A.Shivarova. NATO ASI Series 3: High Technology 67, Kluwer Acad. Publ. 1999, 123-135.

320. *Wilhelm, R.:* ECR Plasmas for Thin-Film Deposition. In: Advanced Technologies Based on Wave and Beam Generated Plasmas, (Eds.) H.Schlüter, A.Shivarova. NATO ASI Series 3: High Technology 67, Kluwer Acad. Publ. 1999, 111-122.

321. *Wobig, H.:* Theory of Advanced Stellarators. Plasma Physics and Controlled Fusion **41**, A159-A173 (1999).

322. *Wobig, H.:* Theory of Advanced Stellarator Reactor. Problems of Atomic Science and Technology. Series: Plasma Physics, Issues **1**(1), **2**(2), 3-7 (1999).

323. *Wobig, H. and H. Renner:* Stellarator Research at the IPP in Garching. Stellarator News **65**, 11-14 (1999), http://www.ornl.gov/fed/stelnews.

324. *Wolf, R., O. Gruber, M. Maraschek, R. Dux, C. Fuchs, S. Günter, A. Herrmann, A. Kallenbach, K. Lackner, P. McCarthy, H. Meister, G. Pereverzev, J. Schweinzer, U. Seidel and ASDEX Upgrade Team:* Stationary Advanced Scenarios with Internal Transport Barrier on ASDEX Upgrade. Plasma Physics and Controlled Fusion **41**, B93-B107 (1999).

325. *Wolle*, B., R. Bätzner*, T. Baloui, D. Gonda, H. Klein*, B. Wiegel* and J. Wittstock*:* Special Absorber Neutron Detector Moderator Assembly: A New Detector System for Flux Measurements of Collimated 2.5 MeV Neutrons. Review of Scientific Instruments **70**, 1194-1196 (1999).

326. *Wolle*, B., G. Beikert* and T. Baloui:* Refined Monte Carlo Modelling of Fusion Neutron Emission in Magnetically Confined Plasmas. Computer Physics Communications **123**, 46-55 (1999).

327. *Wolle*, B., G. Beikert* and F. Gadelmeier:* Effect of Anisotropic Neutron Emission on Counter Calibration Using Activation Techniques. Nuclear Instruments and Methods in Physics Research A **424**, 561-568 (1999).

328. *Wolle*, B., A. Weller, S. Schill*, F. Gadelmeier, T. Baloui and G. Beikert*:* Measurements and Simulations of the Neutron Production at W7-AS. Review of Scientific Instruments **70**, 1197-1200 (1999).

329. *Yu*, Q. and S. Günter:* Numerical Modelling of Neoclassical Double Tearing Modes. Nuclear Fusion **39**, 487-494 (1999).

330. *Zebisch, P., E. Taglauer and W7-AS Team:* A New Sniffer Probe for the Determination of Hydrogen Isotope Ratios in the W7-AS Stellarator. Review of Scientific Instruments **70**, 3007-3014 (1999).

331. *Zebisch, P., E. Taglauer, W7-AS Team and NBI Team:* The Hydrogen Isotope Ratio in W7-AS during Deuterium NBI Heating. Nuclear Fusion **39**, 451-457 (1999).

332. *Zehrfeld, H.-P.:* Resistive Equilibrium States of Axisymmetric Plasmas with Compressible Viscous Fluid Flow. In: Proc. 26th EPS Conf. Control. Fusion and Plasma Phys., Maastricht 1999, (Eds.) B.Schweer, G.Van Oost, E.Vietzke. ECA 23J. Europ. Phys. Soc., Geneva 1999, 1421-1424.

333. *Zeiler, A.:* Anomalous Transport in Tokamaks. In: Interrelation between Plasma Experiments in Laboratory and Space, Kreuth 1999, (Ed.) MPI für Extraterrestr. Physik, Garching 1999, 2.9.

334. *Zilker, M., K. Hallatschek, P. Heimann and F. Hertweck:* Multiprocessor Systems for Real Time Data Acquisition on the ASDEX Upgrade and Future Plasma Experiments. Fusion Engineering and Design **43**, 417-423 (1999).

335. *Zohm, H., G. Gantenbein*, G. Giruzzi*, S. Günter, F. Leuterer, M. Maraschek, J. Meskat*, A.G. Peeters, W. Suttrop, D. Wagner*, M. Zabiego* and ASDEX Upgrade Team:* Experiments on Neoclassical Tearing Mode Stabilization by ECCD in ASDEX Upgrade. Nuclear Fusion **39**, 577-580 (1999).

336. *Zoletnik*, S., M. Anton, M. Endler, S. Fiedler, M. Hirsch, K. McCormick, J. Schweinzer and W7-AS Team:* Density Fluctuation Phenomena in the Scrape-off Layer and the Edge Plasma of the Wendelstein 7-AS Stellarator. Physics of Plasmas **6**, 4239-4247 (1999).

337. *Zoletnik*, S., M. Anton, M. Endler, S. Fiedler, M. Hirsch, K. McCormick and W7-AS Team:* Statistical Analysis of Fluctuation Events in the SOL and the Edge Regions of the W7-AS Stellarator. In: Proc. 26th EPS Conf. Control. Fusion and Plasma Phys., Maastricht 1999, (Eds.) B.Schweer, G.Van Oost, E.Vietzke. ECA 23J. Europ. Phys. Soc., Geneva 1999, 849-852.

338. *Zoletnik*, S., M. Saffman*, N.P. Basse, W. Svendsen*, G. Kocsis* and M. Endler:* Relationship between Confinement and Core Plasma Fluctuations in the W7-AS Stellarator. In: Proc. 26th EPS Conf. Control. Fusion and Plasma Phys., Maastricht 1999, (Eds.) B.Schweer, G.Van Oost, E.Vietzke. ECA 23J. Europ. Phys. Soc., Geneva 1999, 1493-1496.

## Diploma Theses

339. *Jensen, O.:* Messungen von Ionentemperatur und -strömungsgeschwindigkeit an einem Plasma in einer linearen Magnetfeldkonfiguration. Humboldt-Univ. Berlin 1999.

340. *Keller, M.:* Experimentelle Studie über die Detektion geladener Teilchen. Univ. Heidelberg 1999.

## Doctoral Theses

341. *Brandenburg, R.:* Lithiumstrahldiagnostik von Kernfusionsplasmen. Techn. Univ. Wien 1999.

342. *Herre, G.:* Untersuchung der Plasmarandschicht am Stellarator Wendelstein 7-AS. Techn. Univ. München 1999.

343. *Landkammer, B.:* Untersuchung der Erosion von Kohlenwasserstoffschichten in Sauerstoff-Gasentladungen. Univ. Bayreuth 1999.

344. *Lindig, S.:* Aufbau eines dE-E-Teleskopdektors für ERDA und Reichweitenmessung von Wasserstoff in oberflächennahen a-C:H bzw. a-C:D Schichten mit ERD-Ionenstrahlanalyse. Fachhochschule München 1999.

345. *Poli, E.:* Diffraction Effects on Electromagnetic Gaussian Wave Beams in Anisotropic Inhomogeneous Plasmas. Univ. Pavia 1999.

346. *Steltenpohl, A.:* Wachstum von Palladium auf Palladium(111). Univ. Bayreuth 1999.

347. *Ullrich, W.:* Heliumtransport in der Plasmarandschicht an ASDEX Upgrade. Univ. Augsburg 1999.

348. *Vetter, S.:* Struktur und Dynamik von reinen und sauerstoffbedeckten gestuften Kupferoberflächen. Univ. Bayreuth 1999.

## Habilitations

349. *Schweinzer, J.:* Atomare Prozesse mit schnellen Lithiumatomen zur Diagnose und Optimierung von Fusionsplasmen. Techn. Univ. Wien 1999.

350. *Zeiler, A.:* Tokamak Edge Turbulence. Univ. Ulm 1999.

## Patents

351. *Biedermann, C., R. Radtke and S. Deuchler*:* Hochflexibler Membranbalg mit vorgelagertem Drehpunkt. Patentanmeldung Deutschland: 22.12.99.

352. *Gehringer, K.:* Vitondichtungen. Verlängerung des Gebrauchsmusters 295 19 353.0 bis 2001: 1.6.99.

353. *Haas, G.:* Heißkathoden Ionisations-Manometer. Verlängerung des Gebrauchsmusters 93 05 441.6 bis 2001: 13.9.99.

354. *Mast, K.-F., G. Schramm and M. Münch*:* Einleitung der nationalen Phasen. Europa, USA, Japan: 6.5.99; Veröffentlichung der deutschen Patenturkunde: 12.8.99; Patentanmeldung USA: 17.9.99, Japan: 21.9.99.

355. *Schauer, F.:* Gasdurchlässige Hochspannungsisolation. Stellung des Prüfantrags: August 1999.

356. *Schäftner, J.:* Dichtringabziehvorrichtung. Deutsches Gebrauchsmuster 29601651.9.

357. *Schneider, F.:* Hybrider Regler. Freigabe des deutschen Patents P 3931133.3: 12.11.99.

358. *Weber, G.:* Vakuum-Stromdurchführung. Stellung des Prüfantrags: April 1999.

359. *Wittenbecher, K., P. Turba and K. Klaster:* Lichtschranke mit hoher Störsicherheit. Patenterteilungsbeschluß: 18.2.99; Verzicht auf Auslandsanmeldungen: Juli 1999.

360. *Wittenbecher, K.:* Verfahren und Vorrichtung zur Frequenzmultiplikation und -division. Patentanmeldung Europa: 3.3.99; USA: 1.3.99; Japan: 10.3.99; Offenlegung des deutschen Patents DE 198 10 576 A 1: 16.9.99.

# Lectures

361. *Amano*, T., C.D. Beidler, E. Harmeyer, F. Herrnegger, A. Kendl, J. Kisslinger, I.N. Sidorenko, E. Strumberger and H. Wobig:* Progress in Helias Reactor Studies. 12th Int. Stellarator Conf., Madison,WI 1999.

362. *Anton, M., J. Geiger, R. Jaenicke, C. Wendland, H. Maaßberg, W7-AS Team and ECRH Group*: Toroidal Current Densities Viewed by Magnetic Diagnostics at W7-AS. 12th Int. Stellarator Conf., Madison,WI 1999.

363. *Bachmann, P.:* Remarks on 1D Temperature Bifurcation. Theory Meeting, Zinnowitz 1999.

364. *Bachmann, P., D. Sünder and H. Wobig:* Bifurcation of Temperature in Edge Plasmas. 7th Int. Workshop on Plasma Edge Theory in Fusion Devices, Toki 1999.

365. *Balden, M. and M. Mayer:* Removal of Deuterium from Codeposited Carbon-Silicon Layers. 9th Int. Conf. on Fusion Reactor Materials, Colorado Springs,CO 1999.

366. *Baldzuhn, J., L. Giannone, M. Kick, K. McCormick and W7-AS Team:* Optimised Confinement Discharges in W7-AS. 12th Int. Stellarator Workshop, Madison,WI 1999.

367. *Baloui, T., B. Wolle*, S. Schill*, F. Gadelmeier, R. Bätzner* and K. Hübner*:* Numerische Modellierung des Neutronentransports für Aktivierungsmessungen in der Experimentierhalle von W7-AS. Verhandl. DPG (IV) **34**, 374, P27.2 (1999).

368. *Basse, N.P. and S. Zoletnik*:* Two-Point Correlation Measurements of Density Fluctuations in the W7-AS Stellarator. 12th Int. Stellarator Conf., Madison,WI 1999.

369. *Bäumel, S. and H.-J. Hartfuß:* ECE Imaging Development at W7-AS. 11th Joint Russian-German Meeting on ECRH and Gyrotrons, Karlsruhe, Stuttgart, Garching 1999.

370. *Bäumel, S., M. Rodriguez* and H.-J. Hartfuß:* Mehrdimensionale ECE-Messungen. Verhandl. DPG (IV) **34**, 356, P20.6 (1999).

371. *Becker, G.:* Radiation Limits in ITER. ITER Combined Core-Pedestal Transport Database and Modelling Workshop, Garching 1999.

372. *Beckmann, M.:* Advanced Current Drive. 11th Joint Russian-German Meeting on ECRH and Gyrotrons, Karlsruhe, Stuttgart, Garching 1999.

373. *Beckmann, M.:* Calibration of the ECRH Polarization Mirrors at ASDEX Upgrade. 11th Joint Russian-German Meeting on ECRH and Gyrotrons, Karlsruhe, Stuttgart, Garching 1999.

374. *Beckmann, M.:* Nichtlineare Elektronenzyklotronheizung im Teilchenbild. Verhandl. DPG (VI) **34**, 374, P27.1 (1999).

375. *Beckmann, M.:* Nonlinear Effects in the Absorption of Electron Cyclotron Waves. 11th Joint Russian-German Meeting on ECRH and Gyrotrons, Karlsruhe, Stuttgart, Garching 1999.

376. *Beckmann, M. and F. Leuterer:* Electron Cyclotron Current Drive at $\omega \approx \omega_c$ with X-Mode Launched from the Low Field Side. 11th Joint Workshop on ECE and ECRH, Oh-arai 1999.

377. *Behler, K., H. Blank, A. Buhler, R. Drube, K. Förster, R. Merkel, G. Raupp, H. Reuter, M. Zilker and ASDEX Upgrade Team:* Recent Developments in the ASDEX Upgrade Data Acquisition Environment. 2nd IAEA Techn. Comm. Meeting on Control, Data Acquisition and Remote Participation for Fusion Research, Lisbon 1999.

378. *Behler, K., A. Buhler, R. Merkel, G. Neu, G. Raupp, W. Treutterer, D. Zasche, T. Zehetbauer and ASDEX Upgrade Team:* Real-Time Information Exchange between Data Acquisition. 11th IEEE NPSS Real Time Conf., Santa Fe,NM 1999.

379. *Behringer, K.:* IPP Diagnostic Expertise and JET Cooperation. Workshop on Diagnostics, Lisbon 1999.

380. *Behringer, K.:* Physikalische Grundlagenforschung auf dem Gebiet der Plasmatechnologie. 9. Bunddt. Fachtagung Plasmatechnologie und Workshop Plasmaanwendungen in der Textilindustrie, IPF Stuttgart 1999.

381. *Behringer, K.:* Spektroskopie und Modellierung von Niederdruckplasmen. Kolloquium, Univ. Düsseldorf 1999.

382. *Behringer, K.:* Spektroskopie und Modellierung von Niederdruckplasmen. Kolloquium, Techn. Univ. München 1999.

383. *Behringer, K.:* Spektroskopie von Nichtgleichgewichtsplasmen. Vorlesung, Univ. Augsburg, SS 1999.

384. *Behringer, K., M. Stritzker*, U. Fantz* and H. Schreck*:* Seminar über Anwendungen und Diagnostik von Niederdruckplasmen. Seminar, Univ. Augsburg, SS 1999.

385. *Behringer, K., U. Fantz* and T. Hamacher:* Seminar über Probleme der zukünftigen Energieversorgung. Seminar, Univ. Augsburg, SS 1999.

386. *Behrisch, R.:* Nachweis der Wasserstoffisotope in den Oberflächenschichten von Wandproben aus Plasmaexperimenten. Techn. Univ. München, Univ. München, WS 1999/2000.

387. *Behrisch, R.:* Wasserstofftiefenprofile in Wandmaterialien von Fusionsexperimenten. Techn. Univ. München, Univ. München, WS 1999/2000.

388. *Beidler, C.D. and H. Maaßberg:* An Improved Formulation of Ripple-Averaged Kinetic Theory. 12th Int. Stellarator Conf., Madison,WI 1999.

389. *Beidler, C.D. and H. Maaßberg:* Ripple Averaged Kinetic Theory for Stellarators. IAEA Techn. Comm. Meeting on First Principle Based Transport Theory, Kloster Seeon 1999.

390. *Beikler, R.:* Investigation of Alloy Surfaces by Low Energy Ion Scattering. Sektion Physik and Center of Nano Science, Univ. München 1999.

391. *Beikler, R.:* Ion Scattering Studies of Ordered Alloy Surfaces: NiAl (100), CuAu (100). 2nd Int. Workshop on Surface and Grain Boundary Segregation, Schloss Ringberg 1999.

392. *Beikler, R. and E. Taglauer:* Investigation of Alloy Surfaces by Low-Energy Ion Scattering. Symp. on 25 Years of Structural Research at LS Peisl, Univ. München 1999.

393. *Beikler, R. and E. Taglauer:* Ion Scattering Studies of Ordered Alloy Surfaces: NiAl(100). 14th Int. Conf. on Ion Beam Analysis/Europ. Conf. on Accelerators in Appl. Research and Technology, Dresden 1999.

394. *Beikler, R. and E. Taglauer:* Ion Scattering Studies of Ordered Alloy Surfaces: NiAl(100) and CuAn(100). 2nd Int. Workshop on Surface and Grain Boundary Segregation, Schloss Ringberg 1999.

395. *Bessenrodt-Weberpals, M.:* Diagnostik der Plasmadynamik in Tokamaks. Kolloquium, Univ. Düsseldorf 1999.

396. *Bessenrodt-Weberpals, M.:* Hochtemperatur-Plasmaphysik. Vorlesung, Univ. Düsseldorf, WS 1999/2000.

397. *Bessenrodt-Weberpals, M.:* Plasma-Material-Bearbeitung (Plasma-Aided Manufacturing). Vorlesung, Univ. Düsseldorf, SS 1999.

398. *Biedermann, C., T. Fuchs, G. Fußmann and R. Radtke:* Einschluß hochgeladener Ionen in einer Elektronenstrahl-Ionenfalle. Verhandl. DPG (VI) **34**, 258, A18.16 (1999).

399. *Biskamp, D.:* Collisionless Magnetic Reconnection. Centennial Meeting of the APS, Atlanta,GA 1999.

400. *Bleuel, J., M. Endler, H. Niedermeyer and W7-AS Team:* The Comparison of Global Confinement Times with Radial Fluxes Induced by Electrostatic Fluctuations in W7-AS. TTF Turbulence Workshop, Fluctuation Studies in Fusion and Non-Fusion Plasmas, Padua 1999.

401. *Bohmeyer, W.:* Plasmadiagnostik an einer linearen magnetisierten Entladung. Hahn-Meitner-Inst., Berlin 1999.

402. *Bolt, H.:* Influence of Plasma-Surface Interaction on Steady State Operation - Materials Related Issues. 2nd IAEA Techn. Comm. Meeting on Steady-State Operation of Magnetic Fusion Devices, Fukuoka 1999.

403. *Bolt, H.:* Plasma Facing Materials and Component for Steady State Operation. Workshop on Plasma Facing Materials and Components, Sapporo 1999.

404. *Bolt, H., J. Linke* and M. Rödig*:* Thermal Loading of Materials in Fusion Applications. CEIT, San Sebastian 1999.

405. *Bolt, H., J. Linke*, M. Rödig*, M. Scheerer* and H. Greuner:* Research Activities Concerning Plasma Facing Materials and Component Development. Fusion Reactor Technology Seminar, Nat. Inst. for Fusion Science, Toki 1999.

406. *Bolt, H., J. Linke*, M. Rödig*, M. Scheerer* and H. Greuner:* Research Activities Concerning Plasma Facing Materials and Component Development. Japan Atomic Energy Res. Inst., Naka 1999.

407. *Bolt, H. and M. Nöthe*:* Interaction between Surface and Plasma - Plasma Processes and Film Deposition Using TEOS. 2nd Asean-Europ. Conf. on Plasma Surface Engineering, Beijing 1999.

408. *Bolt, H., M. Nöthe*, A. Buuron* and F. Koch:* Plasmaunterstützte Abscheidung von Metall/Nichtmetall-schichten - Prozeßanalytik und Strukturuntersuchungen. Kolloquium, Univ. Greifswald 1999.

409. *Bonoli*, P.T., A.E. Hubbard*, E. Nelson-Melby*, M. Porkolab*, S.J. Wukitch*, M. Brambilla, G. Schilling* and G. Taylor*:* Mode Conversion Electron Heating Experiments in Alcator C-Mod: Theory and Experiment. Bull. Am. Phys. Soc. **44**, 206 (1999).

410. *Bosch, H.-S.:* Als Physiker in der Großforschung. Max-Planck-Gesellschaft. Univ. Ulm 1999.

411. *Bosch, H.-S.:* Basic Nuclear Fusion. Summer Univ. for Plasma Physics, Greifswald 1999.

412. *Bosch, H.-S.:* ITER. Summer Univ. for Plasma Physics, Greifswald 1999.

413. *Bosch, H.-S.:* Plasmadiagnostik. Vorlesung, Humboldt-Univ. Berlin, SS 1999.

414. *Bosch, H.-S.:* Safety and Environment. Summer Univ. for Plasma Physics, Greifswald 1999.

415. *Bosch, H.-S.:* Was haben die Sterne mit unserer Energieversorgung zu tun? Schulvortrag, MPG Hauptversammlung, Dortmund 1999.

416. *Bosch, H.-S., D.P. Coster, R. Dux, O. Gruber, G. Haas, A. Kallenbach, M. Kaufmann, R. Schneider, A. Stäbler, R. Wolf and ASDEX Upgrade Team:* Helium Transport Investigations in ASDEX Upgrade. 4th Int. Workshop on Helium Transport and Exhaust, Jekyll Island,GA 1999.

417. *Bowman*, J.C., A. Zeiler and D. Biskamp:* A Multi-Grid Algorithm for Nonlocal Collisional Electrostatic Drift-Wave Turbulence. Bull. Am. Phys. Soc. **44**, 354 (1999).

418. *Bowman*, J.C., A. Zeiler and D. Biskamp:* A Multi-Grid Algorithm for Nonlocal Collisional Electrostatic Drift-Wave Turbulence. IAEA Technical Comittee Meeting on First Principle Based Transport Theory, Kloster Seeon 1999.

419. *Bradshaw, A.M.:* Oberflächenstrukturuntersuchungen mittels Synchrotronstrahlung. Kolloquium, Forschungszentrum Jülich 1999.

420. *Bradshaw, A.M.:* Strukturbestimmung von Adsorbaten mittels Synchrotronstrahlung. Physikal. Kolloquium, Univ. Jena 1999.

421. *Brakel, R.:* Die Abhängigkeit des magnetischen Einschlusses von Rotationstransformation und magnetischer Verscherung im W7-AS Stellarator. Verhandl. DPG (IV) **34**, 344, P7.4 (1999).

422. *Brakel, R.:* Experimental Results from Stellarators. Summer Univ. for Plasma Physics, Greifswald 1999.

423. *Brakel, R., M. Anton, J. Geiger, H.-J. Hartfuß, G. Kühner, A. Weller, E. Würsching, W7-AS Team and ECRH-Group:* An Empirical Model of Electron Energy Transport in the Presence of Rational Surfaces in W7-AS. 12th Int. Stellarator Conf., Madison,WI 1999.

424. *Braun, F.:* Fast Matching of Load Charges in the ICRF Range. 18th IEEE/NPSS Symp. on Fusion Engineering, Albuquerque,NM 1999.

425. *Burhenn, R.:* Vom W7-AS zum W7-X. Graduiertenkollegstreffen, Forschungszentrum Jülich, Univ. Düsseldorf, Bad Honnef 1999.

426. *Dinger*, A., C. Lutterloh*, J. Biener* and J. Küppers:* Adsorption of Propylene Oxide on Pt(111) Surfaces and its Reactions with Gaseous and Adsorbed H Atoms. 46th AVS Symp., Seattle,WA 1999.

427. *Dinger*, A., C. Lutterloh*, and J. Küppers:* Kinetics of Abstraction of Monohydride and Dihydride D from Si(100) Surfaces. 46th AVS Symp., Seattle,WA 1999.

428. *Dohmen R. and J. Pichlmeier*:* Parallelization of the FP-LAPW Code WIEN 97 for Message-Passing Systems. Europ. Centre for Parallel Computing at Vienna, Vienna 1999.

429. *Dohmen R. and J. Pichlmeier*:* Parallelization of WIEN 97 for Message-Passing Systems. 5th WIEN-WORKSHOP on Full-Potential LAPW Calculations with the WIEN 97 Code, Vienna 1999.

430. *Dose, V. and P. Pecher:* Cross Sections and Rate Coefficients for Partial Electron Impact Ionization of $CH_4$ and $H_2$. 5. Greifswalder Gespräch zur Plasmaphysik "Databases for Modelling and Simulation of Plasmas", Greifswald 1999.

431. *Drevlak, M.:* Optimization of Heterogenous Magnet Systems. 12th Int. Stellarator Conf., Madison,WI 1999.

432. *Düchs, D.F.:* Methoden zur numerischen Beschreibung von heißen Plasmen. Vorlesung, Univ. Bochum, SS 1999.

433. *Düchs, D.F.:* The Role of Fusion Energy. 3rd Symp. on Current Trends in Int. Fusion Research: Review and Assessment, Washington,D.C. 1999.

434. *Düchs, D.F.:* Wellenausbreitung in Plasmen. Vorlesung, Univ. Bochum, WS 1999/2000.

435. *Düchs, D.F.:* Wozu Energie aus kontrollierter Kernfusion? Vorlesung, Univ. Bochum, WS 1989/99.

436. *Dux, R.:* Impurity Behaviour in Advanced Tokamak Scenarios on ASDEX Upgrade. Meeting on Advanced Tokamak Operation at JET, Garching 1999.

437. *Dux, R.:* Plasmaphysik und Fusionsforschung I., Vorlesung, Univ. Augsburg, WS 1999/2000.

438. *Dux, R.:* Plasmaphysik und Fusionsforschung II. Vorlesung, Univ. Augsburg, SS 1999.

439. *Dux, R., C. Fuchs, A. Gude, J. Schweinzer and ASDEX Upgrade Team:* Messung des neoklassischen Transportes und des Strahlungsprofils von Verunreinigungen in ASDEX Upgrade. Verhandl. DPG(VI) **34**, 342, P6.1 (1999).

440. *Endler, M.:* Hochtemperatur-Plasmaphysik I. Univ. Greifswald, WS 1999/2000.

441. *Endler, M. and J. Bleuel:* Vergleich zwischen Langmuir-Sondenmessungen an W7-AS und Driftwellencodes von B. Scott - bisherige Erfahrungen. Workshop on Simulation of Turbulence in Low-Temperature Plasmas and Comparison with Experiment, Kiel 1999.

442. *Endler, M., J. Bleuel, P. Grigull, H. Niedermeyer and G. Theimer:* Die Bedeutung des radialen Teilchentransports durch Fluktuationen in der Randschicht des Stellarators Wendelstein 7-AS für den Einschluß. Verhandl. DPG (IV) **34**, 344, P7.5 (1999).

443. *Endler, M., J. Bleuel, H. Niedermeyer, U. Pfeiffer, G. Theimer and W7-AS Team:* Die räumliche Struktur der Randschichtturbulenz am Stellarator Wendelstein 7-AS. Seminar zur Oberflächen- und Grenzflächenphysik, Univ. Greifswald 1999.

444. *Endler, M., H.-J. Hartfuß and W7-X Diagnostic Team:* The W7-X Diagnostic Programme. Workshop on Diagnostics, Lisbon 1999.

445. *Erckmann, V.:* High Power ECCD Experiments at W7-AS, Status of ECRH for W7-X. Kolloqium, Inst. for Applied Physics, Nizhny Novgorod 1999.

446. *Erckmann, V., G. Dammertz*, W. Kasparek*, H.P. Laqua, H. Maaßberg, M. Thumm*, W7-X Team and W7-AS Team, W7-X Team (FZ Karlsruhe)* and W7-X Team (IPF Stuttgart)*:* ECRH and ECCD Experiments at W7-AS, Status at W7-X. 11th Joint Workshop on ECE and ECRH, Oh-arai 1999.

447. *Feng, Y. and J. Kisslinger:* Status and Application of the EMC3/EIRENE Code. 7th Int. Workshop on Plasma Edge Theory in Fusion Devices, Toki 1999.

448. *Feng, Y., J. Kisslinger and F. Sardei:* Formulation and Application of the EMC3 Code. Theory Meeting, Zinnowitz 1999.

449. *Feng, Y., J. Kisslinger and F. Sardei:* Modeling and Simulation of the W7-AS Island Divertor. 12th Int. Stellarator Conf., Madison,WI 1999.

450. *Fischer, R.:* Background Estimation in Experimental Spectra. 19th Int. Workshop on Maximum Entropy and Bayesian Methods, Boise,ID 1999.

451. *Fischer, R.:* The Adaptive Resolution Concept in Form-Free Distribution Estimation. Verhandl. DPG (VI) **34**, 292, KY3.4 (1999).

452. *Fischer, A., F.C. Jenoft*, U. Wild*, G. Weinberg*, H. Sack-Kongehl*, K. Weiss*, R. Schlögl*, T. Wagner*, A.D. Polli*, M. Rühle* and C. Linsmeier:* Naßchemische Herstellung dünner sulfathaltiger Zirkonoxidfilme. 32. Jahrestreffen dt. Katalytiker, Friedrichroda 1999.

453. *Fuchs, C., J. Geiger, H.-J. Hartfuß, H. Maaßberg and W7-AS Team:* Shafranov Shift in the "Electron Root" Feature at the W7-AS. 11th Joint Workshop ECE and ECRH, Oh-arai 1999.

454. *Fuchs, C. and H.-J. Hartfuß:* Cotton-Mouton Polarimetry at W7-X. 11th Joint Russian-German Meeting on ECRH and Gyrotrons, Karlsruhe, Stuttgart, Garching 1999.

455. *Fuchs, C. and H.-J. Hartfuß:* Technology of the New W7-AS Broadband Radiometer System. 11th Joint Workshop on ECE and ECRH, Oh-arai 1999.

456. *Fuchs, T., C. Biedermann, G. Fußmann and R. Radtke:* Experimentelle Bestimmung der Strahlungsfunktion hochgeladener Krypton-Ionen. Verhandl. DPG (VI) **34**, 352, P15.8 (1999).

457. *Fuchs, T., P. Beiersdorfer*, C. Biedermann, G. Fußmann and R. Radtke:* Measurement of Radiative Cooling Rates for Highly Charged Krypton Using an Electron Beam Ion Trap. 18th Int. Conf. on X-Ray and Inner-Shell Processes, Chicago,IL 1999.

458. *Fußmann, G.:* Atom- und Molekülphysik. Vorlesung, Humboldt-Univ. Berlin, SS 1999.

459. *Fußmann, G.:* EBIT: Eine neue Quelle zur Erzeugung hochionisierter Atome. Berliner Physikal. Kolloquium der drei Universitäten, Berlin 1999.

460. *Fußmann, G.:* EBIT: Eine neue Quelle zur Erzeugung hochionisierter Atome. Kolloquium, Fritz-Haber-Inst., Berlin 1999.

461. *Fußmann, G.:* EBIT: Eine neue Quelle zur Erzeugung hochionisierter Atome. Kolloquium, Univ. Bochum 1999.

462. *Fußmann, G.:* Einschluss und Beobachtung hochionisierter Atome in einer EBIT-Quelle. Kolloquium, Forschungszentrum Jülich 1999.

463. *Fußmann, G.:* Evolution der Materie. Rotary-Club, Berlin 1999.

464. *Fußmann, G.:* Die Sonnenfinsternis 1999 – ein Jahrhundertereignis. Rotary-Club, Berlin 1999.

465. *Geier, A., K. Asmussen, A. Bard, H. Maier and R. Neu:* Eine Sublimationssonde zur Untersuchung des Divertorrückhaltevermögens für schwere Verunreinigungen. Verhandl. DPG (VI) **34**, 342, P6.3 (1999).

466. *Geiger, J., C.D. Beidler, V. Erckmann, U. Gasparino, H.P. Laqua, S.V. Kasilov*, H. Maaßberg, N.B. Marushchenko* and M. Romé*:* Fokker-Planck Estimation of Electron Distribution Functions for High Power ECCD at W7-AS. 12th Int. Stellarator Conf., Madison,WI 1999.

467. *Goldstraß, P. and C. Linsmeier:* Combined Ion and Electron Spectroscopy Study of the Surface Reactions of Beryllium with Carbon. 14th Int. Conf. on Ion Beam Analysis/Europ. Conf. on Accelerators in Appl. Research and Technology, Dresden 1999.

468. *Goldstraß, P. and C. Linsmeier:* Surface Reactions and Adlayer Formation on Beryllium after Carbon and Oxygen Bombardment. 4th IEA Int. Workshop on Beryllium Technology for Fusion, Karlsruhe 1999.

469. *Gori, S., J. Nührenberg, R. Zille, S. Okamura and K. Matsuoka:* Alpha-Particle Confinement Optimization in Quasi-Axisymmetric Configurations. 12th Int. Stellarator Conf., Madison,WI 1999.

470. *Grigull, P., M. Hirsch, K. McCormick, J. Baldzuhn, R. Brakel, S. Fiedler, C. Fuchs, L. Giannone, H.-J. Hartfuß, D. Hildebrandt, J. Kisslinger, R. König, G. Kühner, F. Wagner, H. Wobig and W7-AS Team:* A New H-Mode Operational Range in W7-AS. 12th Int. Stellarator Conf., Madison,WI 1999.

471. *Gruber, O.:* Collaborations and Remote Access on ASDEX Upgrade. Tripartite Workshop Collaborative Exploitation of Large Fusion Facilities, JET, Abingdon 1999.

472. *Gruber, O. and ASDEX Upgrade Team:* Advanced Tokamak Studies on ASDEX Upgrade. Seminar, ENEA, Frascati 1999.

473. *Gruber, O. and ASDEX Upgrade Team:* Internal Transport Barrier Discharges on ASDEX Upgrade: Progress towards Steady-State. Tripartite Workshop Advanced Scenarios with Internal Barriers, JET, Abingdon 1999.

474. *Gruber, O. and ASDEX Upgrade Team:* Internal Transport Barriers with Reactor-Relevant $T_e \approx T_i$. Joint Meeting of ITER Confinement Database and Modelling Expert Group, Transport and Internal Barrier Expert Group, Edge and Pedestal Physics Expert Group, JET, Abingdon 1999.

475. *Gruber, O. and ASDEX Upgrade Team:* Plasmas with Internal Barriers and Similar Electron and Ion Temperatures. Tripartite Workshop Advanced Scenarios with Internal Barriers, JET, Abingdon 1999.

476. *Gruber, O. and ASDEX Upgrade Team:* Thresholds for ITB Formation. Joint Meeting of ITER Confinement Database and Modelling Expert Group, Transport and Internal Barrier Expert Group, Edge and Pedestal Physics Expert Group, JET, Abingdon 1999.

477. *Gruber, O., R. Wolf, R. Dux, S. Günter, P. McCarthy, K. Lackner, M. Manso*, M. Maraschek, H. Meister, G. Pereverzev, W. Treutterer and ASDEX Upgrade Team:* Internal Transport Barrier Discharges on ASDEX Upgrade: Progress towards Steady-State. IAEA Techn. Comm. Meeting on H-Mode and Transport Barrier Physics, Oxford 1999.

478. *Gruber, O., R. Wolf, R. Dux, S. Günter, P. McCarthy, K. Lackner, M. Maraschek, H. Meister, G. Pereverzev, W. Treutterer and ASDEX Upgrade Team:* Quasi-Steady-State H-Mode and $T_e > T_i$ Operation with Internal Transport Barriers on ASDEX Upgrade. 2nd IAEA Techn. Comm. Meeting on Steady-State Operation of Magnetic Devices-Plasma Control and Plasma Facing Components, Fukuoka 1999.

479. *Grulke, O.:* Fluktuationen in toroidalen Plasmen. Seminarvortrag, Univ. Kiel, SS 1999.

480. *Grulke, O.:* Turbulence in KIWI and TEDDI. Workshop on Simulation of Turbulence in Low-Temperature Plasmas and Comparison with Experiment, Kiel 1999.

481. *Gubanka, E., H.-S. Bosch, W. Ullrich, M. Hoek* and ASDEX Upgrade Team:* Tritonen Burnup an ASDEX Upgrade. Verhandl. DPG (VI) **34**, 343, P6.6 (1999).

482. *Gude, A., S. Günter, M. Maraschek, S. Sesnic and ASDEX Upgrade Team:* Beobachtung von Fishbone-ähnlichen Frequenzsprüngen der neoklassischen Tearing Mode an ASDEX Upgrade. Verhandl. DPG (VI) **34**, 374, P26.3 (1999).

483. *Günter, S.:* Confinement Degrading MHD Instabilities on ASDEX Upgrade. Seminarvortrag, Culham 1999.

484. *Günter, S., A. Gude, M. Maraschek, S. Schade, S. Sesnic, Q. Yu*, H. Zohm and ASDEX Upgrade Team:* Theoretische und experimentelle Untersuchungen von neoklassischen tearing Moden an ASDEX Upgrade. Verhandl. DPG (VI) **34**, 347, P11.1 (1999).

485. *Hackl, A.:* Ein neues Netz am IPP. 16. DV-Tagung der Max-Planck-Institute, Göttingen 1999.

486. *Hallatschek, K., A. Zeiler and D. Biskamp:* Nonlocal Simulation of the Transition from Ballooning to ITG Mode Turbulence in the Tokamak Edge. 8th Europ. Fusion Theory Conf., Como 1999.

487. *Hallatschek, K., A. Zeiler, D. Biskamp, J.F. Drake* and B.N. Rogers*:* Nonlocal Simulation of the Transition from Ballooning to ITG Mode Turbulence in the Tokamak Edge. IAEA Techn. Comm. Meeting on First Principle Based Transport Theory, Kloster Seeon 1999.

488. *Hallatschek, K.:* Nonlocal Simulations of Tokamak Edge Turbulence. MPE-Tagung, Schloss Ringberg 1999.

489. *Hartfuß, H.-J.:* Plasmadiagnostik I, Wellen in Plasmen und aktive Mikrowellendiagnostiken. Univ. Greifswald, WS 1998/1999.

490. *Hartfuß, H.-J.:* Plasmadiagnostik II, Wellenführung an Drähten, in Hohlleitern und Gauß'sche Optik, Mikrowellentechnik. Univ. Greifswald, SS 1999.

491. *Hartfuß, H.-J.:* Plasmadiagnostik III, Radiometrie und passive Mikrowellendiagnostiken. Univ. Greifswald, WS 1999/2000.

492. *Hartfuß, H.-J. and W7-X Diagnostic Team:* Overview of the W7-X Diagnostic System. 12th Int. Stellarator Conf., Madison,WI 1999.

493. *Hartmann, D.A.:* Experimental Stellarator Physics. 4th Carolus Magnus Summer School on Plasma Physics, Maastricht 1999.

494. *Hartmann, D.A.:* Plasma Heating. Summer Univ. for Plasma Physics, Greifswald 1999.

495. *Hartmann, D.A.:* Results with the Double Strap Antenna on W7-AS. Coordinating Comm. Fast Waves, Garching 1999.

496. *Hartmann, D.A.:* Das Sonnenfeuer auf die Erde holen. Tag der offenen Tür, Max-Planck-Haus, München 1999.

497. *Hartmann, D.A., R. Brakel, V. Erckmann, S. Fiedler, C. Fuchs, L. Giannone, P. Grigull, H.-J. Hartfuß, K. Itoh, S.-I. Itoh, R. Jaenicke, R. König, H. Laqua, K. McCormick and F. Wagner:* Contributions of W7-AS to Steady-State Operation of Magnetic Fusion Devices. 2nd IAEA Techn. Comm. Meeting on Steady-State Operation of Magnetic Fusion Devices, Fukuoka 1999.

498. *Hartmann, D.A. and G. Cattanei:* Recent Results of ICRF Heating on the Stellarator W7-AS. 12th Int. Stellarator Conf., Madison,WI 1999.

499. *Hartmann, D.A., G. Cattanei, W7-AS Team and ICRH Group:* Comparison of RF Heating on the Stellarator W7-AS Using Different Antennas. US-Japan Workshop on RF Heating Technology and EU-Japan Workshop on Antenna/RF Source and Related Technology, Oh-arai 1999.

500. *Hartmann, D.A., G. Cattanei, W7-AS Team and ICRH Group:* Recent Progress with ICRF Heating on the Stellarator W7-AS. 12th Int. Stellarator, Conf. Madison,WI 1999.

501. *Hatzky, R.:* Nicht-lineare gyrokinetische Berechnungen von ITG-Moden. Theory Meeting, Zinnowitz 1999.

502. *Hatzky, R.:* Simulation of Ion-Temperature-Gradient-Driven (ITG) Modes: on the Way to W7-X. IAEA Techn. Comm. Meeting on First Principle Based Transport Theory, Kloster Seeon 1999.

503. *Heger*, B., U. Fantz*, K. Behringer, D.P. Coster and ASDEX Upgrade Team:* Messungen und Rechnungen zur Bedeutung der Wasserstoffmoleküle im ASDEX Upgrade Divertorplasma. Verhandl. DPG (VI) **34**, 374, P26.2 (1999).

504. *Heinemann, B., O. Vollmer, W. Kraus, P. Massmann*, P. McNeely, R. Riedl, E. Speth, R. Trainham* and R. Wilhelm:* Progress in the Development of RF Sources for NBI Heating Systems. 18th IEEE/NPSS Symp. on Fusion Engineering, Albuquerque,NM 1999.

505. *Heller*, R., W. Maurer* and W7-X Team:* Test Results for an Advanced Conductor for the Wendelstein 7-X Magnet System. 16th Int. Conf. on Magnet Technology, Jacksonville,FL 1999.

506. *Hildebrandt, D., L. Giannone, P. Grigull, J. Kisslinger, R. König, K. McCormick, D. Naujoks, W7-AS Team and NBI Group:* Limiter Thermography on the Stellarator W7-AS with Magnetic Island Topology at the Plasma Edge. 12th Int. Stellarator Conf., Madison,WI 1999.

507. *Hirsch, M., P. Grigull, H. Wobig, J. Kisslinger, K. McCormick, M. Anton, J. Baldzuhn, S. Fiedler, C. Fuchs, J. Geiger, L. Giannone, H.-J. Hartfuß, E. Holzhauer*, R. Jaenicke, M. Kick, H. Maaßberg, F. Wagner, A. Weller and W7-AS Team:* Operational Conditions and Characteristics of ELM-Events during H-Mode Plasmas in the Stellarator W7-AS. 7th IAEA Techn. Comm. Meeting on H-Mode and Transport Barrier Physics, Oxford 1999.

508. *Hirsch, M. and E. Holzhauer*:* Doppler Reflectometry for the Investigation of Poloidally Propagating Density Pertubations. 11th Joint Russian-German Meeting on ECRH and Gyrotrons, Karlsruhe, Stuttgart, Garching 1999.

509. *Hirsch, M., A. Weller and K. Toi*:* Global MHD in Stellarators. 11th General Conf. of the EPS: Trends in Physics, London 1999.

510. *Holzhauer*, E.:* On the Potential of Microwave Scattering Plasma Diagnostics. 11th Joint Russian-German Meeting on ECRH and Gyrotrons, Karlsruhe, Stuttgart, Garching 1999.

511. *Hopf, C., A. von Keudell and W. Jacob:* Oberflächen-Reaktionswahrscheinlichkeit von Radikalen aus Methan- und Acetylen-Plasmen. 9. Bundesdt. Fachtagung Plasmatechnologie, Stuttgart 1999, PS10.

512. *Huber*, A., W. Biel*, H.G. Esser*, R. Jaspers*, M. Lehnen*, G. Mank*, R. Neu, Ph. Mertens*, V. Phillips*, A. Pospieszczyk*, J. Rapp*, U. Samm*, B. Schweer*, B. Unterberg* and E. Vietzke*:* Untersuchung des Verunreinigungshaushaltes von TEXTOR 94 mit siliziumbeschichteter Wand. Verhandl. DPG (VI) **34**, 354, P18.2 (1999).

513. *Jacob, W.:* Ion-Induced Processes and Surface Reactions during Growth and Erosion of Hydrocarbons. TRANS-DIAM 1 Meeting, Amiens 1999.

514. *Jacob, W.:* Ion-Induced Processes and Surface Reactions during Growth and Erosion of Hydrocarbon Films. Materials Science Seminar, Federal Univ. of Rio de Janeiro 1999.

515. *Jacob, W.:* Review of Experimental Work in the Plasma Technology Group at IPP. Theoriekonzil, MPI für Extraterr. Physik, Garching 1999.

516. *Jacob, W., C. Hopf, A. von Keudell, M. Meier and T. Schwarz-Selinger:* Microscopic Processes at Carbonaceous Surfaces in Contact with Hydrogen Plasmas. Meeting on Modelling of Erosion/Deposition in the Plasma Boundary, Culham 1999.

517. *Jacob, W., C. Hopf, A. von Keudell and T. Schwarz-Selinger:* Surface Loss Probabilities of Neutral Hydrocarbon Radicals on Amorphous Hydrogenated Carbon Film Surfaces: What are the Dominant Growth Precursors in Plasma Deposition of a-C:H Films. TRANS-DIAM 1 Meeting, Amiens 1999.

518. *Jacob, W., C. Hopf, A. von Keudell and T. Schwarz-Selinger:* Surface Loss Probabilities of Neutral Hydrocarbon Radicals on Amorphous Hydrogenated Carbon Film Surfaces: What are the Dominant Neutral Growth Precursors in Plasma Deposition of a-C:H Films. Materials Science Seminar, Federal Univ. of Rio de Janeiro 1999.

519. *Jacob, W., C. Hopf, A. von Keudell, T. Schwarz-Selinger and B. Landkammer:* Surface Loss Probabilities of Hydrocarbon Radicals on Amorphous Hydrogenated Carbon Film Surfaces: Consequences for the Formation of Re-Deposited Layers in Fusion Experiments. NATO Advanced Research Workshop on Hydrogen Recycle at Plasma Facing Materials, St. Petersburg 1999.

520. *Jacob, W., A. von Keudell, T. Schwarz-Selinger and C. Hopf:* Surface Loss Probabilities of Neutral Hydrocarbon Radicals on Amorphous Hydrogenated Carbon Film Surfaces: Consequences for the Formation of Re-Deposited Layers in Fusion Experiments. ITER Seminar, Garching 1999.

521. *Jaenicke, R. and W7-AS Team:* Conclusions from Experiments with Large Toroidal Currents on W7-A and W7-AS. US-Japan Workshop Stellarator/Helical System Concept Improvement, Oak Ridge,TN 1999.

522. *Jaenicke, R. and W7-AS Team:* Overview on Recent W7-AS Results. 12th Int. Stellarator Conf., Madison,WI 1999.

523. *Jandl O.:* Modelling of Plasma Facing Components for the Fusion Experiment W7-X. ANSYS Users Meeting, Cejkovice 1999.

524. *Jüttner B.:* Apparition et Paramètres des Plasmas Denses Auprès des Électrodes d'Arc Électrique. Congrès Général de la Societé Française de Physique, Clermont-Ferrand 1999.

525. *Jüttner, B.:* Feldemission in elektrischen Entladungen im Vakuum. Fachdiskussion des VDE ITG-FA 8.6, Magdeburg 1999.

526. *Jüttner, B.:* Le Mouvement Rétrograde des Spot Cathodiques dans le Vide. Réunion EDF, Club Arc Électrique, Paris (Clamart) 1999.

527. *Jüttner, B.:* Physik der Elektrodenprozesse elektrischer Lichtbögen. Kolloquium, Techn. Univ. Chemnitz 1999.

528. *Jüttner B.:* Technische Plasmaphysik. Vorlesung, Humboldt- Univ. Berlin, WS 1998/99.

529. *Kallenbach, A.:* Plasmadiagnostik. Vorlesung, Univ. Hannover, WS 1998/1999.

530. *Kardaun, O.J.W.F.:* Importance of Using $q_{95}$ as Regressor Variable. ITER Confinement Database and Modeling Workshop, Garching 1999.

531. *Kardaun, O.J.W.F.:* Physical Error Propagation. ITER Confinement Database and Modeling Workshop, Garching 1999.

532. *Kardaun, O.J.W.F.:* Physical Regression with Errors in Variables. ITER Confinement Database and Modeling Workshop, JET, Abingdon 1999.

533. *Kardaun, O.J.W.F.:* Plasma Shape Dependence of the Thermal Energy. ITER Confinement Database and Modeling Workshop, JET, Abingdon 1999.

534. *Kardaun, O.J.W.F.:* Point and Interval Predection of Energy Confinement in ITER: a Case for ITERH-98P(y,2). ITER Confinement Database and Modeling Workshop, JET, Abingdon 1999.

535. *Kastelewicz, H.:* Numerische Plasmamodellierung für den linearen Plasmagenerator PSI-1. Univ. Düsseldorf 1999.

536. *Kaufmann, M.:* Die Bedeutung der ASDEX Upgrade Experimente für ITER. Jahrestagung Kerntechnik, Karlsruhe 1999.

537. *Kaufmann, M.:* Einführung in die Plasmaphysik und Fusionsforschung II. Vorlesung, Univ. Bayreuth, SS 1999.

538. *Kaufmann, M.:* Fusion Research on ASDEX Upgrade. Kolloquium, Athens 1999.

539. *Kaufmann, M.:* Sollen wir die gleiche Quelle, die die Sonne mit Energie versorgt, als Energiequelle auf der Erde entwickeln? Garching 1999.

540. *Kendl, A., B.D. Scott and H. Wobig:* Simulation of Drift-Alfvén Turbulence in Advanced Stellarator Geometry. 12th Int. Stellarator Conf., Madison,WI 1999.

541. *Kendl, A., H. Wobig and B.D. Scott:* Geometrische Effekte in der Mikroturbulenz. Verhandl. DPG (IV) **34**, 342, P5.6 (1999).

542. *Kendl, A.:* Geometrische Effekte in der Mikroturbulenz. Workshop on Simulation of Turbulence in Low-Temperature Plasmas and Comparison with Experiment, Kiel 1999.

543. *Kendl, A.:* Randschichtturbulenz in Wendelstein 7-X. Theory Meeting, Zinnowitz 1999.

544. *Kendl, A.:* Transition from Tokamak to Stellarator Turbulence. 8th Europ. Fusion Theory Conf., Como 1999.

545. *Kersten*, H., D. Rohde*, P. Pecher, W. Jacob and R. Hippler*:* Untersuchungen zum Energieeinstrom bei der a-C:H Schichtabscheidung: Vergleich zwischen ECR-Plasma und Magnetronsputtern. 9. Bundesdt. Fachtagung Plasmatechnologie, Stuttgart 1999, PD11.

546. *Keudell, A. von:* Auf der Suche nach dem Wachstumsprecusor in Beschichtungsplasmen. Univ. Essen 1999.

547. *Keudell, A. von:* Surface Loss Probabilities of $CH_x$ Radicals: Consequences for the Formation of Co-Deposited Layers in Fusion Experiments. EU Meeting on Plasma Wall Interaction, Jülich 1999.

548. *Keudell, A. von:* Surface Loss Probabilities of $CH_x$ Radicals: Consequences for the Formation of Co-Deposited Layers in Fusion Experiments. 10th Workshop SOL and Divertor Physics ITER Expert Group, Garching 1999.

549. *Keudell, A. von:* Surface Mechanisms during Growth of a-Si:H Films. 14th Int. Symp. on Plasma Chemistry, Prag 1999.

550. *Keudell, A. von:* Surface Processes during Thin Film Growth. Erasmus Summer School 99, Eindhoven 1999.

551. *Keudell, A. von:* Surface Reactions of $CH_x$ Radicals. Univ. Erlangen 1999.

552. *Keudell, A. von:* Surface Reactions of $CH_x$ Radicals in Low Temperature Plasmas. Univ. Greifswald 1999.

553. *Keudell, A. von:* Surface Reactions of $SiH_x$ and $CH_x$ Radicals during Growth of a-Si:H and a-C:H Films. AVS Fall Meeting, Seattle,WA 1999.

554. *Keudell, A. von and J.R. Abelson*:* Interaction of $SiH_3$ Radicals with a-Si:H Surfaces, Monitored by In-situ Real-Time Infrared Absorption Spectroscopy. Workshop Frontiers in Low Temperature Plasma Diagnostics III, Saillon 1999.

555. *Keudell, A. von, C. Hopf and W. Jacob:* Oberflächen-reaktionswahrscheinlichkeit der dominanten Wachstumsspezies in Methan- und Acetylen-Plasmen. VI. Erfahrungsaustausch „Oberflächentechnologie mit Plasmaprozessen", Mühlleithen 1999.

556. *Kisslinger, J., C.D. Beidler, E. Strumberger and H. Wobig:* Low Aspect Ratio Helias Configurations. 12th Int. Stellarator Conf., Madison,WI 1999.

557. *Kleberg, I. and B. Jüttner:* Mikroskopische Eigenschaften der Brennfleckbewegung bei externem Magnetfeld. Verhandl. DPG (VI) **34**, 369, P24.14 (1999).

558. *Kleiber, R.:* Resistive Drift-Mode-Instability for a Sequence of l=2 Stellarators. IAEA Techn. Comm. Meeting on First Principle Based Transport Theory, Kloster Seeon 1999.

559. *Knauer, J.P., G. Kühner, J. Baldzuhn, S. Fiedler, C. Fuchs, L. Giannone, M. Hirsch, K. McCormick, A. Weller, C. Wendland and W7-AS Team:* Densitiy Profile Effects in "H-Mode" Discharges Observed by High Resolution Thomson Scattering at W7-AS. 12th Int. Stellarator Conf., Madison,WI 1999.

560. *Kohl, A.:* Morphologie und Oberflächenreaktionen an Rh/Vox/SiO2-Modellkatalysatoren. 32. Jahrestreffen dt. Katalytiker, Friedrichroda 1999.

561. *Kohl, A.:* Surface Analytical and Catalytic Investigations of Rh/Vox/SiO2 Model Catalysts. Summer School on Surface Science: Understanding Catalysis, Dronten 1999.

562. *Kohl, A., S. Labich, E. Taglauer and H. Knözinger*:* Agglomeration of Supported Rhodium on Model Catalysts. 18th Europ. Conf. on Surface Science, Vienna 1999.

563. *Kolovos-Vellianitis*, D., Th. Kammler* and J. Küppers:* Interaction of Gaseous H Atom with Cu(100) Sufaces: Adsorption, Absorption, and Abstraction. 18th Europ. Conf. on Surface Science, Vienna 1999.

564. *Könies, A.:* Investigation of a Kinetic Energy Principle in Three Dimensional Geometrie. Int. Sherwood Theory Conf., Atlanta,GA 1999.

565. *König, R., H.-J. Hartfuß and W7-X Diagnostic Team:* Overview of the W7-X Diagnostic System. 12th Int. Stellarator Conf., Madison,WI 1999.

566. *König, R., K. McCormick, P. Grigull, A. Werner, Y. Feng, D. Hildebrandt, J. Kisslinger, J.P. Knauer, G. Kühner, D. Naujoks, J. Sallander, F. Sardei, F. Wagner and W7-AS Team:* Island Divertor Investigations on the W7-AS Stellarator. 12th Int. Stellarator Conf., Madison,WI 1999.

567. *Kottmair*, A., U. Fantz* und K. Behringer:* VUV-Emissionsspektroskopie an mikrowellenangeregten $H_2$- und $D_2$-Plasmen. Verhandl. DPG (V) **34**, 357, P20.14 (1999).

568. *Kraus, W.:* Status of RF Source Development for Negative Ions. Joint Development Comm. Meeting, JET, Abingdon 1999.

569. *Kraus, W.:* Status of the RF Source Development for the W7-AS Radial Injector and for Negative Ions. Super Joint Development Comm. Meeting, JAERI, Naka 1999.

570. *Krieger, K.:* Comparison of Low-Z and High-Z Wall Materials. EU Meeting on Plasma-Wall Interaction, Jülich 1999.

571. *Krieger, K.:* Materialien für die erste Wand in Fusionsmaschinen mit magnetischem Einschluß. Kolloquium, Forschungszentrum Karlsruhe 1999.

572. *Krieger, K., A. Bard, A. Geier, U. von Toussaint and ASDEX Upgrade Team:* Direkte Messung von Kohlenstofferosionsraten im Divertor von ASDEX Upgrade. Verhandl. DPG (VI) **34**, 338, P2.1 (1999).

573. *Lackner, K.:* The Case for the Next Step. Vortrag, Thermonuclear Tokamak Panel, Paris 1999.

574. *Lackner, K.:* Prospects of Magnetic Confinement Fusion. 4th Carolus Magnus Summer School on Plasma Physics, Maastricht 1999.

575. *Lackner, K.:* Stand und Perspektiven der kontrollierten Kernfusion. Kolloquium, Univ. Würzburg 1999.

576. *Landkammer, B., P. Pecher and W. Jacob:* Variation des Ionenflusses aus einem ECR-$O_2$-Plasma durch Edelgasbeimischung. 9. Bundesdt. Fachtagung Plasmatechnologie, Stuttgart 1999, PS23.

577. *Lang, P.T.:* Efficient Plasma Refueling Using Pellets. Large Tokamak Seminar, JAERI, Naka 1999.

578. *Lang, P.T.:* Pellet Injection Technology at IPP and JET. Seminarvortrag, JAERI, Naka 1999.

579. *Lang, P.T., J. Gafert, M. Maraschek, H. Murmann, J. Neuhauser, H. Salzmann, J. Schweinzer and ASDEX Upgrade Team:* Operationsgrenzen in H-Mode-Entladungen mit Pelletnachfüllung. Verhandl. DPG (VI) **34**, 339, P3.2 (1999).

580. *Lang, R.S., W. Beck, P. Cierpka, P.T. Lang, A. Lorenz, V. Mertens and G. Weber:* $D_2$-Pelletinjektor auf der Basis des Leidenfrost-Effektes. Verhandl. DPG (VI) **34**, 284, K2.4 (1999).

581. *Laqua, H. and F. Schneider:* Improvement of Diamagnetic Loop Measurements in Stellarators Using Digital Signal Processing Techniques. 2nd IAEA Techn. Comm. Meeting on Control, Data Acquisition and Remote Participation for Fusion Research, Lisbon 1999.

582. *Laqua, H.P.:* Fusionsplasmen. Vorlesungsreihe zur Plasmatechnologie, Fachhochschule Stralsund, WS1999/2000.

583. *Laqua, H.P.:* Overview on ECRH Experiments at the Wendelstein-AS Stellarator. 12th Int. Stellarator Conf., Madison,WI 1999.

584. *Laqua, H.P.:* Plasma Waves. Summer Univ. for Plasma Physics, Greifswald 1999.

585. *Laqua, H.P.:* Die Sonne als Vorbild. Schulvortrag, Hildegardis Gymnasium, Bochum 1999.

586. *Laqua, H.P., V. Erckmann, C. Fuchs and W. Kasparek*:* High Field Launch ECRH Experiments at the Wendelstein-AS Stellarator. 11th Joint Russian-German Meeting on ECRH and Gyrotrons, Karlsruhe, Stuttgart, Garching 1999.

587. *Laqua, H.P. and H. Maaßberg:* Non-Linear ECRH Absorption Experiments at the Wendelstein-AS Stellarator. 11th Joint Russian-German Meeting on ECRH and Gyrotrons, Karlsruhe, Stuttgart, Garching 1999.

588. *Lederer, H.:* Höchstleistungsrechnen für die Grundlagenforschung in der Max-Planck-Gesellschaft. Statustagung des BMBF, HPSC 99, Bonn 1999.

589. *Lederer, H.:* Metacomputing in German Testbeds: Gigabit Testbed South. 2nd Metacomputing Workshop, Stuttgart 1999.

590. *Lederer, H.:* Parallelisierung von LAPW und Leistungsvergleich T3E/SX-5. Herbsttreffen des Arbeitskreises Supercomputing des ZKI, Univ. Düsseldorf 1999.

591. *Lederer, H.:* Stand der Gigabitprojekte mit MPG-Beteiligung. 16. DV-Tagung der Max-Planck-Institute, Göttingen 1999.

592. *Leuterer, F.:* The ASDEX Upgrade ECRH System. Nat. Inst. for Fusion Science, Toki 1999.

593. *Leuterer, F.:* ECRH Experiments in ASDEX Upgrade. Far Infrared Centre, Fukui Univ. 1999.

594. *Leuterer, F.:* ECRH Experiments in ASDEX Upgrade. Kyoto Univ. 1999.

595. *Leuterer, F.:* ECRH Experiments in ASDEX Upgrade. Meeting of Japan. Univ., Plasma Physics Lab., Nat. Inst. for Fusion Science, Toki 1999.

596. *Leuterer, F.:* Experiments with ECRH in ASDEX Upgrade. JAERI, Naka 1999.

597. *Leuterer, F.:* Simultaneous Attainment of High Electron and Ion Temperatures in ITB Discharges in ASDEX Upgrade. 11th Joint Russian-German Meeting on ECRH and Gyrotrons, Karlsruhe, Stuttgart, Garching 1999.

598. *Leuterer, F.:* X-1-Mode Current Drive and Prospects for LHD. Nat. Inst. for Fusion Science, Toki 1999.

599. *Leuterer, F., F. Monaco, M. Münich and H. Schütz:* Calorimetric Measurements of ECRH Power Transmission at ASDEX Upgrade. 11th Joint Russian-German Meeting on ECRH and Gyrotrons, Karlsruhe, Stuttgart, Garching 1999.

600. *Leuterer, F., G. Gantenbein*, S. Günter, M. Maraschek, F. Ryter, W. Suttrop, R. Wolf, H. Zohm and ASDEX Upgrade Team:* ECRH Experiments in ASDEX Upgrade. 11th Joint Workshop on ECE and ECRH, Oh-arai 1999.

601. *Leuterer, F., M. Beckmann, H. Brinkschulte, F. Monaco, M. Münich, F. Ryter, L. Empacher*, G. Gantenbein*, W. Förster*, W. Kasparek*, P. Schüller*, K. Schwörer*, A. Borchegowski*, A. Fix*, V. Illin*, L. Popov*, V. Sigalaev* and E. Tai*:* Experience with the ECRH System of ASDEX Upgrade. 11th Joint Workshop on ECE and ECRH, Oh-arai 1999.

602. *Linsmeier, C.:* X-Ray Photoelectron Spectroscopy. 14th Int. Conf. on Ion Beam Analysis/Europ. Conf. on Accelerators in Appl. Research and Technology, Dresden 1999.

603. *Linsmeier, C., R. Behrisch, W. Eckstein and K. Schmid:* Sputtering of a Chromium Layer during Analysis with 10 MeV Silicon Ions. 14th Int. Conf. on Ion Beam Analysis/Europ. Conf. on Accelerators in Appl. Research and Technology, Dresden 1999.

604. *Linsmeier, C. and J. Wanner*:* Reactions of Oxygen Atoms and Molecules with Au, Be, and W Surfaces. 18th Europ. Conf. on Surface Science, Vienna 1999.

605. *Lorenz, A., W. Beck, P. Cierpka, P.T. Lang, R.S. Lang and G. Weber:* Untersuchung der Vorgänge beim Auftreffen von $D_2$-Pellets auf starre Wände. Verhandl. DPG (VI) **34**, 284, K2.3 (1999).

606. *Luthin, J. and C. Linsmeier:* Carbon Films and Carbide Formation on Tungsten. 18th Europ. Conf. on Surface Science, Vienna 1999.

607. *Maaßberg, H.:* Stellarator Kinetic Theory. 4th Carolus Magnus Summer School on Plasma Physics, Maastricht 1999.

608. *Maaßberg, H.:* Stellarator Kinetic Theory. Theory Meeting, Zinnowitz 1999.

609. *Maaßberg, H., C.D. Beidler, V. Erckmann, U. Gasparino, H. Laqua, N. Marushchenko*, S. Murakami* and W7-AS Team:* ECRH and ECCD at High Power Density at W7-AS. 4th Int. Workshop on Strong Microwaves in Plasmas, Nizhny Novgorod 1999.

610. *Maaßberg, H., C.D. Beidler, V. Erckmann, U. Gasparino, H.P. Laqua, S. Murakami* and W7-AS Team:* The ECRH-Driven Electron Root Feature. 11th Joint Russian-German Meeting on ECRH and Gyrotrons, Karlsruhe, Stuttgart, Garching 1999.

611. *Maaßberg, H, V. Erckmann, U. Gasparino, H.P. Laqua, N. Marushchenko* and W7-AS Team:* High Power Density ECCD at the W7-AS Stellarator. 11th Joint Russian-German Meeting on ECRH and Gyrotrons, Karlsruhe, Stuttgart, Garching 1999.

612. *Maier, H.:* Erosion/Deposition and Deuterium Retention in the ASDEX Upgrade Divertor. 10th Workshop of the SOL and Divertor Physics ITER Expert Group, Garching 1999.

613. *Maier, H., A. Tabasso, K. Krieger, V. Rohde, J. Roth and ASDEX Upgrade Team:* Deuterium-Inventare in verschiedenen Divertor-Konfigurationen von ASDEX Upgrade. Verhandl. DPG **(VI) 34**, 365, P22.1 (1999).

614. *Maraschek, M., A. Gude, S. Günter, P.T. Lang, H.W. Müller, S. Sesnic and ASDEX Upgrade Team:* Pellet-induzierte neoklassische Tearing Moden bei hoher Dichte. Verhandl. DPG (VI) **34**, 374, P26.4 (1999).

615. *McCormick, K., J. Baldzuhn, S. Fiedler, L. Giannone, P. Grigull, H.-J. Hartfuß, D. Hildebrandt, J.P. Knauer, G. Kühner, R. König, D. Naujoks and J. Sallander:* Edge Diagnostics Overview for the W7-AS Divertor Phase. 12th Int. Stellarator Conf., Madison,WI 1999.

616. *Meir*, S., U. Fantz* und K. Behringer:* Vergleich von Messungen und Rechnungen der Balmer-Linienverhältnisse in Niederdruckplasmen. Verhandl. DPG (VI) **34**, 357, P20.13 (1999).

617. *Meister, H., A. Kallenbach, J. Stober and ASDEX Upgrade Team:* Charakterisierung der internen Transportbarriere mittels Ladungsaustauschspektroskopie an ASDEX Upgrade. Verhandl. DPG (VI) **34**, 343, P7.2 (1999).

618. *Mertens*, Ph. und R. König:* Laserinduzierte Fluoreszenz in Divertor und Randschicht. Workshop on W7-X Diagnostics, Schloss Ringberg 1999.

619. *Meyer-Spasche, R.:* Analysis und Numerik von Erhaltungsgleichungen. Vorlesung, Techn. Univ. München, SS 1999.

620. *Meyer-Spasche, R.:* Invention as Tool for Discovery: Mathematical Modeling of Taylor Vortex Flows. 5. Österr. Symp. zur Geschichte der Mathematik, Neuhofen an der Ybbs 1999.

621. *Meyer-Spasche, R.:* Nichtlineare Eigenwertprobleme - Theorie und Numerik. Vorlesung, Techn. Univ. München, WS 1999/2000.

622. *Meyer-Spasche, R. and F. Pohl:* Secondary Bifurcations of Steady Flows Revisited. 11th Int. Couette-Taylor Workshop, Bremen 1999.

623. *Michel, G., M. Kuntze*, B. Piosczyk* and M. Thumm*:* Considerations on Multimode Quasi-Optical Converters. 24th Int. Conf. on Infrared and Millimeter Waves, Monterey 1999.

624. *Michel, G., M. Kuntze*, B. Piosczyk* and M. Thumm*:* Design Issues of Broadband Quasi-Optical Mode Converters. 11th Joint Russian-German Meeting on ECRH and Gyrotrons, Karlsruhe, Stuttgart, Garching 1999.

625. *Milch, I.:* Energie aus dem Sternenfeuer – Kernfusionsforschung. Frauen führen Frauen. Deutsches Museum, München 1999.

626. *Milch, I.:* Fusionsforschung mit WENDELSTEIN 7-X in Greifswald. Fortbildungsveranstaltung für Stadtführer, VHS Greifswald 1999.

627. *Müller, H.W., M. Kaufmann, P.T. Lang, R.S. Lang, A. Lorenz, V. Mertens, J. Neuhauser and ASDEX Upgrade Team:* Nachweis der Hoch-β-Plasmoid Drift bei Pelletinjektion in Plasmen mit toroidalem Magnetfeldeinschluß. Verhandl. DPG (VI) **34**, 340, P3.4 (1999).

628. *Münich, M., M. Beckmann, F. Brandl, H. Brinkschulte, F. Leuterer, F. Monaco, F. Ryter and H. Schütz:* Status of the ECRH System Construction at ASDEX Upgrade. 11th Joint Russian-German Meeting on ECRH and Gyrotrons, Karlsruhe, Stuttgart, Garching 1999.

629. *Neilson*, G., A. Reiman*, M. Zarnstorff*, A. Brooks*, G.Y. Fu*, R. Goldston*, L.P. Ku*, Z. Lin*, R. Majeski*, D.A. Monticello*, H. Mynick*, N. Pomphrey*, M. Redi*, W. Reiersen*, J. Schmidt*, S. Hirshman*, J.F. Lyon*, A. Berry*, B.E. Nelson*, R. Sanchez*, D. Spong*, A. Boozer*, W. Miner*, P. Valanju*, W.A. Cooper*, M. Drevlak, P. Merkel and C. Nührenberg:* Physics Basis for High-Beta, Low-Aspect-Ratio Stellarator Plasmas. 41st Annual Meeting of the Division of Plasma Physics of the APS, Seattle,WA 1999.

630. *Nelson-Melby*, E., P.T. Bonoli*, A.E. Hubbard*, M. Porkolab*, S.J. Wukitch* and M. Brambilla:* Mode Conversion Electron Heating Using GSVD Analysis. Bull. Am. Phys. Soc. **44**, 205 (1999).

631. *Neu, G., V. Mertens, G. Raupp, W. Treutterer, D. Zasche, T. Zehetbauer and ASDEX Upgrade Team*: A Configuration Environment for the ASDEX Upgrade Control System. Int. Conf. on Accelerator and Large Experimental Physics Control Systems, Trieste 1999.

632. *Neu, R.:* Diagnostics for Fusion Plasmas. Summer Univ. for Plasma Physics, Greifswald 1999.

633. *Neu, R.:* Einführung in die Plasmaphysik (Plasmaphysik I). Vorlesung, Univ. Tübingen, WS 1999/2000.

634. *Neu, R.:* Fusionsforschung (Plasmaphysik II). Vorlesung, Univ. Tübingen, SS 1999.

635. *Neu, R.:* Future Works on Plasma Wall Interaction at ASDEX Upgrade. EU Meeting on Plasma Wall Interaction, Jülich 1999.

636. *Neu, R.:* Kernfusion - Energiequelle der Zukunft? Studium Generale, Univ. Tübingen, SS 1999.

637. *Neu, R., V. Rohde, R. Dux, A. Bard, H.G. Esser*, A. Kallenbach, K. Krieger, H. Maier, V. Philipps*, D. Schlögl, U. Wenzel and ASDEX Upgrade Team:* Ergebnisse der Silizierung an ASDEX Upgrade. Verhandl. DPG (VI) **34**, 354, P18.1 (1999).

638. *Niedner, S., B.D. Scott, A. Kendl and U. Stroth:* Shear and Curvature in TJ1-U. Workshop on Simulation of Turbulence in Low-Temperature Plasmas and Comparison with Experiment, Kiel 1999.

639. *Nöthe*, M., F. Koch, H.J. Penkalla*, W.P. Rehbach* and H. Bolt:* Investigation of the Structure and Properties of a-C:H Films with Metal and Si-Containing Interlayers. 2nd Asean-Europ. Conf. on Plasma Surface Engineering, Beijing 1999.

640. *Noterdaeme, J.-M.:* Compatibility Issues between Heating Systems. Europ. Programme Workshop, Kloster Seeon 1999.

641. *Noterdaeme, J.-M.:* Influence of the Heating Method on Sawteeth in a Tokamak Plasma. Vorlesung, Univ. of Gent 1999.

642. *Noterdaeme, J.-M.:* Sawtooth Behaviour in H/$He^3$ ICRH Mode Conversion Heated Plasmas. Coordinating Comm. on Fast Waves, Brussels 1999.

643. *Noterdaeme, J.-M.:* Variation of the ICRF Resonance Position. Effect on the Plasma. Coordinating Committee on Fast Waves, Culham 1999.

644. *Noterdaeme, J.-M., R. Wolf and F. Leuterer:* ASDEX Upgrade, Overview of Recent ICRF Results, Plans for ICRF CD and Advanced Scenarios. ITER Physics Expert Group Meeting on Fast Particles, Cadarache 1999.

645. *Nührenberg, J.:* Neuere Fragen in der Stellaratortheorie. Greifswald-Rostock Seminar, Rostock 1999.

646. *Nührenberg, J.:* New German-European Magnetic Fusion Centre Greifswald. Nuclear Fusion Inst., Kurchatov Inst., Moscow 1999.

647. *Nührenberg, J.:* Theoretische Physik III: Elektrodynamik. Vorlesung, Univ. Greifswald, WS 1998/99.

648. *Nührenberg, J.:* Das Wendelstein 7-X Projekt. Univ. Greifswald 1999.

649. *Nührenberg, J., U. Schwenn and E. Strumberger:* Neoclassical Transport in Stellarators. IAEA Techn. Comm. Meeting on First Principle Based Transport Theory, Kloster Seeon 1999.

650. *Ott, W., D.A. Hartmann, P. McNeely, F.-P. Penningsfeld, E. Speth, NI Group and W7-AS Team:* Plasma Generation in W7-AS Stellarator by Neutral Beams Alone. Super Joint Development Comm. Meeting, JAERI, Naka 1999.

651. *Ott, W., F.-P. Penningsfeld, C. Fuchs, L. Giannone, H.-J. Hartfuß, J.P.T. Koponen*, W. Kraus, E. Speth, NI Group and W7-AS Team:* Neutral Beam Power Deposition Profiles in W7-AS Stellarator: Comparison of Theory and Experiment. Super Joint Development Comm. Meeting, JAERI, Naka 1999.

652. *Paulin*, H., U. Fantz* und K. Behringer:* Bestimmung der Ausbeute der chemischen Erosion von Kohlenstoffmaterialien in $H_2$- und $D_2$-Plasmen. Verhandl. DPG (VI) **34**, 365, P22.2 (1999).

653. *Pecher, P.:* Modeling of the Composition of the Ion Flux Emanating from a Methane Electron Cyclotron Resonance Plasma. Workshop on Frontiers in Low Temperature Plasma Diagnostics III, Saillon 1999.

654. *Pecher, P. and V. Dose:* Elektronentemperaturen und chemische Ratenkoeffizienten aus Ionenmassenspektren. IPF/IPP-Seminar Techn. Anwendung von Plasmen, Garching 1999.

655. *Pecher, P. and V. Dose:* Neue Elektronenstoß-Wirkungsquerschnitte und Ratenkoeffizienten für Methan und Wasserstoff. 9. Bundesdt. Fachtagung Plasmatechnologie, Stuttgart 1999, PD9.

656. *Pecher, P. and W. Jacob:* Wie entstehen schwere Ionen in Methanplasmen? 9. Bundesdt. Fachtagung Plasmatechnologie, Stuttgart 1999, PD10.

657. *Pecher, P., B. Landkammer and W. Jacob:* Welche Teilchen treffen aus einem Sauerstoffplasma auf das Substrat? VI. Erfahrungsaustausch „Oberflächentechnologie mit Plasmaprozessen", Mühlleithen 1999.

658. *Peeters, A.G.:* Kinetic Theory. Summer Univ. for Plasma Physics, Greifswald 1999.

659. *Phillips*, C.K., D. Clark*, J.C. Hosea*, B. LeBlanc*, D. McCune*, G. Schilling*, J.R. Wilson*, P.T. Bonoli* and M. Brambilla:* Modeling of ICRF Experiments in C-Mod. Bull. Am. Phys. Soc. **44**, 206 (1999).

660. *Pinches, S.D., S. Günter, M. Maraschek, S. Sesnic and ASDEX Upgrade Team:* Simulations of Fast Particles Behaviour during Fishbones in ASDEX Upgrade. Bull. Am. Phys. Soc. **44**, 1628 (1999).

661. *Pinches, S.D. and A. Könies:* Wave-Particle Interactions in 3D Geometry. 7th Europ. Fusion Physics Workshop, Kloster Seeon 1999.

662. *Pinkau, K.:* Auf dem Weg zur Fusion: Zielorientierte Grundlagenforschung. MPG Heidelberg 1999.

663. *Pinkau, K.:* Towards a Burning Fusion Plasma. IPP, Schloß Blutenburg, München 1999.

664. *Pinkau, K.:* Wirklichkeit. Kath. Akad. Thüringen, Bad Kösen 1999.

665. *Pinkau, K.:* Zukunft der Forschung - Zukunft der Aufklärung. Radiokulturhaus, Vienna 1999.

666. *Poli, E., A.G. Peeters and G. Pereverzev:* Electromagnetic Beam Propagation in Anisotropic Inhomogeneous Plasmas. 11th Joint Russian-German Meeting on ECRH and Gyrotrons, Karlsruhe, Stuttgart, Garching 1999.

667. *Poli, E., G. Pereverzev, A.G. Peeters and M. Bornatici*:* EC Beam Tracing in Fusion Plasmas. 11th Joint Workshop on ECE and ECRH, Oh-arai 1999.

668. *Pospieszczyk*, A. and R. König:* Hochauflösende Spektroskopie. Workshop on W7-X Diagnostics, Schloss Ringberg 1999.

669. *Preuss, R. and V. Dose:* Einschlußskalierung verschiedener Stelleratoren. Verhandl. DPG (VI) **34**, 343, P7.3 (1999).

670. *Preuss, R., P. Pecher and V. Dose:* Handling Discordant Data Sets. 19th Int. Conf. on Maximum Entropy and Bayesian Methods, Boise,ID 1999.

671. *Puri, S.:* Anomalous Enhanced Transport via Kirchhoff Radiation. Joint US-EU TTF Meeting, Portland,OR 1999.

672. *Puri, S.:* Anomalous Transport via Kirchhoff Radiation. IAEA Techn. Comm. Meeting Workshop on First Principle Based Plasma Transport Theory, Kloster Seeon 1999.

673. *Raupp, G. and ASDEX Upgrade Team:* Die Steuerung des Tokamaks ASDEX Upgrade: Vom Experiment zum Reaktor. Kolloquium, IPF Stuttgart 1999.

674. *Redi*, M., A. Diallo*, J.L. Johnson*, G.Y. Fu*, L.P. Ku*, N. Pomphrey*, A. Reiman*, R. White*, M. Zarnstorff*, C. Nührenberg, W.A. Cooper* and NCSX Team*:* Robustness and Flexibility in NCSX: Global Ideal MHD Stability and Energetic Particle Transport. 12th Int. Stellarator Conf., Madison,WI 1999.

675. *Redi*, M., G.Y. Fu*, D.A. Monticello*, N. Pomphrey*, C. Nührenberg and W.A. Cooper*:* Calculation of Vertical Stability for Quasi-Axial Stellarators. Sherwood Theory Meeting, Sherwood 1999.

676. *Reiman*, A., B. Blackwell*, A. Boozer*, A. Brooks*, W.A. Cooper*, M. Drevlak, G.Y. Fu*, R. Goldston*, J. Harris*, S. Hirshman*, M. Isaev*, C. Kessel*, L.P. Ku*, Z. Lin*, J.F. Lyon*, P. Merkel, M. Mikhailov*, W. Miner*, D.A. Monticello*, H. Mynick*, N. Nakajima*, G. Neilson*, C. Nührenberg, M. Okamoto*, N. Pomphrey*, M. Redi*, W. Reiersen*, R. Sanchez*, J. Schmidt*, D. Spong*, A. Subbotin*, P. Valanju*, K.Y. Watanabe*, R. White* and M. Zarnstorff*:* Plasma Configuration Design of the National Compact Stellarator Experiment (NCSX). 12th Int. Stellarator Conf., Madison,WI 1999.

677. *Reimbold, S., B. Wolle*, A. Weller*, M. Kick and K. Hübner*:* Einschluß und Verluste schneller Teilchen an W7-AS. Verhandl. DPG (IV) **34**, 343, P6.7 (1999).

678. *Reinecke, N. and E. Taglauer:* The Kinetics of Oxygen-Induced Faceting of Cu(115) and Cu(119) Surfaces. 18th Europ. Conf. on Surface Science, Vienna 1999.

679. *Renner, H., J. Boscary, V. Erckmann, H. Greuner, H. Grote, J. Sapper, E. Speth, F. Wesner, M. Wanner and W7-X Team:* The Capabilities of Steady State Operation at the Stellarator W7-X with Emphasis on the Divertor Design. 2nd IAEA Techn. Comm. Meeting on Steady-State Operation of Magnetic Fusion Devices, Fukuoka 1999.

680. *Reuter H.:* Mass Storage System and AFS. Decorum '99, New Orleans,LA 1999.

681. *Riedl, R.:* 100 kV Operation of the Second AUG Injector. Joint Development Comm. Meeting, JET, Abingdon 1999.

682. *Rodriguez*, M., J. Pascual*, S. Bäumel and H.L. Hartnagel*:* A New Approach to Imaging Techniques for ECE Radiometry: A Subharmonic Mixer Array with On-Chip Pumping Power. 7th Int. Symp. on Recent Advances in Microwave Technology, Malaga 1999.

683. *Roth, J.:* Tritium Codeposition: Mechanisms for the Formation of Redeposited Layers. IAEA Advisory Group Meeting on "Critical Assessment of Tritium Detention in Fusion Reactor Materials", Vienna 1999.

684. *Roth, J., K. Ertl and C. Linsmeier:* Beschleunigeranalysen am IPP. Beschleunigerseminar, Garching 1999.

685. *Roth, J.:* Problems of Material Mixing in Plasma-Wall-Interactions. Particle Surface Interaction Group, Nat. Laboratories, Oak Ridge,TN 1999.

686. *Roth, J.:* Material for the First Wall of Future Fusion Devices. Univ. of Vanderbuilt 1999.

687. *Roth, J. and M. Balden:* Chemical Erosion of Si, C and SiC under H+ Bombardment. EU-PSI Meeting, Jülich 1999.

688. *Ryter, F., R. Brückner, B. Brüsehaber, F. Leuterer, G. Pereverzev, J. Schweinzer, W. Suttrop and ASDEX Upgrade Team:* Transport Studies with ECRH in ASDEX Upgrade. 11th Joint Russian-German Meeting on ECRH and Gyrotrons, Karlsruhe, Stuttgart, Garching 1999.

689. *Ryter, F., F. Leuterer, M. Beckmann, H. Brinkschulte, R. Brückner, B. Brüsehaber, F. Monaco, M. Münich, G. Pereverzev, H. Schütz, W. Suttrop and ASDEX Upgrade Team:* ECRH Experiments in the ASDEX Upgrade Tokamak. 4th Int. Workshop on Strong Microwaves in Plasmas, Nizhny Novgorod 1999.

690. *Saarelma*, S., S. Günter, T. Kurki-Suonio* and H.-P. Zehrfeld:* LM Phenomenon as an Interaction between Bootstrap Current Driven Peeling Modes and Pressure Driven Ballooning Modes. 7th IAEA Techn. Comm. Meeting on H-Mode and Transport Barrier Physics, Oxford 1999.

691. *Salat A. and J.A. Tataronis*:* Singular Modes of Ideal Magnetohydrodynamics. Int. Sherwood Fusion Theory Conf., Atlanta,GA 1999.

692. *Salat, A. and J.A. Tataronis*:* Spatial Singularities of the Ideal and Continuum Modes. 41st Annual Meeting of the Division of Plasma Physics of the APS, Seattle,WA 1999.

693. *Sallander*, E., A. Weller and W7-AS Team:* Effects of Non-Vanishing Toroidal Current Densities on the Stability in the Wendelstein 7-AS. Annual Meeting of the Swedish Fusion Research Unit, NFR-EURATOM, Gothenburg 1999.

694. *Sallander*, E., A. Weller and W7-AS Team:* Effects of Non-Vanishing Toroidal Current Densities on the Stability in the Wendelstein 7-AS. 12th Int. Stellarator Conf., Madison,WI 1999.

695. *Sallander, J., R. König and K. McCormick:* A High-Spatial Resolution H-alpha-Diagnositic for the Divertor Phase of Wendelstein-7. 12th Int. Stellarator Conf., Madison,WI 1999.

696. *Sapper, J.:* The Superconducting Magnetsystem for W7-X. 4th Europ. Conf. on Applied Superconductivity, Barcelona 1999.

697. *Sardei, F.:* Magnetohydrodynamik. Vorlesung, Univ. der Bundeswehr, München 1999.

698. *Sardei, F.:* Die Physik des Inseldivertors am Beispiel des Stellarators W7-AS. Seminar, Berlin 1999.

699. *Sardei, F.:* Rechneranwendungen in der Fluidynamik. Vorlesung, Univ. der Bundeswehr, München 1999.

700. *Sardei, F., Y. Feng, P. Grigull, J. Kisslinger and W7-AS Team:* Physik des Inseldivertors am Beispiel des Stellarators W7-AS. Verhandl. DPG (IV) **34**, 337, P7 (1999).

701. *Sardei, F., Y. Feng and J. Kisslinger:* Island Divertors for Helical Systems. Kyoto Univ. 1999.

702. *Sardei, F., Y. Feng and J. Kisslinger:* Island Divertors for Helical Systems. 7th Int. Workshop on Plasma Edge Theory in Fusion Devices, Tajimi 1999.

703. *Schalk*, B., U. Fantz* und K. Behringer:* Rechnung und Interpretation der $H_2$- und $D_2$-Kontinuumsstrahlung. Verhandl. DPG (VI) **34**, 345, P9.2 (1999).

704. *Schauer, F.:* Present Status of the W7-X Project. Symp. on Large-Scale Superconducting Technology of Nuclear Fusion Experiment Facilities, Toki 1999.

705. *Schauer, F.:* Zukünftige Energiegewinnung mit Hilfe von Kernfusion. Vortragsveranstaltung, Balcke-Dürr Energietechnik GmbH, Ratingen 1999.

706. *Schmidtmann, K., J. Gafert, S. Günter, U. Schumacher* and ASDEX Upgrade Team:* Stark-Effekt-Messungen in dichten Divertorplasmen im Tokamak ASDEX Upgrade. Verhandl. DPG (VI) **34**, 346, P9.4 (1999).

707. *Schwarz-Selinger, T.:* Wer ist der Täter? Auf der Suche nach dem Wachstumsprecursor in Beschichtungsplasmen. IPF/IPP-Seminar Techn. Anwendung von Plasmen, Garching 1999.

708. *Schwarz-Selinger, T., A. von Keudell and W. Jacob:* Eine einfache Methode zur Charakterisierung von a-C:H-Schichten. 9. Bundesdt. Fachtagung Plasmatechnologie, Stuttgart 1999, PS18.

709. *Schweer*, A. and R. König:* Aktive Divertor- und Randspektroskopie. Workshop on W7-X Diagnostics, Schloss Ringberg 1999.

710. *Schwenn, U.:* Computer Simulation in Plasmas. Summer Univ. for Plasma Physics, Greifswald 1999.

711. *Schwenn, U.:* Videokonferenzen am IPP. 16. DV-Tagung der Max-Planck-Institute, Göttingen 1999.

712. *Scott, B.D.:* Computation of Electromagnetic Gyrofluid Turbulence in Tokamak Edge Geometries. 8th Europ. Fusion Theory Conf., Como 1999.

713. *Scott, B.D.:* 2D Drift Waves and Large Scale Structures. Workshop on Simulation of Turbulence in Low-Temperature Plasmas and Comparison with Experiment, Kiel 1999.

714. *Scott, B.D.: E* x *B* Shear Flows and Electromagnetic Gyrofluid Turbulence. Bull. Am. Phys. Soc. **44**, 90 (1999).

715. *Scott, B.D.:* Electromagnetic Gyrofluid Turbulence in Realistic Tokamak Geometry. 7th Europ. Fusion Physics Workshop, Kloster Seeon 1999.

716. *Scott, B.D.:* Electromagnetic Gyrofluid Turbulence in Realistic Tokamak Geometry. Verhandl. DPG (VI) **34**, 366, P23.2 (1999).

717. *Scott, B.D.:* Hydro-Driftdynamik der magnetisierten Plasmen. Vorlesung, Univ. Düsseldorf, SS 1999.

718. *Scott, B.D.:* Magneto-Hydrodynamics. Summer Univ. for Plasma Physics, Greifswald 1999.

719. *Scott, B.D.:* Properties of Nonlinear Drift Wave Turbulence and Relevance to Submarginal Transport. Joint US-EU TTF Meeting, Portland,OR 1999.

720. *Scott, B.D.:* State Transition in Tokamak Edge Turbulence Inducted by $E \times B$ Shear. Joint US-EU TTF Meeting, Portland,OR 1999.

721. *Scott, B.D.:* Turbulence Simulations Diagnostics. Workshop on Simulation of Turbulence in Low-Temperature Plasmas and Comparison with Experiment, Kiel 1999.

722. *Scott, B.D.:* Turbulence Simulations Formulation. Workshop on Simulation of Turbulence in Low-Temperature Plasmas and Comparison with Experiment, Kiel 1999.

723. *Scott, B.D.:* Turbulence Simulations Results. Workshop on Simulation of Turbulence in Low-Temperature Plasmas and Comparison with Experiment, Kiel 1999.

724. *Sergeev*, V.Yu., L. Ledl*, R. Burhenn, B.V. Kuteev*, V.G. Skokov*, S. Egorov* and W7-AS Team:* Studies of Carbon Pellet Injection into WVII-AS Plasmas. 26th Annual Russian Conf. on Plasma Phys. and Control. Fusion, Zvenigorod 1999.

725. *Simon-Weidner, J. and N. Jaksic:* Kriterien zur Beurteilung der Sicherheit von Bauteilen mit den Anforderungen an die Ergebnisauswertung. MacNeal-Schwendler GmbH Users Conf., Weimar 1999.

726. *Speth, E.:* On the Optimum Beam Energy of Neutral Beam Current Drive in Tokamaks. Verhandl. DPG (VI) **34**, 375, P27.3 (1999).

727. *Steuer, K.-H.:* Fusionsreaktoren, schnelle Brüter und Sonnenkraftwerke - Stand und Perspektiven bei der Erschließung neuer Energiequellen. 3 Schulvorträge, MPG Hauptversammlung, Dortmund 1999.

728. *Steuer, K.-H.:* Perspektiven der Kernfusion. Kolloquium, Fachhochschule Kempten gemeinsam mit VDI, VDE, Kempten 1999.

729. *Steuer, K.-H.:* Unsere Sonne, ein gigantischer Fusionsreaktor. Astronomietage, Ingolstadt 1999.

730. *Stroth, U.:* Experiments in the Stellarator W7-AS. California Inst. of Technology, San Diego,CA 1999.

731. *Stroth, U.:* Experiments in the Stellarator W7-AS. Univ. of San Diego,CA 1999.

732. *Stroth, U.:* The Role of the Radial Electric Field for Confinement in W7-AS. Joint US/EU TTF Meeting, Portland,OR 1999.

733. *Strumberger, E.*: Deposition Patterns of Fast Ions on Plasma-Facing Components. Theory Meeting, Zinnowitz 1999.

734. *Sünder, D., P. Bachmann and H. Wobig:* Temperatur-Bifurkationen in 3-D-Plasmagleichgewichten. Verhandl. DPG (VI) **34**, 366, P23.8 (1999).

735. *Suttrop, W.:* Ergänzungen zur Einführung in die Plasmaphysik und Fusionsforschung, Teil I. Vorlesung, Univ. Bayreuth, WS 1998/99.

736. *Suttrop, W.:* Ergänzungen zur Einführung in die Plasmaphysik und Fusionsforschung, Teil II. Vorlesung, Univ. Bayreuth, SS 1999.

737. *Taglauer, E.:* Katalysatoren: Morphologie und Oberflächenreaktionen. Vortrag, Univ. Osnabrück 1999.

738. *Taglauer, E.:* Segregation on Bimetallic Surfaces and Relations to Metallic Catalysts. 2nd Int. Workshop on Surface and Grain Boundary Segregation, Schloss Ringberg 1999.

739. *Taglauer, E.:* Wo's heiß hergeht - Energie aus der kontrollierten Kernfusion - wie steht's damit? Deutsches Zentrum für Luft- und Raumfahrt e.V., Oberpfaffenhofen 1999.

740. *Taglauer, E., A. Kohl and H. Knözinger*:* Agglomeration of Rhodium Metal Supported on Oxide Substrates. ESF Workshop on Atomic Layers Epitaxy, Helsinki 1999.

741. *Taglauer, E., J. du Plessis* and R. Beikler:* Segregation and Prefential Sputtering of Alloy Surfaces. 18th Int. Conf. on Atomic Collision Schilds, Odense 1999.

742. *Taglauer, E., A. Steltenpohl, R. Beikler and L. Houssiau*:* Scattered Ion Yields from Bimetallic Crystal Surfaces. 12th Int. Workshop on Inelastic Ion Surface Collisions, South Padre Island 1999.

743. *Tasso, H.:* On Lyapunov Stability of Dissipative Mechanical Systems. 4th Int. Congress on Industrial and Applied Mathematics, Edinburgh 1999.

744. *Thomsen, H., M. Endler, J. Bleuel, A.V. Chankin*, S. Davies*, S.K. Erents*, G.F. Matthews* and JET Team:* Parallele Korrelation elektrostatischer Fluktuationen in der Randschicht des JET Tokamaks. Seminar, Univ. Greifswald 1999.

745. *Throumoulopoulos*, G.N. and H. Tasso:* Ideal Magneto-hydrodynamic Equilibria with Helical Symmetry and Incompressible Flows. Bull. Am. Phys. Soc. **44**, 597-598 (1999).

746. *Throumoulopoulos*, G.N. and H. Tasso:* On Resistive MHD Tokamak Equilibria with Flow. 8th Europ. Fusion Theory Conf., Como 1999.

747. *Toussaint, U. von:* Depth Profile Determination with Confidence Intervals from Rutherford Backscattering. 14th Int. Conf. on Ion Beam Analysis/Europ. Conf. on Accelerators in Appl. Research and Technology, Dresden 1999.

748. *Toussaint, U. von:* Tiefenprofile von Ionenstrahl-diagnostiken mittels Bayesscher Wahrscheinlichkeitstheorie. Techn. Univ. München, Univ. München 1999.

749. *Ullrich, W., H.-S. Bosch and ASDEX Upgrade Team:* Helium Transport und Plasmaströmung in der Randschicht an ASDEX Upgrade. Verhandl. DPG (VI) **34**, 342, P6.5 (1999).

750. *Vasquez-Borucki, S. and W. Jacob:* Einfluß amorpher Kohlenwasserstoffschichten auf die Gaspermeation durch Polymerfolien. 9. Bundesdt. Fachtagung Plasmatechnologie, Stuttgart 1999, PO16.

751. *Vollmer, O.:* Status of RF Negative Ion Sources at IPP Garching. Super Joint Development Comm. Meeting, JAERI, Naka 1999.

752. *Vollmer, O., H. Falter*, P. Frank*, B. Heinemann, W. Kraus, P. Massmann*, P. McNeely, R. Riedl, E. Speth, R. Trainham* and R. Wilhelm*: Development of Large RF Driven Ion Sources for Fusion. 8th Int. Conf. on Ion Sources, Kyoto 1999.

753. *Volpe, F., H.P. Laqua and W. Kasparek*:* The Development of an Electron Bernstein Wave Emission Diagnostic for Temperature Profile Measurement above the ECE-Cutoff Density. 11th Joint Russian-German Meeting on ECRH and Gyrotrons, Karlsruhe, Stuttgart, Garching 1999.

754. *Wagner, F.:* Achievements and Proposals of the German Stellarator Programme. PLASMA 99, 4th Symp. on Research and Applications of Plasmas, Warschau 1999.

755. *Wagner, F.:* Considerations Regarding the EU Fusion Programme. Fusion Summer Study, Snowmass 1999.

756. *Wagner, F.:* The Early Years at IPP. Festkolloquium Prof. Keilhacker, Culham 1999.

757. *Wagner, F.:* Das Garchinger Stellaratorprogramm unter Günter Grieger. Festkolloquium Prof. Grieger, Greifswald 1999.

758. *Wagner, F.:* Modern Physics of Stellarators. Festkolloquium Prof. Troyon, Lausanne 1999.

759. *Wagner, F.:* Die physikalischen Grundlagen des Fusionsprojektes W7-X. Kolloquium, Forschungszentrum Rossendorf 1999.

760. *Wagner, F.:* Die Zielsetzung für das Greifswalder Experiment Wendelstein 7-X. Rotary Club, Greifswald 1999.

761. *Wanner, M.:* Design Goals and Status of the Wendelstein 7-X Project. 12th Int. Stellarator Conf., Madison,WI 1999.

762. *Weller, A., M. Anton, C. Fuchs, J. Geiger, M. Hirsch, R. Jaenicke, C. Nührenberg, E. Sallander*, D. Spong*, A. Werner and W7-AS Team:* Survey on MHD Instabilities in W7-AS. 12th Int. Stellarator Conf., Madison,WI 1999.

763. *Weller, A., M. Anton, J. Geiger, M. Hirsch, C. Nührenberg, D. Spong*, A. Werner, W7-AS Team and NBI-Group:* Interaction of Fast Ions with MHD-Modes in the Stellarator W7-AS. 7th Europ. Fusion Physics Workshop, Kloster Seeon 1999.

764. *Weller, A. and E. Sallander*:* Stability Studies of Plasmas with Significant Rotational Transform from Toroidal Currents. US-Japan Workshop on Stellarator/Helical System Concept Improvement, Oak Ridge,TN 1999.

765. *Wendland, C., H. Maaßberg, E.R. Solano and W7-AS Team:* Bootstrap and Neutral Beam Driven Current at the W7-AS Stellarator. 12th Int. Stellarator Conf., Madison,WI 1999.

766. *Wenzel, U.:* Experiments and Modelling on Molecular Activated Recombination in the Divertor of ASDEX Upgrade. Symp. on Molecular Processes in Fusion Divertor Plasmas, Nagoya 1999.

767. *Werner, A., J. Baldzuhn and W7-AS Team:* Aktive Hα-Spektroskopie am Stellarator W7-AS zur Bestimmung der Ionentemperatur und Plasmarotation. Verhandl. DPG (IV) **34**, 346, P9.5 (1999).

768. *Werner, A., A. Weller, D.S. Darrow* and W7-AS Team:* Fast Ion Losses in Wendelstein 7-AS. 6th IAWA Techn. Comm. Meeting on Energetic Particles in Magnetic Confinement Systems, Naka 1999.

769. *Wilhelm, R.:* Plasmaphysik I. Vorlesung, Techn. Univ. München, WS 1999/2000.

770. *Wilhelm, R.:* Plasmaphysik II. Vorlesung, Techn. Univ. München, SS 1999.

771. *Wilhelm, R.:* Stand und Aussichten der Kernfusion. Techn. Univ. München 1999.

772. *Wobig, H.:* Remarks on Plasma Equilibria in Toroidal Geometry. Theory Meeting, Zinnowitz 1999.

773. *Wobig, H.:* Theoretische Plasmaphysik I. Vorlesung, Techn. Univ. München, WS 1999/2000.

774. *Wobig, H.:* Theoretische Plasmaphysik II. Vorlesung, Techn. Univ. München, SS 1999.

775. *Wobig, H.:* Wendelstein 7-X und die Hausdorff-Dimension. Seminar, Greifswald 1999.

776. *Wobig, H. and D. Pfirsch:* Destruction of Drift Surfaces in Toroidal Systems. IAEA Techn. Comm. Meeting on First Principle Based Transport Theory, Kloster Seeon 1999.

777. *Wobig, H. and D. Pfirsch:* On Guiding Center Orbits in Stellarator Configurations. 12th Int. Stellarator Conf., Madison,WI 1999.

778. *Wolf, R.:* Advanced Tokamak Experimente an ASDEX Upgrade. Kolloquium, IPF Stuttgart 1999.

779. *Wolf, R.:* Response of Internal Transport Barriers to Central Electron Heating and Current Drive on ASDEX Upgrade. Bull. Am. Phys. Soc. **44**, 20 (1999).

780. *Wolf, R., O. Gruber, R. Dux, C. Fuchs, S. Günter, A. Kallenbach, K. Lackner, M. Maraschek, H. Meister, G. Pereverzev, F. Ryter, J. Schweinzer, U. Seidel, A. Sesnic, A. Stäbler and J. Stober:* Interne Transportbarrieren am Tokamak ASDEX Upgrade. Verhandl. DPG (VI) **34**, 343, P7.1 (1999).

781. *Zasche, D., K. Behler, G. Neu, G. Raupp, W. Treutterer, T. Zehetbauer and ASDEX Upgrade Team:* Automatic Setting of Machine Control with Physics Operation Parameters. 2nd IAEA Techn. Comm. Meeting on Control, Data Acquisition and Remote Participation for Fusion Research, Lisbon 1999.

782. *Zeiler, A.:* Wie entsteht das Magnetfeld der Erde? Habilitationsvortrag, Univ. Ulm 1999.

783. *Zeiler, A., J.F. Drake* and B.N. Rogers*:* Electromagnetic ITG Mode Turbulence at the Plasma Edge. IAEA Techn. Comm. Meeting on First Principle Based Transport Theory, Kloster Seeon 1999.

784. *Zeiler, A., J.F. Drake* and B.N. Rogers*:* Electromagnetic $\eta_i$ Mode Turbulence at the Plasma Edge. Bull. Am. Phys. Soc. **44**, 1014 (1999).

785. *Zeiler, A., J.F. Drake* and B.N. Rogers*:* Magnetic Reconnection in Toroidal $\eta_i$ Mode Turbulence. Bull. Am. Phys. Soc. **44**, 320 (1999).

786. *Zeiler, A., J.F. Drake* and B.N. Rogers*:* Two-Fluid Simulations of Plasma Edge Turbulence. H-Mode Workshop, Oxford 1999.

787. *Zohm, H.:* Aktive Kontrolle magnetischer Inseln an ASDEX Upgrade. Verhandl. DPG (VI) **34**, 347, P11.2 (1999).

788. *Zohm, H.:* Einsatz von Hochleistungsmikrowellen in Kernfusionsplasmen. Seminar, Forschungszentrum Karlsruhe 1999.

789. *Zohm, H.:* Einsatz von Hochleistungsmillimeterwellen in Kernfusionsplasmen. Kolloquium, Univ. Stuttgart 1999.

790. *Zohm, H.:* Neues von der Fusionsforschung mit magnetischem Einschluss. Kolloquium, GSI Darmstadt 1999.

791. *Zohm, H.:* Stabilisation of Neoclassical Tearing Modes in ASDEX Upgrade. 11th Joint Russian-German Meeting on ECRH and Gyrotrons, Karlsruhe, Stuttgart, Garching 1999.

792. *Zohm, H.:* The Stabilisation of Neoclassical Tearing Modes by ECCD in ASDEX Upgrade. 4th Int. Workshop on Strong Microwaves in Plasmas, Nizhny Novgorod 1999.

793. *Zohm, H.:* Tokamak Equilibrium, Stability and Transport. Summer Univ. for Plasma Physics, Greifswald 1999.

794. *Zohm, H.:* Tokamak MHD. 11th General Conf. of the EPS: Trends in Physics, London 1999.

## Internal Laboratory Reports

IPP 1/319 *Bosch, H.-S. and A. Gude (Eds.):* ASDEX Upgrade Results, Publications and Conference Contributions Period 1/98 to 2/99.

IPP 1/320 *Hoek*, M., H.-S. Bosch and W. Ullrich:* Triton Burnup Measurements at ASDEX Upgrade by Neutron Foil Activation.

IPP 1/321 *Ullrich, W.:* Heliumtransport in der Plasmarandschicht an ASDEX Upgrade.

IPP 1/322 *Gruber, O., K.H. Finken*, G. Fuchs*, J. Neuhauser, J.-M. Noterdaeme, B. Streibl and F. Wesner:* Combined Application to the HGF Strategy Fund for the Funding Period 1999 - 2002 from the HGF Centres, IPP Garching and FZ Jülich, for "Optimized Stationary Tokamak Operation".

IPP 1/323 *Schweinzer, J.:* Atomare Prozesse mit schnellen Lithiumatomen zur Diagnose und Optimierung von Fusionsplasmen.

IPP 2/343 *Herrnegger, F., F. Rau and H. Wobig (Eds.):* Contributions to Wendelstein 7-X and the Helias Reactor 1991-1998.

IPP III/238 *Salat, A. and J.A. Tataronis*:* Radial Dependence of Magnetohydrodynamic Continuum Modes in Axisymmetric Toroidal Geometry.

IPP III/239 *Herre, G.:* Untersuchung der Plasmarandschicht am Stellarator Wendelstein 7-AS.

IPP III/240 *Itoh, S.-I. and K. Itoh:* Statistical Theory of Subcritically-Excited Strong Turbulence in Inhomogeneous Plasmas (II).

IPP III/241 *Harmeyer, E., J. Kisslinger and H. Wobig:* The Effect of Ferritic Structural Material on the Magnetic Field of Stellarators.

IPP III/242 *Salat, A. and J.A. Tataronis*:* On the Existence of Orthongonal, Magnetic Field Line Coordinate Systems.

IPP III/243 *Itoh, S.-I. and K. Itoh:* Statistical Theory of Subcritically-Excited Strong Turbulence in Inhomogeneous Plasmas (III).

IPP III/244 *Wobig, H., E. Harmeyer, F. Herrnegger and J. Kisslinger:* On Blanket Concepts of a Helias Reactor.

IPP III/245 *Wobig, H. and D. Pfirsch:* Guiding Center Orbits of Passing Particles in Toroidal Systems.

IPP III/247 *Itoh, S.-I. and K. Itoh:* Statistical Theory of Subcritically-Excited Strong Turbulence in Inhomogeneous Plasmas (IV).

IPP III/248 *Keller, M.:* Experimentelle Studie über die Detektion geladener Teilchen.

IPP III/249 *Strumberger, E., H. Wobig, J. Kisslinger and C. Nührenberg:* Equilibrium and Stability Properties of al Helias Reactor.

IPP III/250 *Wobig, H. and J. Kisslinger:* Viscous Dumping of Rotation in Wendelstein 7-AS.

IPP III/251 *Wobig, H., I.N. Sidorenko and A.A. Shishkin*:* Resonant Diffusion of Passing Alpha-Particles in a Helias Reactor.

IPP III/252 *Giannone, L.:* Physics of the Density Limit in the W7-AS Stellarator.

IPP 4/279 *Puri, S.:* Anomalous Particle Pinch in Tokamaks.

IPP 5/83 *Büchl, K. and W. Sandmann:* Launching of Cryogenic Pellets through Guide Tubes.

IPP 5/84 *Bosch, H.-S. and A. Gude (Eds.):* ASDEX Upgrade Results, Publications and Conference Contributions Period 1/98 to 2/99.

IPP 5/85 *McCarthy, P., P. Martin and W. Schneider:* The CLISTE Interpretive Equilibrium Code.

IPP 5/86 *Brandenburg, R. and J. Schweinzer:* Lithiumstrahldiagnostik von Kernfusionsplasmen.

IPP 5/87 *Max-Planck-Institut für Plasmaphysik:* IAEA Technical Committee Meeting on First Principle-Based Transport Theory. Abstracts. Kloster Seeon 1999.

IPP 5/88 *Zeiler, A.:* Tokamak Edge Turbulence.

IPP 5/89 *Becker, G.:* Effect of Perpendicular Momentum Dissipation on Anomalous Inward Drift.

IPP 9/120 *Vetter, S.:* Struktur und Dynamik von reinen und sauerstoffbedeckten gestuften Kupferoberflächen = Structure and Dynamics of Clean and Oxygen Covered Stepped Copper Surfaces.

IPP 9/121 *Lindig, S.:* Aufbau eines dE-E-Teleskopdetektors für ERDA und Reichweitenmessung von Wasserstoff in oberflächennahen a-C:H- bzw. a-C:D-Schichten mit ERD-Ionenstrahlanalyse = Installation of dE-E Telescope Detector for ERDA and Measurements of Range of Hydrogen in near Surface a-C:H and a-C:D Layers with ERDA.

IPP 9/122 *Landkammer, B.:* Untersuchung der Erosion von Kohlenwasserstoffschichten in Sauerstoff-Gasentladungen = Erosion of Hydrogenated Carbon Films in Oxygen Glow Discharges.

IPP 9/123 *Steltenpohl, A.M.:* Wachstum von Palladium auf Palladium (111) = Growth of Palladium on Palladium(111).

IPP 10/12 *Bosch, H.-S. and A. Gude (Eds.):* ASDEX Upgrade Results, Publications and Conference Contributions Period 1/98 to 2/99.

## External Laboratory Reports

NET 97-457 *Balden, M. and J. Roth:* Post-Test Examination of Divertor Mock-Up Tiles after High Power Load Testing. Final Report on NET Contract ERB 5004 CT 97 0093. NET, Garching 1999.

ITER-Task 227 *Bohmeyer, W., G. Fußmann and P. Kornejew:* Tritium Permeation and Inventory Characteristic of Co-Deposited Materials Produced in Plasma Generator and via CD4-Chemical Deposition. Final Report.

NIFS-585 *Kumazawa*, R., T. Mutoh*, T. Seki*, F. Shimpo*, G. Nomura*, T. Ido*, T. Watari*, J.-M. Noterdaeme and Y. Zhao*:* Liquid Stub Tuner for Ion Cyclotron Heating. Nat. Inst. for Fusion Sciences, Nagoya 1999.

# Author Index

# Teams

**ASDEX Upgrade Team:** R.Arslanbekov, C.Atanasiu*, A.Bard, G.Becker, W.Becker, M.Beckmann, K.Behler, K.Behringer, A.Bergmann, M.Bessenrodt-Weberpals, R.Bilato, D. Bolshukhin, K.Borrass, H.-S.Bosch, B.Braams*, M.Brambilla, R.Brandenburg*, F.Braun, H.Brinkschulte, R.Brückner, B.Brüsehaber, A.Buhler, H.Bürbaumer*, A.Carlson, M.Ciric, G.Conway, D.Coster, C.Dorn, R.Drube, R.Dux, S.Egorov*, W.Engelhardt, H.-U.Fahrbach, U.Fantz*, H.Faugel, M.Foley*, R.Fritsch, P.Fu*, J.C.Fuchs, J.Gafert*, O.Gehre, A.Geier, J.Gernhardt, O.Gruber, E.Gubanka, A.Gude, S.Günter, G.Haas, D.Hartmann, B.Heinemann, G.Herppich, A.Herrmann, J.Hobirk, F.Hofmeister, H.Hohenöcker, L.Horton, L.Hu*, D.Jacobi, A.Kallenbach, O.Kardaun, M.Kaufmann, K.Kirov, R.Kochergov, H.Kollotzek, W.Kraus, K.Krieger, B.Kurzan, G.Kyriakakis*, K.Lackner, P.T.Lang, R.S.Lang, M.Laux, F.Leuterer, A.Lorenz, H.Maier, M.-E.Manso*, M.Maraschek, K.-F.Mast, P.McCarthy*, D.Meisel, P.Meissner, H.Meister, F.Meo, R.Merkel, V.Mertens, J.P.Meskat, R.Monk, H.W.Müller, H.Murmann, G.Neu, R.Neu, J.Neuhauser, J.-M.Noterdaeme, I.Nunes*, G.Pautasso, A.G.Peeters, S.Pinches, R.Pugno, G.Raupp, T.Ribeiro*, R.Riedl, V.Rohde, H.Röhr, J.Roth, F.Ryter, H.Salzmann, W.Sandmann, S.Schade, H.-B.Schilling, D.Schlögl, K.Schmidtmann, R.Schneider, W.Schneider, G.Schramm, J.Schweinzer, S.Schweizer, B.D.Scott, U.Seidel, F.Serra*, S.Sesnic, C.Sihler, A.Silva*, E.Speth, A.Stäbler, K.-H.Steuer, J.Stober, B.Streibl, E.Strumberger, W.Suttrop, A.Tabasso, G.Tardini, C.Tichmann, W.Treutterer, M.Troppmann, N.Tsois*, W.Ullrich, P.Varela, U.Wenzel, F.Wesner, R.Wolf, R.Wunderlich, N.Xantopoulus*, Q.Yu*, M.Zarrabian, D.Zasche, T.Zehetbauer, H.P.Zehrfeld, A.Zeiler, H.Zohm.

**ECRH Group (AUG):** M.Beckmann, H.Brinkschulte, F.Leuterer, K.Kirov, F.Monaco, M.Münich, F.Ryter.

**ECRH Group (W7-AS):** V.Erckmann, G.Grünwald, J.Hofner, F.Hollmann*, H.Laqua, G.Michel, F.Noke, F.Purps.

**ICRH Group:** W.Becker, V.Bobkov, F.Braun, H.Faugel, D.Hartmann, F.Hofmeister, F.Meo, J.-M.Noterdaeme, S.Puri, F.Wesner.

**NI Group:** M.Ciric, P.Franzen, B.Heinemann, W.Kraus, P.McNeely, S.Obermayer; W.Ott, F.-P.Penningsfeld, F.Probst, R.Riedl, W.Schärich, E.Speth, A.Stäbler, R.Süß, O.Vollmer, K.Wittenbecher.

**NI Team(W7-AS):** W.Ott, F.-P.Penningsfeld, F.Probst, E.Speth, R.Süß.

**W7-AS Team:** M.Anton, S.Bäumel, T.Baloui, M.Basse, C.Beidler, J.Bleuel, R.Brakel, H.Callaghan, G.Cattanei, D.Dorst, H.Ehmler, A.Elsner, M.Endler, K.Engelhardt, V.Erckmann, Y.Feng, S.Fiedler, N.Franz, C.Fuchs, F.Gadelmeier, U.Gasparino, J.Geiger, L.Giannone, P.Grigull, O.Grulke, H.Hacker, E.Harmeyer, H.-J.Hartfuß, D.Hartmann, F.Herrnegger, M.Hirsch, E.Holzhauer, J.K.Hübner, R.Jaenicke, F.Karger, A.Kendl, M.Kick, A.Kislyakov*, J.Kisslinger, T.Klinger*, S.Klose, J.Knauer, J.P.Koponen, H.Kroiss, G.Kühner, A.Kus, H.Laqua, L.Ledl, R.Liu, H.Maaßberg, K.McCormick, G.Michel, S.Niedner, W.Ott, M.G.Pacco-Düchs, F.-P.Penningsfeld, S.Reimbold*, M.Rodriguez, N.Ruhs, N.Rust, J.Saffert, A.Salat, J.Sallander, F.Sardei, M.Schubert, I.Sidorenko, E.Speth, N.Stöferle, U.Stroth, H.Thomsen, F.Volpe, F.Wagner, H.Walter, A.Weller, C.Wendland, A.Werner, E.Würsching, D.Zimmermann, M.Zippe.

# University Contributions to IPP Programme

# LEHRSTUHL FÜR EXPERIMENTELLE PLASMAPHYSIK DER UNIVERSITÄT AUGSBURG

(Prof. Dr. Kurt Behringer)

## PLASMA EDGE DIAGNOSTICS

(K. Behringer, U. Fantz, B. Heger, A. Lotter, S. Meir, H. Paulin, T. Ondak, P. Starke and D. Wünderlich)

Diagnostics of low temperature plasmas is one of the main topics of the group. Here, interpretation of molecular spectra in laboratory experiments (RF, MW and ECR discharges) as well as in divertor plasmas (see: *The role of molecules in divertors* in the tokamak section) is of special interest. Detailed information about plasma parameters, $n_e$ and EEDF in low pressure plasmas was obtained from a combination of the following diagnostics: Langmuir probes for spatial profiles, microwave interferometry as a non-disturbing method and emission spectroscopy in the visible and uv/vuv spectral range. For determination of molecular or atomic densities from measured radiation, rate coefficients and collisional radiative (CR) models are necessary. In the case of hydrogen and deuterium plasmas, the radiation of various molecular bands allows determination of effective rate coefficients and evaluation of CR models for $H_2$. By increasing the pressure, i.e. particle densities, the influence of heavy particle collisions can be investigated. Another application is diagnostics by means of Balmer lines. Here, the optical thickness of Lyman lines and dissociative excitation of molecules plays an important role. In addition, line ratios can be determined, as shown in the contributions of the IPP E4 division. Further main subjects are diagnostics of methane plasmas and chemical erosion of carbon in hydrogen and deuterium plasmas.

### Methane Plasmas and Chemical Erosion of Carbon

For a better understanding of dissociative channels of methane and formation of higher hydrocarbons, methane plasmas in ECR discharges with high (95%) and low (5%) percentage of methane in helium have been investigated. The latter mixture is important for interpretation of chemical erosion of carbon in hydrogen plasmas. Particle densities were determined by mass spectrometry and emission spectroscopy in the wavelength range 115 - 900 nm. In the plasmas, depletion of methane is in the range of a factor four to ten and the density is comparable to the produced molecular hydrogen density dominating the plasmas. The formation of higher hydrocarbons ($C_2H_x$) is due to heavy particle collisions and leads to densities typically 10% of methane. The main species of higher hydrocarbons is always $C_2H_2$ followed by $C_2H_4$ and $C_2H_6$, the proportions depending on the methane partial pressure. Therefore, when determining densities from measured CH bands, $C_2$ bands, Balmer line and carbon line radiation, dissociative excitation from higher hydrocarbons ($C_2H_2$) must be considered. Especially in the case of CH, the contribution to the radiation can be about 30%. Comparing the results for $C_2$ densities from the $C_2$ Swan ($\lambda$ = 516 nm) with the $C_2$ Mulliken ($\lambda$ = 231 nm) bands, the relative dependencies on plasma parameters are nearly identical, but differ by a factor of 2.5 in absolute value. The Mulliken transition is directly coupled to the ground state and therefore much better suited for density determinations than the Swan bands in the metastable system, but it is more difficult to measure (weak transition at 231 nm). Chemical erosion measurements were carried out in RF plasmas in combination with detailed diagnostics of plasma parameters (see: *annual report 1998, university contributions*). When determining atomic hydrogen and deuterium fluxes onto the substrate (EK98), two cases must be distinguished: The incoming fluxes on the surface (derived from the density directly above the surface) are $\Gamma_H = \Gamma_D = 1.7 \cdot 10^{22}$ $m^{-2}s^{-1}$, whereas the balance of incoming and reflected fluxes derived from the diffusion of the particles leads to $\Gamma_H = \Gamma_D = 2.6 \cdot 10^{21}$ $m^{-2}s^{-1}$. As a consequence, the reflection coefficient of the surface was determined to be about 80%. Ion fluxes are estimated to be $\Gamma_{H2+} = \Gamma_{D2+} = 6 \cdot 10^{19}$ $m^{-2}s^{-1}$. The radiation of the CH(CD) and the $C_2$ Swan bands gives dependencies of the erosion on substrate temperature, ion energy (physically enhanced chemical erosion) and isotopes. Absolute yields were measured by weight losses. The results can be compared with calculations using the Roth model (J. Roth, J.Nucl.Mat. **266-269**, 51, 1999). An example is given in figure 1, the yields refer to the diffusion fluxes.

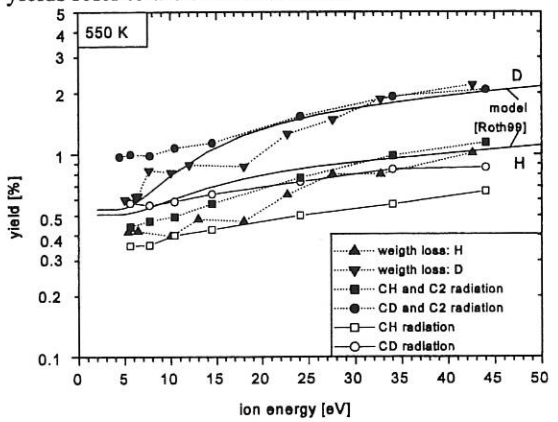


*FIG.1: Yields of carbon in hydrogen/deuterium plasmas depending on ion energy at a substrate temperature of 550 K.*

At 550K, yields from the model and the weight losses are in good agreement for deuterium, whereas weight loss measurements give a higher isotope effect. Concerning the spectroscopic data, only the combination of the CH (CD) bands with the $C_2$ signal correctly reproduces the dependencies, as can be seen from a comparison of the filled and the open symbols (H: square, D: circle). This demonstrates the influence of higher hydrocarbons as discussed for methane plasmas. The results indicate that higher hydrocarbons are particularly important for deuterium. At 300K and low ion energies (7 eV), the isotope effect vanishes but a yield of 0.25% remains, which is not predicted by the model.

Oral Presentations

Fantz, U.: Methoden und Ergebnisse der Atom- und Molekülemissionsspektroskopie in Niederdruckplasmen. Augsburger Physikalisches Kolloquium, Universität Augsburg 1999.

Fantz, U.: Spectroscopic Diagnostics and Modelling of Particle Densities in Low Pressure Plasmas, 12th Symp. on Application of Plasma Processes (SAPP), Slowakei 1999.

# LEHRSTUHL FÜR EXPERIMENTALPHYSIK III
# DER UNIVERSITÄT BAYREUTH

(Prof. Dr. Jürgen Küppers)

## Elementary Reactions Of Hydrogen Atoms with Adsorbates and Solid Surfaces.

(J. Biener, C. Lutterloh, M. Kappel, A. Horn, Th. Zecho, A. Dinger, B. Brandner, A. Theobald)

IPP-University of Bayreuth cooperation is concentrated on investigating fusion-relevant plasma-wall interaction processes. Accordingly, the hydrogen atom surface chemistry on possible wall reactor materials is the primary research topic.

A considerable fraction of the species impinging the first wall of a fusion experimental vessel are neutrals and ions in the energy range below about 10 eV kinetic energy. These particles are not capable to cause physical sputtering, but can induce several processes, like chemical erosion, abstraction etc, by which the plasma gets contaminated. It is therefore desirable to understand the elemental processes and mechanisms of these processes. Recent work of the IPP/UBT collaboration was concentrated on investigations of these issues. Since low energy ions are neutralized in the immediate vicinity of a substrate by resonance neutralization, it is sufficient to study the low energy atom-surface interaction. From experimental reasons, the work utilized only thermal atoms with energies in the .1 eV range.

Using reaction kinetics measurements, in the past two years we have demonstrated that gas phase H atoms react with adsorbates according to the Eley-Rideal (ER) and hot-atom (HA) mechanisms. Reactions on surfaces on which H is strongly bound, e.g. on metals and semiconductors, proceed along the HA mechanism. On weakly bonding substrates, e.g. the basal plane of graphite, the reactions proceed along an ER scheme.

HA reactions exhibit kinetics and products which are unexpected in the classical ER scheme. This was shown in investigations of reactions between D and adsorbed alkyl halides, methyl bromide, ethyl iodide and isopropyl iodide, on H admission to Si surfaces leads to chemical etching via silane formation. The kinetics of this reaction was studied between 100 K and 800 K. It was demonstrated that the final reaction step in the stationary etching reaction is the abstraction of adsorbed $SiH_3$ by H(gas) towards $SiH_4$. The instationary etching reaction, most efficient around 630 K, proceeds between surface silyl groups and adjacent dihydride.

H covered Pt(111) surfaces. As expected from the exothermicity, D abstracts methyl, ethyl, and propyl, respectively, from the halides via formation of methane, ethane, and propane. In addition, undeuterated alkanes were observed which provide evidence for the operation of HA mechanisms on the Pt surface. In contrast, the same reactions on graphite as substrates revealed only deuterated products. The kinetics of the products in these latter reactions can be strictly expressed as

$$d[\text{products}]/dt = \sigma\Phi[\text{iodine}]_0 \exp(-\sigma\Phi t)$$

with $\sigma$ as reaction cross section, $\Phi$ as atom flux, t as time, and $[\text{iodine}]_0$ as concentration of the iodines on the surface at reaction start. This is a required result. The kinetics of product formation in HA reactions cannot be expressed analytically, but is available from model calculations.

In addition to simple abstraction, H/substrate reactions can lead to hydrogenation. A study of the hydrogenation of graphite on Pt(111) revealed that only the edges of graphite islands could be hydrogenated. This result is in accordance with an earlier study on C/Pt(100) surfaces and confirms that the main reaction pathway is not structure-sensitive.

In view of the growing importance of silicidation of plasma facing components, studies were performed on the interaction of H with clean and D (monodeuteride) covered Si(100) surfaces. In contrast to commonly accepted experimental evidence, measurements of the HD product kinetics in abstraction of adsorbed D by gaseous H revealed that this reaction is not an ER reaction. In agreement with this, a significant fraction of homonuclear products ($D_2$) were observed. This fraction is markedly reduced in abstraction from the dideuteride surface and the abstraction kinetics phenomenology is similar to an ER scenario. However, even on this substrate the abstraction is a HA reaction.

Publications:

Dinger[1], A., C. Lutterloh[1], J. Biener[1*] and J. Küppers[1,2**]
Hydrogen Atom Reactions with Graphite Island Edges on Pt(111) Surfaces: Hydrogenation through Eley-Rideal and Hot-Atom Processes.
Surf. Sci. 421 (1999) 17

Dinger[1], A., C. Lutterloh[1], J. Biener[1*] and J. Küppers[1,2**]
Reactions of Hydrogen Atoms with Acetone Monolayers adsorbed on Graphite Monolayer covered Pt(111) Surfaces
Surf. Sci. 437 (1999) 116

Dinger[1], A., C. Lutterloh[1], J. Biener[1*] and J. Küppers[1,2**]
Reactions of Gaseous H Atoms with Propylene Oxide Monolayers adsorbed on Graphite covered Pt(111) Surfaces.
Surf. Sci. 421 (1999) 44

Wehner, S. and J. Küppers[*]
Interaction of Gaseous D Atoms with Alkyl Halides adsorbed on Pt(111), H/Pt(111), and C/Pt(111) Surfaces: Hot-Atom and Eley-Rideal Reactions. I. Methyl Bromide.
J. Chem. Phys. 111 (1999) 3209

Wehner, S. and J. Küppers[*]
Interaction of Gaseous D Atoms with Alkyl Halides adsorbed on Pt(111), H/Pt(111), and C/Pt(111) Surfaces: Hot-Atom and Eley-Rideal Reactions. II. Ethyl Iodide.
J. Chem. Phys. 111 (1999) 3218

Wehner, S. and J. Küppers[*]
Interaction of Gaseous D Atoms with Alkyl Halides adsorbed on Pt(111), H/Pt(111), and C/Pt(111) Surfaces: Hot-Atom and Eley-Rideal Reactions. III. Isopropyl Iodide.
J. Chem. Phys. 111 (1999) 3225

Kappel[1], M and J. Küppers[1,2,*]
Ripening of Subsurface Amorphous C Clusters formed by Low Energy He Ion Bombardment of Graphite.
Surf. Sci. 440 (1999) 387

Kammler[1], Th and J. Küppers[1,2*]
Interaction of H Atoms with Cu(111) Surfaces: Adsorption, Absorption and Abstraction.
J. Chem. Phys. 111 (1999) 8115

Dinger[1], A., C. Lutterloh[1], and J. Küppers[1,2*]
Kinetics of D Abstraction with H atoms from the Monodeuteride Phase on Si(100) Surfaces.
Chem. Phys. Lett. 311 (1999) 202

Schimmel, T., T. Koch, J. Küppers, and M. Lux-Steiner
True Atomic Resolution under Ambient Conditions obtained by Atomic Force Microscopy in the Contact Mode.
Appl. Phys. A (Mat. Sci. Process) 68 (1999) 399

Kolovos-Vellianitis[1*], D., Th. Kammler[1], and J. Küppers[1,2]
Interaction of Gaseous H Atoms with Cu(100) Surfaces: Adsorption, Absorption, and Abstraction.
Surf. Sci. in press

Dinger[1], A., C. Lutterloh[1], J. Biener[1*] and J. Küppers[1,2**]
Adsorption of Propylene Oxide on Pt(111) Surfaces and its Reactions with Gaseous and adsorbed H atoms.
Surf. Sci. in press

Dinger[1], A., C. Lutterloh[1], and J. Küppers[1,2*]
Stationary and Instationary Etching of Si(100) Surfaces with Gas Phase and Adsorbed Hydrogen.
Chem. Phys. Lett. submitted

Oral Presentations:

Dinger[1], A., C. Lutterloh[1], and J. Küppers[1,2*]
Kinetics of Abstraction of Monohydride and Dihydride D from Si(100) Surfaces.
46th AVS Symposium, Seattle, October 1999

Dinger[1], A., C. Lutterloh[1], J. Biener[1*], and J. Küppers[1,2**]
Adsorption of Propylene Oxide on Pt(111) Surfaces and its Reactions with Gaseous and Adsorbed H Atoms.
46th AVS Symposium, Seattle, October 1999

Kolovos-Vellianitis[1*], D., Th. Kammler[1], and J. Küppers[1,2]
Interaction of Gaseous H Atom with Cu(100) Sufaces: Adsorption, Absorption , and Abstraction.
COSS-18, When, September 1999

Zecho, T.
Hydrogen induced Chemical Erosion of Thin Amorphous Carbon Films.
Equine Plasma-Surface, CARS University de Provence, Marseille
November 1999

Diploma Theses:

A. Theobald: Wechselwirkung von Ionen mit Graphit-Oberflächen.
Universität Bayreuth, Juli 1999

D. Kolovos-Vellianitis: Adsorption, Absorption und Abstraktion von H an Cu(100)-Oberflächen.
Universität Bayreuth, November 1999

Doctoral Theses:

A. Horn: Der Einfluss von Bor-Heteroatomen auf die Reaktionen von thermischen Wasserstoffatomen mit Kohlenwasserstoffen.
Dissertation, Universität Bayreuth, Juli 1999

M. Kappel: Rastersondenmikroskopische Untersuchungen zur Wechselwirkung niederenergetischer Edelgasionen mit Graphitoberflächen.
Dissertation, Universität Bayreuth, Juli 1999

**LEHRSTUHL FÜR EXPERIMENTALPHYSIK II**
**DER UNIVERSITÄT GREIFSWALD**
(Prof. Dr. Rainer Hippler)

# ON THE ENERGY INFLUX AT PLASMA DEPOSITION OF a-C:H LAYERS

(D.Rohde, P. Pecher, H. Kersten, W. Jacob, R. Hippler)

The cooperation of the IPP and the University of Greifswald is concentrated on investigating fusion-relevant plasma wall interaction processes.

Plasma enhanced techniques for the deposition of thin layers experienced an extraordinarily strong spreading in the last decades. A special importance received amorphous hydrocarbon films (a-C:H-layers), which are interesting for a multiplicity of applications as wear protection, optical surface coatings, fusion research, etc. The technological interest is triggered by a broad range of technologically useful properties which are intermediate between diamond, graphite, and hydrocarbon polymers. Moreover, hydrocarbon films play a significant role in today's thermonuclear fusion experiments either as protective coating of the first wall of fusion reactors or as non-desired by-products in form of redeposited C:H-layers from previously eroded carbon and abundantly available hydrogen /1-4/.

In these complex processes the thermal and energetic conditions at the substrate surface play an important role. The thermal conditions at the surface affect elementary processes like adsorbtion, desorbtion, and diffusion as well as chemical reactions, microstructure, and morphology of the films /5,6/.
Therefore, the integral energy influx $Q_{in}$ from the plasma to the substrate was determined at a-C:H-film deposition by means of magnetron sputtering (Greifswald) and by means of an electron cyclotron resonance (ECR) discharge (IPP). The measurements, for which a thermal probe was designed, are based on the time course of the substrate temperature $dT_S/dt$ during the deposition process /7/:

$$Q_{in} = mc\left[\left(\frac{dT_S}{dt}\right)_{heating} - \left(\frac{dT_S}{dt}\right)_{cooling}\right]_{TA} \qquad (1)$$

The heat capacity $mc$ of the Cu- substrate was $0.6J/K$.

The different contributions to the integral energy influx were estimated by model calculations on the basis of assumptions for the kinetic energy of the charge carriers, recombination, and film condensation /8/.
It could be shown that the energy influx during the deposition in the $CH_4$-ECR-plasma is predominantly determined by ions and chemical reactions, while the energy influx during magnetron sputtering of a-C:H films is dominated by fast neutrals and target radiation. The values of the energy influx ($Q_{in}$) are in both deposition devices in the same order of magnitude for comparable discharge parameters as process pressure and discharge power.
The results emphasize that the energy influx can be regarded as a key parameter in thin film deposition and is important for comparison and scaling-up of different plasma process systems /9/.

The thermal probe was tested for typical discharge conditions in the magnetron discharge sputter equipment and the ECR source deposition reactor in order to investigate the energy and particle fluxes onto the surface during layer growth and to compare the different deposition systems concerning the influence of energetic fluxes. For the calculation of the several contributions the plasma parameters have to be known. The dependence of the electron density $n_e$ and electron temperature $kT_e$ on the external deposition parameters (discharge power, sputter time, gas mixture) in the magnetron experiment has been determined by using Langmuir-probe measurements.
Simultaneously to these measurements, the time behaviour of the discharge, of the neutral gas mixture, and of target oxidation state has been monitored by mass spectroscopy, and evaluation of the current-voltage discharge characteristics. TRIM calculations were used to obtain the energy of the sputtered and reflected particles ariving from the target to the substrate /10/. Furthermore, XPS and XRD studies of the deposited films have been carried out to determine the mass density and to calculate the condensation energy of the deposited material.

It should be mentioned that the energy influx $Q_{in}$ is a surface integral of the related energy flux density $J_{in}$ over the substrate surface $A_S$:

$$Q_{in} = \int_{A_S} J_{in} dA \qquad (2)$$

where $J_{in}$ consists of various controbutions:

$$J_{in} = J_{cond} + J_{ion} + J_{electron} + J_{rad} + J_{rec}, \qquad (3)$$

which have been determined by typically elementary processes appearing while sputtering /11/ or ECR deposition, respectively.

- condensation of the deposition material carbon ($J_C$)

$$J_C = q_C \cdot \rho \cdot R_{dep} = j_C \cdot E_C \qquad (4)$$

$E_c$: condensation heat, $j_c$: particle flux density, $q_c$: specific condensation heat

- kinetic energy of the sputtered and reflected particles ($J_n$)

$$J_n = j_C \cdot E_n = R_{dep} \frac{N_A \rho}{M} \cdot E_n \quad (5)$$

$R_{dep}$: deposition rate, $N_A$: Avogadro- constant, $\rho$: mass density of the film, $E_n$: kinetic particle energy

- kinetic energy of electrons ($J_e$) and ions ($J_i$)

$$J_e = n_e \sqrt{\frac{kT_e}{2\pi m_e}} \exp\left\{-\frac{e_0 V_{bias}}{kT_e}\right\} \cdot 2kT_e$$

(for Maxwell- energy distribution) (6)

$$J_i = n_e \sqrt{\frac{kT_e}{m_i}} \exp\{-0.5\}\, e_0 V_{bias}$$

(criterion of Bohm) (7)

$$V_{bias} = V_{pl} - V_s$$

$V_{pl}$: plasma potential, $V_s$: substrate potential

- recombination energy of the electrons and ions ($J_{rec}$) in case of a floating substrate

$$J_{rec} = j_e \cdot (E_i - \Phi) \quad (8)$$

$E_i$: ionization energy, $j_e$: electron flow density ,
$\Phi$: work function

- target radiation ($J_{rad}$)

$$J_{rad} = \sigma(\varepsilon_T T_T^4 - \varepsilon_S T_S^4) \quad (9)$$

$T_T$: target temperature, $\varepsilon$: emissivity

In the case of carbon sputtering in a pure argon plasma only the contributions $J_n$, $J_e$, $J_i$, and $J_{rec}$ influence the thermal balance of the substrate. If hydrogen is added during the sputtering process, the thermal load is remarkably higher than for pure argon. This is due to an additional energetic contribution by the recombination of hydrogen atoms on the surface.
By applying a bias voltage on the thermal probe (substrate) the ions are accelerated from the plasma to the surface. The energy influx at ECR deposition increases significantly with increasing bias voltage $V_{bias}$. In magnetron deposition there was only a very small effect on $Q_{in}$ due to a negative bias voltage. One can conclude that in the ECR source the positive ions are mainly determine the thermal balance, whereas in the magnetron device the sputtered particles arriving from the target determine the energy influx in this case.
The measured energy influx for carbon deposition were in the order of *0.03 ... 0.1 J/cm²s* . The values are in a good agreement with the energetic contributions which are calculated on the basis of the model.

**References**


[1] G. Federici, C.H. Wu,
J. Nucl. Mater., 207 (1993) 62.
[2] J. Winter,
Plas. Phys. Contr. Fusion, 38 (1996) 1503.
[3] A. Annen, A. von Keudell, W. Jacob,
J. Nucl. Mater., 231 (1996) 151.
[4] W. Wang, W. Jacob, J. Roth,
J. Nucl. Mater. 245 (1997) 66.
[5] H. Deutsch, H. Kersten, A. Rutscher, Contrib. Plasma Phys.29(1989),203.
[6] J. A. Thornton, J.Vac.Sci.Technol.11(1974) 606.
[7] H. Kersten, E. Stoffels, W.W. Stoffels, M. Otte, C. Csambal, H. Deutsch, R. Hippler, accepted for publication in J.Appl.Phys. 4/2000.
[8] H. Kersten, D. Rohde, J. Berndt, H. Deutsch, R. Hippler, submitted to Thin Solid Films
[9] N. Hershkowitz, D. Breuner, J.Ding, K. Kirmse, Does it matter what type of source is used for plasma etching of semiconductors, ISPC12(1995) 533
[10] W. Eckstein, J.P. Biersack,
Z. Physik B, 63 (1986) 471.
[11] H. Kersten, G. M. W. Kroesen, R. Hippler;
Thin Solid Films, 332 (1998) 282.


Presentations:

D. Rohde, H. Kersten, P. Pecher, W. Jacob, R. Hippler: „Sputtern von metalldotierten a-C:H-Schichten mittels DC-Magnetron", Doktorandenkolloquium IPP Garching 1999.

D. Rohde, H. Kersten, P. Pecher, W. Jacob, R. Hippler: „Untersuchungen zum Energieeinstrom bei der a-C:H-Schichtabscheidung" DPG-Tagung „Dünne Schichten", Münster 1999, DPG-Verhandlungen S.656.

H. Kersten, D. Rohde, P. Pecher, W. Jacob, R. Hippler: „Untersuchungen zum Energieeinstrom: Vergleich zwischen ECR-plasma und Magnetronsputtern", 9. Bundesdeutsche Fachtagung „Plasmatechnologie", Stuttgart 1999, S.102.

H. Kersten, A. Knuth, R. Hippler: „Eine einfache Thermosonde zur Bestimmung des Energieeinstroms beim Plasma-Processing" , Stuttgart 1999, S.103.

Publications:

H. Kersten, D. Rohde, J. Berndt, H. Deutsch, R. Hippler: „Investigations on the energy influx at plasma processes by means of a simple thermal probe",
submitted to Thin Solid Films.

D. Rohde, P. Pecher, H. Kersten, W. Jacob, R. Hippler: „On the energy influx at plasma deposition of a-C:H layers",
submitted to Contrib. Plasma Phys.

# INSTITUT FÜR EXPERIMENTELLE UND ANGEWANDTE PHYSIK DER CHRISTIAN-ALBRECHTS-UNIVERSITÄT ZU KIEL

(Prof. Dr. Ulrich Stroth)

Cooperation with IPP on the fields plasma turbulence in toroidally confined plasmas and comparison with numerical turbulence simulations as well as diagnostic development for turbulence measurements.

## 1. Turbulence Studies in the TJ-K Torsatron

(N. Krause, C. Lechte, S. Niedner, F. Greiner)

Understanding the plasma turbulence is one of the most challenging topics in the physics of toroidally confined plasmas. Although numerical simulation of MHD and drift-wave turbulence has much progressed in the past years, detailed experimental tests of the models are difficult to carry out. Due to advanced plasma parameters of fusion plasmas, detailed probe measurements are not possible. Other diagnostics are not able to provide the necessary full set of density, temperature, potential and magnetic field fluctuation data.

At Kiel University the TJ-K torsatron is operated with low temperature plasmas. This will enable probe measurements with high temporal and spatial resolution to investigate core plasma turbulence in a fusion relevant magnetic topology. TJ-K is the former TJ-IU torsatron built and operated at CIEMAT. Major and minor radii are 0.6 and 0.1 m, respectively; the magnetic field strength will be limited to 0.2 T. TJ-K will be operated at reduced plasma parameters. Using a 5 kW helicon-wave heating system, electron temperatures in the order of 10 eV and densities of up to $10^{18}\,m^{-3}$ are envisaged.

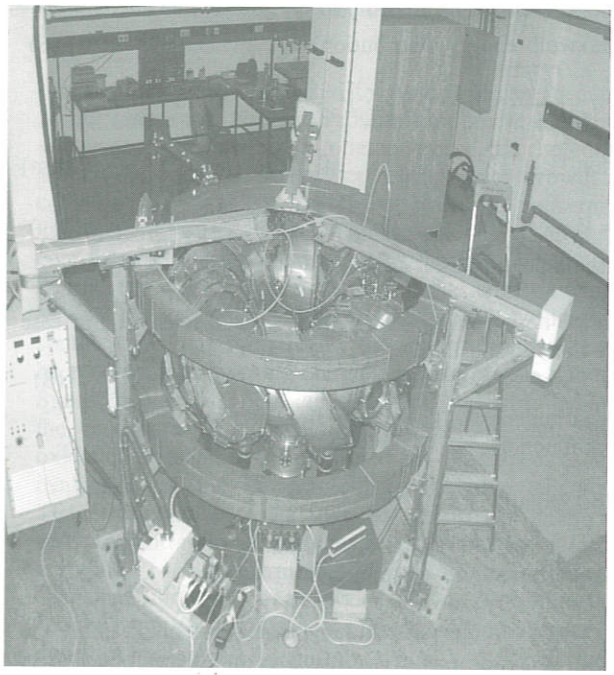

*FIG.: The Torsatron TJ-K in its new laboratory.*

## 2. Project Status

In October 1999, TJ-K was transferred from Madrid to Kiel. It was moved into the experimental Hall, reassembled and welded to the basement. A vacuum system was installed and helium glow discharges were used for vessel cleaning. Without baking, the base pressure is now $< 5\ 10^{-7}$. The magnetic field coils were connected to an existing power supply. Since the available current is limited to 1.2 kA, all coils had to be connected in series. The ratio between the currents flowing in the toroidal and vertical field coils is controlled by a shunt, which was also installed at the end of the year. Coil tests were successfully carried out. Field measurements with a electron beam will follow in 2000. Remote machine control and data acquisition software was developed in LabView. The programs are running on two PCs and the software is currently being tested.

## 3. Heating and Diagnostics Development

The plasma will be heated by Helicon waves. A 5 kW amplifier with the necessary RF equipment will be installed in February 2000. For initial tests, a small half-wavelength helical antenna (Nagoya Type III) is available. A larger antenna, encompassing the whole plasma cross-section, is under design.

Langmuir probe arrays will be used to measure the fluctuating plasma parameters. For initial measurements, a movable probe was built. The probe allows to scan the full plasma cross-section. A poloidal 32-tip probe array and magnetic probes

will be built in 2000. Furthermore, a interferometer and a field-line-tracing diagnostic are planned for the near future.

## 4. Theoretical Studies

To explore the accessible plasma parameter range, the global power balance of a low temperature plasma was investigated. The available heating power is mainly balanced by ionization, radiation and convective losses. Heat conduction was neglected and the convection was calculated from the particle balance. The calculation is based on rate coefficients which were obtained by folding the cross-sections for helium and argon with a Maxwellian. The power balance shows that in Helium a density of $10^{18}$ $m^{-3}$ and a temperature of 10 eV are possible. Higher temperatures are possible at lower density and vice versa. The estimated plasma parameters will be compared with parameter variations in TJ-K and other devices. Control parameters are neutral gas pressure, heating power and the kind of gas used. Microscopic and statistical properties of the turbulence are theoretically investigated with a drift-Alfvén turbulence code from B. Scott, IPP. The realistic magnetic configuration of TJ-K and Wega, Greifswald, will be implemented with the help of A. Kendl, IPP. Changing the plasma beta, the transition from drift-wave to MHD turbulence is studied with the goal to identify statistical parameters or microscopic correlation characteristics, which can be used to disentangle experimentally the mechanism driving the plasma turbulence in TJ-K and Wega. This work is in progress. The flexibility of the magnetic configuration of TJ-K will be exploited to investigate the influence of magnetic curvature, shear and well on turbulence.

# TECHNISCHE UNIVERSITÄT MÜNCHEN
# LEHRSTUHL FÜR MESSSYSTEM- UND SENSORTECHNIK

(Prof. Dr. Alexander W. Koch*)

The cooperation IPP – Technische Universität München is concentrated on the development of speckle-measurement techniques to detect arc traces, deformation, erosion, surface roughness, surface structure and surface shape in the divertor region of experimental fusion devices. The optical method is superior to any mechanical method with respect to data acquisition time and non-perturbing measurement.

## DETECTION OF EROSIVE AREAS

(M. Jakobi, P. Evanschitzky*, M. Kassasia*)

The use of phase-shifting methods in speckle interferometry allow, for example, determination of deformations of rough objects with three-dimensional information, and the detection of surface micro relief changes. Fig. 1a shows a surface deformation measurement of a graphite tile performed with a Twyman-Green interferometer set-up, an argon laser and a CCD camera. The detected image corresponds to a measurement area of 14 x 14 mm² and is perturbed by the surface micro relief change caused by an electric arc.

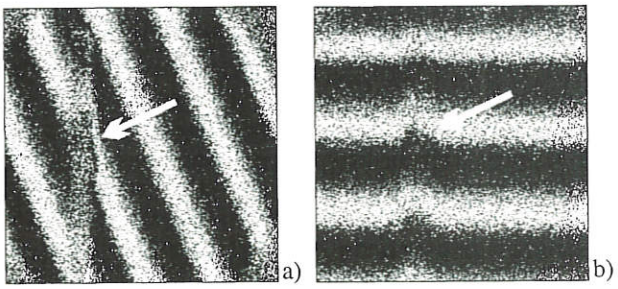


*FIG. 1: Detection of arc traces in phase-shifting images of strong erosion (a) and slight erosion (b).*

The amount of deformation is 250 nm if the grey scales change from black over different levels of grey to white. The fringes are introduced by tilting the test object. The erosion shown in Fig. 1a is stronger than that of Fig. 1b since the fringes in Fig. 1a are interrupted and those of Fig. 1b are only slightly curved. Hence, the erosion can be clearly detected. The erosion shown in Fig. 1b changes the phase by approximately a fourth of the fringe spacing. This corresponds to a maximum erosion depth of 80 nm on the assumption that the distribution of the surface height change is a Gaussian distribution. Since the erosion shown in Fig. 1a interrupts the fringes and is detected as strong perturbation in the phase-shifting image, the erosion depth is larger than the amount that completely disturbs the phase, i.e. 240 nm.

During a speckle experiment it is very difficult to change experimental parameters and study their influences separately one after the other. Therefore, speckle image simulation puts a method to hand that can check the practicability of the speckle method for new measurement needs. The simulation is based on coherent ray tracing allowing image evaluation with conventional personal computers.

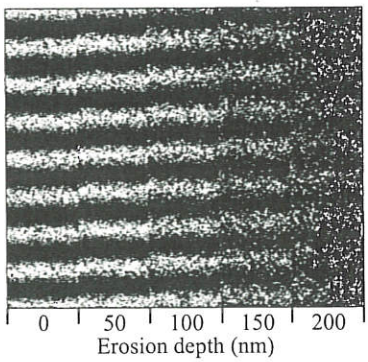


*FIG. 2: Simulation of fringe contrast affected by erosion.*

The simulation result of a deformation measurement affected by erosion, shown in Fig. 2, is divided in five vertical stripes, which have different fringe contrasts caused by different quantities of erosion depth ranging from 0 nm to 200 nm. The simulation results agree well with analytically derived results.

# INSTITUT FÜR PLASMAFORSCHUNG (IPF) DER UNIVERSITÄT STUTTGART

(Prof. Dr. U. Schumacher)

Since about three decades Max-Planck-Institute of Plasma Physics (IPP) at Garching and Institute of Plasma Research (IPF) at Stuttgart University are collaborating closely on developments, measurements, and interpretations of heating and diagnostic systems. The cooperation primarily aims at application of microwave heating, current drive, and diagnostics - mainly for W7-X - and contributions to emission and absorption spectroscopy for bulk and divertor plasma diagnostics.

## 1. PLASMA HEATING

(H. Z o h m[1] , L. Empacher[2], W. Förster, G. Gantenbein, H. Hailer, E. Holzhauer, S. Klenge, W. Kasparek, A. Letsch, J. P. Meskat, A. Mück, G. A. Müller, B. Plaum, P. G. Schüller, K. Schwörer, R. Wacker, W. Xu)

[1] until October 31, 1999 [2] until April 30, 1999

In collaboration with IPP Garching, FZK Karlsruhe, and IAP Nizhny Novgorod.

The investigation of the application of ECRH to fusion plasmas was continued. On the technical side, the work on the W7-X ECRH system was the major part, although the support for W7-AS and ASDEX Upgrade was continued. In addition, studies of the MHD stability of ASDEX Upgrade high-β discharges and the use of ECRH / ECCD to influence this stability became a major issue. Also, our general developments in the field of millimetre wave technology as well as the study of microwaves as a plasma diagnostic tool are reported here.

### 1.1 Electron cyclotron resonance heating (ECRH)

#### *1.1.1 ECRH on W7-AS*

Plasma heating using 70 GHz for fundamental and second harmonic electron resonance was used from the beginning on W7-AS. Two 70 GHz gyrotrons with 200 kW power per unit will be replaced by one gyrotron on the Bravo socket with a power of around 0.5 MW equipped with a voltage depressed collector (VDC). The benefit of this new technique is an efficiency increase of microwave power generation from 30% to nearly 50%. The technique was tested on a 140 GHz, 800 kW VDC gyrotron from Gycom which was installed on the Alpha socket powered by a high voltage power supply specially designed for operation with voltage depression of the electron beam collector. Stable microwave output power could be achieved by stabilisation of the beam acceleration voltage (70-80 kV). This stabilisation could be attained using a low power high voltage regulator (20-30 kV) connected between resonator body and collector of the gyrotron. This circuitry allows the use of a high power high voltage supply for the electron beam current without need for a high precision and expensive voltage regulation.

Following this scheme a high precision regulator for high voltage body supply for the new 70 GHz gyrotron was developed. This regulator modulator consists of a 45 kV switch mode power supply which feeds a linear amplifier with a final stage consisting of two high voltage tetrodes connected in serial push pull. The socket for the Bravo gyrotron is completed by a supply for cathode filament heating and monitoring of voltages and currents together with alarm for tube protection by fast high voltage switch off.

#### *1.1.2 ECRH system for ASDEX Upgrade*

Contributions of IPF to the ECRH system on ASDEX Upgrade aim at construction, operation, and maintenance of the 140 GHz system. Experiments to control MHD instabilities with ECRH/ECCD were planned, performed, and evaluated (cf Section 1.2). The construction of the transmission system for the millimetre wave power was finished for three gyrotrons and it is routinely in operation.

To improve the transmission efficiency measurements of the amplitude distribution of the gyrotron beams were performed (see Annual Rep. 1998). From these data the complex field distribution of the beams was reconstructed numerically and the transformation with existing mirrors was modeled. The average losses in the transmission lines are about 10 % which is in good agreement with estimates. When the fourth gyrotron will be available it is planned to measure the beam profile and to calculate optimised mirrors for the transmission system.

#### *1.1.3 ECRH system for W7-X*

##### *1.1.3.1 Multibeam transmission system*

The transmission of the millimetre waves for ECRH on W7-X will be realised fully optically using a modular mirror system. In 1999, the thermo-mechanical calculations for the mirrors were essentially completed. In contrast to earlier plans, it is envisaged to fabricate the mirrors from stainless steel with a copper surface. This concept shows smaller deformations in case of excursions of the cooling water temperature, furthermore the risk of material stress in the mirror is lower compared

to the former Al/Cu sandwich design. The cooling structures were optimised leading to a maximum increase of the surface temperature of only 20 °C. Several test pieces to verify mirror concept and fabrication method were produced. Cooled mirrors for test purposes as well as for the gyrotron test facility at FZK Karlsruhe are under construction.

The parameters of the transmission system are mainly frozen, the design of the standard mirrors for the MBWG, the matching optics and the polarisers is finished. After a successful test of a MBWG-mount, the parts for the non-cooled prototype MBWG at IPF were ordered. Purchasing, mounting, and test of measurement systems were continued. The multiple beam simulator was put into operation, a measured far-field pattern is shown in **Fig. 1.1**.

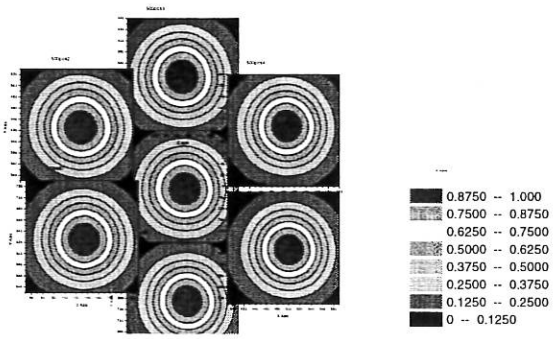


*FIG. 1.1: Far-field pattern of the multiple beam simulator measured at the position of the first MBWG mirror.*

*1.1.3.2 Voltage regulator for gyrotron power control*

The microwave output power generated in gyrotrons with voltage depressed collector is controlled by the acceleration voltage for the electron beam between cathode and resonator which is insulated from the electron collector. Typical values for this acceleration voltage are 80 kV. A fraction of this electron beam energy can be recovered after interaction with the microwave field of the resonator by a deceleration voltage between resonator (body) and electron collector. A typical value for this voltage is 30 kV. Therefore the main power supply, connected between cathode and collector has a voltage in the range of around 50 kV with a corresponding current of about 40 A for a gyrotron with 1 MW microwave output power. The current to the resonator body stays below 100 mA.

For the completion of the equipment of the FZK gyrotron test site a supply for the body voltage (0-30 kV, 0-300 mA) was built at IPF. This supply is a modification of the type developed for W7-AS (see 1.1.1).

The development of the corresponding devices for the 10 gyrotrons for ECRH on W7-X at Greifswald was continued. This development is profiting from experiments with the prototype from the test site and incorporates additional modules with microcomputer systems which act as interfaces to the general control system of the W7-X stellarator experiment.

*1.1.4 ITER contributions*

In 1999, work on the ITER-relevant concept of remotely steerable antennas continued with the aim to increase the scanning range. This scheme is based on the imaging properties of rectangular corrugated waveguides which would allow the installation of the movable mirrors outside of the ITER vacuum vessel. Numerical calculations were started to optimise the corrugation depth of the guides to reduce the phase slippage between the modes which carry the power for high scanning angles. An experimental proof of this concept failed up to now due to the limited precision of the corrugations. In addition, the integration of mitre bends into the antenna for neutron screening was investigated. It could be shown, that such "dog-legs" are in principal possible, however, at the price of a reduced beam quality.

## 1.2 MHD stability studies

The study of the MHD stability of fusion plasmas mainly concentrated on the formation of magnetic islands due to neoclassical tearing modes at the resistive β-limit. The possibility of removing these islands by small amounts of ECRH power is studied theoretically and experimentally in ASDEX Upgrade. In addition, ECE diagnostics is used on ASDEX Upgrade to infer details about the structure of the magnetic island.

*1.2.1 Active control of neoclassical tearing modes (NTM) using ECRH / ECCD*

*1.2.1.1 Experiments on ASDEX Upgrade*

Experiments on the stabilisation of neoclassical tearing modes on ASDEX Upgrade were continued. For the strongly NBI heated (10 - 12.5 MW) plasma (lower single null ELMy H-mode, plasma current 0.8 MA, electron density of $n \approx 5\times10^{19}$ m$^{-3}$), the achievable β is usually limited to $\beta_N = 2.2 - 2.8$ by the occurrence of neoclassical tearing modes with mode numbers m = 3, n = 2. In previous experiments partial stabilisation of NTM by applying ≈ 800 kW of RF power was successfully demonstrated. These experiments were performed with phased ECCD injection (AC) where the gyrotrons were feedback controlled to launch their power in the O-point of the island. However, it was shown that stabilisation can also be achieved by continuous injection (DC) with practically the same efficiency. For the DC ECCD experiments reported here three gyrotrons at 140 GHz were used (2$^{nd}$ harmonic X mode, B= 2.5 T), each delivering 0.4 MW of RF power to the plasma. The injection was performed from the low field side of the tokamak, and the beams were launched with an angle of -15° (co-CD) and +15° (counter-CD) with respect to the radial direction. The magnetic field was changed slowly during a discharge (5 %, within 1.5 s) to match the position of the EC resonance and the island.

**Figure 1.2** shows the temporal evolution of a discharge with co-CD. The Mirnov coil which detects the mode shows that the island vanishes and is completely suppressed by ECCD injection.

In case of counter CD we used the same operating parameters of the tokamak but reversed launching angle of the antennas. Here heating and counter-CD are competing effects and may cancel each other partially. **Figure 1.3** shows a discharge with counter ECCD injection, where the island did not vanish, but was reduced to about half the width.

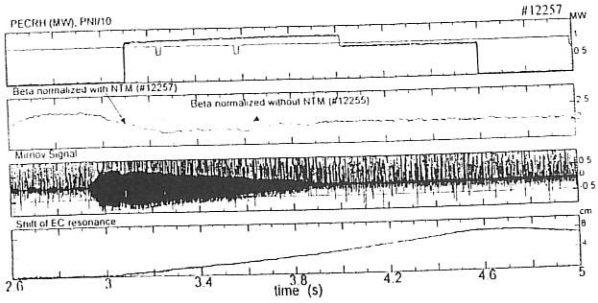


*FIG. 1.2: Stabilisation of a 3/2 neoclassical tearing mode by ECCD power. $\beta_N$ of this discharge is compared to a (nearly) identical discharge without NTM.*

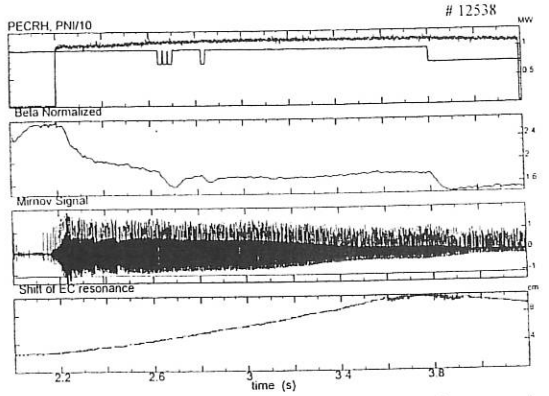


*FIG. 1.3: Example of a counter CD experiment where a partial stabilisation of the NTM can be observed.*

### 1.2.2 *Analysis of the structure and dynamics of magnetic islands*

For further work on active control of tearing-modes, detailed knowledge of tearing-mode dynamics and island structure is important. Therefore, a new analysis method for the temperature profile of magnetic islands and the associated magnetic structure was developed.

The ECE system of ASDEX Upgrade was used to measure the temperature profile with improved temporal (500 kHz, 1 MHz, 5 MHz) and high spatial resolution at fifteen radial positions in the island region (see **Fig. 1.4**). The analysis of the radial profile of the first Fourier component of an island temperature profile yields the position of the resonant surface and the island width. To relate these data to the magnetic structure of the island, a model of the helical equilibrium and perturbed flux is applied. Using the heat flux equation, the perturbed plasma temperature profile is computed numerically. The island geometry determines the Fourier spectrum of the temperature oscillation. By fitting the theoretically predicted temperature oscillation to the experimental data it is possible to determine the equilibrium flux and the perturbation flux. This can be used in order to assess the nonlinear stability parameter Δ' from ECE data.

The steady-state temperature profile obtained by the numerical solution of the stationary heat flux equation will be compared with the results of a time dependent plasma transport code developed at IPP Garching [Q. Yu and S. Günter, Phys. Plasmas, Vol. 5, No. 11, 1998]. This may contribute to a further investigation of the temperature profiles inside magnetic

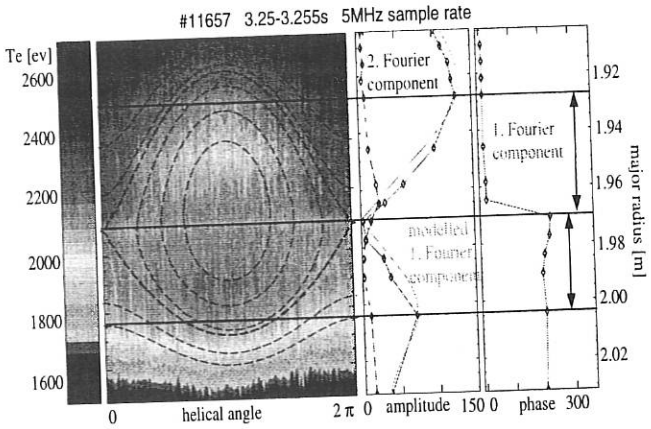


*FIG. 1.4: Temperature profile of a neoclassical magnetic (3,2) island at the β-limit. The dashed lines indicate the reconstructed magnetic flux structure of which the modelled first Fourier component matches the experimental data best (Δ' = -11).*

islands which, in contrast to simple theory, are not completely flattened. This phenomenon seems to be due to the finite ratio of heat conductivity parallel and perpendicular to the magnetic field, and localised heat sources inside the island.

### 1.2.3 *Analysis of the effects of ECRH on sawteeth in ASDEX Upgrade*

Work was started to study the sawtooth behaviour of the plasma during ECRH injection both, experimentally and using a numerical model. In ECRH discharges, the radial temperature profile of the plasma and the sawtooth period are strongly correlated to the deposition radius of the heating power. Depending on this radius the ECRH power may have a destabilising or a stabilising effect.

A model based on a resistive kink developed by B. B. Kadomtsev was implemented in a code of F. Porcelli and E. Rossi in order to simulate the data of ECE- and SXR-diagnostics. The code predicts frequency doubling, which is consistent with the experimental data and can be explained with the formation of a hot island. Fourier analysis (cf Section *1.2.2*) will be used to determine if the sawteeth are driven by a kink or by a tearing instability.

## 1.3 General developments in millimetre wave technology

### 1.3.1 *Investigations of materials for in-vessel components and absorbers*

The knowledge of the properties of dielectric materials suited for absorption of high power microwave radiation in calorimetric loads and dummy loads and for the design of wall coatings and in-vessel structures is of great importance. Therefore, a measuring device was built consisting of an open resonant cavity in a vacuum vessel mounted on a vacuum oven allowing sample temperatures up to 1800 °C.

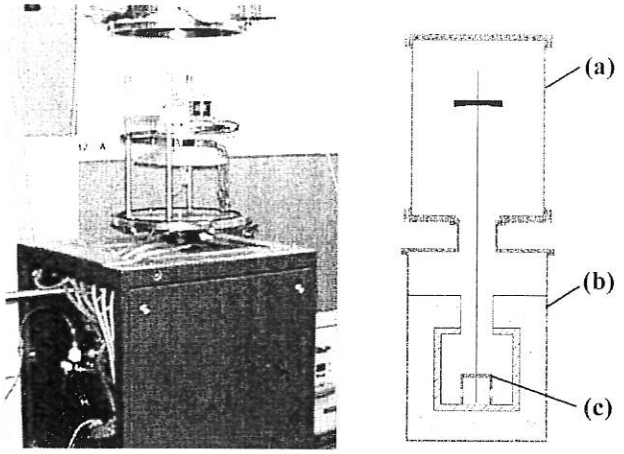


*FIG. 1.5: Photograph and scheme of the resonator (a) and oven vessel (b), and test sample position (c).*

**Figure 1.5** shows a photograph of the experimental setup and a scheme of the combined resonator (a) and oven (b) vacuum vessel.

In combination with a vector-network-analyzer measuring amplitude and phase of the wave field in the resonant cavity the Q-factor and resonance frequency with and without sample can be determined. This allows calculation of permittivity ε and loss tangent tan δ of the test material. With the given dimensions of the oven the length of the nearly hemispherical Fabry-Perot resonator was set to 820 mm leading to a beam waist of $w_0$ = 17 mm for 140 GHz at the sample position (c) close to the bottom of the heated chamber.

### *1.3.2 Numerical optimisation of waveguide components*

The development of codes for the optimisation of waveguide components (especially bends) was continued. The curvature is approximated by Chebycheff-polynomials or a Fourier series. The coefficients of the approximation as well as the corrugation depth for corrugated waveguides are taken into account for the optimisation. The code works for rectangular and corrugated or smooth cylindrical waveguides. In the present implementation, the optimisation is done with a genetic algorithm.

A corrugated 28 GHz $TE_{01}$ bend with a total angle of 90° for high power application (10 kW) was optimised for both low spurious mode power inside the bend and little spurious modes at the output. Starting with a constant curvature, the code found a curvature function with two maxima (see **Fig. 1.6**). This optimised curvature is significantly different from the analytic curvature functions (e.g. sin, $\sin^2$), which are normally used for the design of waveguide bends.

**Figure 1.7** shows the mode spectrum along the bend for the initial and optimised case. One can see, that both, the peak power of spurious modes inside the bend and the output power of spurious modes at the bend output are optimised simultaneously. This optimised bend is currently under construction and will be tested soon. The present codes will also be extended for the optimisation of bended mode converters and the implementation of other optimisation techniques (e.g. Downhill Simplex).

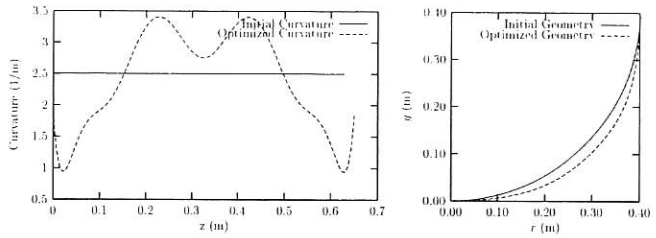


*FIG. 1.6: Initial and optimised curvatures (left) and correspondingly bent shapes (right).*

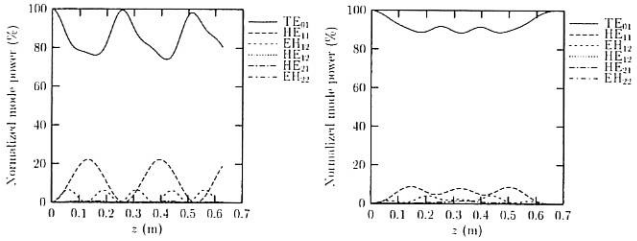


*FIG. 1.7: Mode spectrum along the initial (left) and the optimised (right) bend.*

### *1.3.3 Microwave beam diagnostics by thermographic recording*

Program components set up in past years in order to read and evaluate the data from a thermographic system and to derive the information needed for beam correcting mirrors were developed further with the aim to accept also the data sets from another, recently acquired thermo-camera, and to get a consistent package that shall also become portable to other computer systems.

## 1.4 Millimetre wave diagnostics

### *1.4.1 Reflectometry experiments on W7-AS*

On the stellarator W7-AS heterodyne measurements with the existing tilted antenna (fixed tilt angle) were continued. First measurements show that it is possible to extract information about **E×B** plasma rotation from the asymmetric frequency shift in the frequency spectra. As an example, in ECRH experiments which were performed in the context of the "electron-root" studies the shift of the drift wave spectra from the electron-diamagnetic to the ion-diamagnetic direction indicates the occurrence of a positive radial electric field. In addition a new antenna system has been installed which allows to change the tilt angle continuously. With this antenna the poloidal wavenumber spectra of the density turbulence could be scanned. Another significant result is the observation that the width and frequency shift of the measured frequency power spectra can change dramatically in different confinement regimes.

### *1.4.2 Microwave reflectometry on ASDEX Upgrade*

In 1999, a tunable heterodyne reflectometer (V-band, 48 - 75 GHz) was built and tested on ASDEX Upgrade. The tilted antenna system (tilt angle ≈ 8 deg.) allows the system to operate as a Doppler reflectometer. In this frequency range both, the plasma edge and bulk can be scanned. First measurements of turbulent density fluctuations were performed for various discharge parameters. The observed asymmetric frequency spectra allow to determine the propagation velocity of the fluctuations in the laboratory frame. Currently a computer based frequency control and data acquisition system with a sampling rate of 20 MHz is being installed.

As an example for the output of the I/Q detector **Fig. 1.8** shows the complex signal, measured during a time interval of ≈ 15 µs in an H-mode discharge with 5.0 MW NBI. The microwave frequency of 58.6 GHz corresponds to a nominal cut-off layer at a minor radius r/a ≈ 0.3 in the bulk of the plasma.

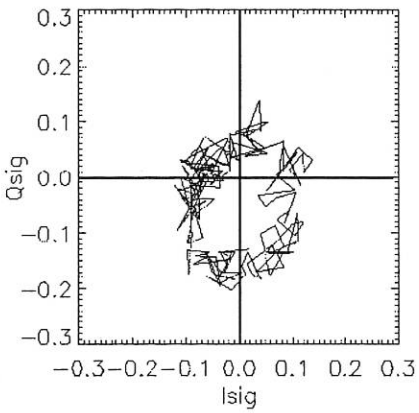


*FIG. 1.8: I/Q signal, shot number 12560, f = 58.6 GHz ≙ 1/3 minor radius, NBI power 5.0 MW.*

In the time interval of 15 µs the vector in the complex plane approximately describes a circle which includes the origin. This is typical for an output which contains both the unshifted $0^{th}$ order reflected signal and the Doppler shifted $1^{st}$ order backscattered signal. As can be seen the turbulence level in the reflecting plasma layer is high enough that the Doppler shifted microwave power scattered into the first order dominates the $0^{th}$ order (no Doppler shift), therefore precise measurements of propagation velocity and direction are expected.

## 1. 5 WEGA

In connection with the intended revival of the WEGA experimental device at Greifswald, work was contributed in preparing the transfer of this device and in planning its new setup. In addition, a new version of the Gourdon code for WEGA is being created, based on the latest version of this code and adapting routines especially developed for the WEGA configuration. Using preliminary versions of this code, calculations of magnetic field distributions inside and outside of the torus vessel were done. Also, work is in progress to revise the Gourdon code, to convert it to the FORTRAN 95 standard, and to improve its applicability and performance.

# 2. PLASMA EDGE DIAGNOSTICS

( U. S c h u m a c h e r, I. Altmann, G. Dodel, K. Hirsch, E. Holzhauer, B. Roth, D. Schinköth, K. Schmidtmann, and J. Schneider)

## 2.1 Spectroscopic measurements of plasma parameters in the divertor of ASDEX Upgrade

Low electron temperatures in the range of 1 eV were measured spectroscopically in the divertor of ASDEX Upgrade. These plasmas are dominated by three-body recombination. Because of the strong volume recombination the plasma flux is changed into an isotropic neutral flux. Thus the power entering the divertor is spread onto a larger area of the divertor target than for the directed plasma flow, and hence the plasma wall interaction is reduced substantially.

The recombination radiation from neutral hydrogen was used for the determination of the plasma parameters. Various spectroscopic methods exist for the determination of the electron temperature. They rely on the observation of the continuous radiation from bound-bound transitions and free-bound transitions in atomic hydrogen. The Boltzmann plot is based on the measurements of the population densities and line intensities, respectively, of the hydrogen levels above the collision limit, which sensitively depend on the electron temperature. Another method to derive the electron temperature is based on the intensity ratio of the hydrogen continua. The application of the intensity ratio of the Balmer and Paschen continuum around the wavelength $\lambda$ = 364 nm is called the Balmer sprung method.

The measurements show, that the Boltzmann plot and Balmer sprung methods do not give the same results. The temperatures derived from the Boltzmann plot (Balmer line intensities from quantum numbers n = 6 ($\lambda$ = 410.2 nm) up to n = 10 ($\lambda$ = 379.8 nm)) are found to be significantly lower than those obtained from the Balmer sprung method. This discrepancy can be explained by taking the inhomogeneity of the divertor plasma into account. The measured intensities are line-of-sight integrated along density and temperature gradients. Due to the different dependencies of the Balmer and Paschen continua and of the Balmer line intensities on temperature, the weighting effect of the emission results in deviations of the temperature values obtained from the different diagnostic methods applied.

The interpretation of these experimental data was supported by B2-EIRENE code calculations. The line and continuum intensities were calculated with the results of the density and temperature profiles along the lines-of-sight obtained with this code. It was found, that the temperatures determined by the spectroscopic methods of the Boltzmann plot and the Balmer sprung tend to be lower and upper bounds of the line averaged electron temperature when applied to an inhomogeneous divertor plasma.

The electron density in the divertor region was measured by the Stark broadening of the Balmer line H$\beta$ ($\lambda$ = 486.1 nm) and by the absolute Balmer continuum radiation. The electron density is determined from the Stark broadened Balmer line by fitting profiles from model calculations (S. Günter) of the Stark profiles of H$\beta$ which take the ion dynamics and the static magnetic field into account. Both methods yield electron densities of several $10^{20}$ $m^{-3}$.

## 2.2 Erosion studies from emission and absorption spectroscopy

The determination of erosion mechanisms and of erosion rates as a function of the plasma parameters is of major importance not only for tests of thermal protection materials for reusable space transportation systems but also for plasma facing components in thermonuclear fusion devices. Plasma jets interacting with targets of the material in question are applied for these measurements and material tests. One of the methods is to study the erosion of a C/C-SiC target in such a plasma jet by high resolution emission and absorption spectroscopy of Si I resonance spectral lines at 251 nm and 288 nm, respectively. The silicon is eroded by the plasma jet and forms a disc like radiating cloud in front of the target. Spectrally resolved profiles of the Si I resonance lines are obtained applying an Echelle spectrometer, whereas line integrals were measured with a ¾ m spectrometer.

Various methods to determine the silicon neutral density from the absorption measurements are applied. The influence of self absorption on the resonance lines of Si I in the $3p^2\ ^3P$ - $3p4s\ ^3P^o$ multiplet was investigated in detail by short time (1 ms) spectroscopy of the correlated multiplet line integrals. Due to the exponential dependence on the electron temperature the excitation of the Si I resonance lines is mainly concentrated in the high temperature central region of the plasma jet.

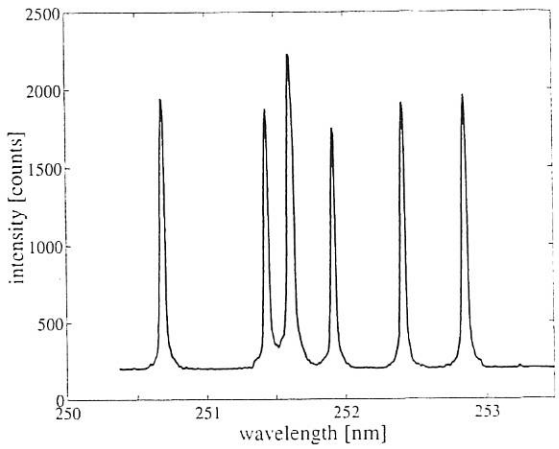


*FIG. 2.1: Silicon multiplet emission from the highly absorbing Si cloud.*

**Figure 2.1** gives an example of the Si I multiplet for the case of relatively high self absorption, which is expressed by the optical depth $\tau_{251.6\ nm}$ of the strongest line of this multiplet being larger than 15. Besides the line at the wavelength of 251.9 nm all spectral lines of that multiplet show saturation at the black body (Kirchhoff-Planck) limit. Detailed investigations of these short time emission spectra of the Si I resonance line multiplet are under way. First rough temperature estimates from the absolute maximum line intensities yield an electron temperature in the range of 4500 K.

The conditions of plasmas with high concentrations of eroded neutral Silicon are additionally investigated by transmission experiments. First results of the transmission were obtained from measurements with a periodically pulsed Xe flash lamp imaged onto the central part of the interaction region of the plasma jet with the C/C-SiC target. The flash lamp operates at a light pulse e-folding length of about 100 µs, which is sufficiently short compared to the characteristic fluctuation timescales of more than 300 ms. The repetition rate was varied in the range of 1 to 10 Hz depending on the read-out cycle of the ICCD camera system.

High resolution spectral transmission measurements of the line pair of the multiplet at the wavelengths 251.6 nm and 251.4 nm were performed using the Echelle spectrometer, while line integrated measurements of the complete multiplet spectrum were taken with a ¾ m ACTON spectrometer. The spectra of both spectrometers were recorded using a double pulse ICCD camera. **Figure 2.2** shows an example of simultaneous transmission and emission measurements taken with the Echelle spectrometer. The spectra show pronounced absorption effects, which allow to determine the optical depth directly and hence, together with the length of the line of sight and the atomic data, the silicon neutral density. Since the line width of the absorption profile also depends on the optical depth (assuming a Voigt profile), an independent support for the value of the optical depth results from the different profile widths of the two spectral lines.

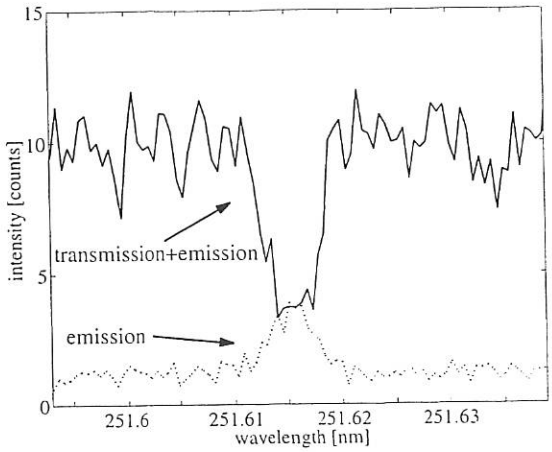


*FIG. 2.2: Example of a spatially integrated absorption and emission spectrum of two lines in the Si I multiplet showing pronounced absorption effects.*

## 2.3 Contributions to atomic data of silicon

The evaluation of the silicon density in the interaction region of a plasma jet with a C/C-SiC target is based on the interpretation of the measured spectra of the silicon multiplet at 251 nm, which consists of the $^3P$ - $^3P^o$ transitions. Electron impact is one important channel for excitation. For the low temperature region the Born approximation (widely used for the high energy range) is not an appropriate approach to calculate the electron impact cross section near the threshold. Earlier R-matrix calculations of electron impact excitation cross sections took only three spectral terms ($^3P$, $^1D$ and $^1S$) into account.

New calculations were performed in collaboration with the University of Strathclyde in the ADAS framework. Up to 19 terms (like $^3F^o$, $^1F$ and $^3D^o$) in LS-coupling and new orbitals like 3d and 4p were included. The N+1 electron collision problem (N = 14 for Si I) was solved and convergence has been

reached for the orbital angular momentum $L \leq 18$ for energies below 8 eV. The calculations using orbitals of Thomas-Fermi type yield oscillator strengths for the transition of interest within 1 % of the measured values. Therefore cross sections of electron impact excitation including their complex resonance structure are calculated and will be applied in population models. For practical applications this resonance structure will be smoothed owing to multi-particle statistical behaviour. Collisional radiative model calculations for all Si I transitions observed are planned for the near future.

# PUBLICATIONS, CONFERENCE REPORTS, PATENTS, DOCTORAL THESES, DIPLOMA THESES, REPORTS, AND SEMINAR TALKS

## PUBLICATIONS


*Altmann, I., G. Bauer, K. Hirsch, H. Jentschke, S. Klenge, B. Roth, D. Schinköth, and U. Schumacher:* In-situ diagnostics of the interaction region between a nitrogen-oxygen plasma jet and hot C/C.SiC ceramic materials. Accepted for publication in High Temperatures - High Pressures, (see also SFB-Report 1999/46).

*Dodel, G.:* On the history of far-infrared (FIR) gas lasers: Thirty-five years of research and application. Infrared Phys. Technol. **40** (1999) 127-139.

*Empacher, L. and W. Kasparek:* Analysis of a multiple-beam waveguide for free-space transmission of microwaves. Submitted to IEEE Transactions on Antennas and Propagation (1999).

*Erckmann, V., G. Dammertz, D. Dorst, L. Empacher, W. Förster, G. Gantenbein, T. Geist, W. Kasparek, H.P. Laqua, G.A. Müller, M. Thumm, M. Weißgerber, H. Wobig, W7-AS team, and W7-X team:* ECRH and ECCD with high-power gyrotrons at the stellarators W7-AS and W7-X. IEEE Transactions on Plasma Science, **PS-27** (1999) 538-546.

*Gafert, J., K. Behringer, D. Coster, C. Dorn, A. Kallenbach, R. Schneider, U. Schumacher, and ASDEX Upgrade Team :* Spectroscopic investigation of the dynamics of ions and neutrals in the ASDEX Upgrade Divertor II. Journal of Nuclear Materials **266-269** (1999) 365-369.

*Hirsch, K., B. Roth, I. Altmann, K.-L. Barth, H. Jentschke, A. Lunk, U. Schumacher:* Plasma-induced silica-like protection layer formation on C/C-SiC heat-shield materials for reentry vehicles. High Temperatures-High Pressures **31** (1999) 455-465.

*Jentschke, H., K. Hirsch, S. Klenge, and U. Schumacher:* High resolution emission and absorption spectroscopy for erosion product analysis in boundary plasmas. Rev. Sci. Instrum. **70** (1999) 336-339.

*Kurzan, B. and E. Holzhauer et al.:* Measurement and scaling of the radial correlation length of density turbulence in AUG. Accepted for publication in Plasma Phys. Contr. Fusion.

*Mehringer, P., G.A. Müller, and H. Zohm:* Distribution of microwave intensity in a multi-mode cavity. Submitted to J. Microwave Power and Electromagn. Energy (1999).

*Ogawa, I., T. Idehara, S. Maekawa, W. Kasparek, and G.F. Brand:* Conversion of gyrotron output into a gaussian beam using the far field. Int. J. Infrared Millimeter Waves **20** (1999)801-822.

*Ogawa, I., T. Idehara, M. Pereyaslavets, and W. Kasparek:* Design of a quasi-optical system converting the TE06 output mode of a gyrotron into a gaussian -like beam. Int. J. Infrared Millimeter Waves **20** (1999) 543-558.

*Ogawa, I., A. Sakai, T. Idehara, and W. Kasparek:* Application of the complex beam parameter to the design of a quasi-optical transmission line for a submillimetre wave gyrotron. Int. J. Electronics **86** (1999) 1071-1084.

*Plaum, B., G. Gantenbein, W. Kasparek, M. Thumm, and D. Wagner:* Far-field calculations and measurements of an S-bend deformed oversized HE11-wavguide antenna. Int. J. Infrared Millimeter Waves **20** (1999) 1009-1018.

*Wagner, D., M. Thumm, and W. Kasparek:* Hybrid modes in highly oversized corrugated rectangular waveguides. Int. J. Infrared Millimeter Waves **20** (1999) 567-582.

*Zohm, H., G. Gantenbein, G. Giruzzi, S. Günter, F. Leuterer, M. Maraschek, J.P. Meskat, A.G. Peeters, W. Suttrop, D. Wagner, M. Zabiego, ASDEX Upgrade Team, and ECRH Group:* Experiments on neoclassical tearing mode stabilization by ECCD in ASDEX Upgrade. Nucl. Fusion **39** (1999) 577-580.


## CONFERENCE REPORTS

9. Bundesdeutsche Fachtagung für Plasmatechnologie, Stuttgart, March 3 - 5, 1999

*Altmann, I., G. Bauer, K. Hirsch, H. Jentschke, S. Klenge, B. Roth, D. Schinköth und U.Schumacher:* Untersuchung der Wechselwirkung eines Plasmastrahls mit einem C/C-SiC-Target. Poster PD1.

*Hirsch, K., B. Roth, I. Altmann, K.-L. Barth, H. Jentschke, A. Lunk und U. Schumacher:* Aufwachsverhalten einer $SiO_2$-ähnlichen Schutzschicht auf C/C-SiC-Hitzeschutzmaterial in einem Stickstoff-Sauerstoff-Plasma bei hohen Oberflächentemperaturen. Poster PS8.

Frühjahrstagung der Deutschen Physikalischen Gesellschaft, Fachausschuß Plasmaphysik, Heidelberg, March 15 - 19, 1999

*Altmann, I., K.-L. Barth, K. Hirsch, H. Jentschke, S. Klenge, A. Lunk, B. Roth, D. Schinköth und U. Schumacher:* In situ Diagnostiken für die Wechselwirkungszone zwischen Plasmafreistrahl und C/C-SiC Materialproben. Verhandl. DPG (VI) **34** (1999) P 20.16.

*Gantenbein, G., G. Giruzzi, S. Günter, F. Leuterer, M. Maraschek, J. Meskat, W. Suttrop, D. Wagner, M. Zabiego, and H. Zohm:* Einsatz von ECRH zur Stabilisierung neoklassischer Tearing Moden. Verhandl. DPG (VI) **34** (1999) P 11.4.

*Klenge, S., I. Altmann, K. Hirsch, H. Jentschke, B. Roth und U. Schumacher:* Untersuchungen der Selbstabsorption des SiI Multipetts bei 251nm mit korrelierter Emissionsspektroskopie. Verhandl. DPG (VI) **34** (1999) P 15.7.

*Meskat, J. P., S. Günter, S. Schade, W. Suttrop, H. Zohm, and ASDEX Upgrade Team:* Untersuchung von Tearing Moden in ASDEX Upgrade. Verhandl. DPG (VI) **34** (1999) P 11.3.

*Schinköth, D., G. Bauer, H. Jentschke, K. Hirsch und U. Schumacher:* Charakterisierung eines Freistrahlplasmas durch Emissionsspektroskopie und Laser-Thomson-Streuung. Verhandl. DPG (VI) **34** (1999) P 20.15.

*Schmidtmann, K., J. Gafert, S. Günther, U. Schumacher, and the ASDEX Upgrade Team:* Stark-Effekt-Messungen in dichten Divertorplasmen im Tokamak ASDEX Upgrade. Verhandl. DPG (VI) **34** (1999) P 9.4.

*Zohm, H., G. Gantenbein, G. Giruzzi, S. Günter, F. Leuterer, M. Maraschek, J.P. Meskat, W. Suttrop, M. Zabiego und ASDEX Upgrade Team:* Aktive Kontrolle magnetischer Inseln an ASDEX Upgrade. Verhandl. DPG (VI) **34** (1999) P 11.2.

III. Workshop on Microwave Reflectometry for Fusion Plasma Diagnostics, Cadarache, France, March 22 - 24, 1999

*Hirsch, M., E. Holzhauer, J. Baldzuhn, and B. Kurzan:* Doppler reflectometry for the investigation of poloidally propagating density perturbations. EUR-CEA-FC-1674, ed. F. Clairet, (1999).

26th EPS Conference on Controlled Fusion and Plasma Physics, Maastricht, The Netherlands, June 14 - 18, 1999

*Meskat, J. P., S. Günter, S. Schade, W. Suttrop, H. Zohm:* Analysis of the structure of tearing modes in ASDEX Upgrade. Conference Digest, P4.002 (1999).

*Zohm, H., G. Gantenbein, G. Giruzzi, S. Günter, F. Leuterer, M. Maraschek, J.P. Meskat, S. Schade, W. Suttrop, M. Zabiego:* Stabilization of neoclassical tearing modes by ECRH in ASDEX Upgrade. Conference Digest, P4.001 (1999).

4th International Workshop "Strong Microwaves in Plasmas", Nizhny Novgorod, August 2 - 9, 1999:

*Kasparek, W., V. Erckmann, H.P. Laqua, E. Borie, G. Dammertz, L. Empacher, W. Förster, G. Gantenbein, S. Illy, G. Michel, G. Müller, B. Piosczyk, M. Thumm, D. Wagner, M. Weißgerber, H. Zohm, W7-AS Team, and W7-X teams:* ECRH and ECCD for the stellarator W7-X. In "Strong Microwaves in Plasmas 1999" ed. A.G. Litvak, Inst. of Applied Physics, Nizhny Novgorod.

*Zohm, H. et al.:* The stabilization of neoclassical tearing modes by ECCD in ASDEX-Upgrade. In "Strong Microwaves in Plasmas 1999" ed. A.G. Litvak, Inst. of Applied Physics, Nizhny Novgorod.

International Workshop on Electron Cyclotron Resonance Heating Transmission Systems, Carmel, California, September 1 - 3, 1999

*Empacher, L., G. Gantenbein, F. Hollmann, W. Kasparek, P.G. Schüller, H. Zohm, D. Arz, V. Erckmann, H.P. Laqua, and M. Weißgerber:* Development of water-cooled mirrors for the 140 GHz transmission system for ECRH on the stellarator W7-X.

15th European Conference on Thermophysical Properties, Würzburg, Germany, September 5 - 9, 1999

*Altmann, I., G. Bauer, K. Hirsch, H. Jentschke, S. Klenge, B. Roth, D. Schinköth, and U. Schumacher:* In situ diagnostics of the interaction region between a nitrogen-oxygen plasma jet and hot C/C-SiC ceramic materials. Book of Abstracts, O6-3, p 87.

24. International Conference on Infrared and Millimeter Waves, Monterey, California, September 6 - 10, 1999

*Empacher, L., G. Gantenbein, F. Hollmann, W. Kasparek, P.G. Schüller, H. Zohm, D. Arz, V. Erckmann, H.P. Laqua, and M. Weißgerber:* Development of water-cooled mirrors for the 140 GHz transmission system for ECRH on the stellarator W7-X. Conf. Digest, TU-D7

*Plaum, B., D. Wagner, W. Kasparek, and M. Thumm:* Numerical optimization of waveguide bends using a genetic algorithm. Conf. Digest, TH-A5.

*Schüller, P. G., H. Hailer, and H.P. Laqua:* Compact absorber loads for high-power microwaves. Conf. Digest, TU-F3.

7th IAEA TCM on H-mode and Transport Barrier Physics, Oxford, UK, September 27 - 29, 1999

*Hirsch, M., E. Holzhauer et. al.:* Operational conditions and characteristics of ELM-events during H-modes in the stellarator W7-AS. To appear in Plasma Phys. Contr. Fusion.

11th Joint Workshop on ECE and ECRH, EC-11 and IAEA-TCM, Oh-arai, Japan, October 4 - 8, 1999

*Chirkov, A. V., G.G. Denisov, F. Hollmann, G. Gantenbein, M. Haug, W. Kasparek, and D. Wagner:* Simulation and experimental study of a remote steering system for ECRH/ECCD antenna beams. JAERI Report, submitted to Fusion Engineering and Design.

*Empacher, L., G. Gantenbein, F. Hollmann, W. Kasparek, P.G. Schüller, H. Zohm, D. Arz, V. Erckmann, H.P. Laqua, and M.Weißgerber:* Developments for the 140 GHz ECRH transmission system for the stellarator W7-X. JAERI Report, submitted to Fusion Engineering and Design.

*Erckmann, V., G. Dammertz, W. Kasparek, H.P. Laqua, H. Maassberg, M.Thumm, and W7-X and W7-AS teams:* ECRH and ECCD experiments at W7-AS, status at W7-X. JAERI Report, submitted to Fusion Engineering and Design.

*Leuterer, F., S. Günter, M. Maraschek, F. Ryter, R. Wolf, G. Gantenbein, H. Zohm, ASDEX Upgrade Team, and ECRH Group:* ECRH experiments in ASDEX Upgrade. JAERI Report.

*Plaum, B., D. Wagner, W. Kasparek, and M. Thumm:* Optimization of oversized waveguide bends using a genetic algorithm. JAERI Report, submitted to Fusion Engineering and Design.

First French-German Symposium on Simulation of Atmospheric Entries by Means of Ground Test Facilities (SSAE 99), Stuttgart, Germany, November 17 - 19, 1999

*Hirsch, K., I. Altmann., G. Bauer, H. Jentschke, S. Klenge, B. Roth, D. Schinköth, and U. Schumacher:* In situ diagnostic methods for investigating the interaction region between a plasma jet and C/C-SiC targets. Contrib. paper 3.7, p 1-8.

*Hirsch, K., B. Roth, I. Altmann, K.-L. Barth, H. Jentschke, A. Lunk, and U. Schumacher:* Visualisation of surface phenomena on C/C-SiC targets exposed to a nitrogen-oxygen plasma jet. Contrib. paper 3.4, p 1-8.

## PATENT

*Aldinger, F., J. Bill, A. Greiner, K. Hirsch und M. Kaiser:* Beschichtung zur Verminderung der Erosion an thermisch hochbelasteten Oberflächen aus faserverstärkter Keramik und Verfahren zu deren Herstellung. (Coatings to reduce the erosion on surfaces of fibre fortified ceramics under high thermal loads and their processing). Deutsches Patentamt, München, 19928173.4, (99/35160-ICT)

## DIPLOMA THESIS

*Schneider, W.:* Holographische Bestimmung von Phasenfronten von Millimeterwellenstrahlung. (Holographic determination of phase fronts of millimetre radiation.) Universität Stuttgart, 1999.

## DOCTORAL THESIS

*Empacher, L.:* Analyse eines Vielstrahl-Wellenleiters zur Übertragung hoher Mikrowellenleistungen. (Analysis of a multiple beam waveguide for transmission of high microwave power.) Universität Stuttgart, 1999.

## REPORTS

*Altmann, I., G. Bauer, K. Hirsch, H. Jentschke, S. Klenge, B. Roth, D. Schinköth, and U. Schumacher:* In situ diagnostics of the interaction region between a nitrogen-oxygen plasma jet and hot C/C.SiC ceramic material. SFB-report 1999/46 and IPF-Report 99-1.

*Hirsch, K., I. Altmann, G. Bauer, H. Jentschke, S. Klenge, B. Roth, D. Schinköth, and U. Schumacher:* In situ diagnostic methods for investigating the interaction region between a plasma jet and C/C-SiC targets. IPF-Report 99-3.

*Hirsch, K., B. Roth, I. Altmann, K.-L. Barth, H. Jentschke, A. Lunk, and U. Schumacher:* Visualisation of surface phenomena on C/C-SiC targets exposed to a nitrogen-oxygen plasma jet. IPF-Report 99-4.

## SEMINAR TALKS

*Gantenbein, G.:* Übertragungssystem für die ECRH an W7-X. W7-X Seminar, Usedom, November 1999

*Hirsch, K.:* Developments with technical plasmas at Stuttgart, Applications and Diagnostics, ADAS Workshop, Loch Lomond, Scotland, September 26-28, 1999

*Kasparek, W.:* ERCH and ECCD for the stellarator W7-X. Colloquium, Fukui University, Japan, October 11, 1999

*Plaum, B.:* Optimization of oversized Waveguide bends using a genetic algorithm. Colloquium, Fukui University, Japan, October 11, 1999

*Schmidtmann, K.:* Spektroskopische Messung von Divertorparametern. ASDEX Upgrade Seminar, Max-Planck-Institut für Plasmaphysik, Garching, January 20, 1999

*Schumacher, U.:* Plasmaforschung zur Lösung des globalen Energieproblems. LEU Stuttgart, March 16 and March17, 1999

*Schumacher, U.:* Durchbrüche in Plasmen. Kolloquium, Max-Planck-Institut für Plasmaphysik, Garching, July 16, 1999

*Schumacher, U.:* Stand und Perspektiven des Fusionsreaktors. Physikalisches Kolloquium, Universität Tübingen, November 17, 1999

*Zohm, H.:* Einsatz von Hochleistungsmikrowellen in Fusionsplasmen. Seminar, Forschungszentrum Karlsruhe, 1999

*Zohm, H.:* Neues von der Fusionsforschung mit magnetischem Einschluß. GSI Darmstadt 1999

*Zohm, H.:* Einsatz von Hochleistungs-Millimeterwellen in Kernfusionsplasmen. Kolloquium der Fakultät Elektrotechnik und Informationstechnik, Universität Stuttgart, November 2, 1999

# How to reach
# Max-Planck-Institut für Plasmaphysik (IPP)

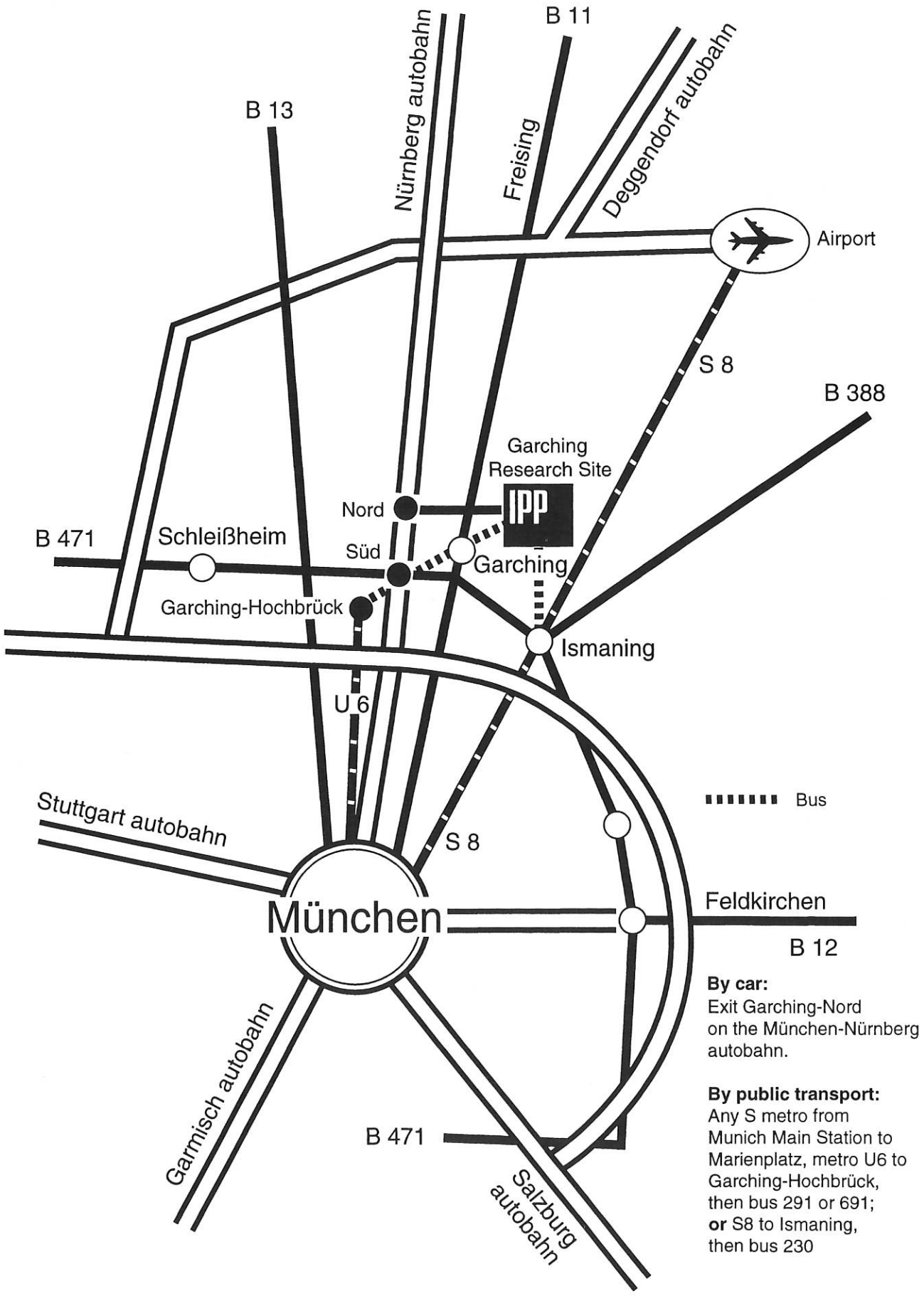


**By car:**
Exit Garching-Nord
on the München-Nürnberg
autobahn.

**By public transport:**
Any S metro from
Munich Main Station to
Marienplatz, metro U6 to
Garching-Hochbrück,
then bus 291 or 691;
**or** S8 to Ismaning,
then bus 230

# How to reach Greifswald Branch Institute of Max-Planck-Institut für Plasmaphysik

**Greifswald Branch Institute** of
Max-Planck-Institut für Plasmaphysik
Wendelsteinstraße 1
D-17491 Greifswald

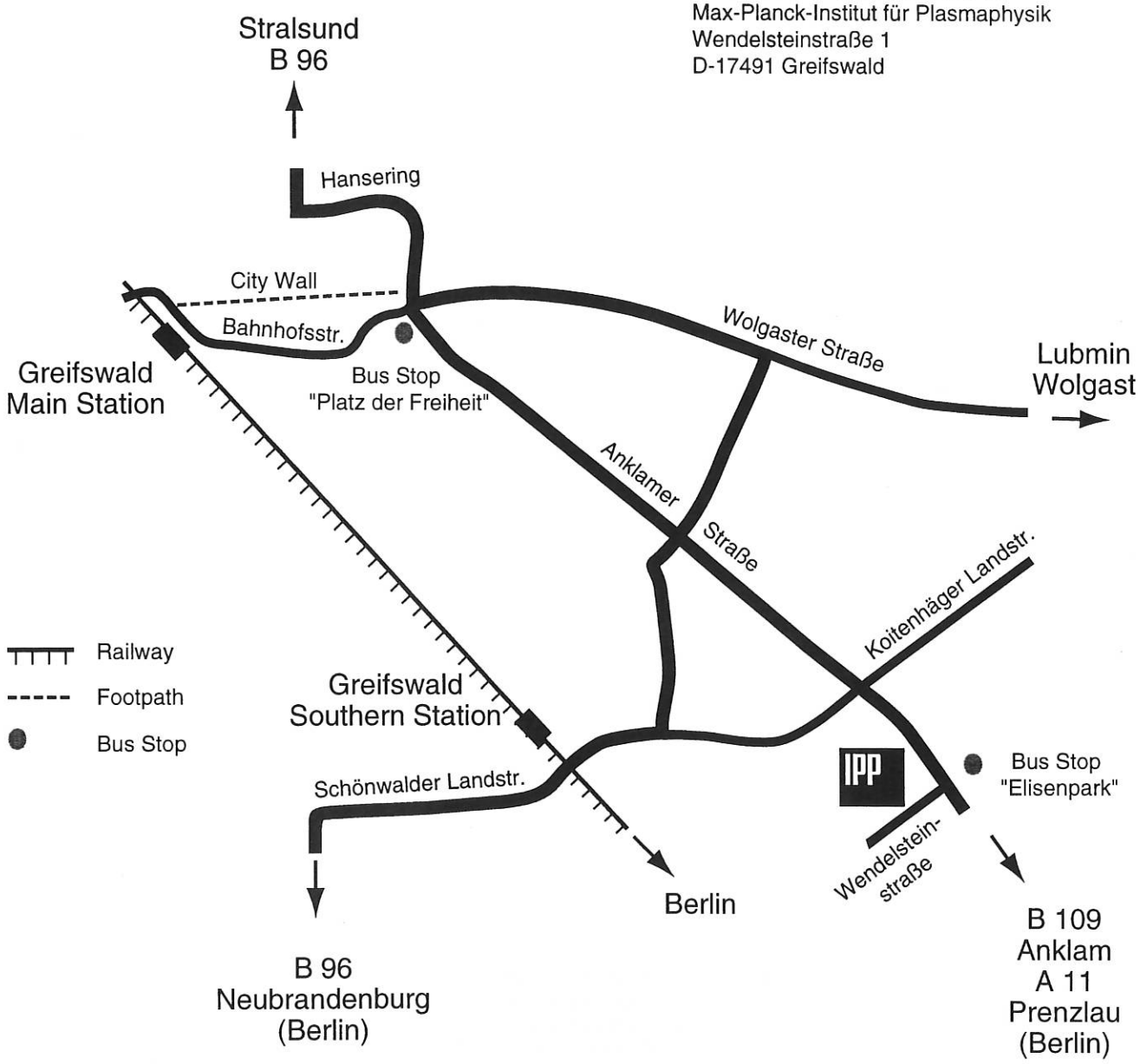


**By air:**
Via Berlin: from Berlin Tegel Airport by bus No. X9 to Zoologischer Garten, S-Bahn to Ostbahnhof Station, by train to Greifswald **or**
Via Hamburg: from the airport to Main Railway Station, by train to Greifswald.

**By car:**
Via Berlin, Neubrandenburg to Greifswald **or** via Hamburg, Lübeck, Stralsund to Greifswald, in Greifswald follow the signs "Max-Planck-Institut".

**By bus:**
From Greifswald Railway Station by bus No. 30, 40, 60, or 61 to the "Platz der Freiheit"s stop. Then by bus 32 or 43 to the "Elisenpark"s stop.

ANNUAL REPORT 1999

Max-Planck-Institut für Plasmaphysik (IPP) • 85748 Garching bei München
Telephone (0 89) 32 99-01 • Telefax (0 89) 32 99-22 00

Printing: Gebr. Giehrl Druckerei GmbH, München

Printed in Germany
ISSN 0179-9347

This work was performed under the terms of the agreement between Max-Planck-Institut für Plasmaphysik and the European Atomic Energy Community to conduct joint research in the field of plasma physics.


Max-Planck-Institut
für Plasmaphysik